Development and Plasticity of Intrinsic Connectivity in the Central Nucleus of the Mouse Inferior Colliculus

by

Joshua Joseph Sturm

AB, Biochemistry and Cognitive Science, Vassar College, 2011

Submitted to the Graduate Faculty of

School of Medicine in partial fulfillment

of the requirements for the degree of

Doctor of Philosophy

University of Pittsburgh

[2015]

UNIVERSITY OF PITTSBURGH

SCHOOL OF MEDICINE

This dissertation was presented

by

Joshua Sturm

It was defended and approved on

November 19, 2015

Alison Barth, PhD, Professor

David Chi, MD, Associate Professor

Lawrence Lustig, MD, Professor

Stephen Meriney, PhD, Professor

Nathaniel Urban, PhD, Professor

Thanos Tzounopoulos, PhD, Associate Professor

Dissertation Advisor: Karl Kandler, PhD, Professor

Development and Plasticity of Intrinsic Connectivity in the Central Nucleus of the Mouse Inferior Colliculus

Joshua Sturm A.B.

University of Pittsburgh, 2015

Development and Plasticity of Intrinsic Connectivity in the Central Nucleus of the Mouse Inferior Colliculus

Joshua Sturm A.B.

University of Pittsburgh, 2015

Proper brain function depends upon the precise organization of neural circuits. In the central auditory system, accurate acoustic processing depends upon the assembly and preservation of tonotopically-organized networks of excitatory and inhibitory synaptic connections.

In this thesis, we investigated the development and plasticity of intrinsic synaptic circuitry in the central nucleus of the mouse inferior colliculus (CNIC), a tonotopically-organized midbrain nucleus that serves as the major subcortical center for auditory integration. In the CNIC, intrinsic connections comprise the majority of synapses, yet the functional organization of these local networks has remained largely obscure.

In Chapter 2, we mapped the functional organization of intrinsic connections in the CNIC during the first three weeks of postnatal development. We found evidence of robust excitatory and inhibitory intrinsic connections already at postnatal day 2 (P2). Excitatory and inhibitory intrinsic connections underwent a period of dramatic refinement after hearing onset, resulting in a predominance of intrinsic inhibition.

In Chapter 3, we examined the role of hearing experience in directing the maturation of intrinsic CNIC circuits by rearing mice in pulsed white noise. We found that pulsed noise delivered from P12-25, but not P19-25, led to a profound reorganization of excitatory and inhibitory intrinsic connections received by both glutamatergic and GABAergic neurons, suggesting that intrinsic CNIC circuits are sculpted by acoustic experience during an early critical period.

In Chapter 4, we investigated the effects of hearing-loss on the organization of CNIC circuits in a mouse model of tinnitus. We found that hearing loss led to reorganizations of excitatory and inhibitory local CNIC circuits, the nature of which correlated with the presence or absence of behavioral evidence of tinnitus. Acoustic enrichment with pulsed white noise delivered immediately after acoustic trauma prevented circuit reorganization and the emergence of behavioral signs of tinnitus.

In addition to providing the first characterization of functional intrinsic connectivity in the auditory midbrain, our findings may also have broader implications for the principles that govern the organization and balance of excitatory and inhibitory networks in subcortical circuits. Our findings also have potentially important clinical implications for the prevention and treatment of tinnitus.

TABLE OF CONTENTS

LIST OF TABLES

LIST OF FIGURES

LIST OF ABBREVIATIONS

ABR: auditory brainstem response

AC: auditory cortex

AE: acoustic enrichment

ASR: acoustic startle reflex

AVCN: anteroventral cochlear nucleus

A1: primary auditory cortex

CNIC: central nucleus of inferior colliculus

DCIC: dorsal cortex of inferior colliculus

DCN: dorsal cochlear nucleus

DNLL: dorsal nucleus of lateral lemniscus

FZ: functional zone

IC: inferior colliculus

LCIC: lateral cortex of inferior colliculus

LL: lateral lemniscus

LSO: lateral superior olive

LSPS: laser-scanning photostimulation

MGB: medial geniculate body

MSO: medial superior olive

NE-AE: noise-exposed with acoustic enrichment

NE-NT: noise-exposed no tinnitus

NE-T: noise-exposed tinnitus

P: postnatal day

PPI: paired pulsed inhibition

SEM: standard error of the mean

SOC: superior olivary complex

SPN: superior paraolivary nucleus

STDP: spike-timing dependent plasticity

VCN: ventral cochlear nucleus

VNLL: ventral nucleus of lateral lemniscus

PREFACE

The work presented herein is based on several manuscripts/chapters that are either published or in preparation.

Figure 1-3 in Chapter 1 was modified from:

Sturm JJ, Nguyen T & Kandler K (2015) Mapping Synaptic Circuits with Photostimulation of Caged Glutamate. Auditory Vestibular Research Methods, New York: Springer. ***Accepted.***

Chapter 2 is a modified version of:

Sturm J, Nguyen T & Kandler K (2014) Development of intrinsic connectivity in the central nucleus of the mouse inferior colliculus. ***J. Neurosci.*** **34(45): 15032-15046.**

Chapters 3 and 4 are versions of manuscripts currently in preparation for journal submission.

Chapter 3 is a version of:

Sturm J, Roos H, Nguyen T & Kandler K (2015) Noise Rearing Induces Local Circuit Reorganization in the Auditory Midbrain During a Critical Period. ***In Preparation*****.**

Chapter 4 is a version of**:**

Sturm J, Roos H, Nguyen T & Kandler K (2015) Reorganization of Synaptic Circuits in the Inferior Colliculus of a Mouse Model of Tinnitus. ***In Preparation*****.**

ACKNOWLEDGEMENTS

First and foremost, I would like to thank my advisor, K. Kandler, for his exceptional support, patience and mentorship. Throughout my time in his laboratory, Dr. Kandler has contributed great care, forethought and rigor to my training. He has treated me as a scientific peer, as well as a trainee, and I am deeply appreciative of his efforts. Sincerest thanks also to the members of my committee, A. Barth, D. Chi, L. Lustig, S. Meriney, N. Urban and T. Tzounopoulos, who graciously took time out of their busy schedules to contribute to my training. Special thanks to D. Chi, for encouraging me to keep in mind the clinical implications of my research and for helping me to develop my clinical skills during my years in the laboratory. Many thanks to L. Lustig, who generously flew in to act as my outsider examiner and offer his valuable insight. I would also like to thank T. Nguyen for providing me with invaluable technical assistance and friendship throughout my training. I would like to thank H. Roos, whose effort and expertise in mouse behavioral testing were crucial. Thanks to E. Aizenman for acting as my career advisor and to R. Steinman for his active and compassionate support. I also appreciate the work of P. Argenzio, D. O'Hara and M. Singh, whose administrative excellence has been essential to my success. Thanks to the NIDCD for providing funds to support my training. Extra special thanks to my family, whose love and support has kept me going through the tough times, and also helped me to fully enjoy the great times. Finally, I would like to thank C. Kelsoe, my partner in life, for her care, compassion and belief in me. Her patience and wisdom have been absolutely paramount.

1.0 GENERAL INTRODUCTION

1.1 ACTIVITY-DEPENDENT CONSTRUCTION OF AUDITORY CIRCUITS

The mature brain is composed of precisely organized neural circuits comprised of excitatory and inhibitory synaptic connections. These connectivity networks enable animals to interact with their external worlds and to develop adaptive behaviors suited to their unique environmental niches. While the initial assembly of neural circuits involves genetically programmed sets of molecular interactions (Goodman and Shatz, 1993), the functional optimization of these circuits requires periods of activity-dependent refinement (Zhang and Poo, 2001). Early in development, activity-dependent refinement of immature circuits is directed by internally generated patterns of correlated spontaneous activity (Kirkby et al., 2013). As the brain progressively matures, circuit refinement becomes increasingly driven by sensory experience (Katz and Shatz, 1996). Although much experience-dependent circuit sculpting takes place early in life, during windows of enhanced synaptic plasticity called critical periods (CP), it is now clear that substantial synaptic reorganization can also take place in adulthood (Hübener and Bonhoeffer, 2014).

The experience-dependent maturation of neural circuits is crucial for the establishment of normal brain function, and changes in sensory experience, either during development or in adulthood, can have dramatic effects on circuit organization. A clear example of this principle can be seen in the central auditory system, where the rapid and accurate processing of sounds is

afforded by the precise topographical structuring of neural circuits according to preferred sound frequency (tonotopy). In the developing rodents, degrading sensory experience during the initial weeks of hearing experience can disturb the maturation of tonotopic organization (Zhang et al., 2001; Zhang et al., 2002; Chang and Merzenich, 2003; Insanally et al., 2010) and have long-lasting consequences for acoustic response selectivity (Sanes & Constantine-Paton, 1983; Sanes & Constantine-Paton, 1985; Seidl and Grothe, 2005; Grecova et al., 2009). Furthermore, in adult animals, where auditory circuits are largely mature, hearing loss can lead to substantial changes in the intrinsic and synaptic properties of auditory neurons, and can contribute to central hearing disorders such as tinnitus and hyperacusis (Roberts et al., 2010; Knipper et al., 2013).

In order to develop effective means of preventing and treating central hearing disorders, it will be crucial to elucidate the processes by which central auditory circuits become precisely organized in development, as well as how changes in sensory experience can modify this functional organization. Here we investigate these questions by examining the development and plasticity of intrinsic synaptic circuitry in the mouse inferior colliculus, the subcortical nexus for auditory integration.

1.2 THE INFERIOR COLLICULUS

The inferior colliculus (IC) is the principal midbrain nucleus of the central auditory system and acts as the major subcortical site for the integration of acoustic information. In the ascending auditory pathway, the IC acts as an obligatory synaptic terminus for nearly all auditory brainstem nuclei (Adams, 1979; Aitken and Phillips 1984b), including the cochlear nucleus (CN) (Oliver, 1984; Oliver, 1987; Cant and Benson, 2008), the superior olivary complex (SOC) (Shneiderman

and Henkel, 1987; Oliver 2000) and the lateral lemniscus (LL) (Saint Marie et al., 1997; Gabriele et al., 2000a) (Figure 1-1). These converging projections carry information about various sound attributes (e.g. duration, frequency, intensity and location), which is assimilated and integrated in the IC. In the descending auditory pathway, the IC receives substantial projections from the auditory cortex (Saldaña et al., 1996; Winer et al., 1998; Bajo and Moore, 2005), which exert top-down control of auditory processing in the IC (Ma and Suga, 2001; Xiao and Suga, 2005; Yan et al., 2005; Ma and Suga, 2008; Nakamoto et al., 2008) and which have recently been shown to modulate sound-driven behavior (Bajo et al., 2010; Xiong et al, 2015). In addition to these ascending and descending inputs, the IC also receives an intercollicular projection from the contralateral IC (Moore et al., 1998; Malmierca et al., 2005; Fathke and Gabriele, 2009), as well as an extensive network of intracollicular (intrinsic) synaptic connections (Saldaña and Merchán, 1992), which gives rise to the majority of IC synapses (Saldaña and Merchán, 1992). The function of these intrinsic networks remains unclear, but recent evidence suggests that they are preferentially engaged at higher sound levels, where they modulate the dynamic range of neuronal responses (Grimsley et al., 2013) and may contribute to the intensity-dependent shaping of spectrotemporal receptive fields (Lesica and Grothe, 2008).

The IC is composed of three principal divisions: a central nucleus (CNIC), a lateral cortex (LCIC) and a dorsal cortex (DCIC) (Fig 1-1) (Aitkin, 1979; Morest and Oliver, 1984). The function of each IC division is reflected by its unique combination of synaptic inputs and postsynaptic targets. For example, the CNIC, which plays a critical role in integration of acoustic stimulus features (Winer and Schreiner, 2005), receives the majority of its synaptic input from the auditory brainstem nuclei (Aitkin et al., 1994; Malmierca, 2004). Output from the CNIC is primarily sent to the ventral division of the thalamic medial geniculate body (MGB), which

serves as the principal relay nucleus to primary auditory cortex (A1) (Calford and Aitkin, 1983; Wenstrup and Grose, 1995). The CNIC also sends descending projections to the dorsal nucleus of the LL (DNLL) (Caicedo and Herbert, 1993), the granule cell domain of the dorsal CN (DCN) (Malmierca et al., 1996) and the efferent medial olivocochlear system (MOC) (Vetter et al., 1992). The DCIC, on the other hand, which plays an important role in top-down modulation of auditory processing (Stebbings et al., 2014), primarily receives synaptic input from the auditory cortex. Outgoing ascending projections from the DCIC are principally sent to the deep dorsal division of the MGB (Winer and Morest, 1984; Mellott et al., 2014), whereas descending DCIC projections are sent to multiple divisions of the DCN (Vater and Feng, 1990). Finally, the LCIC, which is believed to contribute to multimodal sensory integration, is the only IC division to receive considerable non-auditory input (Morest and Oliver, 1984). The LCIC sends ascending projections to both the dorsal and medial divisions of the MGB (Winer and Morest, 1983), and descending projections to the CN (Schofield, 2001) and SOC (Vetter et al., 1992). Thus, the IC is composed of three functional divisions, each of which is distinguishable on the basis of its unique distribution of synaptic inputs and outputs.

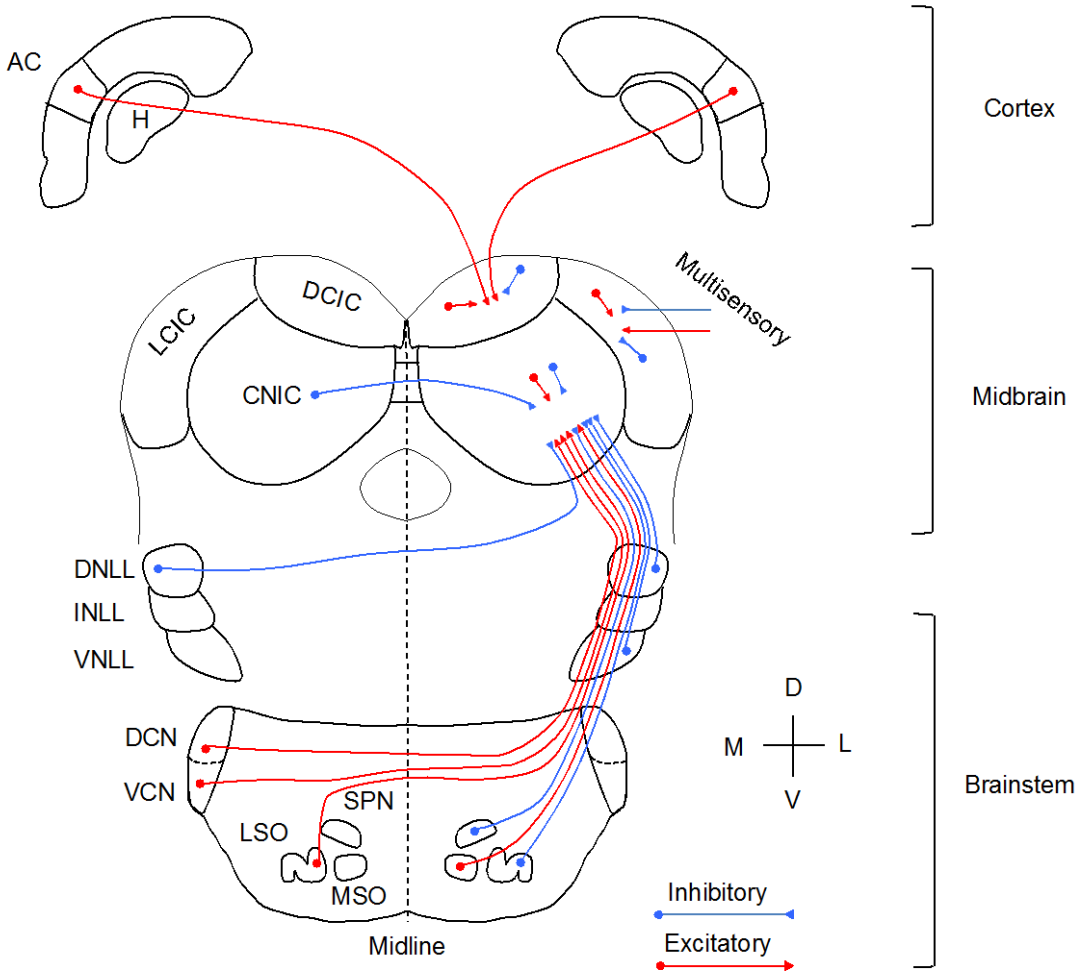

Figure 1-1. Synaptic organization of the inferior colliculus

Schematic of major excitatory (red) and inhibitory (blue) inputs to IC. Synaptic inputs to the IC arise from ascending, commissural, descending and intrinsic sources. Ascending projections primarily terminate in central nucleus (CNIC), whereas descending projections terminate in dorsal cortex (DCIC) and non-auditory (multisensory) projections terminate in lateral cortex (LCIC). Projections shown to single IC for simplicity (mirrored projections are received by contralateral IC). Legend: AC; auditory cortex, CNIC; central nucleus of inferior colliculus, DCIC; dorsal cortex of inferior colliculus, DCN; dorsal cochlear nucleus, DNLL; dorsal nucleus of lateral lemniscus, H; hippocampus, INLL; intermediate nucleus of lateral lemniscus, LCIC; lateral cortex of inferior colliculus, LSO; lateral superior olive, MSO; medial superior olive, SPN; superior paraolivary nucleus, VCN; ventral cochlear nucleus, VNLL; ventral nucleus of lateral lemniscus.

1.3 THE CENTRAL NUCLEUS OF THE INFERIOR COLLICULUS

The central nucleus (CNIC) is the most extensively studied of the three IC divisions, and has been shown to be essential for normal hearing (Jenkins and Masterton, 1982). The CNIC exhibits a robust tonotopic organization, where neurons with similar characteristic frequency (CF) preferences are clustered together into anatomically defined fibrodendritic (isofrequency) laminae (Figure 1-2 A) (Oliver and Morest, 1984; Stiebler and Ehret, 1985; Malmierca, 2004). Isofrequency laminae are approximately 150-200 μm wide and extend lengthwise up to 1,000 μm along the ventrolateral (VL) to dorsomedial (DM) direction (Willott and Shnerson, 1978; Romand and Ehret, 1990). The orientation of these laminae demarcates an "isofrequency axis," which runs orthogonal to the tonotopic axis of the CNIC (Fig 1-2 A) (Stiebler and Ehret, 1985; Romand and Ehret, 1990). In the CNIC, ascending brainstem projections terminate in alignment with fibrodendritic laminae, thereby preserving their tonotopic relations (Morest and Oliver, 1984; Oliver and Morest, 1984; Stiebler and Ehret, 1985; Malmierca et al., 1993; Gabriele et al., 2000a, 2007; Henkel et al., 2005; Miller et al., 2005; Henkel et al., 2007). For example, low-frequency (lateral) parts of the lateral superior olive (LSO) (Guinan et al., 1972 a,b) project to the dorsolateral (DL, low frequency) portion of the CNIC (Merzenich and Ried, 1974; Glendenning and Masterton, 1983), whereas high-frequency (dorsal) parts of the dorsal cochlear nucleus (DCN) project to the ventromedial (VM, high frequency) portion of the CNIC (Oliver, 1984).

In addition to its clear tonotopic organization, the CNIC also exhibits a topographic axis of tone-evoked neuronal response latencies (Hattori and Suga, 1997; Reetz and Ehret, 1999). This axis parallels the isofrequency axis in the VL-to-DM direction, with VL neurons exhibiting shorter response latencies to tones centered at their CFs compared to DM neurons. Interestingly,

this response latency gradient is paralleled by a biochemical gradient of inhibitory neurotransmitter receptor densities (Fubara et al., 1996), where $GABA_A$ receptor density increases from VL to DM and glycine receptor density increases from DM to VL. The predominance of indices of glycinergic inhibition in the VL domain, where CNIC neurons exhibit the fastest tone-evoked response latencies, is consistent with a critical role of glycinergic inhibition in enabling the rapid temporal processing necessary for coincidence detection (Saitoh and Suga, 1995; Myoga et al., 2010). Additionally, differences in the distributions of postsynaptic neurotransmitter receptor types along the isofrequency axis may reflect heterogeneity in the ascending and/or local synaptic network configurations of CNIC neurons with similar CF preferences. Indeed, spectrally matched ascending projections to the CNIC do not terminate uniformly within isofrequency laminae, but rather are segregated into "functional zones" (FZs) according to input source (Aitkin and Schuck, 1985; Maffi and Aitkin, 1987; Shneiderman and Henkel, 1987; Oliver et al., 1997; Loftus et al., 2004; Bajo and Moore, 2005; Cant and Benson, 2006). Neurons in the CNIC that receive input from different FZs exhibit distinct binaural response properties and periodicity preferences (Wenstrup et al., 1986; Schreiner and Langner, 1988; Loftus et al., 2010), likely resulting from a combination of the response properties of their inherited inputs, their intrinsic membrane properties, and their intrinsic connectivity within the CNIC. Thus, multiple levels of functional organization exist within the CNIC, which together contribute to the diversity of spectrotemporal response properties exhibited by CNIC neurons (Escabi and Schreiner, 2002; Lesica and Grothe, 2008).

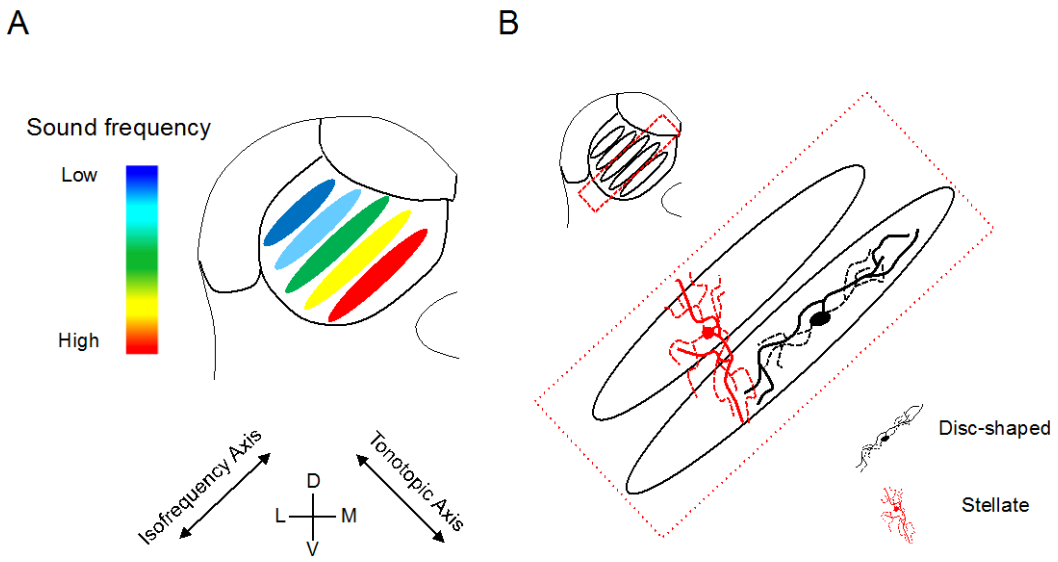

Figure 1-2. Functional organization of central nucleus of inferior colliculus

(A) CNIC neurons with similar characteristic frequency preferences are organized into isofrequency laminae (colored ellipses). Isofrequency laminae extend orthogonal to tonotopic axis, which runs along the ventromedial (high frequency) to dorsolateral (low frequency) direction. (B) Two morphological cell types found in CNIC (cartoon depictions). Dendritic (dashed) and axonal (solid) extensions of disc-shaped cells (black) predominantly restricted to individual isofrequency lamina, whereas extensions of stellate cells (red) cross multiple laminae. Legend: D; dorsal, L; lateral, M; medial, V; ventral.

1.4 INTEGRATION OF EXCITATORY AND INHIBITORY INPUTS IN CNIC

Neurons in the CNIC receive a profound diversity of converging excitatory and inhibitory synaptic inputs (Figure 1-1). Excitatory synaptic inputs to CNIC neurons are glutamatergic, whereas inhibitory synaptic inputs can be either GABAergic or glycinergic. In mammals, major glutamatergic projections to the CNIC arise contralaterally, from the dorsal (DCN) and anteroventral (AVCN) divisions of the CN (Oliver, 1984; Oliver, 1987) and the lateral superior olive (LSO) (Shneiderman and Henkel, 1987), and ipsilaterally, from the medial superior olive (MSO) (Oliver et al., 1995) (Figure 1-1). GABAergic inhibitory projections, on the other hand, predominately arise contralaterally, in the DNLL (Shneiderman et al., 1998) and IC (González-Hernández et al., 1996), and ipsilaterally in the superior paraolivary nucleus (SPN) (González-Hernández et al., 1996), DNLL (Shneiderman et al., 1998) and VNLL (Thompson et al., 1985). In addition to these GABAergic inhibitory pathways, prominent glycinergic inhibitory projections to the CNIC arise ipsilaterally, in the LSO (Saint Marie et al., 1989) and the VNLL (Winer et al., 1995). Neurons in the CNIC can, themselves, be glutamatergic or GABAergic (Ono et al., 2005; Ito et al., 2009), suggesting that intrinsic IC networks likely consist of both excitatory and GABAergic inhibitory connections. However, direct evidence of functional intrinsic excitatory and inhibitory CNIC circuits has been lacking.

Physiological studies in a number of mammalian species (bats, cats, guinea pigs, rats and mice) have revealed by intracellular recordings that excitatory and inhibitory inputs interact to determine sound-evoked responses of CNIC neurons (Covey et al., 1996; Pedemonte et al., 1997; Kuwada et al., 1997; Gitelman et al., 2009; Xiong et al., 2013; Ono and Oliver, 2014). Individual CNIC neurons can receive excitatory and inhibitory inputs from several ascending sources (Ono and Oliver, 2014), and the relative strength and timing of these inputs both contribute to shaping

the sound-evoked discharge patterns of CNIC neurons (Ono and Oliver, 2014; Xiong et al., 2013). For example, CNIC neurons have been shown to detect inter-aural level differences (ILDs), which provide salient cues for localizing binaurally presented sounds in space, by scaling contralaterally evoked synaptic excitation in an ILD-dependent manner, without changing evoked synaptic inhibition (Xiong et al., 2013). Importantly, this ILD-dependent modulation of excitation: inhibition balance left frequency tuning unchanged, thereby providing a modality-specific gain adjustment mechanism that allows CNIC neurons to dynamically encode a sound's location in space without affecting their selectivity for other acoustic features (Xiong et al., 2013). In a second study, directional selectivity for frequency-modulated (FM) sweeps was shown to emerge in CNIC neurons via the assimilation of excitatory and inhibitory input strengths (Gittelman et al., 2009). In this study, direction-dependent shifts in the relative magnitudes of excitatory and inhibitory synaptic conductances were shown to account for the selectivity of IC neurons for upward or downward FM sweeps (Gittelman et al., 2009). Taken together, the evidence from these studies suggests that the dynamic integration of excitatory and inhibitory synaptic inputs onto CNIC neurons contributes to the generation of response selectivity for various acoustic attributes in the IC.

1.5 INTRINSIC CIRCUITRY OF THE CNIC

While the organization and integration of extrinsic projections to the IC have become increasingly well understood in recent years (Brunso-Bechtold et al., 1981; Maffi and Aitkin, 1987; Oliver, 1987, 2000; Faingold et al., 1993; Burger and Pollak, 2001; Malmierca et al., 2002; Henkel et al., 2005; Cant and Benson, 2008; Bajo et al., 2010; Pollak et al., 2011; Xiong et al.,

2013), the anatomical and functional organization of intrinsic connections in the CNIC has remained unclear. Intrinsic axons in the CNIC arise from two major morphological cell types: disc-shaped (flat) and stellate (less flat) neurons (Figure 1-2 B) (Oliver and Morest, 1984; Meininger et al., 1986; Oliver et al., 1991; Malmierca et al., 1993). Disc-shaped neurons exhibit elliptical dendritic fields (200-800 μm long and 50-70 μm wide) and local axon collaterals that are both restricted to the same fibrodendritic lamina as the dendrites of their parent neurons (Oliver et al., 1991). The intralaminar local axons of these disc-shaped neurons likely connect IC neurons that are tuned to similar sound frequencies, but that may reside in different functional zones (Brunso-Bechtold et al., 1981; Maffi and Aitkin, 1987; Shneiderman and Henkel, 1987; Oliver, 2005; Cant and Benson, 2006; Loftus et al., 2010). In contrast to disc-shaped IC neurons, stellate cells exhibit spherical dendritic fields (spanning 200-500 μm) and local axons that extend across several fibrodendritic laminae (Winer & Schreiner, 2005). Thus, whereas disc-shaped cells are morphologically poised to integrate information across tonotopically-matched afferent projections and intrinsic networks, stellate-cells appear suited to facilitate information exchange across isofrequency laminae, between IC neurons with different CF preferences (Merzenich and Reid, 1974; Ehret and Romand, 1994; Schreiner and Langner, 1997; Malmierca et al., 2008).

While the morphological distinctions between disc-shaped and flat IC neurons suggest different cellular specializations, perhaps involving distinct synaptic network architectures, the organization of functional synaptic connectivity in the CNIC has remained elusive. Disc-shaped and stellate IC neurons can be both glutamatergic and GABAergic (Ono et al., 2005; Ito et al., 2009), suggesting that intrinsic IC networks are likely to be excitatory as well as inhibitory, yet little is else is known about the functional organization of these networks. In Chapter 2, we describe a series of studies aimed at elucidating the functional organization of intrinsic CNIC

networks. In these studies, we used laser-scanning photostimulation with caged glutamate (LSPS) (Figure 1-3) to characterize the strength and the spatial distribution of local excitatory and inhibitory inputs received by CNIC neurons in mice during the first three weeks of postnatal development (P2-P22).

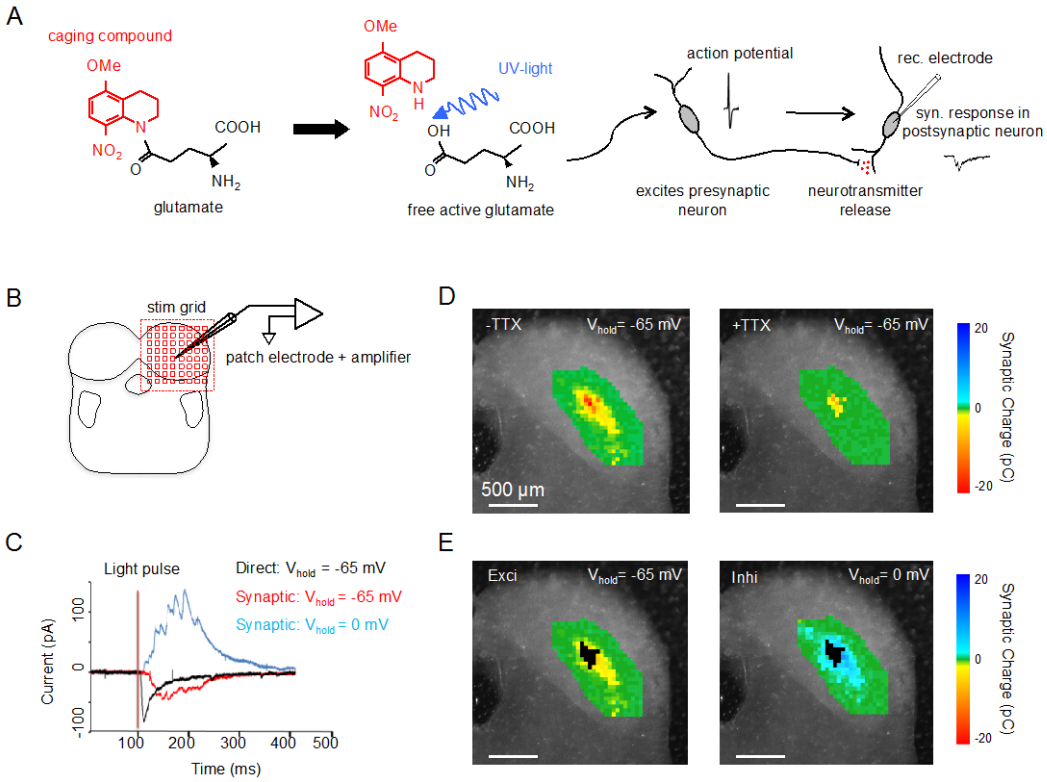

Figure 1-3. Mapping synaptic connections in the CNIC with laser-scanning photostimulation.

(A) UV photostimulation lyses the covalent linkage between glutamate (black) and the caging compound (red, caging group is 4-methoxy-7-nitroindolinyl (MNI) group from MNI-caged-L-glutamate, Tocris) (*left*), thereby releasing free glutamate (*middle*) that drives nearby neurons to spike (*right*). Spiking in presynaptic neurons leads to neurotransmitter release and postsynaptic responses in the recorded cell **(B)** Schematic illustration of input mapping in the inferior colliculus, with whole-cell path clamp recording electrode. Light pulses are delivered to a series of stimulation targets (stim grid) **(C)** Excitatory (red trace) and inhibitory (blue trace) synaptic inputs can be distinguished by holding the membrane potential of the recorded cell near the reversal potential for chloride (-65 mV) and glutamatergic neurotransmission (0 mV), respectively. Compared to direct stimulations (black trace), synaptic responses have longer onset latencies. **(D)** *Left*, Example of an excitatory synaptic input map obtained with laser-scanning photostimulation from an IC neuron in a P7 mouse. *Right*, Synaptic inputs are abolished by mapping in the presence of TTX, which blocks action potential generation leaving only direct responses intact. **(E)** Example average excitatory (left, *same map as 2D, left*) and inhibitory (right) synaptic input maps. Direct responses sites are shown in black. *Figure adapted from Sturm et al., 2015.*

1.6 ACTIVITY-DEPENDENT REFINEMENT IN THE DEVELOPING CNIC

Activity-dependent refinement is a central mechanism by which initially imprecise synaptic connections are sculpted into precise, functionally optimized neural circuits (Wong, 1993; Katz and Shatz, 1996; Kandler, 2004; Spitzer, 2006; Huberman et al., 2008; Kandler et al., 2009; Kirkby et al., 2013). In the rodent auditory system, activity-dependent refinement takes place in two principal stages of development: before hearing onset and after hearing onset. Before hearing onset, which occurs around postnatal day (P) 12 (Rubel, 1984), substantial refinement of functional connectivity has been demonstrated in the auditory brainstem (Kim and Kandler, 2003; Noh et al., 2010; Case et al., 2011), and this refinement has been shown to depend upon spontaneous activity patterns originating in the pre-hearing cochlea (Clause et al., 2014). These spontaneous activity patterns arise when depolarized inner hair cells (IHCs) in the cochlea release glutamate onto auditory nerve afferents, causing them to fire patterned bursts of action potentials that are propagated along the ascending central auditory pathways (Jones et al., 2007; Tritsch et al., 2007; Tritsch and Bergles, 2010). The patterning of spontaneous auditory nerve discharges appears to instruct pre-hearing refinement of auditory circuitry, since disrupting the temporal fine structure of these spontaneous bursts has been shown to profoundly disrupt the functional and structural sharpening of an inhibitory tonotopic map in the auditory brainstem (Clause et al., 2014). Substantial neural circuit refinement also takes place after hearing onset (Sanes and Siverls, 1991; Kapfer et al., 2002; Magnusson et al., 2005; Sun et al., 2010; Clause et al., 2014), as the patterning of neural activity in the auditory system becomes increasingly driven by the spectral and temporal structures of auditory inputs. Changes in the acoustic properties of auditory inputs during early hearing experience can disrupt both structural and functional circuit refinement (Magnusson et al., 2005; Werthat et al., 2008), and have long-lasting effects on

acoustic response selectivity (Sanes and Constantine-Paton, 1983; Sanes and Constantine-Paton, 1985; Zhang et al., 2001; Zhang et al., 2002; Chang and Merzenich, 2003; Chang et al., 2005; Razak et al., 2008; de Villers-Sidani et al., 2008; Zhou et al., 2008; Grecova et al., 2009; Insanally et al., 2010; Oliver et al., 2011; Bures et al., 2014).

In the CNIC, afferent projections from the auditory brainstem are present at birth (Kandler and Friauf, 1993; Okoyama et al., 1995), and are rapidly refined before hearing onset (Oliver, 2000; Gabriele et al., 2000a, 2007; Henkel et al., 2007). This pre-hearing maturation, which involves the segregation of auditory afferents that initially terminate in a uniform manner in the CNIC into distinct isofrequency bands with clear inter-band spaces (Gabriele et al., 2000a), has been shown to depend on cochlear-generated spontaneous activity (Gabreile et al., 2000b; Franklin et al., 2006; Franklin et al., 2008). In contrast to the arrangement of auditory afferents in the CNIC, which appears adult-like at hearing onset, the organization of intrinsic CNIC circuits leading up to hearing onset has remained unclear. Intrinsic CNIC circuit refinement may be largely complete by hearing onset, or it may continue after hearing onset in an experience-dependent manner. Prior studies in rodents have shown that altering the patterning of sound-evoked activity during the first week of hearing with pulsed white noise exposure prevents the maturation of frequency selectivity in CNIC (Sanes and Constantine-Paton, 1983; Sanes and Constantine-Paton, 1985), and since afferent connections are largely mature at hearing onset, these developmental deficits may involve a rewiring of local CNIC circuits. However, it remains to be determined whether changes in the acoustic properties of auditory inputs during early hearing experience can lead to reorganizations of intrinsic CNIC circuits.

In Chapter 3, we describe a series of studies aimed at investigating the role of early hearing experience on the maturation of intrinsic CNIC circuits. In these studies, we exposed

mice to pulsed white noise during the first two weeks of hearing and mapped local connectivity to glutamatergic and GABAergic CNIC neurons using LSPS with caged glutamate.

1.7 PLASTICITY OF THE ADULT CNIC AFTER HEARING LOSS

In addition to playing a critical role in instructing the maturation of central auditory circuits during development, changes in hearing experience can also cause plastic changes in the adult auditory system. In the mature CNIC, experience-dependent plasticity has been most extensively studied after hearing loss, either involving complete deafening with cochlear ablation (McAlpine et al., 1997; Mossop et al., 2000; Vale and Sanes, 2002; Vale et al., 2004; Alvarado et al., 2005) or partial cochlear damage with acoustic trauma (Wang et al., 2002; Ma et al., 2006; Bauer et al., 2008; Dong et al., 2009; Mulders and Robertson, 2009; Dong et al., 2010, Wang et al., 2011; Niu et al., 2013). A number of these studies have linked hearing loss to changes in indices of GABAergic inhibitory neurotransmission in the CNIC, with the majority of studies reporting decreased global indices of GABA signaling (Bledsoe et al., 1995; Mossop et al., 2000; Milbrant et al., 2000; Dong et al., 2009, 2010; but see Bauer et al., 2000). In contrast, few studies have reported hearing loss-related changes in markers of excitatory neurotransmission in the IC (but see Suneja et al., 2000b).

Reductions in GABAergic neurotransmission after hearing loss are thought to underlie multiple changes in the response properties of IC neurons, perhaps by functionally "unmasking" CNIC connections that would otherwise remain inactive. For example, focal cochlear damage has been shown to increase evoked potential (EP) amplitudes in the CNIC at frequencies below the peak of cochlear damage (Salvi et al., 1992), a phenomenon that likely relates to the

recruitment of CNIC neurons. Consistent with this hypothesis, cochlear deafness has been shown to simultaneously decrease GABA release in the CNIC and to increase the number of Fos-immunoreactive CNIC cells activated by electrical stimulation of the cochlea (Nagase et al., 2000). Decreases in GABAergic neurotransmission in the CNIC may also contribute to multiple forms of noise-induced hyperactivity that can emerge in CNIC neurons after cochlear damage, including increased spontaneous firing rates (Ma et al., 2006; Bauer et al., 2008; Dong et al., 2009; Mulders and Robertson, 2009; Dong et al., 2010), Increased burst firing (Bauer et al., 2008; Wang et al., 2011), and increased signal gain (Wang et al., 2002; Niu et al., 2013). Hearing loss-related hyperactivity in the CNIC may initially be inherited from the CN, which can also become hyperactive after cochlear trauma (Brozoski et al., 2002; Mulders and Robertson, 2011; Vogler et al., 2011; Middleton et al, 2011; Manzoor et al., 2012 a/b; Li et al., 2013), and this inherited hyperactivity may be amplified by local decreases in GABAergic neurotransmission in the CNIC.

1.8 PLASTICITY OF THE CNIC IN TINNITUS

A host of studies have also linked hearing loss-induced changes in the CNIC with the perception of phantom sounds in tinnitus (Berger and Coomber, 2015). Hearing loss is the leading risk factor for tinnitus (Helfer et al., 2001; Yankaska et al., 2013), and similar patterns of hyperactivity in CNIC that develop after hearing loss have also been documented in both tinnitus patients and tinnitus animal models (Melcher et al., 2000; Wang et al., 2002; Ma et al., 2006; Bauer et al., 2008; Dong et al., 2009; Mulders and Robertson, 2009; Dong et al., 2010; Manzoor et al., 2012; Niu et al., 2013; Ropp et al., 2014; Berger and Coomber, 2015). Accordingly,

hearing loss-induced decreases in inhibitory neurotransmission in the CNIC may play an important role in the generation of tinnitus-related hyperactivity, similar to how reductions in synaptic inhibition in the DCN contribute to increased spontaneous firing rates in mice with behavioral evidence of tinnitus (Wang et al., 2009; Middleton et al., 2011; Pilati et al., 2012b). However, not all patients that suffer from hearing loss develop tinnitus, and it has remained unclear which (if any) hearing-loss related changes in the CNIC specifically contribute to tinnitus. Furthermore, clear evidence of whether hearing loss and/or the generation of tinnitus involve the reorganization of local synaptic circuits in the CNIC is still missing.

In Chapter 4, we describe a series of studies aimed at identifying hearing-loss-induced reorganizations of synaptic circuits that correlate with tinnitus. We applied LSPS with caged glutamate to map the organization and strength of intrinsic excitatory and inhibitory synaptic inputs onto glutamatergic and GABAergic neurons in the CNIC of noise-traumatized mice with and without behavioral evidence of tinnitus.

1.9 SUMMARY OF DISSERTATION RESEARCH

In this dissertation, we describe a series of studies aimed at elucidating the functional organization of intrinsic synaptic circuits in the central nucleus of the mouse inferior colliculus. We first investigate the development of excitatory and inhibitory synaptic networks in the CNIC during the first three weeks of postnatal development (Chapter 2). We then explore the activity-dependence of intrinsic circuit maturation in the CNIC, by manipulating the quality of early acoustic experience with pulsed white noise exposure, and measuring changes in the excitatory and inhibitory synaptic networks received by identified glutamatergic and GABAergic CNIC

neurons (Chapter 3). Finally, We investigate the effects of hearing loss on synaptic organization in the CNIC, and correlate specific patterns of local circuit rewiring with the emergence of behavioral evidence of tinnitus (Chapter 4). Taken together, the results of these studies highlight a remarkable level of functional plasticity in intrinsic microcircuits of the CNIC.

2.0 DEVELOPMENT OF INTRINSIC CONNECTIVITY IN THE CENTRAL NUCLEUS OF THE MOUSE INFERIOR COLLICULUS

2.1 INTRODUCTION

The inferior colliculus (IC) in the midbrain is the major subcortical auditory integration center. It receives ascending inputs from almost all auditory brainstem nuclei, descending inputs from the thalamus and cortex, and intracollicular projections from the contralateral inferior colliculus (Adams, 1979, 1980; Saldaña and Merchán, 1992; Saldaña et al., 1996; Winer et al., 1998; Malmierca, 2004; Malmierca et al., 2005). In the central nucleus of the IC (CNIC), afferent projections terminate in a tonotopic manner with ascending brainstem projections aligning to anatomically defined fibrodendritic laminae (Morest and Oliver, 1984; Oliver and Morest, 1984; Stiebler and Ehret, 1985; Malmierca et al., 1993; Gabriele et al., 2000a, 2007; Henkel et al., 2005; Miller et al., 2005; Henkel et al., 2007).

In addition to the wide array of ascending and descending projections, the CNIC also contains a dense network of local, intrinsic connections (Oliver et al., 1991; Saldaña and Merchán, 1992; Casseday et al., 2002; Fathke and Gabriele, 2009; Wallace et al., 2013). Local networks are thought to give rise to the majority of synapses in the IC (Saldaña and Merchán, 2005), suggesting that intrinsic connections significantly contribute to the response properties of IC neurons. However, while the organization and integration of extrinsic projections to the IC are

becoming increasingly well understood (Brunso-Bechtold et al., 1981; Maffi and Aitkin, 1987; Oliver, 1987, 2000; Faingold et al., 1993; Burger and Pollak, 2001; Malmierca et al., 2002, 2005; Henkel et al., 2005; Cant and Benson, 2008; Pollak et al., 2011), the anatomical and functional organization of intrinsic connections in the CNIC has remained largely obscure.

Intrinsic axons arise from disc-shaped (flat) as well as stellate (less flat) cells, the two major morphological cell types in the CNIC (Oliver and Morest, 1984; Meininger et al., 1986; Oliver et al., 1991; Malmierca et al., 1993; Wallace et al., 2012). Because both disc-shaped and stellate cells can be glutamatergic or GABAergic (Oliver et al., 1994; Ono et al., 2005), intrinsic connections likely are excitatory as well as inhibitory. Local axon collaterals from disc-shaped cells predominantly project along the same fibrodendritic laminae as the dendrites of their parent neurons (Oliver et al., 1991), and intralaminar local axons likely connect IC neurons that are tuned to similar sound frequencies but may reside in different functional zones (Brunso-Bechtold et al., 1981; Maffi and Aitkin, 1987; Shneiderman and Henkel, 1987; Oliver, 2005; Cant and Benson, 2006; Loftus et al., 2010). In contrast, local axons from stellate cells can spread significantly beyond a fibrodendritic laminae (Oliver et al., 1991), thus potentially connecting neurons that are tuned to different sound frequencies (Merzenich and Reid, 1974; Ehret and Romand, 1994; Schreiner and Langner, 1997; Malmierca et al., 2008).

The contribution of intrinsic connections to an IC neuron's response properties is poorly understood. Recent evidence indicates that intrinsic connections are activated at higher sound intensities than extrinsic inputs (Grimsley et al., 2013). The recruitment of intrinsic networks increases the dynamic range of IC neurons but has little effect on their frequency or intensity tuning. Activation of intrinsic networks at higher sound levels may also contribute to the intensity-dependent dynamic nature of the spectrotemporal receptive fields of IC neurons (Lesica

and Grothe, 2008).

To better understand the functional organization and the development of the intrinsic networks in the CNIC, we used laser-scanning photostimulation in brain slices from developing mice to characterize the strength and the spatial distribution of local excitatory and inhibitory inputs and their developmental refinement.

2.2 MATERIALS AND METHODS

2.2.1 Animals and slice preparation

Experimental procedures were performed in accordance with National Institutes of Health guidelines and were approved by the Institutional Animal Care and Use Committee at the University of Pittsburgh. Brain slices were prepared from neonatal CBA/CaJ mice of either sex (The Jackson Laboratory) that ranged in age from postnatal day 2 (P2) to P22. For brain slice preparation, animals were deeply anesthetized with isofluorane, decapitated, and their brains were immediately removed. Coronal midbrain slices (300 μm) were then prepared using a vibrating microtome. Cuts were in a ~30 degree angle in a dorsocaudal to ventrorostral direction. Consistency of this angle was verified using anatomical landmarks in the slice (IC slice contained fibers of the lateral lemniscus that entered the IC; slice contained ventral areas just rostral to the lateral superior olive). Slices were incubated for 30 min at 34°C in ACSF (composition in mM as follows: 1.3 $7H_2O$ ×$MgSO_4$, 124 NaCl, 5 KCl, 10 dextrose, 1.25 KH_2P0_4, 26 $NaHCO_3$, 2.0 CaCl) followed by 1–3 h incubation at 22°C-25°C (Kim and Kandler, 2003). The synaptic inputs of 89 neurons in the CNIC from 59 mice were mapped. These mice

were grouped into four age ranges: P2-P4 (11 animals, 19 neurons), P7-P9 (18 animals, 21 neurons), P13-P15 (23 animals, 29 neurons), and P19-P22 (7 animals, 20 neurons).

2.2.2 Electrophysiological recordings

Whole-cell recordings were aimed at the CNIC using the inferred demarcations of the lateral and dorsal cortices of the IC, which, in most cases, were visible in our slices. Although the CNIC was clearly recognizable within these defined borders at all ages, individual CNIC neurons cannot be unequivocally distinguished from neurons in the external cortices based on 2D dendritic morphology alone. Thus, to minimize the probability of incorrectly selecting neurons from outside the CNIC, slices that contained the caudal part of the IC (first slice containing the IC in our caudal to rostral series) or that contained the caudal part of the superior colliculus were excluded. Using this procedure, we only recorded from one slice per animal (the second 300 μm slice) and in which we only targeted neurons from within the center of the CNIC. Recordings were performed in a submersion-type chamber (3–4 ml/min perfusion with oxygenated ACSF at 22°C–25°C) mounted on an upright microscope (Zeiss AxioExaminer A1). Borosilicate glass pipettes (5–7 MΩ) were filled with a cesium-based internal solution containing (composition in mM as follows: 110 D-gluconic acid ($C_6H_{12}O_7$), 120 CsOH × H_2O, 11 EGTA, 1 $MgCl_2$ × $6H_2O$, 1 $CaCl_2$ × $2H_2O$, 10 HEPES, 0.3 GTP disodium salt, 2.0 ATP disodium salt, 5 QX314-Cl × H_2O and 0.5% biocytin, pH 7.2, 314 mOsm/L). Whole-cell currents in voltage-clamp mode were acquired with a Multiclamp 700B amplifier (Molecular Devices) and a Digidata-1440A A/D converter (Molecular Devices) at a sampling rate of 10 kHz using pClamp 10 software (Molecular Devices). Voltages were corrected for a junction potential of −13 mV. All pharmacological drugs were bath applied.

2.2.3 Synaptic input mapping

The spatial distribution of presynaptic inputs to CNIC neurons was determined using focal photolysis of *p*-hydroxyphenacyl-glutamate (0.1 mM, MNI glutamate, Tocris Bioscience). A custom-built system was used to guide the size, location, and duration of the UV light spot used to photolyze MNI-glutamate. A UV laser (DPSS Laser, 3510-30, 2 W) was used as a light source, and placement of the uncaging spot was steered with galvanometers (Cambridge Technology, 6210H). Uncaging position, electrophysiological data acquisition, and analysis were under the control of custom-written Labview-programs linked to pClamp software (written by Tuan Nguyen).

Input maps were only collected if cells had a holding current <100 pA and access resistance <50 mΩ. UV light pulses (355 nm) were delivered at 1 Hz in a random order. Light intensity was 2 mW (measured at slice position), light duration was 1 ms, and UV spot size on the slice was 20 μm. For mapping, 5 mM QX314 (Tocris Bioscience) was included in the internal solution to prevent spiking at positive holding potentials. An initial map of the entire IC was collected first with stimulation targets spaced 80 μm apart (Figure 1B). Responsive areas were then mapped at a finer resolution with stimulation sites spaced 40 μm apart (see Figure 2-1 B).

Excitatory and inhibitory synaptic responses were isolated by holding cells at −65 and 0 mV, respectively (Figure 2-1 C). For each condition, 3 input maps were obtained successively and the average map was used for analysis (Figure 2-1 D). To distinguish synaptic responses from direct stimulation of the recorded cell, input mapping was repeated in the presence of 1 μM TTX (Alomone Labs) (see Figure 2-1 D). In the few cases in which maps with TTX could not be obtained, responses elicited close to the recorded neuron were classified as synaptic if their onset

latency was >7 ms. In these cases, choosing this conservative value may miss short-latency synaptic responses arising from locations very close to the recorded cell. When input maps were obtained in the absence and presence of TTX, similar maps were obtained using either onset latencies or TTX sensitivity as criteria.

2.2.4 Excitability mapping

Excitability mapping experiments were performed with loose-seal patches (20–40 MΩ) using patch pipettes (5–10 MΩ) filled with ACSF. After forming a loose seal, UV light was delivered in a 20 μm grid (225 stimulation sites delivered at random locations) surrounding the recording. For each cell, three consecutive excitability maps were obtained, and the average number of spikes per stimulation site was used to create excitability maps.

2.2.5 Data analysis

Input map shape: Elliptical functions of best fit (least-squares fit, ImageJ, National Institutes of Health) were assigned to individual excitatory and inhibitory input maps. An "ellipticity factor" (ratio of minor axis, m; to major axis, M), was then calculated for each map (Figure 2-4 B). Ellipticity factor values that approach 1 describe input maps that were circular, whereas decreasing ellipticity factor values describe input maps that were increasingly elliptical. The angle of the long axis to the horizontal (lateral-to-medial) axis was determined with ImageJ software.

Synaptic input area: Synaptic input area was determined by subtracting the responsive uncaging area obtained in TTX (direct response area) from the total input map. To account for the

expansion of the IC size during development, synaptic input areas were normalized to the cross-sectional IC area for each age group (Figure 2-5 Bi–iii).

Synaptic input strength: Total excitatory and inhibitory synaptic strengths were calculated as the sums of the synaptic charge (pC) elicited from all stimulation sites at holding potentials of −65 and 0 mV, respectively.

2.2.6 Statistical analysis

Data are presented as mean ± SEM. Data were tested for normal distribution, and both unpaired *t* tests (two-tailed) and Mann–Whitney tests were used to determine statistical significance of differences between groups (GraphPad Prism). Statistical significance was set to $p < 0.05$.

2.3 RESULTS

2.3.1 Spatial mapping of local synaptic inputs to single CNIC neurons

To map the organization of intrinsic excitatory and inhibitory synaptic networks in the developing CNIC, we used whole-cell patch-clamp recordings with laser-scanning photostimulation. For each neuron, we first scanned the entire CNIC at a resolution of 80 μm to identify the overall layout of presynaptic sites. We then obtained finer-scale maps at a resolution of 40 μm from the regions that contained responsive stimulation sites (Figure 2-1 B). To distinguish between excitatory and inhibitory synaptic responses, maps were obtained while holding the membrane potential of the recorded neurons at −65 mV, the reversal potential for

chloride, to isolate excitatory responses, and at 0 mV, near the reversal potential of glutamatergic responses, to isolate inhibitory responses (Figure 2-1 C). Both excitatory and inhibitory input maps were highly reproducible in successive iterations and the average map from three iterations was used for all further analysis (Figure 2-1 D). Synaptically elicited responses were distinguished from responses to direct glutamate stimulation of the recorded cell (direct responses) by their onset latencies (>7 ms) (Figure 2-1 C) and their sensitivity to the voltage-gated sodium channel blocker TTX (1 μM) (Figure 1D). Areas from which direct responses were elicited were excluded from the analysis of input maps (Figure 2-1 D). Consistent with previous anatomical studies showing the absence of glycinergic neurons in the IC (Oliver et al., 1994; Ito et al., 2009), all inhibitory responses were abolished by the $GABA_A$-receptor antagonist gabazine (GBZ, 5 μM, n = 6 neurons, p = 0.001, Mann–Whitney test) (Figure 2-2 B). In contrast, GBZ had no effect on excitatory synaptic currents or on excitatory input maps (n = 6, p = 0.741, Mann–Whitney test) (Figure 2-2 A, C).

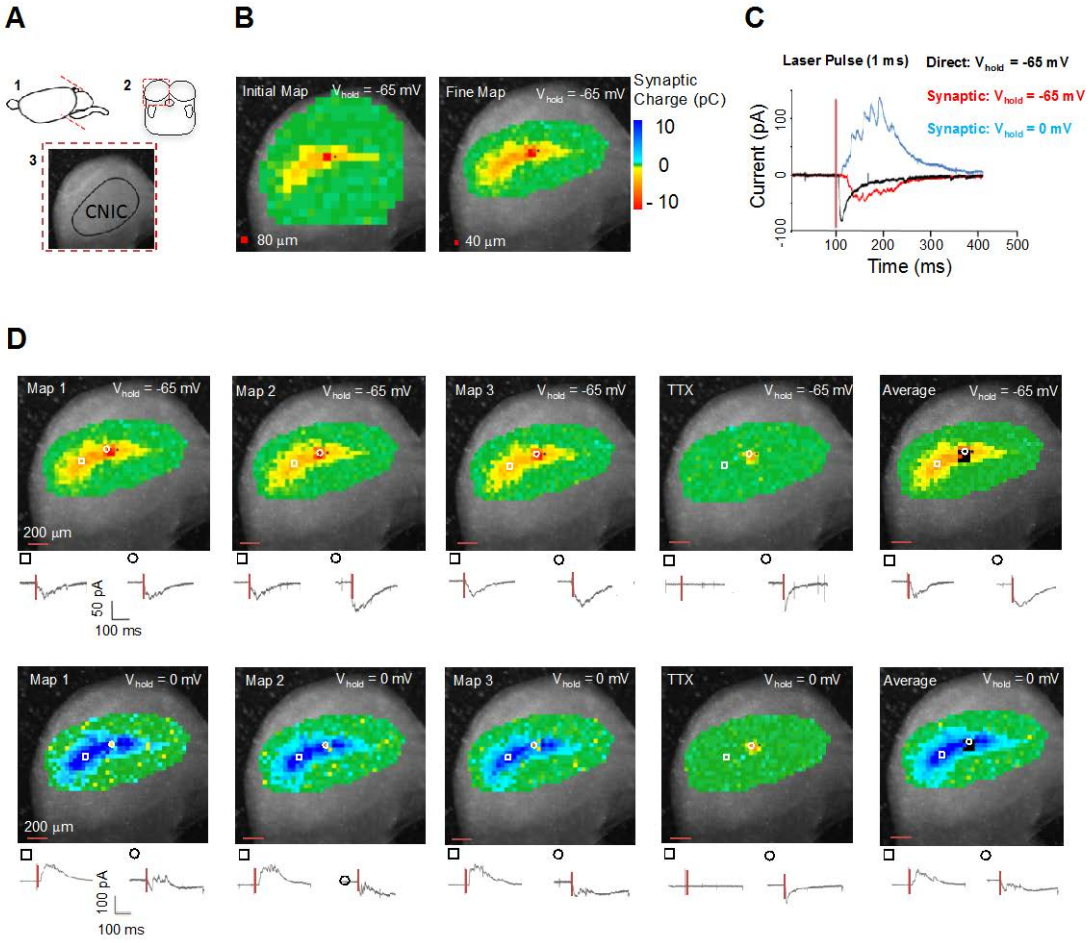

Figure 2-1. Mapping local inputs in the CNIC using laser-scanning photostimulation.

(**A**) Coronal brain slices (300 µm) containing the CNIC were prepared from P2–P15 mice. (**B**) An initial, low-resolution input map of the entire IC is first generated by spacing stimulation sites 80 µm apart. Responsive areas are then rescanned at a finer resolution with a stimulation site spacing of 40 µm. (**C**) Excitatory (red trace) and inhibitory (blue trace) synaptic inputs are distinguished by holding neurons at −65 and 0 mV, respectively. Direct activation of the recorded cell by uncaged glutamate elicits short latency, direct responses. (**D**) Example of three consecutively obtained excitatory (top row) and inhibitory (bottom row) synaptic input maps (P8). TTX (1 µM) abolishes synaptic responses but leaves direct responses intact. Example current traces of synaptic (square) and direct (circle) responses are shown for each map. Red lines indicate laser pulse. Maps 1–3 were used to created average input in which sites with direct responses are marked in black.

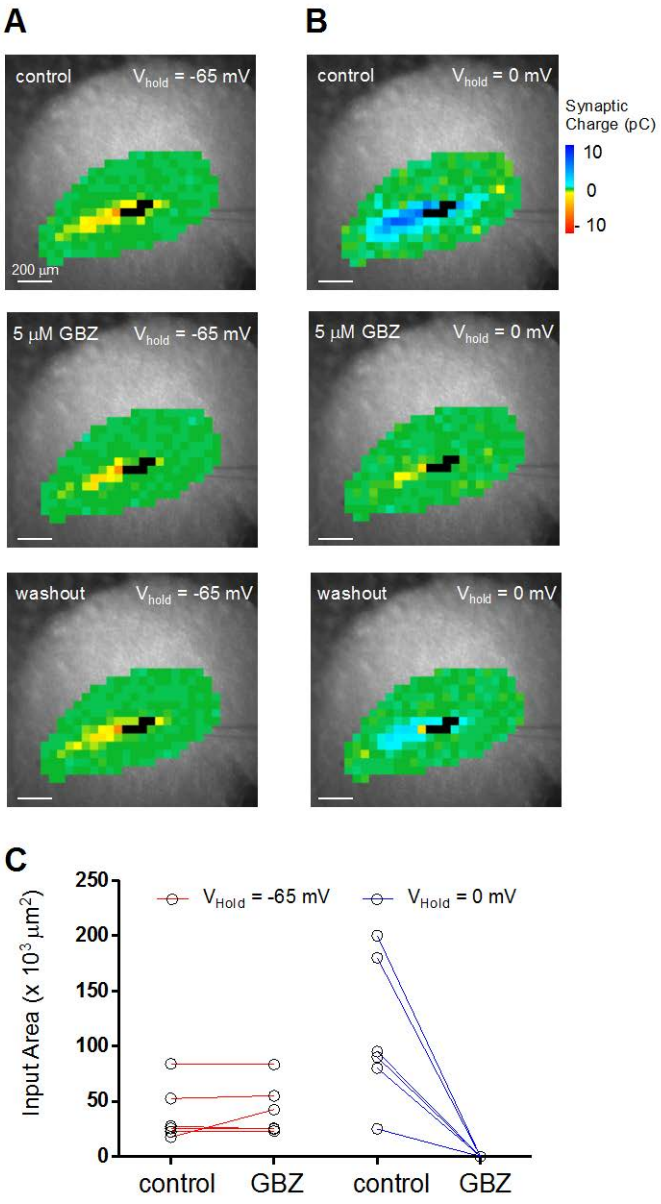

Figure 2-2. intracollicular inhibitory connections are mediated by GABA.

For a subset of neurons (n = 6), 5 µM GBZ was bath-applied during input mapping. (**A**) Excitatory synaptic input maps for a CNIC neuron (P8) before, during, and after washout of 5 µM GBZ. (**B**) Inhibitory synaptic input maps from the same neuron shown in **A**. Direct response areas are marked in black. (**C**) Size of excitatory (red) and inhibitory (blue) input areas from 6 neurons before (control) and after application of GBZ (+ GBZ). Inhibitory map size was calculated exclusively based on outward currents at 0 mV.

2.3.2 Input maps represent monosynaptic connections

Previous studies have shown that disinhibiting the IC favors the recruitment of polysynaptic circuits, leading to an increase in the duration of synaptic responses and response areas (Moore et al., 1998; Sivaramakrishnan and Oliver, 2006; Chandrasekaran et al., 2013). In our mapping experiments, GBZ did not change excitatory input maps (Figure 2-2 C), suggesting that our low-intensity uncaging conditions (0.1 mM caged glutamate and 2 mW of laser power) primarily activated monosynaptic connections, which are not affected by disinhibition. This assumption is further supported by the onset latencies of synaptic currents. First, there was no difference in the latencies of excitatory versus inhibitory responses (Figure 2-3 C, D), which, however, would be expected if a significant fraction of inhibitory responses were caused by the activation of disynaptic connections. Second, onset latencies increased smoothly with increasing stimulation distance at similar rates for excitatory (r^2 = 0.97, slope = 34.4 ms/mm) and inhibitory responses (r^2 = 0.926, slope = 36.4 ms/mm, $Slope_{Inhibitory}$ vs $Slope_{Excitatory}$, p = 0.209, ANCOVA) (Figure 2-3 B), and these rates were similar to those reported for uncaging-activated monosynaptic connections in the cochlear nucleus (Campagnola and Manis, 2014). Finally, if monosynaptic connections are strong enough to generate spikes in postsynaptic neurons, one would expect that neurons close to the recorded cell contribute to the excitability maps, resulting in excitability maps that are larger than direct response areas. This was not the case, however, as the average size of direct response areas (in the presence of TTX) was very similar to the area over which photostimulation generated spikes in cell-attached mode (without TTX, excitability area) (direct

response area = 20,890 ± 1643 μm^2, n = 68 cells; excitability area = 19,840 ± 5020 μm^2, n = 17 cells; direct vs excitability, p = 0.11, Mann–Whitney test). Thus, single stimuli do not elicit synaptically generated spikes in the recorded neuron, which means that unitary connections in the IC are weak, requiring the activity of several to many connections to elicit the postsynaptic neuron to spike. Together, these results suggest that the excitatory and inhibitory input maps obtained with our conditions primarily reflect monosynaptic connections.

2.3.3 Spatial organization of excitatory and inhibitory intrinsic inputs

At all ages examined, intrinsic input maps were elongated and oriented along the ventrolateral to dorsomedial direction, the presumed isofrequency contour of the CNIC (Willott and Shnerson, 1978; Romand and Ehret, 1985; Romand and Ehret, 1990). The angle of the isofrequency axis in the coronal plane of the mouse IC shortly after hearing onset is ~35°–55° (Romand and Ehret, 1990). In each of our age groups, the average orientation angles of both excitatory and inhibitory input maps (determined from the fitted ellipses) fell in that range (excitatory maps: P2-P4 = 43.8 ± 4.2°, n = 18; P7-P9 = 37.4 ± 3.0°, n = 20; P13-P15 = 53.1 ± 7.0°, n = 15; P19-P22 = 45.1 ± 11°, n = 9; inhibitory maps: P2-P4 = 38.1 ± 4.2°, n = 13; P7-P9 = 35.7 ± 3.0°, n = 20; P13-P15 = 47.1 ± 4.3°, n = 14; P19-P22 = 38.2 ± 10°, n = 9; excitatory vs. inhibitory, p = 0.577, Mann–Whitney test).

To quantify the shape of input maps, we fit input maps with an ellipse and calculated the "ellipticity factor" (EF, ratio of minor to major axis; referred to elsewhere as the "compressibility factor," see Maling, 1993) (Figure 2-4 B). At all ages, EFs for excitatory and as well as inhibitory input maps were 0.5, indicating that input maps were elongated, stretching twice as long along the isofrequency direction than along the tonotopic axis (Figure 2-4 C). The degree of

elongation changed during the first three postnatal weeks, such that excitatory maps became more elongated during the first postnatal week (excitatory, $EF_{P2\text{-}P4} = 0.53 \pm 0.14$, n = 18; $EF_{P7\text{-}P9} = 0.44 \pm 0.16$, n = 20; $p < 0.05$, Student's t test), reversed to a more circular shape during the second postnatal week ($EF_{P13\text{-}P15} = 0.58 \pm 0.20$, n = 17; $p < 0.001$, Student's t test), and then became more elongated again during the third postnatal week ($EF_{P19\text{-}P22} = 0.44 \pm 0.05$, n = 9; $p < 0.05$, Student's t test). Inhibitory maps underwent parallel changes during this period (inhibitory, $EF_{P2\text{-}P4} = 0.52 \pm 0.17$, n = 13; $EF_{P7\text{-}P9} = 0.39 \pm 0.09$, n = 20; $EF_{P13\text{-}P15} = 0.60 \pm 0.19$, n = 17; $EF_{P19\text{-}P22} = 0.45 \pm 0.05$, n = 10; P2-P4 vs P7-P9, $p < 0.05$, Student's t test; P7-P9 vs P13-P15, $p < 0.01$, Student's t test; P13-P15 vs P19-P22, $p < 0.05$, Student's t test) (Figure 2-4C). At each age group, excitatory input maps were clustered into two distinct populations, which differed in their EF values (P2-P4, $r^2 = 0.98$, sum of 2 Gaussian fits; P7-P9, $r^2 = 0.98$, sum of 2 Gaussian fits; P13-P15 $r^2 = 0.89$, sum of 2 Gaussian fits; P19-P22, $r^2 = 89$, sum of 2 Gaussian fits) (Figure 2-4 Di–iv). No separation into two populations was evident at any age for inhibitory input maps.

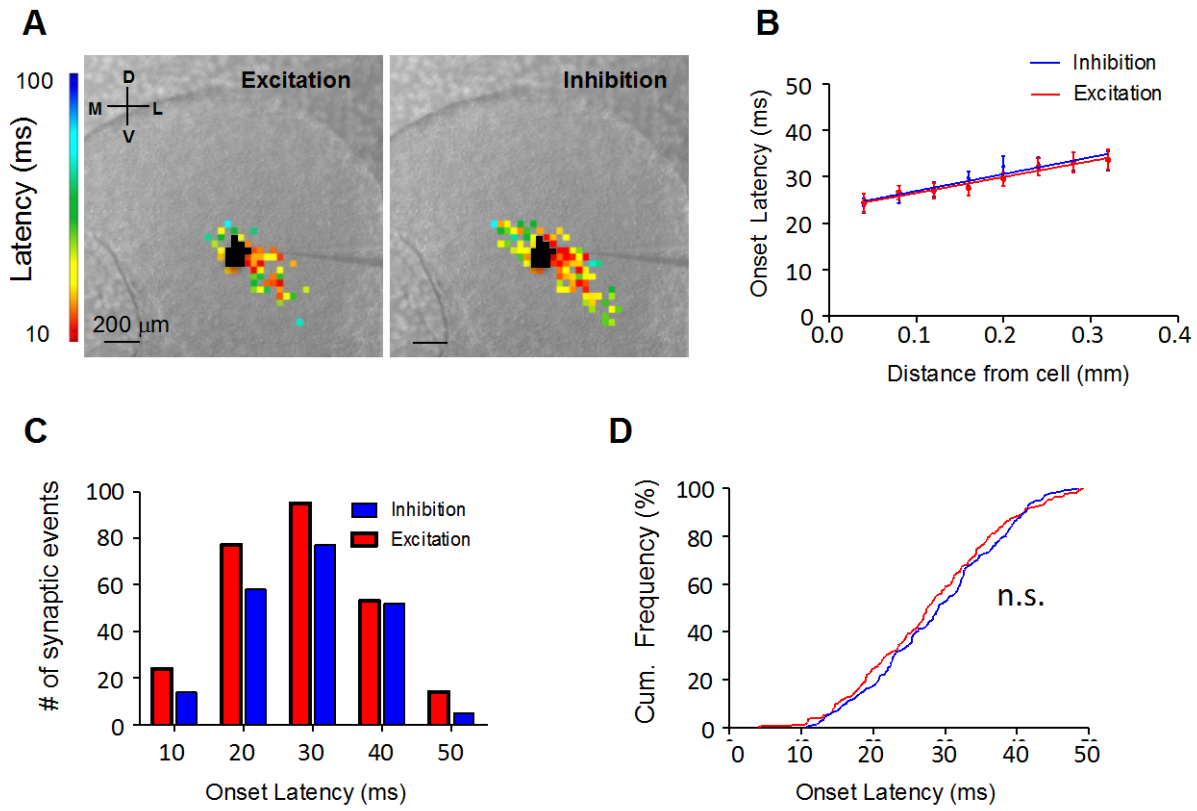

Figure 2-3. Synaptic response latencies are similar for excitatory and inhibitory responses.

(**A**) Example of excitatory and inhibitory synaptic input maps color-coded by onset latency (from a P8 mouse). Black squares represent stimulation sites that elicited direct responses. (**B**) Mean synaptic onset latencies plotted as a function of distance from the recorded cell. Lines are least-squares regression fits for excitation (red, $r^2 = 0.97$, slope = 34.4 ms/mm) and inhibition (blue, $r^2 = 0.926$, slope = 36.4 ms/mm). Error bars indicate SEM. (**C**) Frequency histogram of onset latencies of excitatory (red) and inhibitory (blue) synaptic responses (n = 5 cells). (**D**) Cumulative frequency distributions of excitatory (red line) and inhibitory (blue line) synaptic onset latencies (Kolmogorov–Smirnov, p = 0.192). n.s., Not significant.

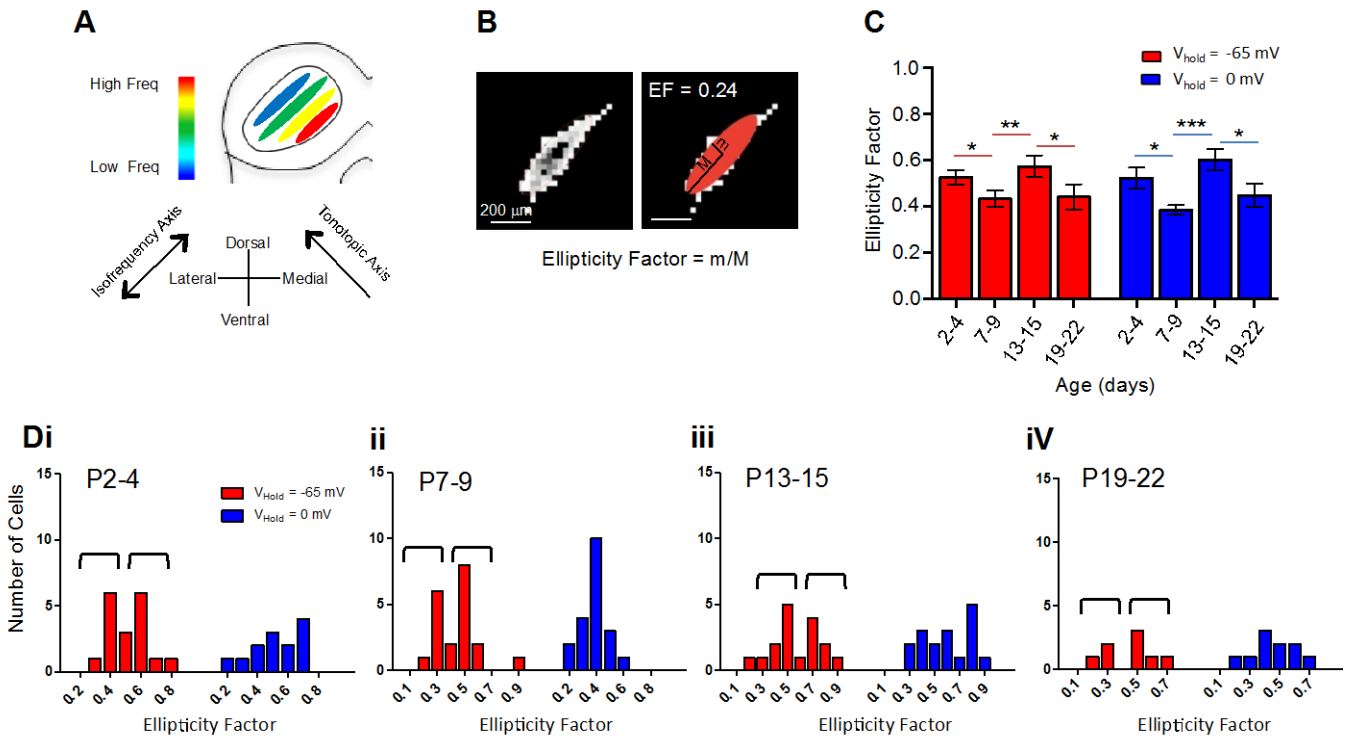

Figure 2-4. Excitatory and inhibitory synaptic input maps are oriented along the isofrequency axis.

(**A**) Schematic illustration of "isofrequency laminae" in the left CNIC. (**B**) Example of an excitatory synaptic input map (left) fitted with an elliptical function (filled red). (**C**) Developmental changes of ellipticity factors for excitatory (red) and inhibitory (blue) input maps. Error bars indicate SEM. *p < 0.05 (two-tailed t test). **p < 0.01 (two-tailed t test). ***p < 0.001 (two-tailed t test). (**D**) Histogram of ellipticity factors for excitatory (red) and inhibitory (blue) input maps at P2-P4 (**i**), P7-P9 (**ii**), P13-P15 (**iii**), and P19-P22 (**iv**). Black brackets represent distinct populations of excitatory input map shapes.

2.3.4 Developmental refinement of excitatory and inhibitory intrinsic input maps

The size of both excitatory and inhibitory input maps changed during development, expanding during the first postnatal week and retracting during the second and third weeks (Figure 2-5 A, Bi). To account for the growth of the IC during this period (Figure 5Bii), we normalized input areas to the cross-sectional areas of the IC (Figure 2-5 Biii). Between P2-P4 and P7-P9, the normalized size of excitatory and inhibitory input maps significantly increased (Figure 2-5 B, C). Excitatory maps increased by ~87% (from 0.14 to 0.26, n = 39; p = 0.01, Student's t test) and inhibitory input maps increased by 63.0% (0.17 to 0.28, n = 34; p = 0.01, Student's t test). This initial map growth was followed by a significant shrinkage of input maps during the second postnatal week. Between P7-P9 and P13-P15, excitatory input area decreased by ~70% (from 0.26 to 0.08, n = 49; $p < 0.001$, Student's t test), and inhibitory input area decreased by 55% (from 0.28 to 0.12, n = 46; $p < 0.001$, Student's t test) (Figure 2-5 B, C). In addition, although input maps were present in virtually all neurons before hearing onset, input maps were observed in only 69% of cells (20 of 29) immediately after hearing onset. Map refinement continued during the third postnatal week. Between P13-P15 and P19-P22, excitatory input area decreased by 70% (from 0.08 to 0.02, n = 36; $p < 0.01$, Mann–Whitney test), and inhibitory input area decreased by ~37%, but this decrease was not statistical significant (from 0.12 to 0.07, n = 36, p = 0.21, Student's t test) (Figure 2-5 B, C). Similar to the P13-P15 age range, input maps were observed in only 70% of cells between P19-P22 (14 of 20).

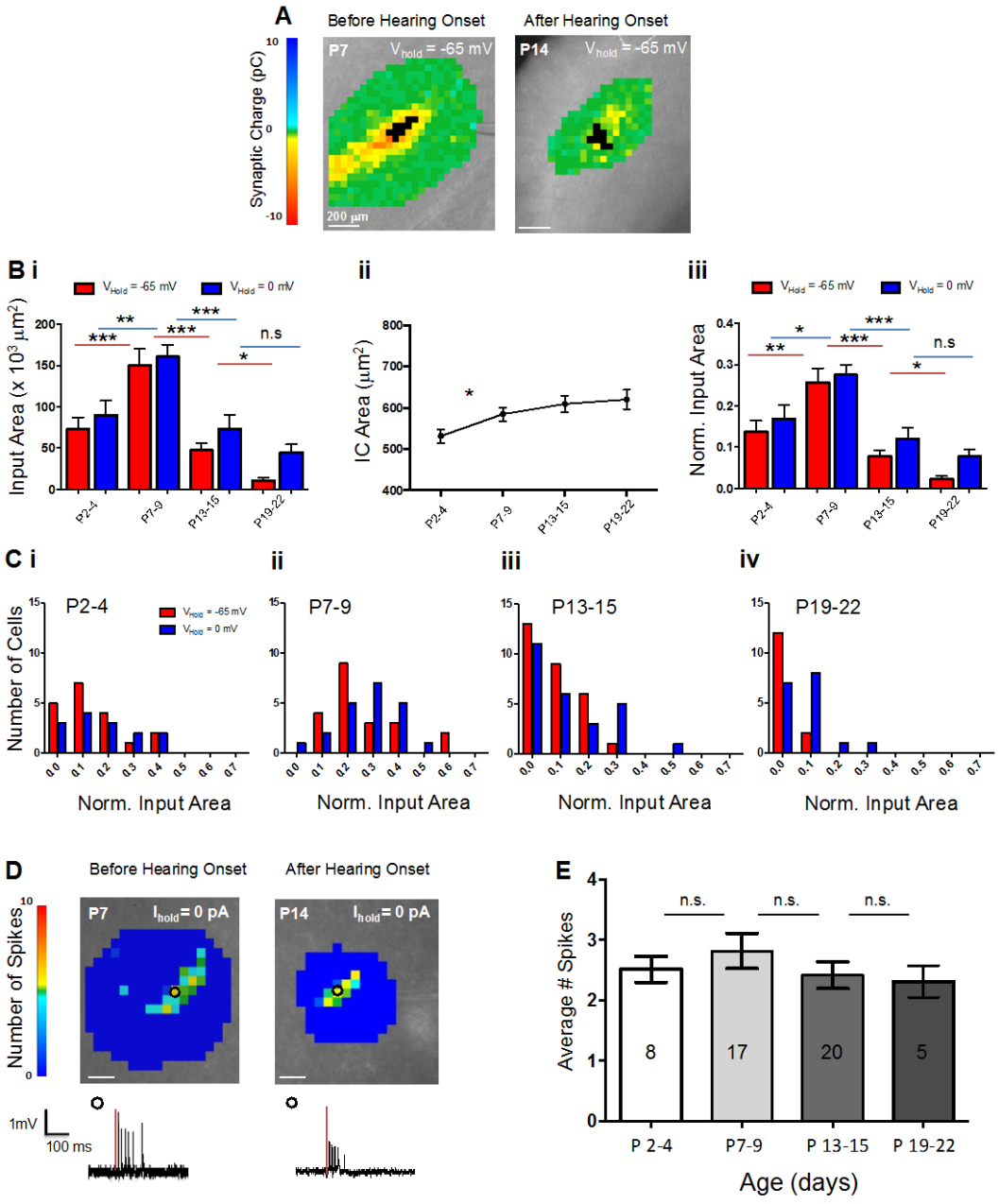

Figure 2-5. Developmental growth and refinement of local synaptic input maps.

Figure 2-5. Developmental growth and refinement of local synaptic input maps.

(A) Examples of synaptic input maps before (left) and after (right) hearing onset. (**B**) Age-dependent changes in the size of excitatory (red) and inhibitory (blue) synaptic input maps. (**Bi)** Absolute sizes of input maps at different ages. **Bii**, Developmental increase of cross-sectional area of IC. (**Biii**) Synaptic input areas normalized to the cross-sectional are of the CNIC for each age group. **C**, Distribution of excitatory and inhibitory synaptic input area sizes in each age group: P2-P4 (**i**), P7-P9 (**ii**), P13-P15 (**iii**), and P19-P22 (**iv**). **D**, Neuronal excitability to glutamate uncaging during cell-attached recordings. Black circles represent stimulus locations from which example traces were recorded. Red line indicates UV light pulse. **E**, The average number of spikes per stimulus was not significantly different between age groups. Numbers in bars indicate number of cells. Error bars indicate SEM. *$p < 0.05$ (two-tailed t test). **$p < 0.01$ (two-tailed t test). ***$p < 0.001$ (two-tailed t test). n.s, Not significant ($p > 0.05$).

To control for possible age-dependent changes in the effectiveness by which uncaged glutamate elicits action potentials in CNIC neurons, which could influence the size of input maps, we used cell-attached recordings to construct excitability maps (Figure 2-5 D). In all age groups, glutamate uncaging over the recorded cell elicited an average of 2–3 action potentials per stimulation (Figure 2-5 E). Thus, the changes in the sizes of input maps reflect the formation of new functional intrinsic connections during the first postnatal week followed by the silencing and/or elimination of connections during the end of the second postnatal week.

To determine whether the addition and elimination of synaptic inputs was biased toward either the isofrequency or the tonotopic axis, we quantified the amount of map changes along the ventrolateral (VL) to dorsomedial (DM) direction (isofrequency axis) and along the ventromedial (VM) to dorsolateral (DL) direction (tonotopic axis) (Figure 2-6 A, B). For the P13-P15 and P19-P22 age groups, this analysis was restricted to those neurons that received input maps exceeding 1% of the IC area (31 of 49 neurons). Between P2-P4 and P7-P9, excitatory as well as inhibitory input maps extended along the isofrequency axis, with similar magnitudes toward the VL (excitatory, $p < 0.001$, $n = 20$; inhibitory, $p < 0.01$, $n = 20$) and the DM directions (excitatory, $p < 0.05$, $n = 20$; inhibitory, $p < 0.05$, $n = 20$) (Figure 2-6 C). In contrast, neither the excitatory nor the inhibitory maps extended along the tonotopic axis (DL direction: excitatory, $p = 0.33$, $n = 20$; inhibitory, $p = 0.64$, $n = 20$: VM direction: excitatory, $p = 0.09$, $n = 20$; inhibitory, $p = 0.11$, $n = 20$).

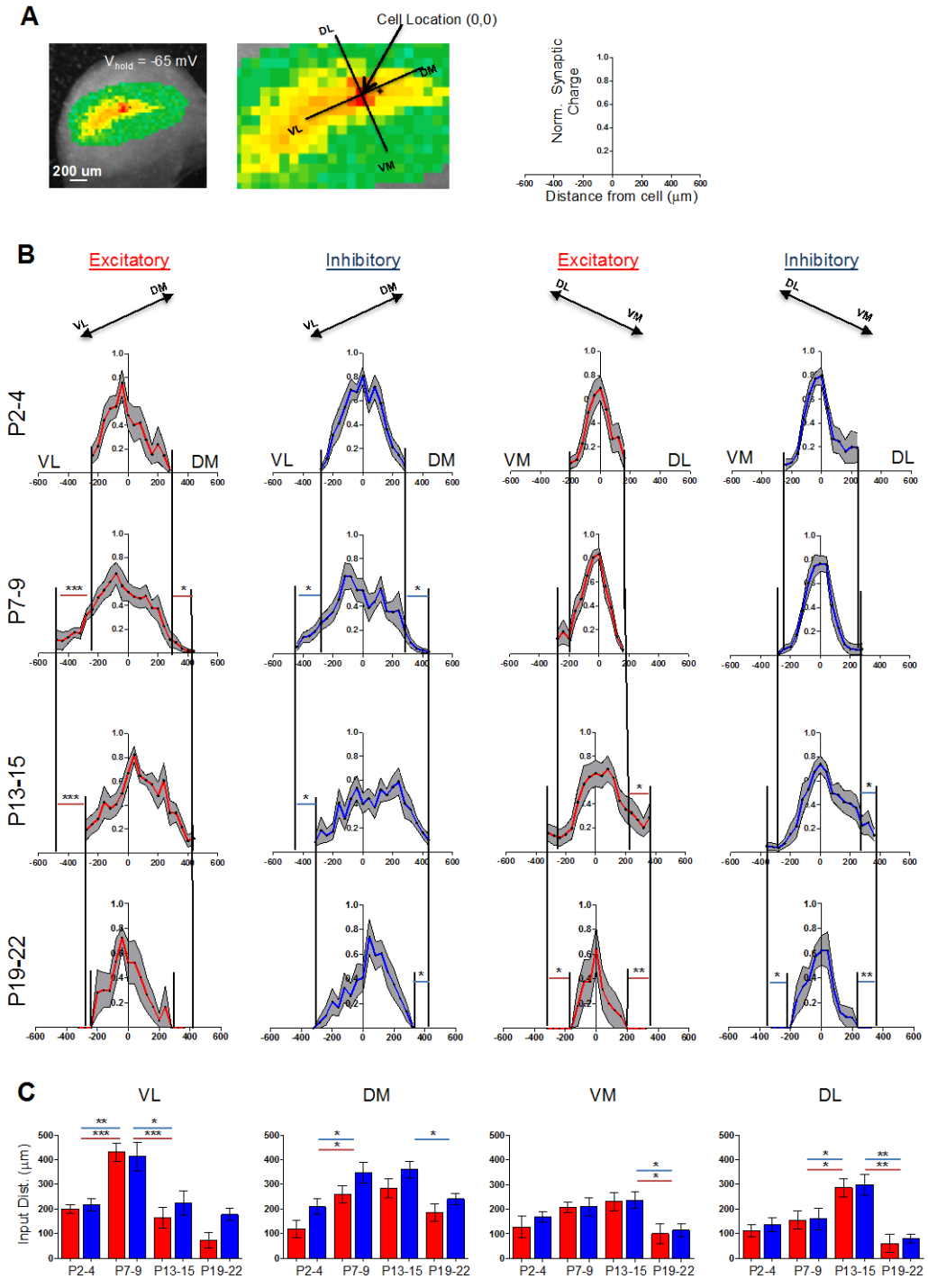

Figure 2-6. Refinement of input maps along the tonotopic and isofrequency axes.

Figure. 2-6. Refinement of input maps along the tonotopic and isofrequency axes.

(**A**) Illustration of analysis. Excitatory and inhibitory synaptic inputs were calculated along each of four axes, relative to the location of the recorded neuron (VL, VM, DL, and DM). Right, Average excitatory and inhibitory synaptic charges (normalized to the maximum excitatory and inhibitory responses for that cell, respectively) are plotted as a function of distance from the recorded cell. (**B**) Excitatory (red) and inhibitory (blue) synaptic charges as a function of distance to the cell body along each of the four axes. Gray shaded areas represent ± SEM. Black lines indicate maximum extent of connections for each age group. (**C)** Average extent of excitatory and inhibitory synaptic input maps along each axis. Error bars indicate SEM. *$p < 0.05$ (two-tailed t test). **$p < 0.01$ (two-tailed t test). ***$p < 0.001$ (two-tailed t test).

Between P7-P9 and P13-P15, both excitatory and inhibitory maps shrank along the isofrequency axis but expanded along the tonotopic axis. Along both axes, these changes were asymmetrical. Along the isofrequency axis, excitatory as well as inhibitory maps retracted exclusively along the VL direction (excitatory, $p < 0.001$, $n = 18$; inhibitory, $p < 0.05$, $n = 18$). Along the tonotopic axis, excitatory and inhibitory input areas expanded exclusively in the DL direction (excitatory, $p < 0.05$; $n = 18$; inhibitory, $p < 0.05$, $n = 18$) (Figure 2-6 C).

Between P13-P15 and P19-P22, both excitatory and inhibitory maps shrank along the tonotopic axis, in both the DL (excitatory, $p < 0.01$, $n = 20$; inhibitory, $p < 0.01$, $n = 20$) and VM (excitatory, $p < 0.05$, $n = 20$; inhibitory, $p < 0.05$, $n = 20$) directions (Figure 2- 6C). Very little refinement occurred along the isofrequency axis between P13-P15 and P19-P22, except that inhibitory maps shrank slightly along the DM direction ($p < 0.05$, $n = 20$, Student's t test) (Figure 2- 6C).

In summary, the sizes of excitatory and inhibitory synaptic input maps underwent two parallel alterations during the first two postnatal weeks. These changes were complex, yet spatially specific, and primarily involved a combination of growth and retraction along the isofrequency axis. During the first postnatal week, input maps expanded symmetrically along the isofrequency axis. During the second postnatal week, this growth was followed by a shrinkage of input maps that was restricted to the VL direction of the isofrequency axis, along which excitatory maps shrank relatively more than inhibitory maps. During the third postnatal week, map refinement was most dramatic and was primarily restricted to the VM and DL directions of the tonotopic axis resulting in excitatory maps that extended 80–320 μm (182 ± 100 μm, $n = 7$) and inhibitory maps that extended 160–360 μm (240 ± 83 μm, $n = 7$) along the tonotopic axis,

which are comparable with the width of a fibrodendritic lamina in the IC (Shneiderman and Henkel, 1987; Malmierca et al., 1993; Fathke and Gabriele, 2009; Wallace et al., 2013).

2.3.5 Relationship of excitatory and inhibitory input

To quantify the spatial relationship of excitatory and inhibitory intrinsic input maps in the developing CNIC, we first determined the spatial overlap of stimulation sites that elicited excitatory and inhibitory responses (Figure 2-7). Overall, the amount of overlap between excitatory and inhibitory input maps was substantial (Figure 2-7 C, D), and there was no systematic shift in the locations of excitatory and inhibitory inputs relative to each other. Approximately 70% of stimulation sites that elicited excitatory responses also elicited inhibitory responses (E:I sites), and this percentage did not change with age (Figure 2-7 C). In contrast, the percentage of inhibitory stimulation sites that also elicited excitatory responses (I:E sites) was age dependent (Figure 2-7 D). At P2-P4, only 45% of sites that elicited inhibitory responses also elicited excitatory responses (n = 15 cells), indicating a dominance of GABAergic over glutamatergic intrinsic connectivity. During the first postnatal week, the I:E fraction increased to 66% at P7-P9 ($p < 0.01$, Mann–Whitney test, n = 31), indicating a relative increase of glutamatergic inputs. From P7-P9 to P13-P15, the I:E fraction significantly decreased again to 47% ($p < 0.05$, Mann–Whitney test, n = 31), indicating a shift back toward more inhibition at the time of hearing onset (Figure 2-7 D). This shift toward inhibition became more pronounced from P13-P15 to P19-P22 and the I:E fraction decreased to 31% ($p < 0.05$, Mann–Whitney test, n = 30). The fact that the I:E fraction decreased from P7-P9 to P13-P15, and from P13-P15 to P19-P22, but the E:I fraction remained constant, indicates that the sizes of excitatory maps decreased more than the sizes of inhibitory maps after hearing onset.

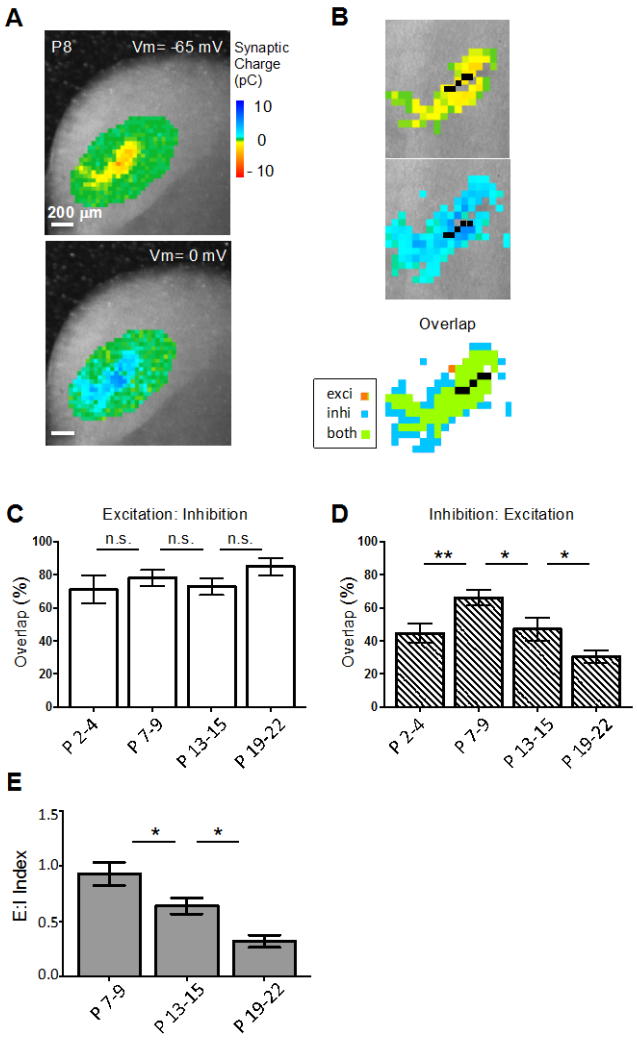

Figure 2-7. Spatial relationship of excitatory and inhibitory synaptic input maps.

(**A**) Example excitatory (top) and inhibitory (bottom) input maps from a CNIC neuron (P7). Direct response areas are in black. (**B**) Same input maps at higher resolution. Bottom, Superimposition of excitatory and inhibitory synaptic maps. (**C**) Percentage of excitatory stimulation sites that also give rise to inhibitory responses: P2-P4, n = 13; P7-P9, n = 18; P13-P15, n = 13; P19-P22, n = 12. (**D**) Percentage of inhibitory stimulation sites that also give rise to excitatory responses. Same neurons as in **C**. (**E**) Mean ratios of area of excitation to area of inhibition for individual neurons: P7-P9, n = 18; P13-P15, n = 13; P19-P22, n = 12. Error bars indicate SEM. *$p < 0.05$ (two-tailed Student's t test). **$p < 0.01$ (two-tailed Student's t test). n.s., Not significant (two-tailed Student's t test).

To quantify the magnitude of this difference, we calculated for each neuron the ratio of excitatory input area to inhibitory input area (E:I area index). Between P7-P9 and P13-P15, the mean E:I index decreased from 0.93 to 0.64, indicating that around the time of hearing onset, excitatory input area decreased by ~29%, relative to inhibitory input area ($p < 0.05$, Student's t test, $n = 31$) (Figure 2-7 E). Between P13-P15 and P19-P22, the mean E:I area index decreased from 0.64 to 0.32, indicating that, during the third postnatal week, excitatory input area decreased by ~32% relative to inhibitory area ($p < 0.05$, Student's t test, $n = 30$).

Although the size of an intrinsic input map illustrates the area in the CNIC from which neurons received synaptic inputs, it does not provide information about the amount of excitation or inhibition that IC neurons can receive from intrinsic sources. To address this question, we determined the total amount of excitation and inhibition received by each neuron by summing the synaptic charge from all stimulation sites. During the first postnatal week, the amount of synaptic excitation as well as inhibition dramatically increased, by approximately sixfold for excitation (from 34.8 pC to 209.8 pC, $n = 22$, $p < 0.01$) and fivefold for inhibition (from 78.9 pC to 385.6 pC, $n = 22$, $p < 0.01$) (Figure 2-8 A, B). Because the increase in the amounts of synaptic excitation and inhibition was similar, the mean E:I charge ratio remained unchanged (Figure 2-8 C). Between P7-P9 and P13-P15, the amount of excitation and inhibition decreased, but this decrease was not statistically significant (excitation, $p = 0.35$, Mann–Whitney test; inhibition, $p = 0.17$, Mann–Whitney test). However, the mean E:I ratio decreased by ~37%, from 0.61 to 0.38 ($p < 0.05$, Mann–Whitney test, $n = 31$) (Figure 2-8 C), indicating that total excitation decreased more than inhibition. Between P13-P15 and P19-P22, there was a dramatic decrease in the amount of excitation and inhibition, from 85.9 pC to 3.9 pC for excitation ($p < 0.05$, $n = 30$, Mann–Whitney test) and from 139.4 pC to 37.8 pC for inhibition ($p < 0.05$, $n = 30$, Mann–

Whitney test). The magnitude of the changes in total strength of inhibition and excitation matched the magnitude of changes we observed in the size of excitatory and inhibitory input maps (Figure 2-7 E).

The dominance of local inhibition that emerged around hearing onset could result from a relative increase in inhibitory input area and/or from an increase in the strength of inhibitory connections. To address this question, we analyzed the charge density of excitatory and inhibitory maps (Figure 2-8 D, E). During the first postnatal week, charge density significantly increased for both excitatory and inhibitory maps ($p < 0.01$, $n = 22$ cells, two-tailed t test), indicating a strengthening of intrinsic connections during this developmental period. An increase in excitatory and inhibitory charge density was also observed during the second postnatal week, although this increase was not statistically significant (excitatory, $p = 0.54$; inhibitory, $p = 0.42$). The increase in excitatory and inhibitory strength was similar and as a result, the E:I charge density ratio remained the same (Figure 2-8 F).

During the third postnatal week, however, charge density decreased for both excitatory ($p < 0.01$, $n = 30$, Student's t test) and inhibitory connections ($p < 0.01$, $n = 30$, Student's t test) (Figure 2-8 D, E). This decrease was slightly greater for excitatory charge density then for inhibitory charge density, but the difference was not large enough to lead to a change in the E:I charge density ratio (Figure 2-8 F). In summary, these results indicate a dominance of GABAergic inhibition during the first three postnatal weeks, which increased in magnitude after hearing onset (Figure 2-8 C) because of a relative increase in inhibitory input area compared with excitatory input area.

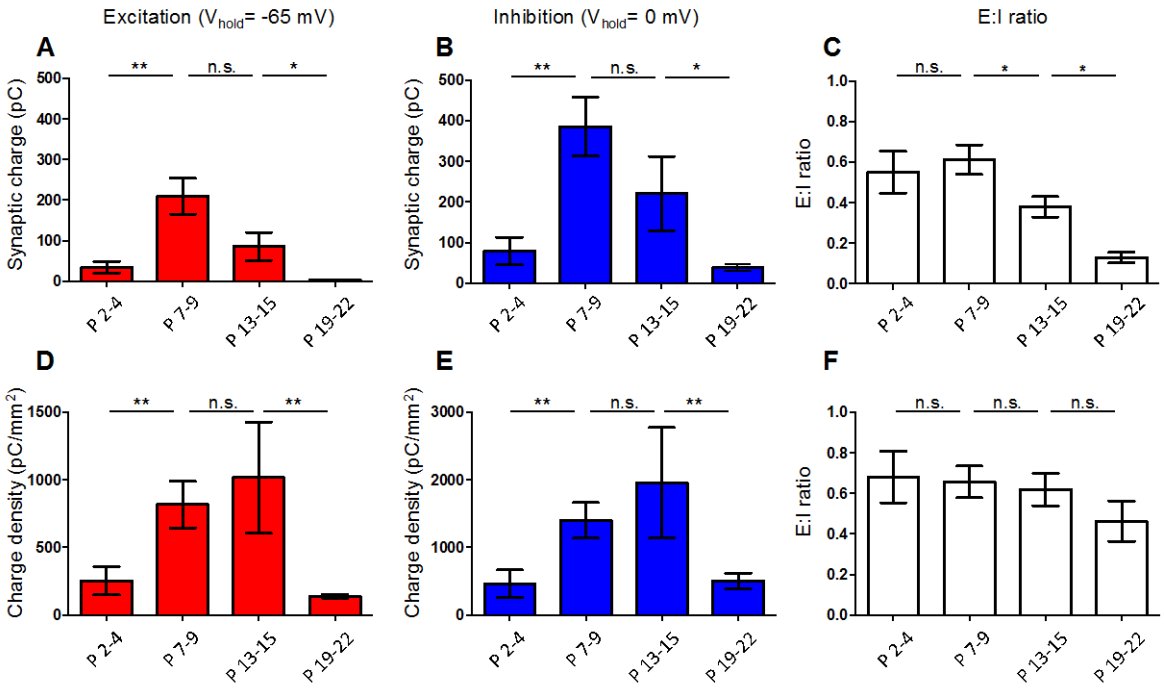

Figure 2-8. Development of the strength of intrinsic excitatory and inhibitory inputs.

(**A**) Developmental changes of mean total excitatory synaptic charge received by CNIC neurons (mean ± SEM; P2-P4, n = 9; P7-P9, n = 14; P13-P15, n = 10; P19-P22, n = 9). (**B**) Mean total inhibitory synaptic charge received by same neurons as in **A**. (**C**) Mean ratio of total excitatory and inhibitory synaptic charge per cell. (**D**) Developmental change of excitatory charge density (P2-P4, n = 8; P7-P9, n = 14; P13-P15, n = 9; P19-P22, n = 11). (**E**) Mean charge density of inhibitory maps (same neurons as in **D**). (**F**) Ratio of excitatory charge density to inhibitory charge density at different ages. Error bars indicate SEM. *p < 0.05 (two-tailed Student's t test). **p < 0.01 (two-tailed Student's t test). ***p < 0.001 (two-tailed Student's t test). n.s., Not significant (two-tailed Student's t test).

Although excitatory and inhibitory inputs maps overlapped considerably, on a microcircuitry level, these maps could be heterogeneous, and individual presynaptic sites within these maps might be dominated by either excitation or inhibition. To address this possibility, we compared the strength of excitatory and inhibitory responses for each individual stimulation site from which both responses could be elicited (Figure 2-9). In some neurons, the amplitudes of excitatory and inhibitory responses elicited from individual stimulation sites were highly correlated (linear correlation with slope approaching 1), whereas in other neurons, many stimulation sites gave rise to predominantly excitatory or inhibitory inputs (linear correlation with slope approaching 0) (Figure 2-9 B–F). In each age group, both the slopes and correlation coefficients were spread between 0 and 1. Negative correlations were rarely encountered, indicating that strong synaptic inputs of one type (either excitatory or inhibitory) were not systemically paired with weak inputs of the other type. Thus, the strengths of overlapping excitatory and inhibitory inputs were more likely to be balanced than antagonistic. Interestingly, in the neurons in which we observed a low correlation of excitatory and inhibitory response amplitudes, either excitation- or inhibition-dominated stimulation sites tended to cluster together (Figure 2-9 F), suggesting that these neurons receive spatially restricted “subclusters” of inputs that are predominately excitatory or inhibitory.

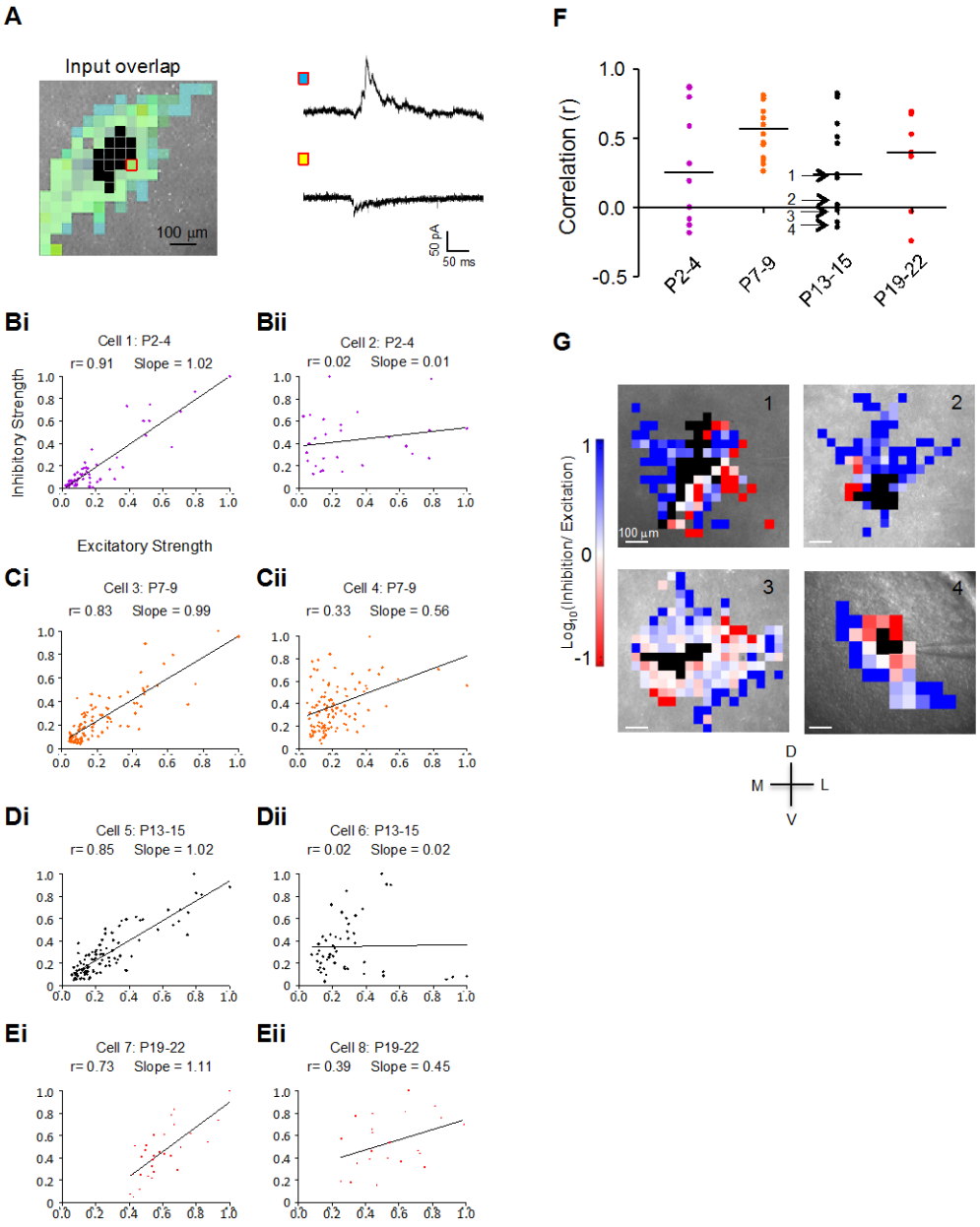

Figure 2-9. Relative synaptic strength of excitatory and inhibitory responses emanating from individual stimulation sites.

Figure 2-9. Relative synaptic strength of excitatory and inhibitory responses emanating from individual stimulation sites.

(A) Example of superimposed excitatory and inhibitory inputs. Red box represents stimulation site that elicited the isolated excitatory and inhibitory responses shown to the right (blue represents inhibitory; yellow represents excitatory). Black boxes represent stimulation sites that elicited direct responses. (**B–E**) Excitatory versus inhibitory synaptic charge from corresponding stimulation sites, normalized to the peak charge. Two example neurons from each age group are shown (**i**, **ii**). Each data point represents a single stimulation site. Lines indicate least-squares linear regressions and Pearson correlation coefficients (r). (**F**) Population of correlation coefficients. Horizontal black lines indicate median. (**G**) Input maps from four cells around hearing onset with r values ∼0 (marked by arrows in **E**). Stimulation sites dominated by inhibition or excitation are clumped together, but the pattern varies highly between cells.

2.4 DISCUSSION

2.4.1 Summary of findings

In this study, we used laser-scanning photostimulation with caged glutamate to provide the first characterization of functional intrinsic connectivity in the central nucleus of the inferior colliculus. Our results demonstrate that, already at P2, the CNIC contains an extensive excitatory and inhibitory intrinsic network. Excitatory and inhibitory inputs were spatially organized, forming continuous maps that largely overlapped with each other and that were aligned with the presumed isofrequency axis. This characteristic organization persisted throughout the first two postnatal weeks of development. However, the size of input maps was developmentally regulated undergoing an expansion during the first postnatal week that was followed by a significant shrinkage that began around the onset of hearing. These changes occurred in parallel for excitatory and inhibitory input maps, although the elimination of intrinsic connections was greater for excitatory than for inhibitory connections, resulting in a predominance of intrinsic inhibition at the end of the third postnatal week.

2.4.2 Technical considerations

An issue to consider when using photostimulation to map the organization of synaptic inputs is whether input maps represent monosynaptic or polysynaptic inputs. In our experiments, we aimed to stimulate monosynaptic inputs by using low concentrations of caged-glutamate (0.1 mM), low laser power (2 mW), and short laser pulse durations (1 ms). Our stimulation conditions

were of significantly lower intensity than those used in other uncaging studies that activated monosynaptic connections in the auditory cortex and brainstem (Noh et al., 2010; Oviedo et al., 2010; Hirtz et al., 2012; Campagnola and Manis, 2014) but still yielded reliable input maps in the IC. Several lines of evidence argue in favor that our conditions primarily activated monosynaptic connections. First, disinhibiting the IC by blocking $GABA_A$ receptors, a condition that allows the recruitment of polysynaptic circuits (Sivaramakrishnan and Oliver, 2006; Chandrasekaran et al., 2013), did not affect excitatory input maps (Figure 2-2). Second, the onset latencies of excitatory and inhibitory responses were indistinguishable (Figure 2-3 C, D), and both increased with distance from the recorded cell at similar rates of ~34 ms/mm (Figure 2-3 B). These rates are comparable with the rates reported for monosynaptic connections in the AVCN of adolescent mice recorded at slightly higher temperatures (Campagnola and Manis, 2014). Third, the average size of spike-eliciting areas obtained with cell-attached recordings was indistinguishable from the average size of direct stimulation areas obtained with whole-cell recordings in the presence of TTX (~400 μm^2), which blocks spike-elicited synaptic transmission. This indicates that presynaptic neurons activated under our photostimulation conditions do not elicit postsynaptic spikes that are necessary for polysynaptic transmission. Together, these results indicate that our input maps predominantly reflect the spatial organization of monosynaptic connections.

2.4.3 Organization of intrinsic synaptic input maps

Our studies demonstrate that functional, intrinsic input maps in the developing CNIC exhibit a laminar organization that closely follows the curvature of isofrequency contours in the CNIC (Ehret and Romand, 1994), thereby connecting neurons with similar best frequencies. This is

consistent with previous anatomical (Oliver et al., 1991; Saldaña and Merchán, 1992; Malmierca et al., 1993, Miller et al., 2005; Wallace et al., 2012) and physiological (Grimsley et al., 2013) studies. Our results also revealed that this organization applies to both excitatory and inhibitory intrinsic circuits. The typical laminar organization was a consistent feature of all neurons that we recorded, despite the fact that our sample likely included many of the anatomically and physiologically distinct cell types that are present in the IC (Oliver and Morest, 1984; Peruzzi et al., 2000; Sivaramakrishnan and Oliver, 2001; Tan et al., 2007). Therefore, a laminar organization appears to be a fundamental feature of intrinsic connectivity that is shared by a wide variety of cell types in the IC.

Along the isofrequency domain, intrinsic input maps were continuous (e.g., not "patchy"), and the strength of both excitatory and inhibitory inputs diminished smoothly with increasing distance from the recorded neuron (Figure 2-6). Thus, intrinsic connections can link different "functional zones," which share a common spectral tuning but receive different ascending (Aitkin and Schuck, 1985; Maffi and Aitkin, 1987; Shneiderman and Henkel, 1987; Oliver et al., 1997; Loftus et al., 2004; Malmierca et al., 2005; Cant and Benson, 2006) and/or descending inputs (Bajo and Moore, 2005). IC neurons in different functional zones exhibit distinct binaural response properties and periodicity preferences (Wenstrup et al., 1986; Schreiner and Langner, 1988; Loftus et al., 2010), and the integration of these elements by intrinsic IC circuits may facilitate the processing of complex acoustic features, such as tempo and rhythm (Bregman et al., 1985).

Along the tonotopic axis, excitatory and inhibitory input maps extended between 400 μm (P2-P4) and 600 μm (Figure 2-5) at hearing onset. This indicates that, at this age, input maps likely span 2–6 frequency bands, or fibrodendritic lamina, each of which is ~100–200 μm wide

(Shneiderman and Henkel, 1987; Malmierca et al., 1993; Fathke and Gabriele, 2009; Wallace et al., 2013). Wide input maps connecting several frequency bands may contribute to the immature frequency filters that are present at this age (Yu et al., 2005). Since the organization of ascending inputs to the IC is mature at hearing onset (Gabriele et al., 2000a, 2007; Henkel et al., 2007), the maturation of frequency filters that occurs after hearing onset (Ehret and Romand, 1994; Yu et al., 2005) may reflect the refinement of intrinsic IC maps that also occurs after hearing onset (Figures 2-5 and 2-6).

Although in 3-week-old animals the average tonotopic width of intrinsic maps corresponded to the width of fibrodendritic laminae, ~30%–40% of maps (6 of 14) extended significantly >200 μm along the tonotopic axis (up to 400 μm), thus connecting 2–3 frequency bands. These tonotopically wide maps across could contribute to the broad tuning of subthreshold synaptic inputs (Xie et al., 2007) that exists despite the strict tonotopic termination patterns of extrinsic inputs (Oliver, 2000; Malmierca et al., 2005; Cant and Benson, 2006). It could also provide a neuronal substrate for the spectral integration of complex sounds seen, for example, in “combination-sensitive” neurons (Portfors and Felix, 2005). In mice, >30% of IC neurons are combination-sensitive and exhibit either combination-sensitive facilitation or inhibition, where a neuron's response to a particular sound frequency is either increased (facilitation) or decreased (inhibition) by the presence of a second sound that is separated by at least an octave (~3 frequency bands) (Portfors and Felix, 2005). Combination-sensitive facilitation and inhibition are important for creating selective responses to species-specific sounds in the IC (Klug et al., 2002), and the organization of intrinsic CNIC circuits is suitable to contribute to the generation of these responses. Because intrinsic circuits are preferentially engaged at higher sound intensities (Grimsley et al., 2013), intensity-dependent recruitment of

excitatory and inhibitory intrinsic inputs from other fibrodendritic lamina may underlie the generation of the complex spectrotemporal receptive fields of CNIC neurons observed at higher sound intensities (Lesica and Grothe, 2008).

2.4.4 Intrinsic excitation: inhibition balance

Intrinsic excitatory and inhibitory synaptic input maps overlapped considerably during the first 3 postnatal weeks. However, after hearing onset, overlapping intrinsic excitatory and inhibitory inputs may be differentially engaged by different acoustic stimuli. For example, frequency response bandwidths in the IC broaden with increasing sound intensity (Egorova et al., 2001; Egorova and Ehret, 2008); and because extrinsic excitatory and inhibitory inputs to the CNIC saturate at higher sound levels (Grimsley et al., 2013), this broadening of tuning may be partly mediated by the recruitment of intrinsic excitatory circuits.

Although most presynaptic sites gave rise to both excitatory and inhibitory inputs, the correlation of the strength of excitation and inhibition arising from individual presynaptic sites varied widely between neurons (Figure 2-9). At each age, we found neurons in which the strength of excitation and inhibition was remarkably correlated, suggesting that the strength of both inputs was adjusted in a coordinated manner. In other neurons, however, the correlation was basically absent, suggesting that, in these neurons, the strength of excitatory and inhibitory inputs is adjusted independently from each other (Figure 2-9). Interestingly, in these neurons, stimulation sites that were dominated by either excitation or inhibition clustered together, giving rise to subinput maps, the organization of which varied considerably between neurons (Figure 2-9). This heterogeneity on the microcircuit level adds to the large degree of heterogeneity of IC

neurons observed in other studies (Peruzzi et al., 2000; Sivaramakrishnan and Oliver, 2001; Tan et al., 2007, Xie et al., 2007) and supports the idea that intrinsic excitatory and inhibitory microcircuits contribute to the generation of response preferences for specific frequency-temporal patterns of sound stimuli in individual IC neurons.

2.4.5 Developmental changes in intrinsic circuitry during the first 3 postnatal weeks

During the first postnatal week, both excitatory and inhibitory intrinsic synaptic input maps expanded along the isofrequency laminae (Figures 2-5 and 2-6), and this expansion was accompanied by synaptic strengthening (Figure 2-8 D, E). During the same period, afferent projections from the DNLL segregate from a uniform to a banded termination pattern (Gabriele et al., 2000a; Henkel et al., 2005). This suggests that, during the first postnatal week, the development and refinement of extrinsic and intrinsic synaptic inputs in the CNIC are independently regulated. However, during the second postnatal week, when extrinsic inputs from the DNLL to the CNIC undergo refinement along the isofrequency domain, intrinsic input maps exhibited refinement along this domain as well. The prehearing refinement of these afferent projections to the CNIC requires cochlear-driven spontaneous activity (Gabriele et al., 2000b), and it remains to be determined whether similar mechanisms are necessary for the refinement of intrinsic input maps.

Although refinement of intrinsic input maps involved both excitatory and inhibitory connections, excitatory input maps shrank more than inhibitory input maps, such after 1 week of hearing a layer of inhibitory inputs surrounded excitatory input maps. The emergence of this surrounding inhibition may relate to the emergence of the inhibitory sidebands, which have been

described in the IC of adult animals (Wang et al., 2002; Fuzessery et al., 2006). After hearing onset, map refinement was most dramatic and most pronounced for excitatory input along the tonotopic axis. The correlation of this refinement with hearing onset may indicate that tonotopic sharpening of excitatory intrinsic IC maps is triggered or guided by early auditory experience.

3.0 NOISE REARING INDUCES LOCAL CIRCUIT REORGANIZATION IN THE AUDITORY MIDBRAIN DURING A CRITICAL PERIOD

3.1 INTRODUCTION

The functional maturation of the auditory system is an activity-dependent process that is instructed by a combination of spontaneously generated and acoustically driven patterns of neuronal firing. Prior to hearing onset, which occurs during embryonic week 24 in humans (Ruben, 1991) and around postnatal day 12 (P12) in rodents (Rubel, 1984), auditory nerve afferents exhibit spontaneous, burst-like discharges (Jones et al., 2007), the precise patterning of which is critical for tonotopic map refinement in the auditory brainstem (Clause et al., 2014). After hearing onset, the patterning of auditory nerve discharges becomes increasingly driven by the spectral and temporal structures of auditory inputs, and changes in the acoustic properties of these inputs during the initial weeks of hearing experience can have profound, long-lasting effects on the emergence of acoustic feature selectivity (Zhang et al., 2001; Zhang et al., 2002; Chang and Merzenich, 2003; Chang et al., 2005; Razak et al., 2008; de Villers-Sidani et al., 2008; Zhou et al., 2008; Grecova et al., 2009; Insanally et al., 2010; Oliver et al., 2011; Bures et al., 2014). In rodents, for example, synchronous activation of auditory nerve afferents with pulsed noise during early hearing experience prevents the maturation of tonotopic maps in primary auditory cortex (A1) (Zhang et al., 2002; Insanally et al., 2010), as well as the

refinement of frequency selectivity in both A1 (Zhang et al., 2002; Insanally et al., 2010) and the inferior colliculus (IC) (Sanes and Constantine-Paton, 1983; Sanes and Constantine-Paton, 1985).

Disruptions in the functional development of the auditory system by noise rearing may relate to a lack of refinement and/or a re-wiring of local synaptic networks. Previous studies in the rodent sound localization system have shown that early omnidirectional noise exposure (Magnusson et al., 2005; Werthat et al., 2008) can disrupt both structural and functional refinement of the inhibitory projection from the medial nucleus of the trapezoid body (MNTB) to the medial superior olive (MSO) (Krapfer et al., 2002), which is responsible for detecting inter-aural time differences (ITD). In these studies, noise-reared animals exhibited impaired ITD selectivity in neurons of the dorsal lateral lemniscus (DLL), a major postsynaptic target of the MSO, whereas adult animals exposed to identical noise exhibited normal ITD tuning (Seidl and Grothe, 2005). Additionally, noise-reared animals exhibited impaired performance in a forced-choice behavioral paradigm that relies upon ITD sensitivity (Maier et al., 2008). Together, these findings suggest that noise-rearing-induced disruptions in synaptic refinement occurring during an early critical period can have significant consequences for hearing performance.

In this study, we investigated the effect of pulsed noise rearing on the organization of local synaptic circuits in the central nucleus of the mouse inferior colliculus (CNIC). The CNIC is the major subcortical integration center in the mammalian brain, receiving ascending inputs from almost all auditory brainstem nuclei (Adams et al., 1979; Malmierca et al., 2005), commissural inputs from the contralateral IC (Saldaña et al., 1992), and descending inputs from the auditory cortex (Saldaña et al., 1996; Gao and Suga, 1998; Bajo and King, 2013). In addition to these extrinsic inputs, the IC also contains an extensive network of intrinsic connections,

which are thought to encompass the majority of IC synapses (Saldaña and Merchán, 2005) and to provide gain control (Grimsley et al, 2013). After hearing onset, both excitatory and inhibitory intrinsic circuits in the CNIC undergo substantial refinement, involving a functional elimination of both excitatory and inhibitory inputs (Chapter 2; Sturm et al., 2014). However, it has remained unknown whether and to what degree the maturation of intrinsic CNIC circuits is shaped by hearing experience.

Here we addressed this question by mapping local connectivity to glutamatergic and GABAergic neurons in the CNIC of mice using laser-scanning photostimulation (LSPS) with caged glutamate, and comparing CNIC circuit connectivity between noise-reared and age-matched control mice. We found that pulsed noise exposure from P12-25 leads to a profound, cell-specific rewiring of glutamatergic and GABAergic IC circuits. In GABAergic IC neurons, noise rearing leads to increases in both excitatory and inhibitory input map areas, as well to a strengthening of excitatory, but not inhibitory synaptic inputs. This leads to a shift in excitation: inhibition balance in favor of excitation. In glutamatergic IC neurons, on the other hand, noise rearing leads to a shrinkage of excitatory input map areas, without changing the size of inhibitory input maps. However, the strengths of inhibitory inputs are weakened relative to closely apposed excitatory inputs, which again leads to a shift in excitation: inhibition balance in favor of excitation. Finally, the effects of noise exposure on GABAergic and glutamatergic IC neurons were absent in mice exposed to pulsed noise rom P19-25, indicating that noise rearing disrupts intrinsic connectivity in the IC during a critical period within the first week of hearing experience.

3.2 MATERIALS AND METHODS

3.2.1 Experimental animals

All experimental procedures were carried out in accordance with US National Institutes of Health (NIH) guidelines and were approved by the Institutional Animal Care and Use Committee (IACUC) at the University of Pittsburgh. Vgat-ires-cre, and dT-loxP mice were purchased from Jackson Labs (Jackson). Vglut2-cre mice were the generous gift of Dr. Rebecca Seal's laboratory. The background strain of all mice was C57BL/6J. In our laboratory, vglut2-cre and vgat-ires-cre mice were crossed with dT-loxP mice to generate vglut2-cre-dT-loxP and vgat-ires-cre-dT-loxP strains.

3.2.2 Pulsed noise exposure

Mice of either sex [postnatal day (P) 11] were assigned to one of three groups: 1) noise-reared P12-25, 2) noise-reared P19-25 or 3) control. Mice in each exposure group were kept together in their original breeding cages with their mother (all mice in a given cage were assigned to the same group). For noise rearing, pulsed white noise (75 dB SPL) was delivered in a sound-attenuating chamber (Coulbourn Instruments) as previously described (Clause et al., 2014). Pulse length was set to 138ms, and pseudorandomly presented with an inter-pulse length of 0-450ms and a duty cycle of 47%.

3.2.3 Slice preparation

Coronal slices were prepared from vglut2-cre-dT and vgat-ires-cre-dT mice of either sex aged 26-30 days. For brain slice preparation, animals were deeply anaesthetized with isoflurane, decapitated, and their brains were immediately removed. Coronal midbrain slices (300 μm) were then prepared using a vibrating microtome and incubated to 34° C in artificial cerebrospinal fluid (ACSF) (composition in mM; 0.25 7 H_2O ×$MgSO_4$, 124 NaCl, 5 KCl, 10 Dextrose, 1.25 KH_2P0_4, 26 $NaHCO_3$, 2 $CaCl_2$) as previously described (Sturm et al., 2014). Brain slices were given 1h (30m incubation at 34° C followed by 30m rest at 22-25° C) prior to beginning recordings.

3.2.4 Electrophysiological recordings

Whole-cell recordings were aimed at the CNIC as previously described (Sturm et al., 2014). Recordings were performed in a submersion-type chamber (3-4 ml/min perfusion with oxygenated ACSF at 22-25° C) mounted on an upright microscope (Zeiss AxioExaminer A1) and were targeted at dT-expressing neurons under fluorescent illumination. Borosilicate glass pipettes (3-6 MΩ) were filled with a potassium-based internal solution containing (composition in mM; 115 K-Gluconic acid ($C_6H_{11}O_7K$), 5 KCl, 11 EGTA, 1 $MgCl_2$ X $6H_2O$, 1 $CaCl_2$ X $2H_2O$, 10 HEPES, 0.3 GTP disodium salt, 2.0 ATP disodium salt and 0.5 % biocytin, pH 7.2, 314 mOsm/l). Whole-cell currents in voltage-clamp mode were acquired with a Multiclamp 700B amplifier (Molecular Devices) and a Digidata- 1440A A/D converter (Molecular Devices) at a sampling rate of 4 kHz using pClamp 10 software (Molecular Devices).

3.2.5 Synaptic input mapping

The spatial distribution of presynaptic inputs to IC neurons was determined using focal photolysis of p-hydroxyphenacyl-glutamate (0.2 mM, MNI- glutamate, Tocris). A custom built system was used to guide the size, location and duration the UV light spot used to photolyze MNI-glutamate (Sturm et al., 2014). A UV laser (DPSS Laser Inc., 3510-30, 2 W) was used as a light source and placement of the uncaging spot was steered with galvanometers (Cambridge Technology, 6210H). Uncaging position, electrophysiological data acquisition and analysis were under the control of custom-written Labview-programs linked to pClamp software (written by Tuan Nguyen). Input maps were only collected if cells had a holding current < -100 pA and access resistance < 50 mΩ. UV light pulses (355 nm) were delivered at 1 Hz in a random order. Light intensity was 20-mW (measured at slice position), light duration was 1-ms. Excitatory and inhibitory synaptic responses were isolated by holding cells at -65 mV and 0 mV, respectively. For each condition, 1-3 input maps were obtained and the average map was used for analysis.

3.2.6 Mapping analysis

During input mapping with LSPS, a combination of spontaneous events, uncaging-evoked synaptic responses and uncaging-evoked direct neuronal responses were measured at the recorded cell. It was therefore necessary to develop a detection method for discerning between these event types. Direct neuronal responses could be reliably distinguished from evoked synaptic response based upon their onset latencies relative to the onset of the uncaging stimulus (direct response onset latencies were < 7 ms post-stimulus, whereas synaptic response onset latencies were > 7ms post-stimulus). This onset latency cut-off was validated previously by

performing input mapping studies in the presence and absence of the voltage-gated sodium channel blocker Tetrodotoxin (TTX), which blocks action potential generation in presynaptic neurons stimulated with glutamate uncaging (Sturm et al., 2014). In these studies, stimulation sites that elicited post-synaptic responses at -65 mV in the absence of TTX were re-mapped in the presence of TTX, and sites where evoked responses persisted in the presence of TTX (e.g. responses that did not require presynaptic action potential generation) were classified as direct response sites. The onset latencies of responses that persisted in TTX (direct responses) were <7 ms, whereas the onset latencies of responses that were eliminated in the presence of TTX (synaptic responses) were >7 ms.

After direct stimulation sites were identified and eliminated, it was then necessary to distinguish between spontaneous synaptic events and synaptic events evoked by glutamate uncaging. The following criteria were utilized to determine whether events observed at individual stimulation sites were treated as synaptic response sites. First, a response amplitude threshold was set to 4σ of the mean baseline activity (recorded over a 100 ms period prior to the laser stimulus at each individual stimulation site). Sampling for potential synaptic events was restricted to a 50 ms window, from 10 ms post-stimulus to 60 ms post-stimulus. If an event occurred during this 50 ms window, with an amplitude that was greater than 4σ of the mean baseline activity (in the case of inhibitory events recorded at 0 mV) or less than -4σ of the mean baseline activity (in the case of excitatory events recorded at -65 mV), then that stimulation site was considered a candidate synaptic response site.

Mean baseline activity was calculated independently for each stimulation trial, and the baseline value from each trial was then used to set the amplitude threshold for that trial. In this

way, amplitude thresholds were adjusted for variations in the level of spontaneous activity that occurred over the course of recordings for each cell. This approach limited the probability that spontaneous synaptic events would be incorrectly considered uncaging-evoked synaptic responses. However, in cases where spontaneous activity levels are high, this approach may lead to a rejection of events that are, in fact, evoked synaptic responses, and in doing so, may underestimate input map size. To account for this possibility, we set the response amplitude threshold to a relatively low value (4σ), in the hopes of minimizing the chance of incorrectly rejecting evoked synaptic responses. Stimulation sites that were determined to be candidate presynaptic sites (e.g. an event that exceeded the amplitude threshold criterion was detected in at least one stimulation iteration at those sites) were only considered *valid* synaptic response sites if they also fulfilled at least 1 of 3 additional criteria. A candidate presynaptic site was only considered *valid* if 1) an event that fulfilled the amplitude response threshold was detected in at least 2 stimulation iterations at that site, 2) an event that fulfilled the response amplitude threshold was detected in a single stimulation iteration at that site, but the event was multi-peaked (likely indicative of a complex synaptic response rather than a spontaneous synaptic current), or 3) an event that fulfilled the response amplitude threshold was detected in a single stimulation iteration at that site, but with a similar onset latency (within 10 ms) to an event observed at an immediately adjacent stimulation site (within 50 μm).

Excitatory and inhibitory synaptic input map areas were calculated as the sum of individual excitatory and inhibitory synaptic response sites, respectively. The synaptic charge transferred (pC) at each valid synaptic response site was calculated over a 150ms window, from 10ms post-stimulus to 160ms post-stimulus, and averaged across all available mapping iterations (1-3). For each cell, the total amounts of excitatory and inhibitory synaptic charge transferred

were determined as the sum of excitatory and inhibitory synaptic charges found at excitatory and inhibitory synaptic response sites, respectively. Synaptic charge per stimulation site was calculated as the total synaptic charge (either excitatory or inhibitory) for a given neuron, divided by the number of synaptic response sites (either excitatory or inhibitory) for that neuron.

Excitation: Inhibition index: Excitation: Inhibition (E: I) indices were calculated at individual dual stimulation sites (e.g. those sites that elicited both excitation and inhibitory response). E: I indices were calculated as the amount of inhibitory synaptic charge elicited at a dual site subtracted from the excitatory synaptic charge elicited at that site, together divided by the sum of excitatory and inhibitory synaptic charges elicited at that site. To calculate cellular E: I indices, the E:I indices of all dual stimulation sites for a given cell were summed together, and this quantity was then divided by the total number of dual stimulation sites for that cell. To calculate pooled E: I indices, the E:I indices of dual stimulation sites were summed across all cells for a given behavioral condition (e.g. control or noise reared) and then divided by the total number of dual stimulation sites for that condition. The above-mentioned calculations are expressed by the following equations:

1) ***E: I index*** $= \dfrac{(exci\ syn.charge - inhi\ syn.charge)}{(exci\ syn.charge + inhi\ syn.charge)}$

2) ***Cellular E:*** $I = \dfrac{\sum_{i=1}^{n}(E{:}I)_i}{N}$ *, where i= synaptic response site number, n= last synaptic response site number for given cell, and N= total number of synaptic response sites that cell.*

3) ***Pooled E: I***= $\frac{\sum_{i=1}^{h}(E:I)_i}{H}$ *, where i= synaptic response site number, h= last synaptic response site number in total population of sites from cell in behavioral condition (i.e. control or noise reared , and H= total number of synaptic response sites.*

3.2.7 Statistical analysis

Data are presented as mean +/- SEM. Data were tested for normal distribution using Bartlett's test. For independent, two-group comparisons, Students t-tests (two-tailed) and Mann-Whitney tests were used to determine statistical significance. For correlational analyses, Pearson correlations were performed. For categorical comparisons, Chi-Square tests were performed (GraphPad Prism). Statistical significance was set to $p < 0.05$.

3.3 RESULTS

3.3.1 Noise rearing increases local excitatory input onto GABAergic neurons

Vgat-ires-cre-dT mice (n= 14 animals) were raised in continuous, pulsed white noise (75 dB white noise in pulses of 138 ms duration, delivered pseudo-randomly at intervals from 0 to 450 ms, duty cycle 47%) during the first 2 weeks of hearing experience (P12-25) (Figure 3-1 A, B). Control mice (n= 15 animals) were raised in standard housing conditions. To detect noise rearing-related changes in intrinsic connectivity in the IC, we mapped local synaptic networks in the IC in brain slices using LSPS of caged glutamate (Sturm et al., 2014), and compared the

distribution and strength of excitatory and inhibitory synaptic inputs received by individual IC neurons between noise-reared and control mice (Figure 3-1 C). Since glutamatergic and GABAergic neurons in the IC cannot be reliably distinguished on the basis of morphological or physiological criteria (Malmierca et al., 1993; Sivaramakrishnan et al., 2001), we targeted recordings to GABAergic neurons using a mouse line in which the expression of the fluorescent protein dtTomato is restricted to GABAergic neurons expressing the Cre protein under the promoter for the vesicular GABA transporter (vgat+). Previous input mapping experiments revealed two types of vgat+ neurons in the IC: neurons that receive both excitatory and inhibitory inputs from intrinsic sources (type 1) and neurons that only receive excitatory inputs (type 2) (Chapter 4, Figure 4-6). In these prior studies, the synaptic input maps of type 1, but not type 2 neurons, were sensitive to noise exposure. We therefore focused the current mapping studies on type 1 GABAergic neurons.

Noise rearing increased the amount of excitatory synaptic input received by GABAergic neurons. This increase in excitation was reflected by larger excitatory input maps (Noise reared: exci input area 166% of control, n= 31 cells, n= 14 animals) (Figure 3-1 C, D), greater amounts of total excitatory synaptic charge (Noise reared: total exci charge 250% of control, n= 30 cells, n= 14 animals) (Figure 3-1 E) and increased excitatory synaptic charge per stimulation site (Noise reared: exci charge per stim. site 165% of control, n= 29 cells, n= 14 animals) (Figure 3-1 F). In contrast, the overall sizes and strengths of inhibitory input maps received by GABAergic IC neurons remained stable (Figure 3-1 C-F).

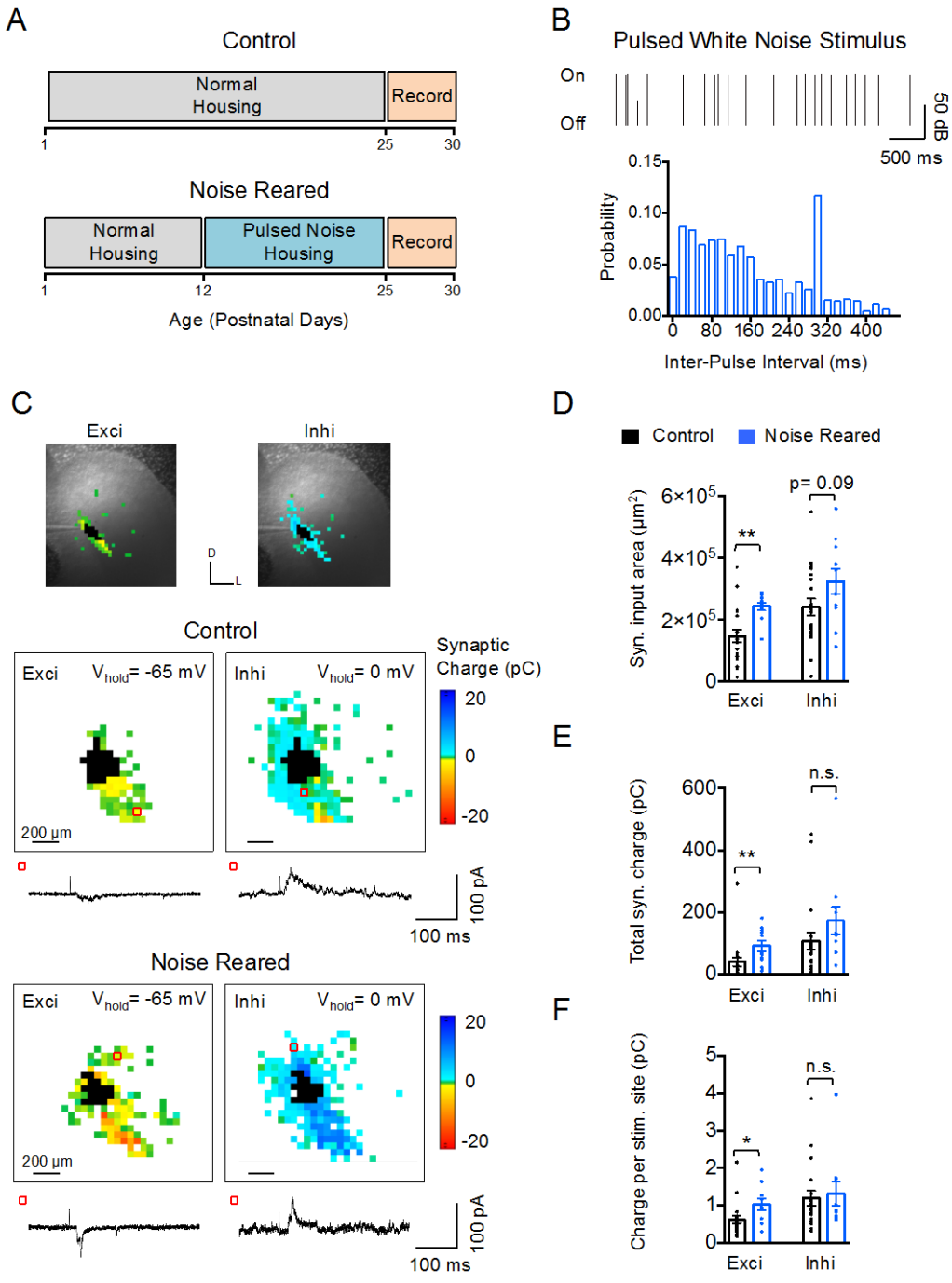

Figure 3-1. Noise rearing increases excitatory input onto GABAergic neurons.

Figure 3-1. **Noise rearing increases excitatory input onto GABAergic neurons**

(A) Noise reared mice are exposed to pulsed white noise from P12-25. **(B)** Pulsed white noise stimulus. Pulse intensity (75 dB) and duration (138 ms) are constant, and inter-pulse interval varies pseudo-randomly at intervals from 0-450 ms. **(C)** Example excitatory and inhibitory maps for a GABAergic neuron are overlaid over a photograph of the corresponding IC slice. Examples of excitatory (left) and inhibitory (right) synaptic input maps from control (top) and noise-reared (bottom) vgat-ires-cre-dT mice. Traces illustrate excitatory and inhibitory synaptic responses to glutamate uncaging at the map locations indicated by symbols. Uncaging sites that elicited direct responses at the recorded neuron are indicated in black. **(D)** Changes in synaptic input area induced by noise rearing. Excitatory input area was increased in noise-reared mice compared to control mice (exci area, control=1.47 x 10^5 μm^2 ± 0.20 x 10^5 μm^2, noise reared: 2.42 x 10^5 μm^2 ± 0.13 x 10^5 μm^2, n= 31 neurons, p= 0.0007, Mann-Whitney Test). **(E)** Changes in total synaptic charge induced by noise rearing. Excitatory input charge was increased in noise-reared mice compared to control mice (exci charge, control= 39.6 pC ± 14.0 pC, noise reared= 99.1 pC ± 16.9 pC, n= 30 neurons, p= 0.0008, Mann-Whitney Test**). (F)** Changes in synaptic charge per stimulation site induced by noise rearing. Excitatory charge per stimulation site was increased in noise-reared mice compared to control mice (exci charge per stim. site, control= 0.62 pC ± 0.10 pC, noise reared= 1.02 pC ± 0.16 pC, n= 29 neurons, Student's t-test, p= 0.0383). Error bars represent SEM. Stars indicate statistical significance. *= $p< 0.05$, **= $p< 0.01$.

Both excitatory and inhibitory synaptic responses in GABAergic neurons were often elicited from the same presynaptic stimulation sites, suggesting that there may be substantial spatial overlap between local sources of excitation and inhibition (Figure 3-2 A). However, in all recorded GABAergic neurons, there were also stimulation sites that elicited excitatory but not inhibitory responses, as well as sites that elicited inhibitory but not excitatory responses (Fig 3-2 A). Thus, presynaptic sites could be divided into three categories: 1) sites that elicited both excitatory and inhibitory synaptic responses (dual), 2) sites that elicited only excitatory synaptic responses (exci alone) and 3) sites that elicited only inhibitory synaptic responses (inhi alone) (Fig 3-2 A).

Given the precise tonotopic organization of the CNIC, where closely apposed neurons share similar CF preferences, excitatory and inhibitory inputs found at dual sites may be activated together *in vivo*. Inputs found at exci-alone and inhi-alone sites, on the other hand, may be recruited by different acoustic stimuli. Thus, noise-rearing-related changes in synaptic input maps may have different consequences for auditory processing depending upon whether they occur at dual sites, exci-alone sites and/or inhi alone sites. Accordingly, the synaptic input maps of control and noise reared animals were compared with respect to dual, exci-alone and inhi-alone sources of synaptic input (Figure 3-2 B-D).

Noise rearing increased dual input area (Noise reared: dual input area 174% of control, n= 30 cells, n= 14 animals), without changing exci-alone or inhi-alone input areas (Figure 3-2 B). Thus, the increase in excitatory input area onto GABAergic neurons (Figure 3-1 D) was due to an increase in dual input area. However, while increases in excitatory input area were restricted to dual sites, increases in total excitatory input charge were found at both dual and exci-alone sites (Noise reared: dual total excitatory charge 267% of control, exci-alone total

excitatory charge 197% of control, n= 30 cells, n= 14 animals) (Figure 3-2 C). Additionally, excitatory input charge per presynaptic site was also increased at both dual and exci-alone sites (Noise reared: dual excitatory charge per stimulation site 165% of control, exci-alone excitatory charge per stimulation site 197% of control, n= 29 cells, n= 14 animals) (Figure 3-2 D). Thus, noise rearing enhanced excitatory synaptic input onto GABAergic neurons at both dual and exci-alone synaptic response sites.

We next investigated whether noise rearing led to changes in the balance of excitatory and inhibitory synaptic strengths at individual dual stimulation sites. In control mice, most GABAergic neurons (16 of 19 cells) exhibited dual stimulation sites where inhibitory synaptic charge was greater than excitatory synaptic charge (Figure 3-2 E). This dominance of inhibition translated into negative excitation: inhibition (E: I) indices, which were calculated as the amount of inhibitory charge elicited at a dual site subtracted from the excitatory charge elicited at that site, together divided by the sum of excitatory and inhibitory charge for that site (see Methods; 3.2) (Figure 3-2 F). Negative E: I indices indicate a dominance of inhibition, whereas positive E: I indices indicate a dominance of excitation. Given that noise rearing led to increases in the strengths of excitatory, but not inhibitory synaptic inputs (Figure 3-2 D), we predicted that E: I indices at dual stimulation sites would be shifted in the positive direction, in favor of synaptic excitation.

To test this hypothesis, we first calculated E:I indices for individual dual sites and determined a mean E:I index for each neuron (Cell E: I index) (*see* Methods; 3.2.6) (Fig 3-2 G). With this method, we detected a trend towards a positive shift in E: I indices in noise-reared mice that failed to reach statistical significance ($p= 0.42$, Mann-Whitney Test) (Fig 3-2 G). A possible confound of this analysis method was that it relies on the size of dual input areas, which greatly

varied among GABAergic IC neurons (ranging from 0.18 x 10^5 μm^2 to 2.3 x 10^5 μm^2). For instance, the statistical confidence associated with the mean E: I index of a cell with 100 dual sites would be far greater than the confidence associated with the mean index of a cell with only 5 dual sites. Therefore, while calculating mean E: I indices for individual cells controls for inter-cell variability, it gives biased weight to E: I indices calculated for dual sites from cells with few dual sites. To account for the variation in dual input areas among GABAergic IC neurons, we also estimated E: I balance by pooling E:I indices calculated for individual dual sites across neurons in each behavioral condition (pooled E: I index) (*see* Methods; 3.2.6) (Fig 3-2 H). This analysis treats all dual stimulation sites as equivalent and therefore avoids giving greater weight to dual sites from neurons with few dual sites. However, in treating all dual sites as equivalent, this method fails to control for inter-cell variability. With the pooled E: I analysis approach, we detected a significant positive shift in the balance of excitatory and inhibitory synaptic strengths in noise reared animals (noise reared: -0.26 ± 0.02, control: -0.37 ± 0.02, n= 1,043 dual stimulation sites, Mann-Whitney test, $p<0.0001$) (Figure 3-2 H). Thus, raising mice in pulsed white noise during the first 2 weeks of hearing experience leads to a significant reorganization of synaptic inputs onto GABAergic IC neurons, involving substantial increases in synaptic excitatory input, which lead to a shift in in the E: I balance of closely apposed excitatory and inhibitory synaptic inputs in favor of synaptic excitation.

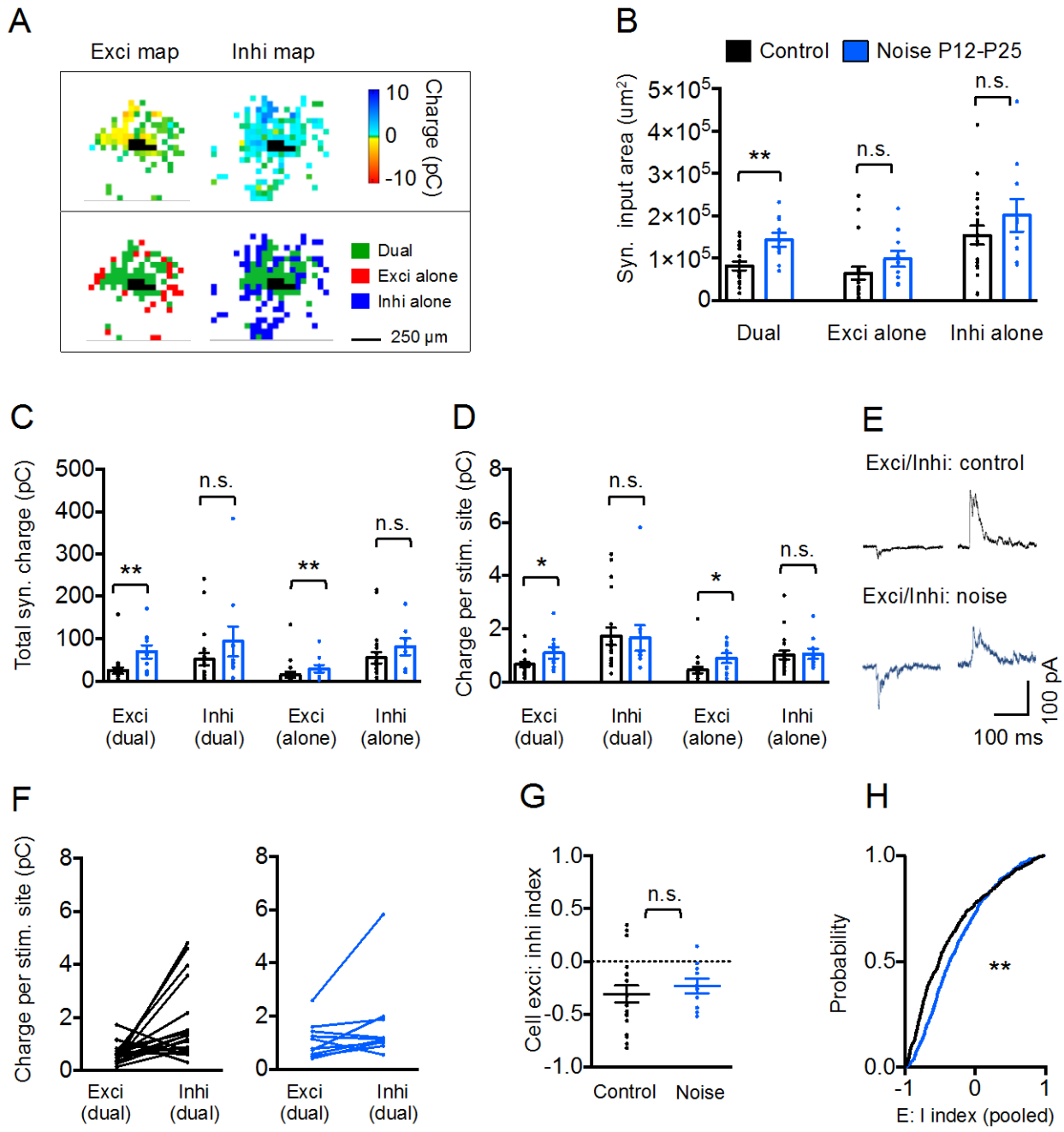

Figure 3-2. Spatial overlap of excitatory and inhibitory inputs on GABAergic neurons after noise rearing from P12-25.

Figure 3-2. Spatial overlap of excitatory and inhibitory inputs onto GABAergic neurons after noise rearing from P12-25. (A) Example Excitatory (left) and inhibitory (right) input maps received by a GABAergic neuron. Input maps consist of uncaging sites that elicit both excitatory and inhibitory responses (dual, green), sites that elicit excitatory responses only (exci alone, red) and sites that elicit inhibitory responses only (inhi alone, blue). **(B)** Changes in synaptic input area induced by noise rearing at dual and non-dual stimulation sites. Dual input area was increased in noise-reared mice compared to control mice (dual input area, control= 0.82 x 10^5 μm^2 ± 0.10 x 10^5 μm^2, noise reared= 1.43 ± 0.17 x 10^5 μm^2, n= 30 neurons, Student's t-test, p= 0.0029). **(C)** Changes in total synaptic charge induced by noise rearing at dual and non-dual stimulation sites. Total excitatory charge was increased in noise-reared mice compared to control mice at both dual (dual exci charge, control= 24.8 pC ± 7.5 pC, noise reared= 69.3 pC ± 15.6 pC, n= 30 neurons, Student's t-test, p= 0.007) and exci-alone stimulation sites (exci-alone exci charge, control= 14.9 pC ± 6.8 pC, noise reared= 29.2 pC ± 8.9 pC, n= 30 neurons, Mann-Whitney Test, p= 0.009). **(D)** Changes in synaptic charge per stimulation site induced by noise rearing at dual and non-dual stimulation sites. Excitatory synaptic charge per stimulation site was increased in noise-reared mice compared to control mice at both dual (dual exci charge per site, control= 0.66 pC ± 0.09 pC, noise reared= 1.98 pC ± 0.21 pC, n= 29 neurons, Mann-Whitney Test, p= 0.031 and exci-alone stimulation sites (exci-alone exci charge per site, control= 0.45 pC ± 0.12 pC, noise reared= 0.89 pC ± 0.19 pC, n= 29 neurons, Mann-Whitney Test, p= 0.034). **(E)** Example excitatory (left) and inhibitory (right) synaptic responses elicited at single, dual uncaging sites at -65 mV and 0 mV, respectively, in a control (top) and a noise-reared mouse (bottom). **(F)** Mean excitatory and inhibitory synaptic charge at dual uncaging sites for control (left) and noise-reared (right) mice. Lines are individual neurons connecting mean excitatory and inhibitory synaptic charges for that neuron. **(G)** Changes in cellular E: I index induced by noise rearing. E: I index measures excitation: inhibition balance and is calculated as the inhibition a neuron receives subtracted from the excitation that neuron receives, divided by the sum of the excitation and the inhibition that neuron receives. Each data point is mean E:I index for an individual neuron, calculated as the average of all indices from dual uncaging sites for that neuron. **(H)** Changes in pooled E: I index induced by noise rearing. E: I indices from individual dual stimulation sites pooled across neurons. In noise reared mice, the pooled E: I index was shifted to more positive values compared to control mice (pooled E: I index, control= -0.37 ± 0.02, noise reared= -0.26 ± 0.02, n= 1,043 dual sites, Mann-Whitney Test, p<0.0001). Error bars represent SEM. Stars indicate statistical significance. *= p< 0.05, **= p< 0.01.

3.3.2 Noise-rearing-induced increases in excitation are restricted to a critical period

The developing brain exhibits heightened responsiveness to changes in the sensory environment during brief postnatal epochs called critical periods (CP). The timing of CPs differs according to sensory modality (e.g. vision vs. audition vs. somatosensation) (de-Villers-Sidani et al., 2007) as well as stimulus feature (e.g. stimulus location, intensity and frequency) (Insanally et al., 2009; Buran et al., 2014). For example, in primary auditory cortex (A1), passive tone exposure disrupts tonotopic organization when delivered between P11-P13, but not after (de Villers-Sidani et al., 2007). We therefore hypothesized that noise rearing with pulsed white noise would lead to synaptic circuit reorganization in the CNIC when delivered during the first week of hearing experience, but not after. To test this hypothesis, we mapped the synaptic inputs received by GABAergic neurons in mice that were reared in standard housing conditions during the first week of hearing experience, from P12-18, and then reared in pulsed white noise from P19-25 (n= 7 animals) (Figure 3-3 A). We predicted that if the CP for intrinsic synaptic circuits in the IC falls within P12-18, then mice exposed to pulsed white noise from P19-25 would exhibit intrinsic synaptic networks similar to those of control, non-noise-reared animals.

Consistent with this prediction, noise rearing between P19-25 did not change the overall distribution or strength of input maps received by GABAergic neurons compared to controls, as indicated by stable input areas (Figure 3-3 B), total input charges (Figure 3-3 C), and amounts of input charge per stimulation site (Figure 3-3 D). When input maps were analyzed on a finer scale, with respect to dual, exci-alone and inhi-alone regions, no differences were found between noise-reared and control mice in terms input area (Figure 3-4 A) or total synaptic charge (Figure 3-4 B), though a trend was observed towards decreased total excitatory synaptic charge for dual stimulation sites (Mann-Whitney Test, p= 0.09) (Figure 3-4 B).

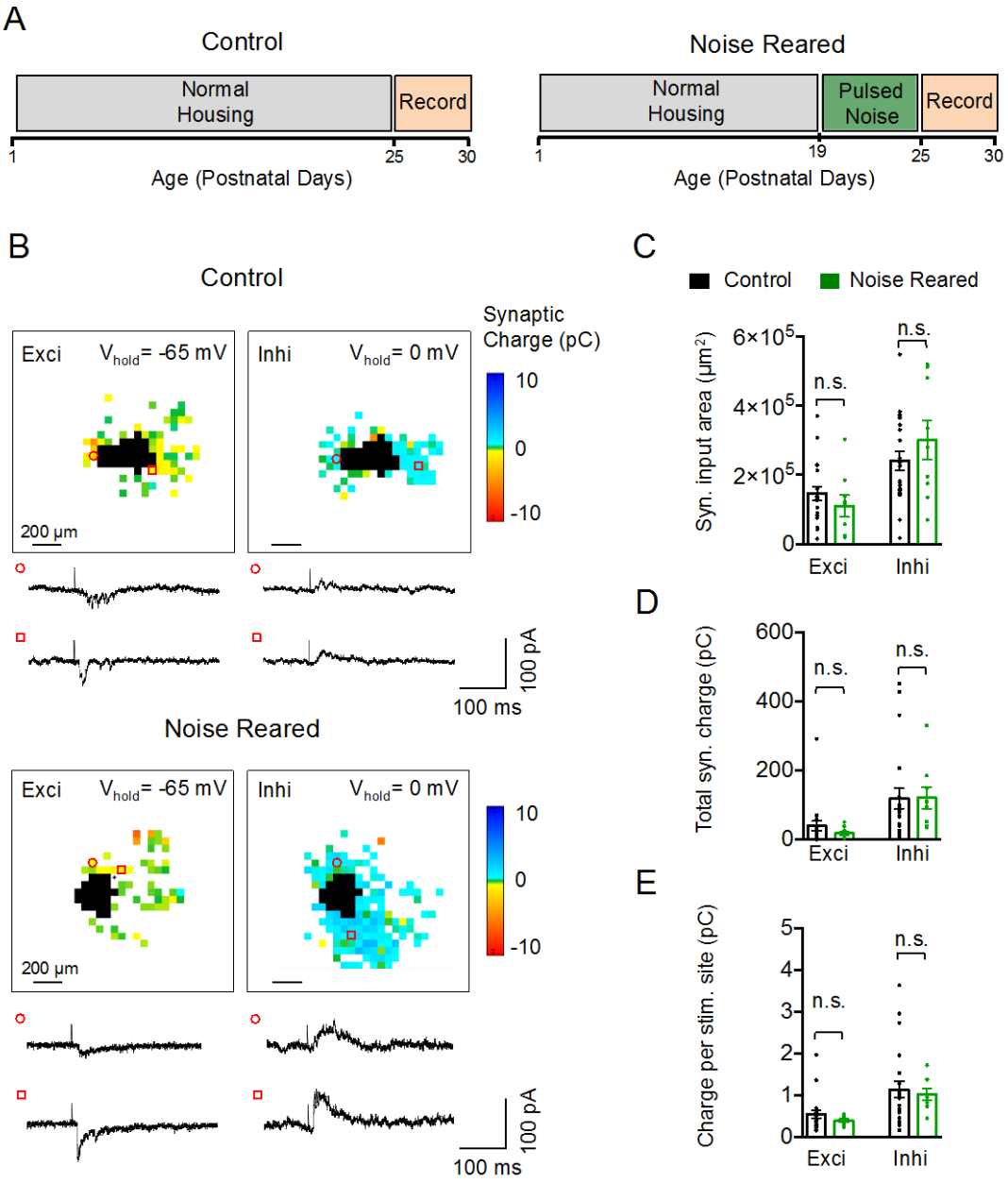

Figure 3-3. A critical period for noise rearing-induced plasticity of local CNIC circuitry.

(A) Noise reared mice are exposed to pulsed white noise from P19-25. **(B)** Examples of excitatory (left) and inhibitory (right) synaptic input maps from control (top) and noise-reared (bottom) mice. Traces illustrate excitatory and inhibitory synaptic responses to glutamate uncaging at the map locations indicated by symbols. Uncaging sites that elicited direct responses at the recorded neuron are indicated in black. **(C-E)** Noise rearing from P19-25 did not alter overall synaptic input area **(C),** total input charge **(D)** or input charge per stimulation site **(E)**. Error bars represent SEM. Stars indicate statistical significance. *= $p < 0.05$, **= $p < 0.01$.

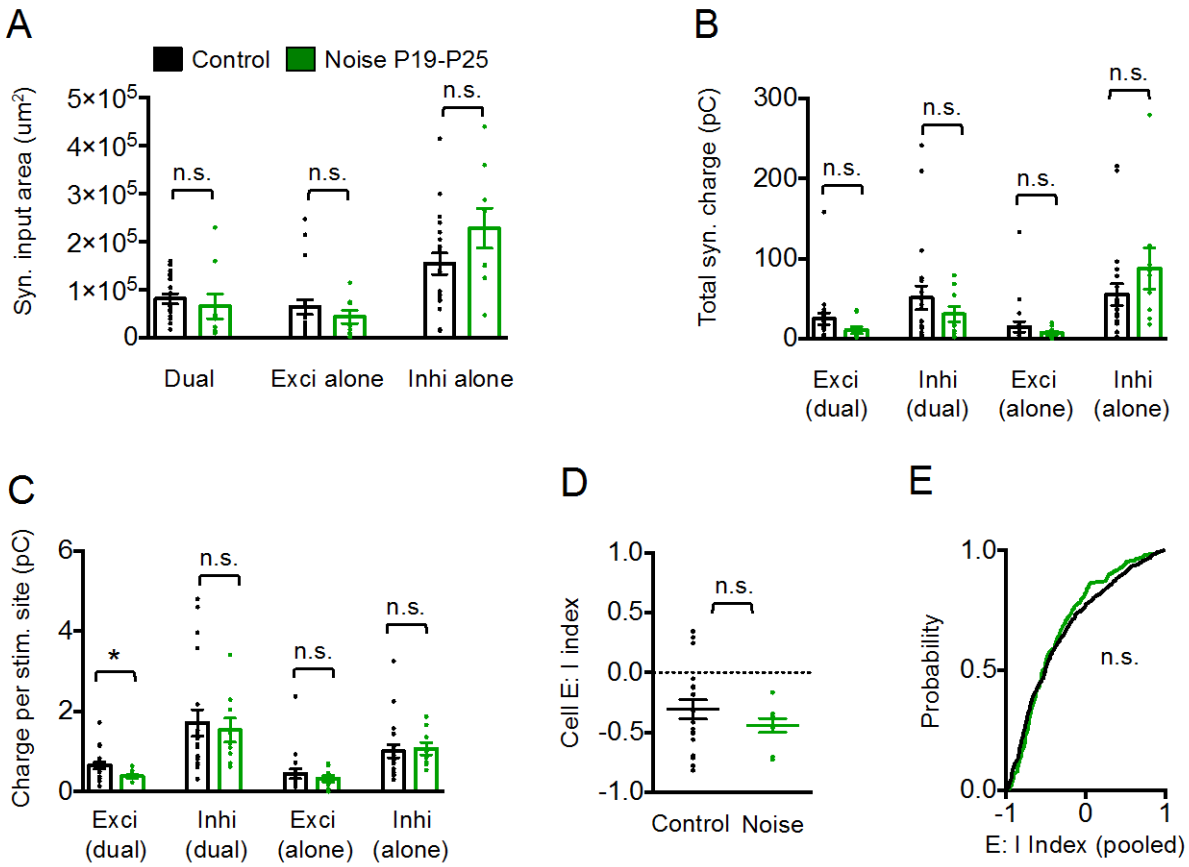

Figure 3-4. Spatial overlap of excitatory and inhibitory inputs onto GABAergic neurons after noise rearing from P19-25.

(A) Noise rearing left synaptic input area unchanged at dual and non-dual uncaging sites. **(B)** Noise rearing left total synaptic input charge unchanged at dual and non-dual uncaging sites. **(C)** Noise rearing decreased excitatory synaptic charge per dual stimulation site (dual exci charge per site, control= 0.66 pC ± 0.09 pC, noise reared= 0.39 pC ± 0.04 pC, n= 28 neurons, Mann-Whitney Test, p= 0.024). **(D-E)** Noise rearing did not change excitation: inhibition balance at dual uncaging sites. Noise rearing had no effect on the mean E: I index calculated for individual neurons **(D)** or on the pooled E: I index **(E).** Error bars represent SEM. Stars indicate statistical significance. *= p< 0.05, **= p< 0.01.

We did observe a decrease in excitatory synaptic charge per stimulation site in noise-reared mice, specifically for dual sites (Noise reared: dual excitatory charge per stimulation site 59% of control, n= 28 cells, n= 12 animals) (Figure 3-4 C), but this change was insufficient to disrupt E: I balance (Fig 3-4 D, E). Thus, noise rearing from P12-25, but not P19-25, led to substantial reorganizations of local synaptic networks received by GABAergic neurons, suggesting that the CP for noise rearing-induced plasticity in intrinsic IC circuits falls within the first week of hearing experience.

3.3.3 Noise rearing enhances E: I synaptic strength correlations in GABAergic neurons

Our group showed previously that while excitatory and inhibitory input maps in the CNIC overlap considerably in the majority of neurons, the correlation between excitatory and inhibitory input strengths at individual presynaptic sites varies substantially between neurons (Sturm et al., 2014). In some neurons, the strengths of excitatory and inhibitory inputs are highly correlated, whereas in other neurons they are weakly or not at all correlated (Sturm et al., 2014). Consistent with these prior findings, we found that in a subpopulation of GABAergic neurons from control mice, the strengths of excitatory and inhibitory synaptic responses elicited at dual input sites were positively correlated (5 of 19 neurons, pearson coefficients ranging from r= 0.24 to r= 0.76) (Figure 3-5).

Interestingly, noise rearing from P12-25, but not P19-25, enhanced both the magnitude and the incidence of this excitation: inhibition coupling (Figure 3-5). When dual stimulation sites were pooled across neurons from each behavioral condition, there were significant linear relationships between excitatory and inhibitory synaptic charge in both control mice (Linear regression, p= 0.17) and mice reared in noise from P12-25 (Linear regression, p<0.0001), but not

in mice reared in noise from P19-25 (Linear regression, p= 0.36) (Figure 3-5 B). Compared to control animals, the strength (r^2 value) and slope of this linear relationship were each significantly greater in mice reared in noise from P12-25 compared to controls (Noise reared r^2= 0.30, slope= 0.70; Control r^2= 0.01, slope= 0.24, n= 30 neurons) (Figure 3-5 C). Additionally, the percentage of neurons that exhibited significant positive correlations between excitatory and inhibitory response strengths was increased in mice reared in noise from P12-25 (8 of 11 cells) compared to both control mice (5 of 19 cells) and mice exposed to noise between P19-25 (1 of 8 cells) (Figure 3-5 D). Thus, in addition to increasing synaptic excitation onto GABAergic IC neurons, noise rearing from P12-25 enhanced the coupling between excitatory and inhibitory response strengths.

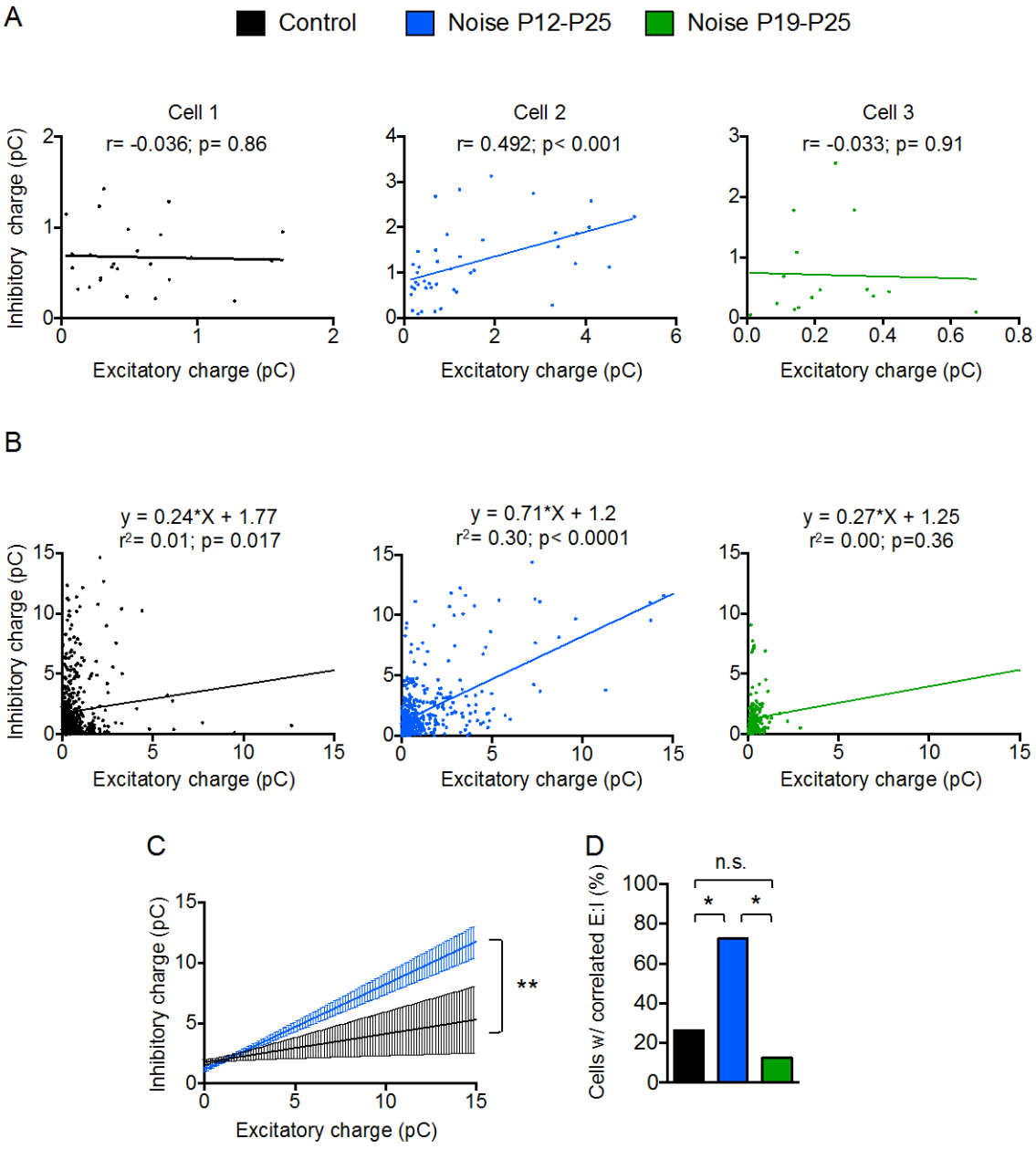

Figure 3-5. Noise rearing increases E: I correlations in GABAergic neurons.

Figure 3-5. Noise rearing increases E: I correlations in GABAergic neurons.

(A) Excitatory versus inhibitory synaptic charge from dual stimulation sites. Example neurons shown from each behavioral condition. Each data point represents an individual dual presynaptic site. Lines indicate least-squares linear regressions and correlation coefficient values (r) are from Pearson correlations. **(B)** Excitatory versus inhibitory synaptic charge for population of dual presynaptic sites, pooled across neurons in each condition. Lines indicate least-squares linear regressions (equations, r^2 and significance shown for each group). **(C)** Comparison of regression line slopes from control (black) and mice reared in noise from P12-25 (blue) (same lines as in B) with 95% confidence intervals (regression line slope, control= 0.235 ± 0.10, noise-reared= 0.71 ± 0.048, F= 19.9, $p<0.0001$). Regression line from mice reared in noise from P19-25 not shown- regression line equation not statistically significant. **(D)** Proportion of neurons in which excitatory and inhibitory synaptic charges are positively correlated. Mice reared in noise from P12-25 exhibit a greater percentage of neurons in which excitatory and inhibitory synaptic charge are correlated compared to both control mice (proportion of cells where excitation and inhibition correlated, control= 5/19 cells, noise-reared P12-25= 8/11 cells, n= 30 neurons, $X^2 = 6.11$, p= 0.013) and mice reared in noise from P19-25 (proportion of cells where excitation and inhibition correlated, noise-reared P12-25= 8/11 neurons, noise-reared P19-25= 1/8 neurons, n= 19 neurons, $X^2 = 6.7$, p= 0.034). Error bars represent 95% CI of regression lines. Stars indicate statistical significance. *= $p< 0.05$, **= $p< 0.01$.

3.3.4 Noise rearing diminishes excitatory input onto glutamatergic neurons

To investigate whether noise rearing also leads to a reorganization of synaptic networks received by excitatory IC neurons, we targeted recordings to glutamatergic neurons using a mouse line in which the expression of the fluorescent protein dtTomato is restricted to glutamatergic neurons expressing the Cre protein under the promoter for the vesicular glutamate transporter 2 (vglut2+). We compared the synaptic networks received by vglut2+ glutamatergic neurons between control and noise-reared mice (Figure 3-6 A).

Noise rearing from P12-25 decreased the amount of excitatory input received by glutamatergic neurons. This decrease was reflected by smaller excitatory input areas (Noise reared: exci input area 49% of control, n= 26 cells, n= 11 animals) (Fig 3-6 B) and decreased total excitatory synaptic charge (Noise reared: total exci charge 30% of control, n= 26 cells, n= 11 animals) (Figure 3-6 C). Excitatory synaptic charge per stimulation site, on the other hand, remained unchanged (Mann-Whitney Test, p= 0.137) (Figure 3-6 C), suggesting that the reduction in synaptic excitation onto glutamatergic neurons was due to a decrease in the number, rather than the strength of excitatory synaptic inputs. Inhibitory input maps received by glutamatergic IC neurons remained stable in noise-reared animals compared to controls (Figure 3-6 B-D).

As in GABAergic neurons, the input maps of glutamatergic IC neurons consisted of a combination of dual, exci-alone and inhi-alone presynaptic sites (Fig 3-7 A). However, unlike GABAergic neurons, glutamatergic neurons exhibited a shrinkage of excitatory input areas (Fig 3-7 B). This shrinkage of excitation was restricted to exci-alone stimulation sites, whereas both dual and inhi-alone areas were unchanged (Fig 3-7 B). No significant differences were detected between control and noise-reared mice in terms of total synaptic charge at either dual or non-dual

sites (Figure 3-7 C), though a trend was observed toward reduced excitatory charge at exci-alone sites (Mann-Whitney Test, p= 0.08). Additionally, no significant differences were observed between control and noise-reared mice in terms of synaptic charge per stimulation site, though a trend was observed toward decreased inhibitory charge per dual stimulation site (Mann-Whitney Test, p= 0.19) (Figure 3-7 D).

When we examined the balance of excitatory and inhibitory synaptic strengths at individual dual stimulation sites, we found that the majority of glutamatergic IC neurons (10 of 11 control cells) exhibited greater inhibitory synaptic charge compared to excitatory synaptic charge (Figure 3-7 E), which translated into negative mean cellular E: I indices (Figure 3-7 F). Interestingly, this dominance of inhibition was reduced in mice exposed to noise from P12-25. In noise-reared animals, we found positive shifts in E:I indices calculated both on an individual cell basis (noise reared: -0.40 ± 0.11, control: -0.03 ± 0.1, n= 21 cells, n= 11 animals) (Figure 3-7 F), and pooled across cells (noise reared: -0.12 ± 0.03, control: -0.50 ± 0.03, n= 486 dual stimulation sites, n= 11 animals) (Figure 3-7 G). Thus, noise rearing from P12-25 decreased excitatory input area, but shifted E:I balance at dual stimulation sites in favor of excitation. In other words, excitatory input area diminished, but at remaining dual sites, excitation became stronger than inhibition.

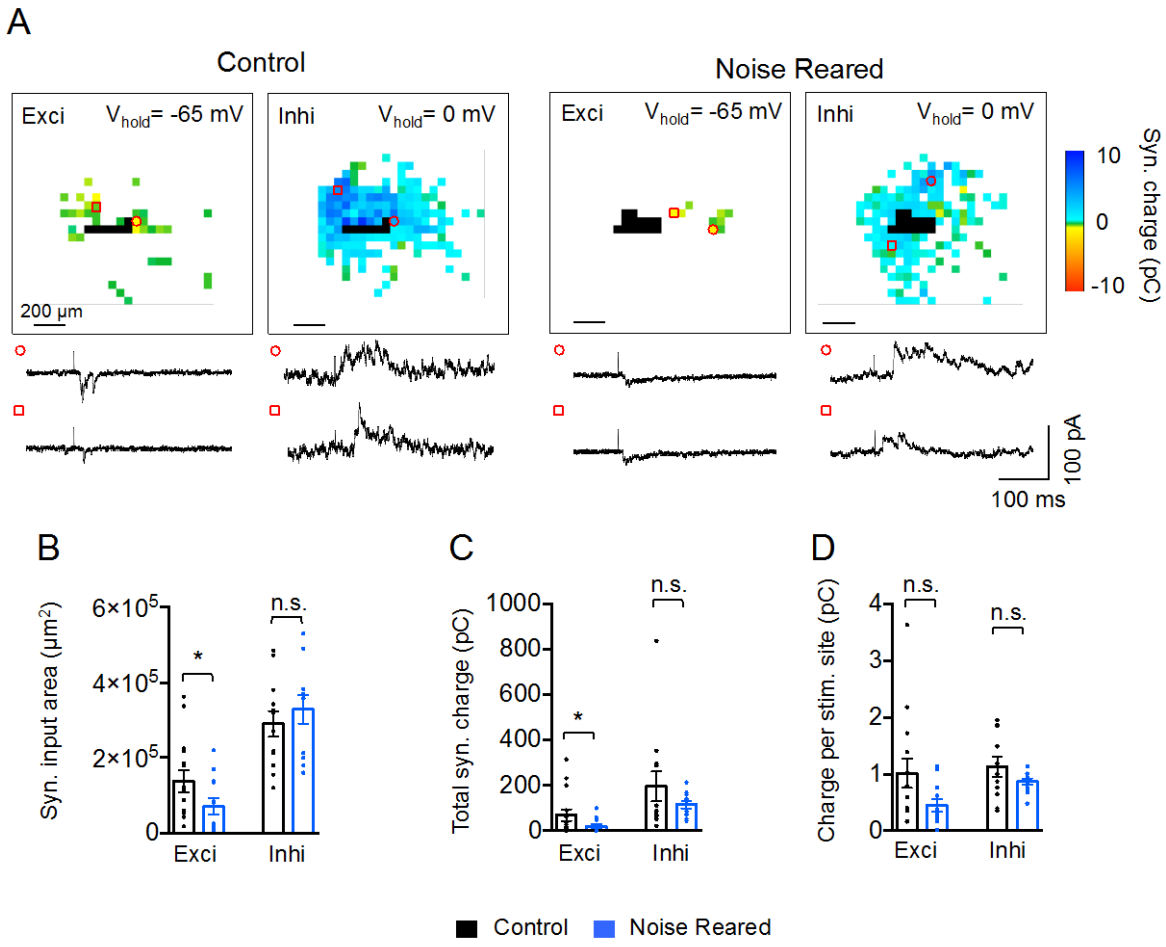

Figure 3-6. Noise rearing decreases synaptic excitation onto glutamatergic neurons.

(A) Examples of excitatory (left) and inhibitory (right) synaptic input maps from control (top) and noise-reared (bottom) vglut2-cre-dT mice. Traces illustrate excitatory and inhibitory synaptic responses to glutamate uncaging at the map locations indicated by symbols. Uncaging sites that elicited direct responses at the recorded neuron are indicated in black. **(B)** Changes in synaptic input area induced by noise rearing. Excitatory input area was decreased in noise-reared mice compared to control mice (exci area, control=1.38 x 10^5 µm^2 ± 0.29 x 10^5 µm^2, 0.68 x 10^5 µm^2 ± 0.23 x 10^5 µm^2, n= 26 neurons, p= 0.040, Mann-Whitney Test). **(C)** Changes in total synaptic charge induced by noise rearing. Excitatory input charge was increased in noise-reared mice compared to control mice (exci charge, control= 68.6 pC ± 25.7 pC, noise reared= 20.4 pC ± 9.3 pC, n= 27 neurons, p= 0.046, Mann-Whitney Test**). (D)** Synaptic charge per stimulation site was unaffected by noise rearing. Error bars represent SEM. Stars indicate statistical significance. *= p< 0.05, **= p< 0.01.

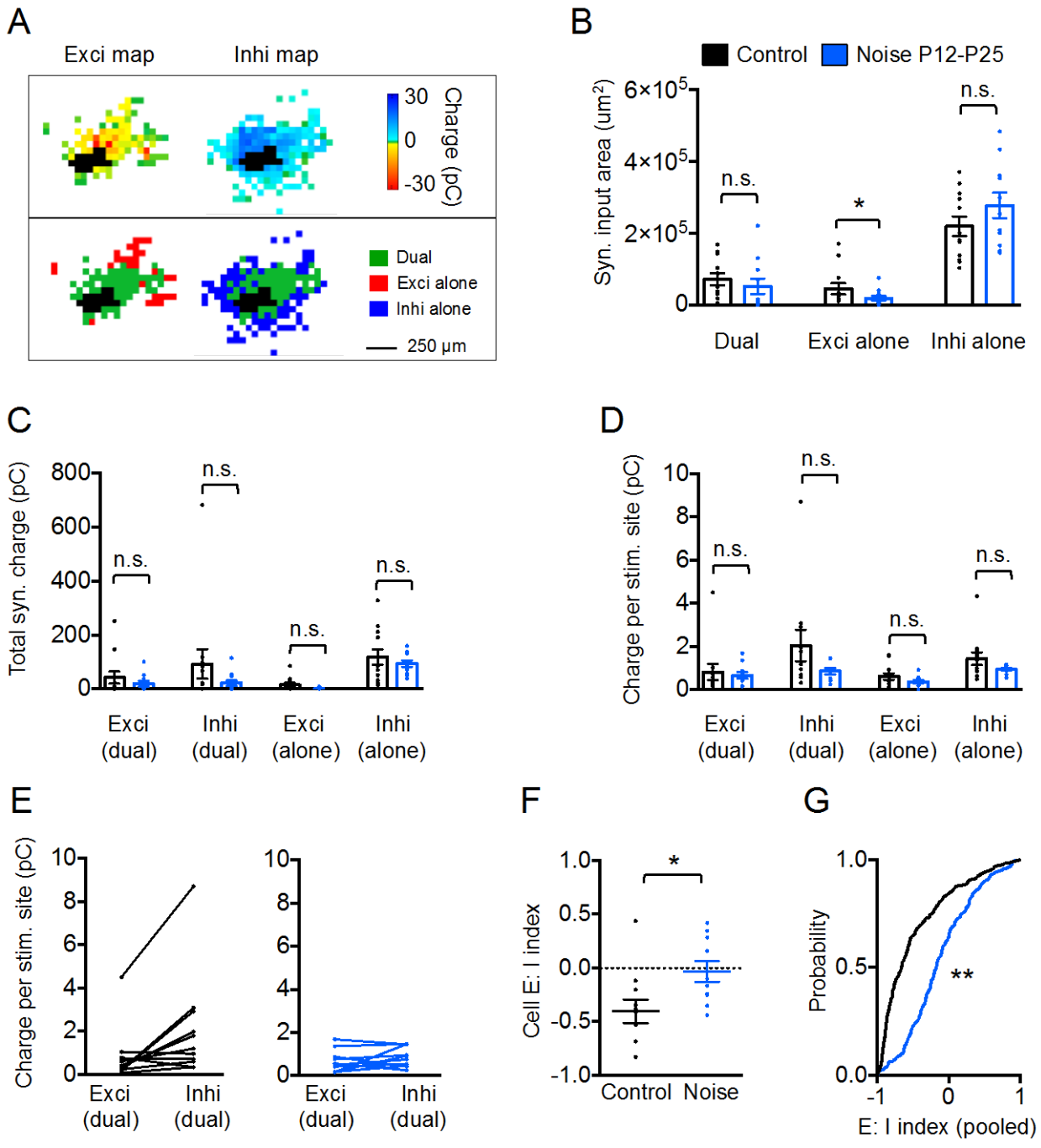

Figure 3-7. Spatial overlap of excitatory and inhibitory inputs onto glutamatergic neurons after noise rearing from P12-25.

Figure 3-7. Spatial overlap of excitatory and inhibitory inputs onto glutamatergic neurons after noise rearing from P12-25.

(A) Example excitatory (left) and inhibitory (right) input maps received by a glutamatergic IC neuron. Input maps consist of uncaging sites that elicit both excitatory and inhibitory synaptic responses (dual, green), sites that elicit excitatory but not inhibitory responses (exci alone, red) and sites that elicit inhibitory but not excitatory responses (inhi alone, blue). **(B)** Changes in dual and non-dual synaptic input areas induced by noise rearing. Exci-alone input area was decreased in noise-reared mice compared to control mice (exci-alone input area, control= 0.45×10^5 $\mu m^2 \pm 0.16 \times 10^5$ μm^2, noise reared= $0.18 \pm 0.07 \times 10^5$ μm^2, n= 23 neurons, Mann-Whitney Test, p= 0.045). **(C)** Total synaptic charge was unchanged by noise rearing at dual and non-dual uncaging sites. **(D)** Synaptic charge per stimulation site was unchanged by noise rearing at dual and non-dual uncaging sites. **(E)** Mean excitatory and inhibitory synaptic charge at dual uncaging sites for control (left) and noise-reared (right) mice. Lines are individual neurons connecting mean excitatory and inhibitory synaptic charges for that neuron. **(F)** Changes in E: I index induced by noise rearing. Each data point is mean E:I index for an individual neuron, calculated as the average of indices from dual uncaging sites for that neuron. The mean E: I index in noise-reared mice was shifted in favor of excitation compared to control mice (E: I index, control= -0.40 ± 0.11, noise reared= -0.03 pC ± 0.10 pC, n= 21 neurons, Student's t-test, p= 0.022). **(G)** Changes in pooled E: I index induced by noise rearing. E: I indices from individual, dual uncaging sites pooled across neurons from control (left) and noise reared (right) mice. In noise reared mice, the pooled E: I index was shifted to more positive values compared to control mice (pooled E: I index, control= -0.50 ± 0.03, noise reared= -0.12 pC ± 0.03 pC, n= 486 dual uncaging sites, Mann-Whitney Test, $p<0.0001$). Error bars represent SEM. Stars indicate statistical significance. *= $p< 0.05$, **= $p< 0.01$.

Finally, we sought to determine whether noise rearing-related changes in the synaptic input maps of glutamatergic neurons were restricted to a similar critical period as GABAergic neurons. Consistent with this prediction, noise rearing between P19-25 (n= 5 animals) did not change either the excitatory or inhibitory synaptic input areas received by excitatory IC neurons (Figure 3-8 A). However, noise rearing between P19-25 did lead to a reduction in total inhibitory charge compared to controls (noise reared: 26.9% of control, n= 17 cells, n= 8 animals) (Figure 3-8 B). This reduction in inhibition was found at inhi-alone presynaptic sites (noise reared: 26.9% of control, n= 18 cells, n= 8 animals), but not dual sites (Figure 3-8 E), and was attributable to a reduction in inhibitory charge per inhi-alone site (noise reared: 43.4% of control, n= 18 cells, n= 8 animals) (Figure 3-8 F). However, despite these changes, we found no differences between control mice and mice exposed to noise from P19-25 in terms of the balance of excitatory and inhibitory synaptic strengths at dual stimulation sites (Fig 3-8 G, H).

It was not possible to investigate changes in excitation: inhibition coupling for glutamatergic neurons through correlational analyses, because the number of dual stimulation targets in many cells was too low (e.g. <10) to gain sufficient statistical power to run correlations and make inter-group comparisons. However, among those glutamatergic neurons that *did* possess sufficiently large dual input areas to perform E: I correlational analysis, we found that a subpopulation of cells exhibited significant positive correlations between excitatory and inhibitory synaptic strengths (4 of 8 cells from control mice, 3 of 5 cells from noise reared P12-25 mice, 1 of 3 cells from noise reared P19-25 mice). Thus, in the CNIC, a subpopulation of both GABAergic and glutamatergic neurons show significant evidence of excitation: inhibition coupling at dual presynaptic sites.

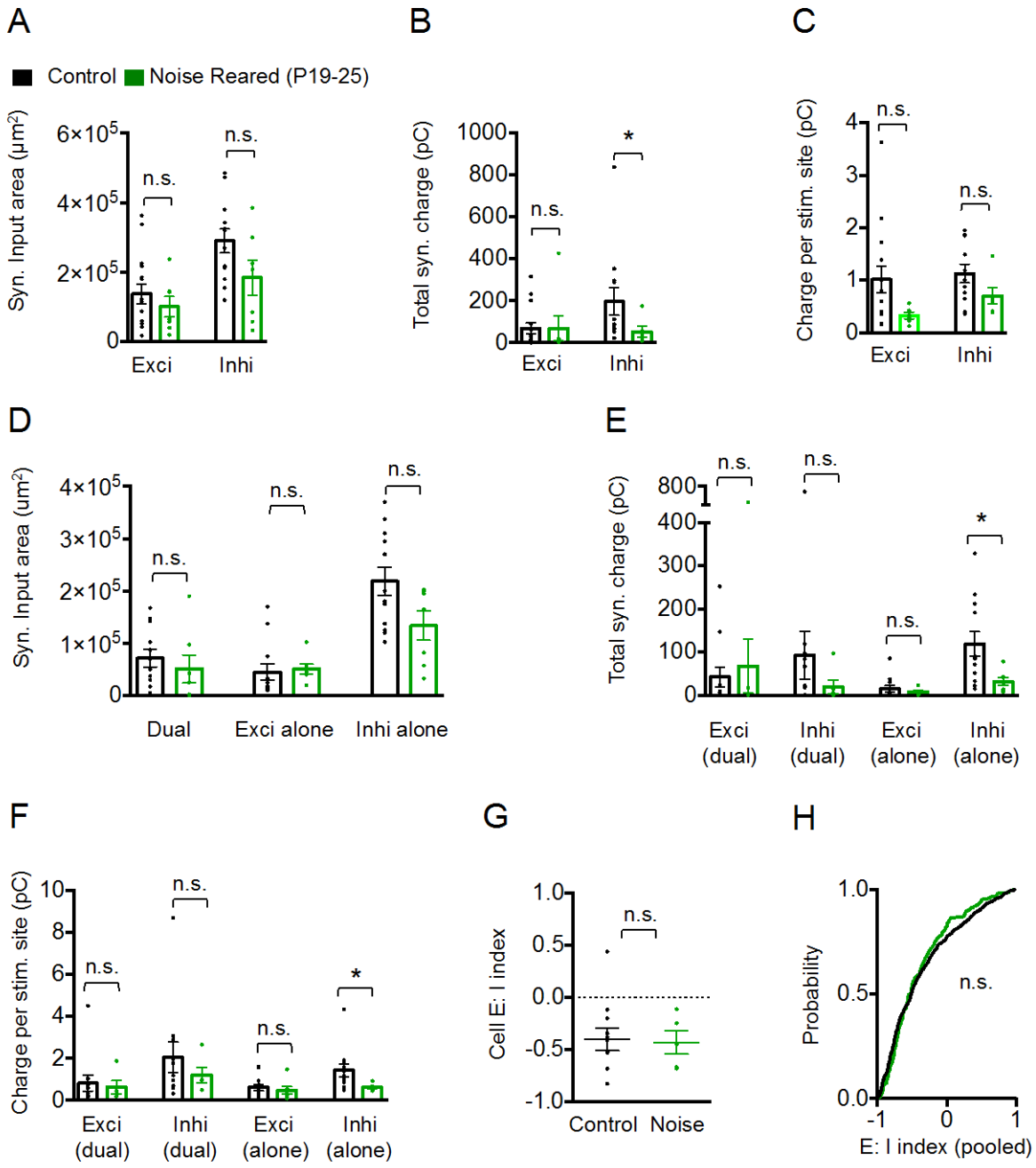

Figure 3-8. Noise rearing leads to reorganization of synaptic inputs onto glutamatergic neurons during a parallel critical period.

Figure 3-8. Noise rearing leads to reorganization of synaptic inputs onto glutamatergic neurons during a parallel critical period.

(A) Noise rearing from P19-25 did not change overall synaptic input area compared to control mice **(B)** Total inhibitory synaptic charge was decreased in noise reared mice compared to controls (total inhibitory synaptic charge, control= 196.6 pC ± 66.3 pC, noise reared P19-25= 51.2 pC ± 25.8 pC, n= 17 neurons, Mann-Whitney Test, p= 0.024). **(C)** Noise rearing did not change overall synaptic input charge per stimulation site. **(D)** Noise rearing from P19-25 did not change dual or non-dual synaptic input areas compared to control mice. **(E)** Total inhibitory synaptic charge was decreased at inhi-alone stimulation sites (total inhibitory synaptic charge from inhi-alone sites, control= 118.4 pC ± 28.7 pC, noise reared P19-25= 31.8 pC ± 9.4 pC, n= 18 neurons, Mann-Whitney Test, p= 0.013). **(F)** Inhibitory synaptic charge per stimulation site was decreased at inhi-alone stimulation sites (inhibitory synaptic charge per inhi-alone site, control= 1.43 pC ± 0.30 pC, noise reared P19-25= 0.62 pC ± 0.06 pC, n= 18 neurons, Mann-Whitney Test, p= 0.013). **(G-H)** Noise rearing did not change E: I balance at dual uncaging sites. Noise rearing had no effect on the mean E: I index calculated for individual neurons **(G)** or on the pooled E: I index **(H).** Error bars represent SEM. Stars indicate statistical significance. *= $p < 0.05$, **= $p < 0.01$.

3.4 DISCUSSION

In this study, we demonstrate that altering the spectrotemporal makeup of acoustic stimulation during early hearing experience profoundly impacts the functional organization of intrinsic synaptic circuits in the central nucleus of the mouse IC. By performing synaptic circuit mapping with LSPS in mice that were reared in pulsed white noise, we were able to link changes in acoustic experience to cell-specific patterns of IC circuit reorganization. Our data support two main conclusions. First, pulsed noise rearing during the first two weeks of hearing experience (P12-25) leads to a substantial reorganization of intrinsic synaptic networks in the IC, with distinct patterns of reorganization occurring for GABAergic and glutamatergic IC neurons. Second, noise rearing-induced reorganizations of local IC circuits are largely restricted to an early critical period during the first week (P12-18) of hearing experience. Taken together, these results demonstrate a powerful link between early acoustic experience and the functional organization of synaptic circuits in the auditory system. Furthermore, our findings provide a possible synaptic circuit basis for the persistent immature frequency tuning that has been observed in the IC of noise-reared mice (Sanes and Constantine-Paton, 1983; Sanes and Constantine-Paton, 1985).

3.4.1 Reorganization of intrinsic IC circuits in noise-reared mice

Synaptic mapping of glutamatergic and GABAergic CNIC neurons enabled us to identify cell-type specific forms of synaptic circuit reorganization in the CNIC of noise-reared animals. In GABAergic inhibitory neurons, noise rearing from P12-25 leads to increases in the sizes of

synaptic input maps, specifically involving an increase in the number of dual stimulation sites (Figure 3-2 B). We cannot be certain of the precise locations of the presynaptic excitatory and inhibitory neurons being stimulated at these dual stimulation sites- only that the 'spike-eliciting areas' of these inputs in response to glutamate uncaging are overlapping. However, this overlap suggests that excitatory and inhibitory presynaptic inputs found at dual sites are located in close spatial approximation to one another. Given the tonotopic organization of the CNIC, inputs evoked at dual stimulation sites may arise from neurons that share similar CF preferences, and these inputs may therefore be driven by similar frequencies of acoustic stimulation. In noise-reared mice, the increase in dual input area for GABAergic neurons may therefore broaden frequency tuning curves.

Noise rearing likely increased dual input area via one of two processes (Figure 3-9). First, the increase in dual input area may involve the addition of excitatory and inhibitory synaptic inputs to regions of the CNIC that were previously unresponsive to glutamate uncaging (Figure 3-9 A). In this case, dual input areas would likely be increased in noise-reared animals, whereas exci-alone and inhi-alone areas would remain stable. Indeed, we found that noise rearing leads to an increase in dual input area, without changing exci-alone or inhi-alone input areas (Figure 3-2 B). An alternative explanation is that noise rearing increases dual input areas via the addition of excitatory and inhibitory synaptic inputs to locations where inhi-alone and exci-alone presynaptic sites were previously found, respectively (Figure 3-9 B). In this case, exci-alone and/or inhi-alone sites would become dual sites, and exci-alone and inhi-alone input areas would likely shrink (Figure 3-9 B). This scenario seems unlikely, however, given that exci-alone and inhi-alone input areas were found to be stable (Figure 3-2 B).

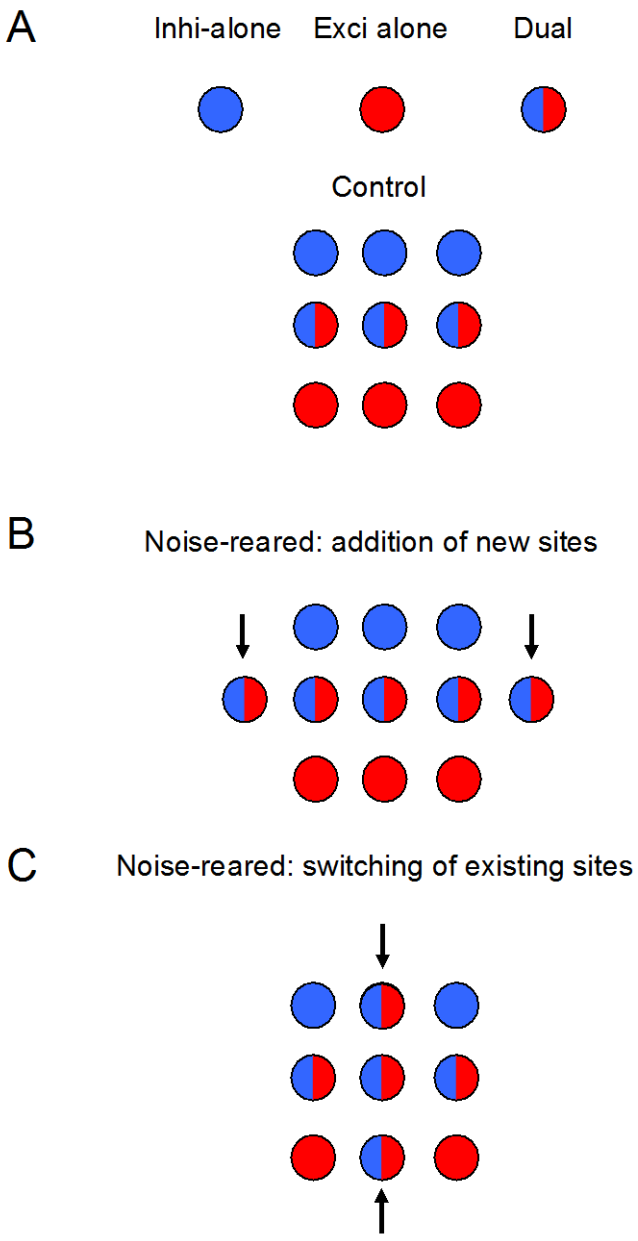

Figure 3-9. Models of noise-rearing-related increases in dual input area onto GABAergic neurons.

(A) Input maps consist of inhi-alone (blue), exci-alone (red) and dual (blue-red) presynaptic sites. Schematized input map shown with equivalent proportions of each site. (B) Noise-rearing from P12-25 may increase dual input area via the addition of excitatory and inhibitory inputs to regions of the CNIC that were previously unresponsive to glutamate uncaging. **(C)** Alternatively, noise rearing may increase dual input area via the addition of excitatory and inhibitory inputs to presynaptic sites that were previously inhi-alone and exci-alone, respectively.

The increase in dual input area onto GABAergic neurons is accompanied by a strengthening of excitatory synaptic inputs at both dual and exci-alone sites. *In vivo*, this increased excitatory input may translate into an increased drive of inhibitory IC networks in response to acoustic stimulation, which could result in a broadening of tuning curves for GABAergic neurons and/or a sharpening of tuning curves for CNIC neurons that receive local inhibitory inputs. Additionally, since intrinsic CNIC circuits are preferentially engaged at higher sound intensities (Grimsley et al., 2013), increases in local excitatory input onto GABAergic neurons may lower the acoustic stimulus intensity threshold for the recruitment of local inhibitory networks. Increasing the amount of local inhibition in the CNIC under conditions of mild acoustic stimulation could alter neuronal tuning properties as well as affect hearing in noisy environments.

In glutamatergic neurons, noise rearing from P12-25 leads to a shrinkage of excitatory input maps (Figure 3-6 A, B), as well as to a loss of total excitatory charge (Figure 3-6 C). However, noise rearing does not change excitatory charge per stimulation target (Figure 3-6 D, Figure 3-7 D), which suggests that the strength of remaining excitatory inputs is preserved. Instead, we find that inhibition is weakened relative to excitation at dual stimulation sites (Figure 3-7 E), and this asymmetry produces a shift in E: I balance at dual sites in favor of excitation. Thus, while the patterns of noise rearing-induced synaptic reorganization differ substantially between excitatory and inhibitory neurons, both changes lead to shifts in the balance of excitatory and inhibitory input strengths in favor of excitation.

The different patterns of noise rearing-induced synaptic reorganization for glutamatergic and GABAergic IC neurons may relate to different spike-timing dependent plasticity (STDP) rules acting at excitatory and inhibitory synapses in the IC. Spike-timing dependent plasticity is

hypothesized to instruct the refinement of synaptic circuits in development (Bennet and Bair, 2015), and in disrupting normal patterns of correlated spiking in auditory circuits, pulsed noise rearing may disturb STDP-dependent circuit refinement. In the DCN, excitatory synapses onto glutamatergic principal cells exhibit long-term potentiation (LTP) when presynaptic excitation is delivered shortly before the occurrence of post-synaptic spiking, whereas excitatory synapses onto GABAergic cartwheel neurons exhibit long-term-depression (LTD) under the same conditions (Tzounopoulos et al., 2004; Tzounopoulos et al., 2007). Similar plasticity rules may function at excitatory synapses onto glutamatergic and GABAergic neurons in the IC, and if pulsed noise exposure disrupts the relative timing of pre- and post-synaptic firing in these neurons, it could theoretically prevent STDP-related strengthening and weakening of excitatory inputs onto glutamatergic and GABAergic IC neurons, respectively. Such a process could explain why pulsed noise exposure from P12-25 results in decreased excitatory input onto glutamatergic IC neurons (if LTP is prevented) as well as to increased excitatory input onto GABAergic IC neurons (if LTD is prevented).

3.4.2 A critical period for intrinsic connectivity in the auditory midbrain

The effects of pulsed noise rearing on synaptic circuit organization in the IC were predominantly restricted to mice that were reared in pulsed noise during the first week of hearing experience (P12-18). Compared to age-matched control mice, mice reared in noise between P19-25 (but not P12-18) exhibited similar excitatory and inhibitory synaptic input maps for both GABAergic (Figures 3-3, 3-4) and glutamatergic (Figure 3-8) IC neurons. Thus, the first week of hearing experience appears to represent a critical period for the effects of noise rearing on intrinsic connectivity in the CNIC.

Although the effects of noise rearing were largely restricted to the first week of hearing experience, pulsed noise delivered exclusively from P19-25 did lead to at least two fine-scale synaptic modifications. Noise-reared animals exhibited a weakening of excitatory synaptic strength at dual presynaptic sites for GABAergic neurons (Figure 3-4 C), as well as a weakening of inhibitory synaptic strength at inhi-alone sites for excitatory neurons (Fig 3-8 B, E, F). It is possible that the critical period for intrinsic circuit plasticity in the CNIC is not completely closed by P19, and that these changes reflect the "tail end" of the plasticity window. However, if this were the case, we would then expect that the synaptic changes occurring in mice that were raised in noise from P19-25 would be similar to those occurring in mice that were raised in noise from P12-25. Instead, whereas the strengths of excitatory synaptic inputs received by GABAergic neurons were slightly weakened in mice exposed to noise between P19-25, excitatory inputs were profoundly strengthened in mice exposed to noise between P12-25. Additionally, whereas the strengths of inhibitory synaptic inputs received by glutamatergic neurons were weakened in mice exposed to noise between P19-25, the strengths of these inhbitory inputs were unchanged in mice exposed to noise between P12-25. We therefore suspect that the fine-scale changes in synaptic strength that result from noise rearing between P19-25 occur after the closure of the initial critical period, and are the result of a distinct, activity-dependent process. In the developing auditory cortex, different intrinsic and synaptic properties of cortical pyramidal neurons exhibit distinct critical periods of plasticity in response to transient hearing loss (Mowery et al., 2015). Therefore, it is plausible that the fine-scale changes in synaptic strength that occurred in the CNIC of mice reared in noise from P19-25 occurred during a distinct critical period from the larger-scale network changes that occurred in mice reared in noise from P12-25.

3.4.3 Consequences of CNIC circuit reorganization for the development of hearing

Frequency tuning in the IC matures rapidly during the first week of hearing experience, as evidenced by a sharpening of tuning curves and a decrease in sound evoked firing thresholds (Shnerson and Willot, 1979, Saunders et al., 1980). Exposing mice to synchronous auditory inputs during this period has been shown to prevent the developmental sharpening of frequency tuning in the IC (Sanes and Constantine-Paton, 1983; Sanes and Constantine-Paton, 1985) and since the organization of ascending inputs to the IC is largely mature at hearing onset (Gabriele et al., 2000a, 2007; Henkel et al., 2007), this disruption in tuning may reflect disturbances in the refinement of intrinsic CNIC maps. Here we demonstrate that pulsed white noise rearing between P12-25 leads to an increase in local excitatory and inhibitory input areas received by GABAergic neurons, as well as to a substantial strengthening of the excitatory synaptic inputs received by these cells. These changes may lead to a widening of tuning curves for GABAergic neurons and to a lowering of their sound-evoked response thresholds.

Neuronal tuning curves in the IC broaden with increasing sound intensity (Egorova et al., 2001; Egorova and Ehret, 2008) and since extrinsic excitatory and inhibitory inputs to the CNIC saturate before intrinsic inputs (Grimsley et al., 2013), this broadening of tuning may be partly mediated by the recruitment of intrinsic IC circuits. In addition to the increased excitation of GABAergic neurons, noise rearing also led to a relative increase in excitatory synaptic strength at dual presynaptic sites (in spite of an overall loss of excitatory area). Together, these noise-reorganizations may shift the intensity-dependent recruitment of intrinsic IC circuits to lower sound intensities and alter neuronal tuning at low-mid sound intensities.

How might pulsed white noise exposure disrupt developmental refinement in intrinsic CNIC circuits? In primary auditory cortex, where pulsed white noise exposure prevents the

maturation of tonotopy and frequency selectivity, the effects of noise rearing have been attributed to premature closure of critical period plasticity (Zhang et al., 2002). This may also be the case in the CNIC, where pulsed noise exposure during early hearing experience may shut the critical period window for experience-dependent plasticity prior to the completion of normal synaptic refinement. Critical period duration is highly dependent on the level of local GABAergic neurotransmission (Hensch et al., 1998; Faglioni and Hensch, 2000; Iwai et al., 2003; Hensch and Stryker, 2004; Hensch, 2005), and critical period closure following pulsed noise exposure may therefore relate to changes in the intrinsic properties of GABAergic IC neurons, as well as to changes in local synaptic inputs received by these cells. In the developing primary visual cortex (V1) of mice, monocular deprivation leads to ocular dominance plasticity via a transient reduction in the evoked firing rates of fast-spiking parvalbumin-positive (PV) GABAergic interneurons, which, in turn, is due to a decrease in local excitatory input onto PV interneurons (Kuhlman et al., 2013). Pharmacologically preventing this reduction in GABAergic neurotransmission just after eye opening has been shown to prevent ocular dominance plasticity in VI and to accelerate critical period closure (Iwai et al., 2003; Kuhlman et al., 2013). The results of these studies parallel our findings in the IC, which demonstrate that pulsed white noise exposure selectively increases excitatory synaptic input onto GABAergic IC neurons. Thus, pulsed white noise exposure may have naturalistically recapitulated the effects achieved by pharmacologically increasing GABAergic neurotransmission in the visual system, and closed the window for experience-dependent plasticity in the auditory system.

3.4.4 Conclusion

In this study, we provide the first evidence that altering the spectrotemporal makeup of acoustic inputs during early hearing experience can lead to profound reorganizations of local synaptic circuits in the auditory midbrain. Raising mice in pulsed white noise during the first two weeks of hearing experience leads to complex yet specific reorganizations of excitatory and inhibitory synaptic inputs onto glutamatergic and GABAergic neurons. Furthermore, our studies demonstrate that noise rearing affects excitatory and inhibitory neurons differently, suggesting that the synaptic networks of each cell type exhibit distinct mechanisms of experience-dependent maturation. Finally, the effects of noise rearing on the distribution of excitatory and inhibitory synaptic networks in the IC are restricted to a critical period window, which falls within the first week of hearing experience.

4.0 REORGANIZATION OF SYNAPTIC CIRCUITS IN THE INFERIOR COLLICULUS IN A MOUSE MODEL OF TINNITUS AND ITS PREVENTION BY ACOUSTIC ENRICHMENT

4.1 INTRODUCTION

Tinnitus is a central hearing condition characterized by the perception of sound without an external source (Baguley et al., 2013). Over 50 million people in the U.S. alone experience tinnitus, more than 2 million of which are debilitated by it (Shargorodsky et al., 2010). Tinnitus predominantly, but not invariably, emerges in individuals who have suffered peripheral hearing loss due to noise damage (Helfer et al., 2011; Yankaskas et al., 2013), ototoxic drugs (Dille et al., 2010), or traumatic brain injury (Yurgil et al., 2015), indicating that cochlear trauma triggers plasticity in central auditory brain circuits that eventually can lead to tinnitus (see Gold and Bajo, 2014 for review).

Studies in both humans and rodent models have identified hyperactivity as a major neuronal correlate of tinnitus (Melcher et al., 2000; Brozoski et al., 2002; Leaver et al., 2011; Middleton et al., 2011; Llano et al., 2012; Li et al., 2013; Kalappa et al., 2014; Luo et al., 2014). This hyperactive state has been observed in several auditory brain regions and is characterized by increased spontaneous firing rates (Brozoski et al., 2002; Seki and Eggermont, 2003; Ma et al., 2006; Vogler et al., 2011; Li et al., 2013; Manzoor et al., 2012; Ropp et al., 2014), a higher

incidence of burst-like firing (Bauer et al., 2008; Pilati et al., 2012a; Kalappa et al., 2014; Coomber et al., 2014), an increase in gain (Wang et al, 2002; Niu et al., 2013; Stefanescu et al., 2015), and enhanced firing synchrony (Seki and Eggermont, 2003; Bauer et al., 2008). Tinnitus-related hyperactivity has been attributed to increased neuronal membrane excitability and to decreased synaptic inhibition. For example, in the dorsal cochlear nucleus (DCN), which is thought to be the initial site of tinnitus generation (Kaltenbach, 2007), noise-induced increases in the spontaneous firing rates of fusiform cells are mediated by a reduction in voltage-gated potassium channel activity (Li et al., 2013; Kalappa et al., 2015; Li et al., 2015), as well as a down regulation of both GABAergic (Middleton et al., 2011) and glycinergic neurotransmission (Wang et al., 2009; Pilati et al., 2012b). In the inferior colliculus (IC) and auditory cortex, noise trauma-induced hyperactivity has been linked to decreased GABAergic inhibition (Dong et al., 2009, 2010; Yang et al., 2011; Llano et al., 2012). However, clear evidence of whether the generation of tinnitus involves the reorganization of central auditory synaptic networks is still missing.

A host of studies have implicated the IC in the generation of tinnitus (Berger and Coomber, 2015). The IC is the major subcortical integration center in the mammalian brain, receiving ascending inputs from almost all auditory brainstem nuclei (Adams et al., 1979; Malmierca et al., 2005), commissural inputs from the contralateral IC (Saldaña et al., 1992), and descending inputs from the auditory cortex (Saldaña et al., 1996; Gao and Suga, 1998; Bajo and King, 2013). In addition to these extrinsic inputs, the IC also contains an extensive and complex network of intrinsic connections, which are thought to encompass the majority of IC synapses (Saldaña and Merchán, 2005). Despite their prominence, the contribution of these intrinsic networks to auditory processing or the generation of tinnitus has remained poorly understood.

During development, both excitatory and inhibitory local IC circuits undergo substantial refinement, both before and after hearing onset (Chapter 2; Sturm et al., 2014) raising the possibility that some degree of plasticity may be retained at older ages. Since intrinsic IC connections provide gain control for IC responses (Grimsley et al., 2013), hearing-loss induced changes in the strength and/or the spatial organization of intrinsic IC circuits are plausible candidates for generating tinnitus-related IC hyperactivity, which is commonly observed in tinnitus patients as well as in animal models (Melcher et al., 2000; Wang et al., 2002; Ma et al., 2006; Bauer et al., 2008; Dong et al., 2009; Mulders and Robertson, 2009; Dong et al., 2010; Manzoor et al., 2012; Niu et al., 2013; Ropp et al., 2014).

To gain better insight into the organization and plasticity of intrinsic synaptic connections in the central nucleus of the IC (CNIC) and to investigate their potential reorganization following noise-induced hearing loss, we mapped local connectivity to glutamatergic and GABAergic neurons in the IC of mice using laser-scanning photostimulation (LSPS) with caged glutamate. We found that noise-induced mild hearing loss leads to profound, yet cell-type and input-specific, reorganizations of excitatory and inhibitory local IC circuits. Interestingly, the specific nature of these reorganizations strongly correlated with the presence or absence of behavioral evidence of tinnitus. In mice with tinnitus, reorganization of excitatory and inhibitory circuits resulted in a significant disruption of the overall synaptic excitation: inhibition balance, whereas in mice without tinnitus, the synaptic reorganization left the excitation: inhibition balance unchanged. Acoustic enrichment (AE) with mild-intensity pulsed white noise immediately following acoustic trauma prevented circuit reorganization and the emergence of evidence of tinnitus without affecting hearing loss. Our results demonstrate that intrinsic synaptic circuits in the IC retain a high degree of plasticity and provide a link between the specific patterns of circuit

reorganization and the behavioral evidence of tinnitus. Finally, our results raise the possibility of using early acoustic enrichment after cochlear trauma to prevent the development of tinnitus.

4.2 MATERIALS AND METHODS

4.2.1 Animals and preparation

Experimental procedures were carried out in accordance with US National Institutes of Health (NIH) guidelines and were approved by the Institutional Animal Care and Use Committee (IACUC) at the University of Pittsburgh. Vgat-ires-cre, and dT-loxP mice were purchased from Jackson Labs (Jackson). Vglut2-cre mice were the generous gift of Dr. Rebecca Seal's laboratory. The background strain of all mice was C57BL/6J. In our laboratory, vglut2-cre and vgat-ires-cre mice were crossed with dT-loxP mice to generate vglut2-cre-dT-loxP and vgat-ires-cre-dT-loxP strains.

4.2.2 Noise exposure

Mice of either sex [postnatal day (P) 20-23] were randomly assigned to one of two groups: 1) noise-exposed group or 2) control group. For unilateral noise exposure, mice in the noise-exposed group were deeply anesthetized with isoflurane and a pipette tip fixed to the end of a 2.5-cm piece of plastic tubing and attached to a speaker was inserted into their left ear canals. Noise exposure consisted of narrow bandpass noise with a 1-kHz bandwidth that was centered at

16 kHz and presented at 116 dB sound pressure level (SPL) for 45 min. Mice in the control group were not given noise exposure.

4.2.3 Gap inhibition of the acoustic startle response

Behavioral evidence of tinnitus was tested using the gap detection methods (Turner et al., 2006; Middleton et al., 2011; Li et al., 2013; Kalappa et al., 2015; Li et al., 2015), which has been cross-validated with other behavioral measures of tinnitus (Bauer & Brozoski, 2001). Gap detection was tested in all mice 1d prior to noise-exposure (P19-22) and then again 7d after noise-exposure (P26-30). Gap detection testing was carried out in a sound-attenuating chamber (Colbourn Instruments). A piezoelectric transducer was used to record of downward force exhibited by the animals during the startle reaction (Clause et al., 2012). During testing, a narrow bandpass background sound (1-kHz bandwidth centered at either 10, 12, 16, 20, 24 and 32 kHz) was presented at 70 dB SPL for 8-25 seconds (randomly varied) prior to presentation of an acoustic startle stimulus (white noise, 140 dB SPL, 20 ms). In 50% of trials, a 50 ms gap was introduced into the background sound 130 ms prior to the presentation of the startle stimulus. Startle response magnitude was measured (in arbitrary units, AU) as the peak-to-peak value of the downward force exerted by mice onto the platform in response to the startle stimulus. Gap detection ability was determined for each sound frequency using the gap startle ratio, which is the ratio of the startle response amplitude in trials with gaps in the background sound at a given sound frequency over the startle response magnitude in trials without gaps at the same sound frequency. Gap startle ratios closer to 0 indicate greater gap inhibition of the acoustic startle reflex while gap startle ratios closer to 1 indicate less gap inhibition.

4.2.4 Tinnitus criteria

In the gap detection paradigm, a decrease in gap detection ability (measured as an increase in the gap detection ratio) serves as the behavioral marker for tinnitus. However, in order to be considered evidence of tinnitus, an increase in the gap detection ratio must exceed an experimenter-defined threshold. Similar to others (Li et al., 2013; Kalappa et al., 2015; Li et al., 2015), we defined this threshold as an increase in the gap detection ratio that was at least 2 standard deviations above the average change in gap detection ratios observed for control mice over a 7d period. To control for potential inter-strain differences in gap detection ability, we determined separate tinnitus threshold scores for vglut2-cre-dTloxP and vgat-ires-cre-dT-loxP mice (Figures 4-1 and 4-2). The probability distributions of changes in gap detection in control mice from each strain were fitted with normal distributions (vglut2-cre-dT-loxP; μ= 0.02, SD σ= 0.141, n= 12 animals: vgat-ires-cre-dT-loxP; μ= 0.02, SD σ= 0.145, n= 12 animals), and tinnitus threshold scores were determined to be 0.30 (vglut2-cre-dT-loxP) and 0.31 (vgat-ires-cre-dT-loxP), similar to the values previously reported for other mouse strains (Li et al., 2013; Li et al., 2015). Noise-exposed mice that exhibited an increase in the gap startle ratio that exceeded these thresholds for at least one sound frequency were considered tinnitus mice (NE-T). Noise-exposed mice that exhibited a change in the gap startle ratio that was less than the tinnitus threshold were considered non-tinnitus mice (NE-NT). To control for tinnitus that was unrelated to noise-exposure, control mice that exhibited an increase in the gap startle ratio that exceeded the tinnitus threshold in the initial testing (1 vglut2-cre-dT-loxP animal and 1 vgat-ires-cre-dT-loxP mouse) were excluded from further analysis. To ensure that all mice were able to detect the gap in the background sounds prior to noise-exposure, gap startle ratios for individual sound frequencies were required to be below 0.9 to be included post-noise-exposure analysis (Li et al.,

2013). One mouse had no gap startle ratios below 0.9 for any tested frequency and was therefore excluded. Utilizing these criteria, 9 out of 18 (50%) noise-exposed vglut2-cre-dT-loxP mice and 10 out of 19 (53%) noise-exposed vgat-ires-cre-dT-loxP showed behavioral evidence of tinnitus.

4.2.5 Prepulse inhibition of the acoustic startle response

Prepulse inhibition (PPI) of the acoustic startle response was assessed in all mice in order to control for noise-induced deficits in acoustic sensitivity and potential changes in the neuronal circuits related to PPI and startle behavior. In the PPI paradigm, a nonstartling prepulse sound decreases startle response amplitudes (Groves et al., 1974). Prior studies have shown that noise-exposed mice with tinnitus exhibit gap detection deficits in the absence of PPI deficits (Li et al., 2013). For PPI testing, a 50-ms pre-pulse sound (1-kHz bandwidth centered at 10, 12, 16, 20, 24 and 32 kHz) was presented 130 ms before the presentation of the startle stimulus (white noise, 140 dB SPL, 20 ms). The sound intensity of the pre-pulse was similar to the intensity of the background sound used in gap detection trials (70 dB SPL). PPI was evaluated for each sound frequency with the PPI startle ratio, which is the ratio of the startle response amplitude without pre-pulse over the startle response amplitude with pre-prepulse. PPI startle ratios closer to 0 indicate stronger PPI of the startle response, while PPI startle ratios closer to 1 indicate weaker PPI of the startle response.

4.2.6 Auditory brainstem response

Auditory brainstem response (ABR) thresholds were assessed in all mice assigned to the noise-exposed group 1d prior to noise exposure (P19-22), and then again 7d after noise-exposure (P26-

30). Measurements were conducted in a sound-attenuating chamber (Coulbourn Instruments) using a Z-Series 3-DSP Bioacoustic System (Tucker Davis Technologies) with subdermal electrodes placed at the vertex, a ground electrode placed ventral to the right pinna, and the reference electrode placed ventral to the left pinna. Stimuli were produced using the System 3 software package (Tucker Davis Technologies). During ABR measurements, animals were anesthetized with Isoflurane anesthesia and their body temperatures were maintained around 36.5-38.5 °C by a heating pad. ABR thresholds were obtained with 1ms clicks as well as 3ms tone bursts of 10, 12, 16, 20, 24, and 32 kHz presented at various sound intensities at a rate of 18.56 per s. Evoked potentials were averaged 1,024 times and filtered using a 300- to 3,000-Hz band- pass filter.

4.2.7 Acoustic enrichment

Acoustic enrichment (AE) consisted of pulsed white noise (75 dB SPL) delivered in a sound-attenuating chamber (Coulbourn Instruments) as described previously (Clause et al., 2014). Pulse length was set to 138ms, and pseudorandomly presented with an inter-pulse length of 0-450ms and a duty cycle of 47%. Acoustic enrichment was started immediately after noise exposure and continued for 7 d before animals were used for ABR measurements, behavioral testing, and preparation of brain slices. Mice in the AE control group (AE-only) were placed in the AE chamber on the same developmental day as NE-AE mice, after which they were treated identically to NE-AE mice.

4.2.8 Slice preparation

Coronal brainstem slices were prepared from vglut2-cre-dT- loxP and vgat-ires-cre-dT-loxP mice of either sex at P26-30. For brain slice preparation, animals were deeply anaesthetized with isoflurane, decapitated, and their brains were removed. Coronal midbrain slices (300 μm) were then prepared as previously described (Sturm et al., 2014) using a vibrating microtome and incubated to 34° C in artificial cerebrospinal fluid (ACSF) (composition in mM; 0.25 7 H_2O x $MgSO_4$, 124 NaCl, 5 KCl, 10 Dextrose, 1.25 KH_2P0_4, 26 $NaHCO_3$, 2 $CaCl_2$). Brain slices were stored in an interface chamber 1h (30m incubation at 34° C followed by 30m rest at 22-25° C) prior to beginning recordings.

4.2.9 Electrophysiological recordings

Whole-cell recordings were aimed at the CNIC as previously described (Sturm et al., 2014). Recordings were performed in a submersion-type chamber (3-4 ml/min perfusion with oxygenated ACSF at 22-25° C) mounted on an upright microscope (Zeiss AxioExaminer A1) and were targeted at dT-expressing neurons under epifluorescent illumination. Borosilicate glass recording pipettes (3-6 MΩ) contained a potassium-based internal solution containing (composition in mM; 115 K-Gluconic acid ($C_6H_{11}O_7K$), 5 KCl, 11 EGTA, 1 $MgCl_2$ X $6H_2O$, 1 $CaCl_2$ X $2H_2O$, 10 HEPES, 0.3 GTP disodium salt, 2.0 ATP disodium salt and 0.5 % biocytin, pH 7.2, 314 mOsm/l). Whole-cell currents in voltage-clamp and current-clamp modes were acquired (Multiclamp 700B amplifier, Digidata- 1440A A/D converter, Molecular Devices) at a sampling rate of 4kHz using pClamp 10 software (Molecular Devices). Current-voltage (IV) plots were generated in current-clamp mode with 15pA current steps. Spontaneous excitatory

(sEPSC) and inhibitory (sIPSC) currents were recorded in voltage-clamp mode, at -65mV and 0mV, respectively.

4.2.10 Blinding procedure

Noise induction, ABR measurements, and behavioral startle measurements where performed by Ms. Hannah Roos (HR). Analysis of ABRs and startle data as well as slice experiments and their analysis were performed by JS.

HR assigned a unique identification number to each animal, and each animal was marked by a system of tattoos. JS performed synaptic input mapping without information about the ABR and startle-behavior data. However, JS was aware of whether or not each animal had been noise-traumatized. For experiments that involved acoustic enrichment with pulsed white noise, JS was aware of whether the experimental animal had received acoustic enrichment at the time of input mapping. While recording and analyzing electrophysiological data and ABR thresholds, JS was blinded to tinnitus behavioral status. For analysis, data from animals in each experimental condition were grouped together into a single software folder, with data from each cell and animal being identified only by the date that the recording was performed. During the analysis period, the behavioral statuses that corresponded to each recording date were maintained on a separate computer not accessed by JS. Only after all data were analyzed did JS match recording dates with tinnitus behavioral status. At this point data were entered into a summary data file, which was then used for inter-group statistical comparisons.

4.2.11 Synaptic input mapping and map analysis

The spatial distribution of presynaptic inputs to CNIC neurons was determined using focal photolysis of caged glutamate as described in Chapter 3 (see Methods Chapter 3, section 3.2). Evoked synaptic responses were distinguished from spontaneous synaptic events and direct stimulations using the same detection criteria described in Chapter 3 (see section 3.2.6). Excitatory and inhibitory input map areas were calculated as the sum of excitatory and inhibitory synaptic response sites, respectively. The synaptic charge transferred (pC) at each response site was calculated over a 150ms window, from 10ms post-stimulus to 160ms post-stimulus, and averaged across all available mapping iterations (1-3). For each cell, the total amounts of excitatory and inhibitory synaptic charge transferred were determined as the sum of excitatory and inhibitory synaptic charges found at excitatory and inhibitory synaptic response sites, respectively.

Excitation: Inhibition index: Excitation: Inhibition indices for individual cells were calculated in terms of input area and input charge according to the following equation:

$\boldsymbol{E: I\ index} = \frac{(exci - inhi)}{(exci + inhi)}$, where the values "exci" and "inhi" are the input areas or input charges for each cell.

4.2.12 Spontaneous synaptic event analysis

Spontaneous post-synaptic currents: sEPSCs and sIPSCs were analyzed using MiniAnalysis software (Synaptosoft). The frequencies and amplitudes of sEPSCs and sIPSCs were determined

for each neuron recorded. E:I indices of total synaptic charge were calculated according to the following equation:

$$\textbf{\textit{E: I index}} = \frac{(total\ sEPSC\ strength - total\ sIPSC\ strength)}{(total\ sEPSC\ strength + total\ sEPSC\ strength)}$$, where total sEPSC strength is the sum of sEPSC amplitudes (pA) recorded over 60s period, and total sIPSC strength is the sum of sIPSC amplitudes (pA) recorded over 60s.

4.2.13 Distinguishing type 1 and type 2 vgat+ neurons

To distinguish between type 1 and type 2 GABAergic neurons, an inhibitory input map threshold was set. Neurons that exhibited inhibitory input map areas $\leq 0.25 \times 10^5\ \mu m^2$ and total inhibitory input charges ≤ 5pC were considered type 2 neurons. Neurons that exhibited either inhibitory input map area $> 0.25 \times 10^5\ \mu m^2$ or total inhibitory input charge > 5pC were considered type 1 neurons.

4.2.14 Intrinsic properties of type 1 and type 2 vgat+ neurons

Intrinsic membrane properties were derived from current-voltage plots collected in current-clamp mode using 15 pA steps. Input resistance was measured with -15 pA injections from rest. Depolarization and repolarization slopes of action potentials were measured as the maximum slope during the depolarization phase and the minimum slope during repolarization phase of a spike, respectively. Action potential half height width was measured as the width of a spike when voltage= spike threshold + (spike amplitude/2). Spike threshold was measured as the membrane potential at which the depolarization slope shows the first abrupt change.

4.2.15 Gap detection behavior analysis

Gap detection ratios were determined individually for each sound frequency as the average startle magnitude in the presence of a background sound gap divided by the average startle magnitude in the absence of a sound gap. Gap ratio changes were defined as the gap detection ratio obtained before noise-exposure (or control) subtracted from the gap detection ratio obtained 7d later.

4.2.16 PPI behavior analysis

PPI ratios were determined individually for each sound frequency as the average startle magnitude in the presence of a prepulse sound divided by the average startle magnitude in the absence of that prepulse sound. PPI ratio changes were defined as the PPI ratio obtained before noise-exposure (or control) subtracted from the PPI ratio obtained 7d later.

4.2.17 ABR threshold analysis

ABR thresholds were analyzed with Biosig software (Biosig) and were defined as the minimum sound intensity (in dB SPL) that a given click or tone burst was able to elicit at least 2 waves in the ABR waveform and.

4.2.18 Statistical analysis

Data are presented as mean +/- SEM. Data were tested for normal distribution using Bartlett's

test. For independent, two-group comparisons, Students t-tests (two-tailed) and Mann-Whitney tests were used to determine statistical significance (GraphPad Prism). For two-group comparisons that involved repeated measures (gap behavior, PPI behavior and ABR thresholds), paired t tests (two-tailed) were used. For 3- and 4- group comparisons, One-way ANOVAs and Kruskal-Wallis tests were used to determine statistical significance (GraphPad Prism). Multiple comparisons were corrected for with the Tukey method (ANOVAs) and the Dunn pairwise method (Kruskal-Wallis). For cumulative probably data, Kolmogorov-Smirnov tests were used. Statistical significance was set to $p < 0.05$.

4.3 RESULTS

4.3.1 Tinnitus behavior emerges in a subset of noise-traumatized mice

In both humans and rodent models, noise-induced hearing loss leads to tinnitus in only a fraction of the population (humans: Nondahl et al., 2011; Yankaskas, 2013, rodents: Dehmel et al., 2012; Li et al., 2013). We elicited noise-induced hearing loss by unilaterally exposing 20-23 day old (P20-23) mice for 45 min to continuous noise (116 dB, 1 kHz band-width centered at 16 kHz). One week later, mice were assessed for hearing threshold shifts using auditory brainstem responses (ABRs) and tested for behavioral evidence of tinnitus using the acoustic startle gap detection method (Turner et al., 2006; Dehmel et al., 2012; Li et al., 2013). This method is based upon inhibition of the acoustic startle reflex (ASR) by a silent gap embedded in a background sound preceding the startle stimulus by 130 ms. Mice that experience tinnitus exhibit a decrease

in gap-mediated inhibition of the ASR at sound frequencies where their presumed tinnitus percept “fills in the gap” (Turner et al., 2006).

Consistent with previous reports (Li et al., 2013), approximately 50% of noise-exposed mice (19/37 animals) exhibited behavioral evidence of tinnitus, as indicated by a significant reduction in gap-mediated inhibition of the ASR (Figure 4-1, Figure 4-2). A reduction in gap detection was found exclusively for sound frequencies that were at or above the hearing-loss frequency range (16-32 kHz) (Figure 4-1, Figure 4-2 and Figure 4-3), which mirrors the situation in human patients, where the frequency of tinnitus is usually at or above the frequency of hearing loss (Schaette and Kempter, 2009; Sereda et al., 2014). The degree of hearing loss after noise exposure was moderate (10-20 dB at 16-32 kHz) and indistinguishable between noise-exposed mice with behavioral evidence of tinnitus (NE-T) and mice without tinnitus (NE-NT) (ABR threshold shift 16-32 kHz: NE-NT: 17.9 ± 2.9 dB, NE-T: 18.2 ± 2.1, n= 33 animals, p= 0.93) (Figure 4-3). Importantly, impaired gap-detection in NE-T mice was not due to impairment in detecting the background sounds in which the silent gaps were embedded, because prepulse inhibition of the ASR (PPI) with prepulses of similar intensities and frequencies as the background sounds used in gap-detection testing was normal (PPI ratio change: Control: -0.12 ± 0.02, NE-NT: -0.10 ± 0.03, NE-T: 0.00 ± 0.03, n= 255 sound frequencies, p= 0.08) (Figures 4-1 and 4-2). Taken together, these behavioral results indicate that while all noise-exposed mice exhibit similar hearing loss, only about 50% of exposed mice develop behavioral evidence of tinnitus.

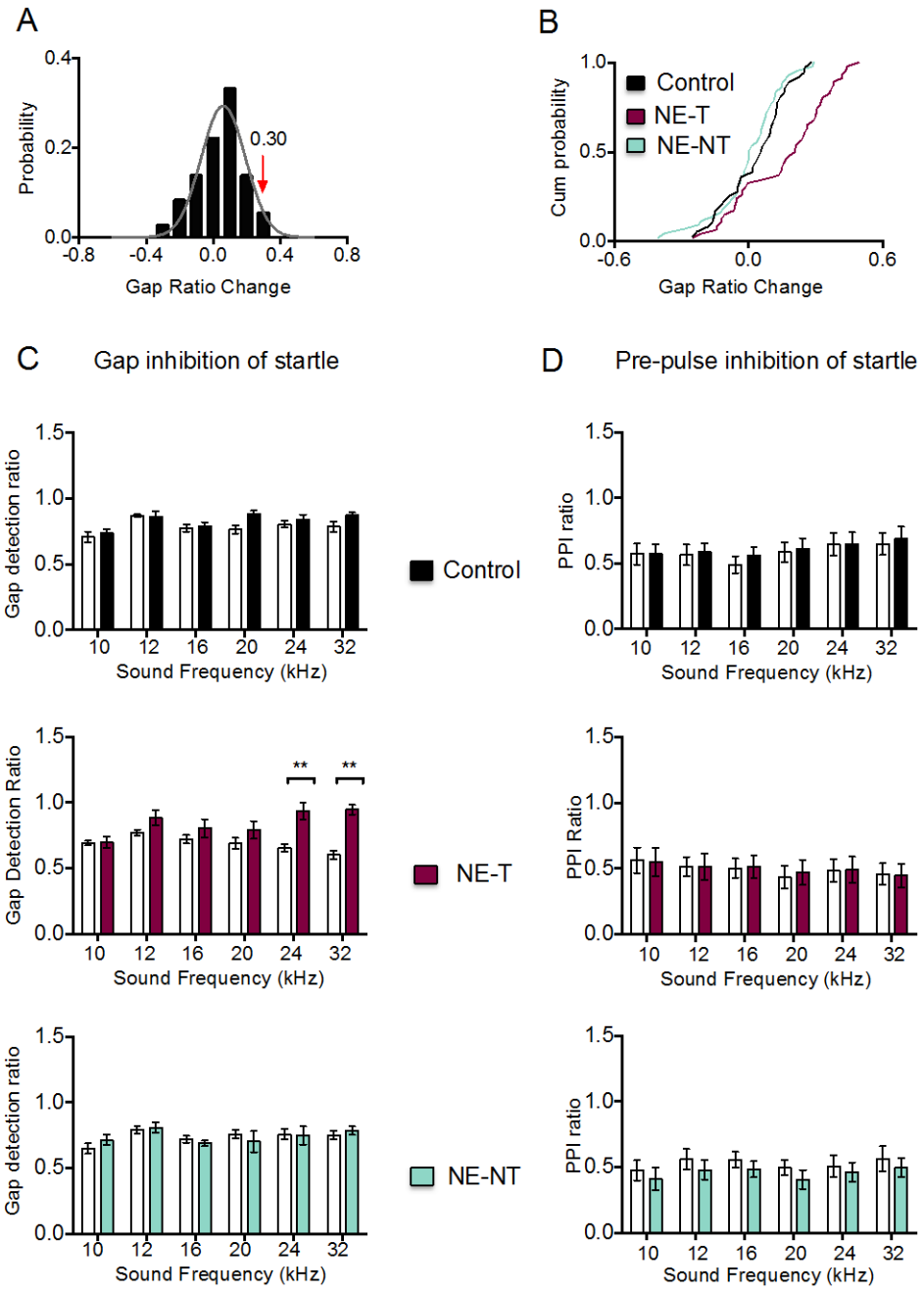

Figure 4-1. Effects of noise exposure on gap detection and PPI in vglut2-cre-dT-loxP mice.

Figure 4-1. Effects of noise exposure on gap detection and PPI in vglut2-cre-dT-loxP mice.

(A) Probability distribution of changes in gap startle ratios (response to startle stimulus with gap present/response to startle stimulus alone) over a one week period in control mice. Data are fitted with normal distribution (gray curve, $\mu = 0.02$, $\delta = 0.140$, $n = 72$ sound frequencies). Gap ratio changes greater than 2δ above the distribution mean (0.30) are considered evidence of tinnitus. **(B)** Cumulative probability distribution for changes in gap ratios following traumatic noise exposure. **(C)** Summary graphs of gap startle ratios before and 7d after noise-exposure. Gap detection ratios remain stable in NE-NT mice, but are increased for higher sound frequencies in NE-T mice (24 kHz, Before= 0.73 ± 0.05; After= 1.03 ± 0.07, n= 9 animals, $p< 0.01$, Paired t test) (32 kHz, Before= 0.74 ± 0.04; After= 0.93 ± 0.08, $p< 0.01$, Paired t-test). **(D)** Summary graphs of PPI startle ratio before and after noise-exposure. Error bars represent SEM. Stars mark statistical significance. *= $p< 0.05$, **= $p< 0.01$.

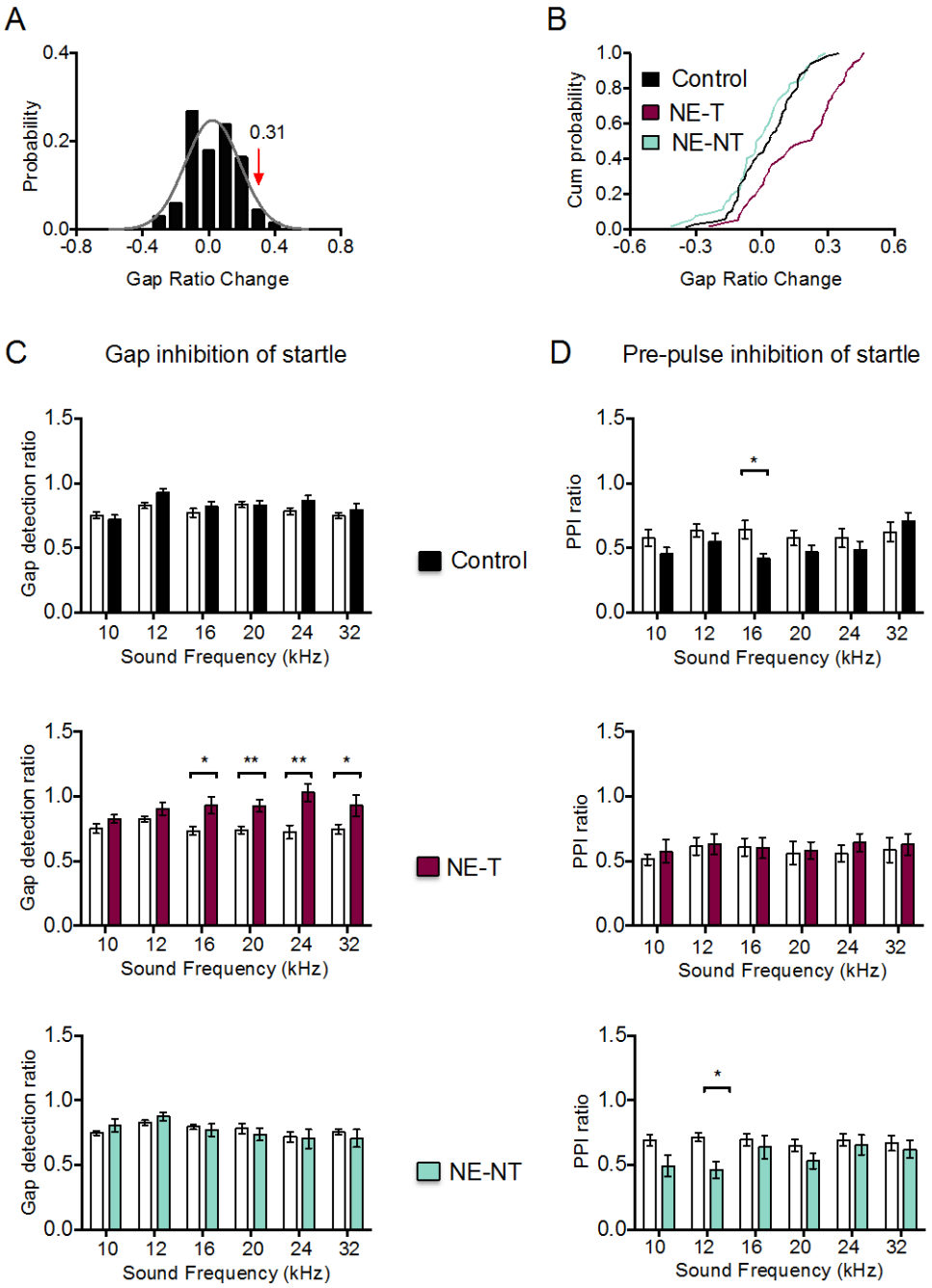

Figure 4-2. Effects of noise exposure on gap detection and PPI in vgat-ires-cre-dT-loxP mice.

Figure 4-2. Effects of noise exposure on gap detection and PPI in vgat-ires-cre-dT-loxP mice.

(A) Probability distribution of changes in gap startle ratios (response to startle stimulus with gap present/response to startle stimulus alone) over 1w period in control mice. Data fitted with normal distribution (gray curve, $\mu = 0.02$, $\delta = 0.145$, $n = 72$). Gap ratio changes greater than 2δ above the distribution mean (0.31) are considered evidence of tinnitus. **(B)** Cumulative probability distribution for changes in gap following noise exposure. **(C)** Summary graphs of gap startle ratios before and 7d after noise-exposure. Gap detection ratios remain stable in NE-NT mice, but are increased for higher sound frequencies in tinnitus mice (16 kHz, Before= 0.73 ± 0.03; After= 0.93 ± 0.07, n= 9 mice, $p< 0.05$, Paired t-test) (20 kHz, Before= 0.74 ± 0.03; After= 0.93 ± 0.05, n= 9 mice, $p< 0.01$, Paired t-test) (24 kHz, Before= 0.73 ± 0.05; After= 1.03 ± 0.07, n= 9 mice, $p < 0.01$, Paired t-test) (32 kHz, Before= 0.74 ± 0.04; After= 0.93 ± 0.08, n= 9 animals, $p< 0.05$, Paired t-test**). (D)** Summary graphs of PPI startle ratio before and after noise-exposure. Error bars represent SEM. Stars mark statistical significance. *= $p < 0.05$, **= $p< 0.01$. Decreases in PPIRs were observed at 16 kHz (Before= 0.64 ± 0.07; After= 0.42 ± 0.04, n= 12 mice, $p< 0.05$, Paired t-test) in control animals and at 12 kHz (Before= 0.71 ± 0.07; After= 0.46 ± 0.03, n= 8 mice $p< 0.01$, Paired t-test) in NE-NT animals.

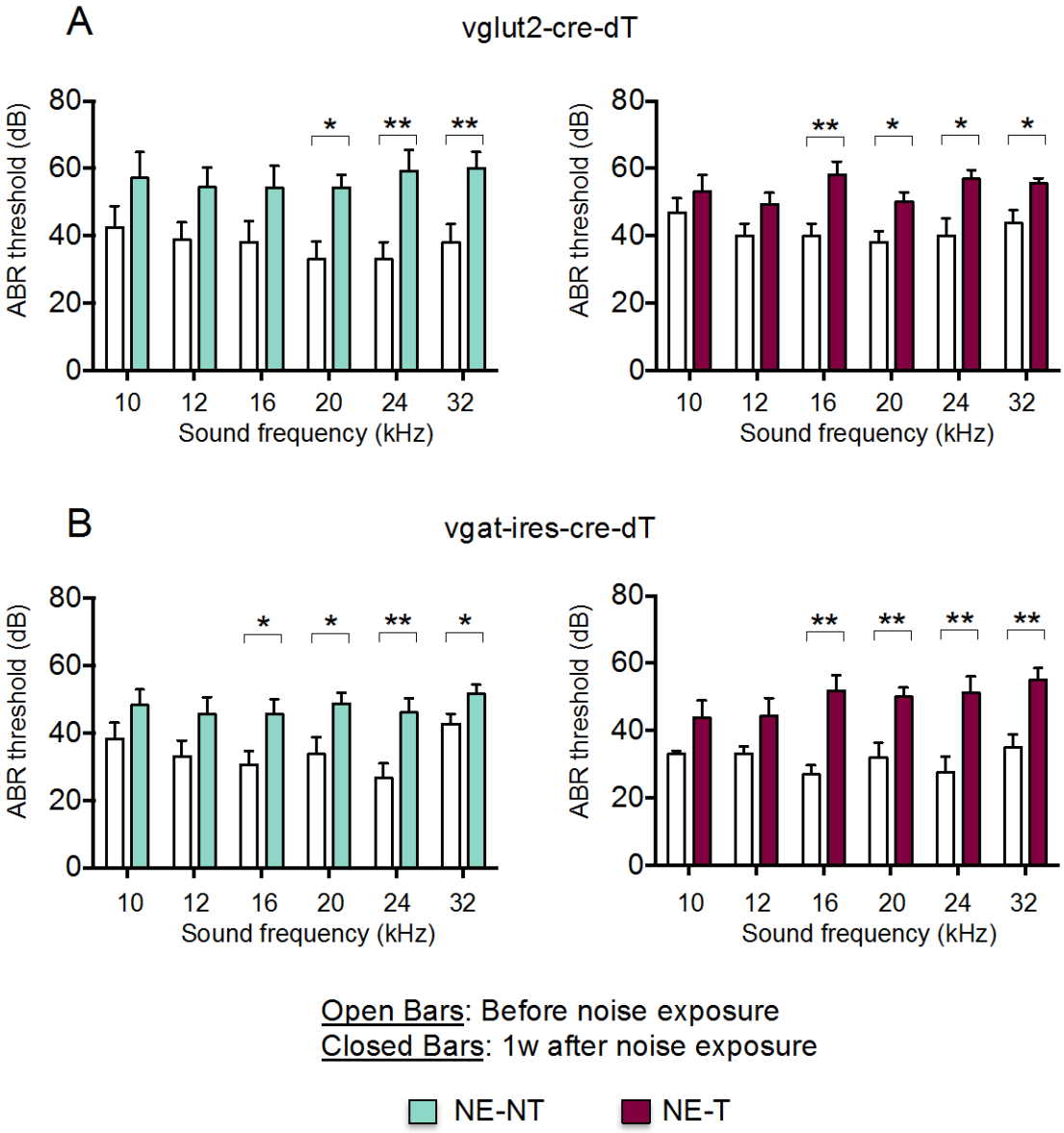

Figure 4-3. ABR thresholds are similarly elevated in mice with or without evidence of tinnitus.

Figure 4-3. ABR thresholds are similarly elevated in mice with or without evidence of tinnitus.

(A) Summary graphs of ABR thresholds before and 7d after noise exposure in vglut2-cre-dT animals. Thresholds for higher sound frequencies were elevated following noise exposure in both NE-NT and NE-T mice. In NE-NT mice, threshold elevations were found at 20 kHz (Before= 33.1 ± 5.0 dB; After= 54.1 ± 3.3 dB, n= 9 mice, p< 0.01, Paired t-test), 24 kHz (Before= 33.1 ± 5.0 dB; After= 58.1 ± 5.5 dB, n= 9 mice, p< 0.01, Paired t-test) and 32 kHz (Before= 38.1 ± 5.3 dB; After= 60.0 ± 4.2 dB, n= 9 mice, p< 0.01, Paired t-test). In NE-T mice, threshold elevations were found at 16 kHz (Before= 40.1 ± 3.3 dB, After= 58.1 ± 3.9 dB, n= 10 mice, p< 0.01, Paired t-test), 20 kHz (Before= 38.1 ± 3.3 dB; After= 50.0 ± 2.0 dB, n= 10 mice p< 0.05, Paired t-test), 24 kHz (Before= 40.0 ± 5.2 dB; After= 56.9 ± 6.7 dB, n= 10 mice, p< 0.05, Paired t-test) and 32 kHz (Before= 43.8 ± 4.0 dB; After= 56.6 ± 1.5 dB, n= 10 mice <0.05, Paired t test**) (B)** same as A, but for vgat-ires-cre-dT animals. Thresholds for higher sound frequencies were elevated following noise exposure. In NE-NT mice, significant threshold elevations were found at 16 kHz (Before= 30.6 ± 4.0 dB; After= 45.6 ± 4.4 dB, n= 9 mice, p< 0.05, Paired t-test), 20 kHz (Before= 33.8 ± 5.0 dB; After= 48.8 ± 3.2 dB, n= 9 mice, p< 0.05, Paired t-test), 24 kHz (Before= 26.7 ± 4.3 dB; After= 46.1 ± 4.2 dB, n= 9 mice, p< 0.05, Paired t-test) and 32 kHz (Before= 42.8 ± 2.9 dB; After= 51.7 ± 2.8 dB, n= 9 mice, p< 0.01, Paired t-test). In NE-T mice, significant threshold elevations were found at 16 kHz (Before: 26.9 ± 2.8 dB; After= 51.9 ± 4.6 dB, n= 10 mice, p< 0.01, Paired t-test), 20 kHz (Before: 31.9 ± 4.5 dB; After= 50.0 ± 2.7 dB, n= 10 mice, p< 0.01, Paired t-test), 24 kHz (Before: 27.5 ± 4.6 dB; After= 51.3 ± 4.7 dB, n= 10 mice, p< 0.01, Paired t-test) and 32 kHz (Before: 35.0 ± 3.9 dB; After= 55.0 ± 3.5 dB, n= 10 mice, p< 0.01, Paired t-test). Error bars represent SEM. Stars indicate statistical significance. *= p< 0.05, **= p< 0.01.

4.3.2 Reorganization of synaptic inputs onto excitatory IC neurons

The presence of behavioral evidence of tinnitus in only a fraction of noise-exposed mice affords the opportunity to associate hearing-loss-induced changes in auditory circuits to the presumed perception of phantom sounds. To identify hearing loss reorganizations of local synaptic circuits in the central nucleus of the IC (CNIC), we obtained whole-cell patch-clamp recordings from IC neurons contralateral to the exposed ear and used LSPS with caged glutamate in brain slices to map their synaptic inputs (Figure 4-4). Since excitatory and inhibitory neurons in the IC cannot be reliably distinguished on the basis of morphological or physiological criteria (Malmierca et al., 1993; Sivaramakrishnan et al., 2001), we targeted recordings from glutamatergic neurons using a mouse line in which the expression of the fluorescent protein dtTomato is restricted to glutamatergic neurons expressing the Cre protein under the promoter for the vesicular glutamate transporter 2 (vglut2+).

In control (unexposed) vglut2+ mice aged P26-30, glutamatergic CNIC neurons received both excitatory and inhibitory local inputs, which were recoded while holding the neurons at -65 mV or 0 mV, respectively (Figure 4-4 C, D). Local input maps were dominated by synaptic inhibition, as indicated by greater inhibitory input map areas (inhi area= 210% ± 25% of exci area, n= 12 neurons, n= 6 animals), greater total inhibitory postsynaptic charge (inhi charge= 287% ± 97% of exci charge, n= 12 neurons, n= 6 animals), and negative excitation: inhibition (E:I) indices for input area ($E:I_{area}$= -0.50 ± 0.09, n= 12 neurons, n= 6 animals) and input charge ($E:I_{charge}$= -0.58 ± 0.15, n= 12 neurons, n= 6 animals) (see Methods; 4.2.10.) (Figure 4-4 D, E). The dominance of inhibition at P26-30 is similar to the dominance of inhibition at P19-22 (Sturm et al., 2014), suggesting that developmental synaptic refinement in intrinsic IC circuits is largely complete by the end of the third postnatal week.

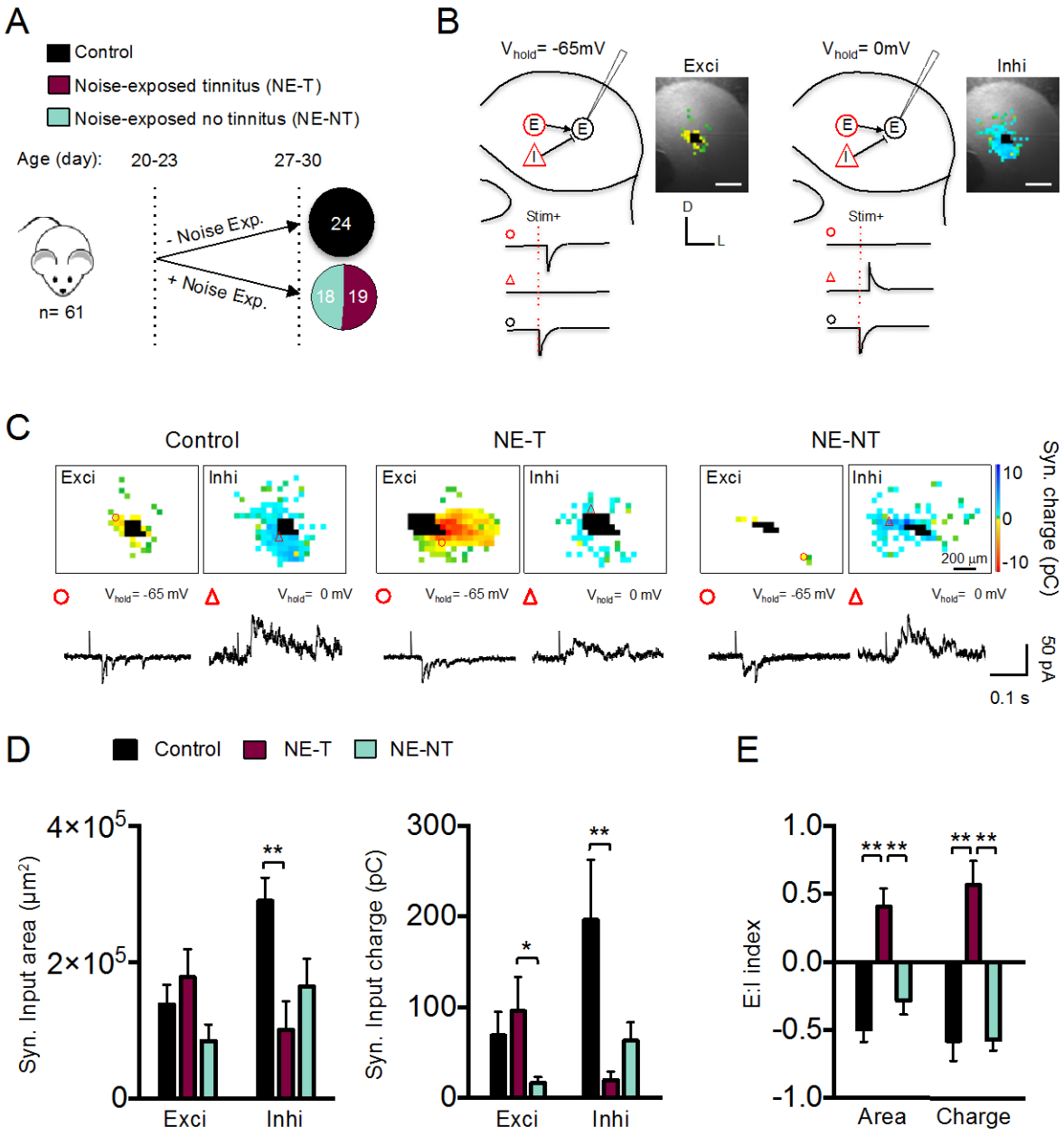

Figure 4-4. Noise-Induced reorganization of synaptic input maps onto glutamatergic IC neurons.

Figure 4-4. Noise-Induced reorganization of synaptic input maps onto glutamatergic IC neurons.

(A) Mice undergo noise trauma at P20-23 and are then tested for behavioral evidence of tinnitus 7d later. 19 of 37 noise-exposed mice (51%) exhibited evidence of tinnitus. **(B)** Schematic of synaptic input mapping of vglut2+ excitatory neurons (black circle). Excitatory (circle) and inhibitory (triangle) inputs are shown in red. Excitatory and inhibitory synaptic input maps are obtained by holding the membrane voltage of the recorded neuron at -65mV (left) and 0mV (right), respectively, during laser stimulation. Example excitatory and inhibitory maps for a neuron are overlaid over a photograph of the corresponding IC slice. Scale bar 400 μm **(C)** Examples of excitatory and inhibitory synaptic input maps from control (left), noise-exposed with tinnitus (NE-T, middle), and noise exposed without tinnitus (NE-NT, right) mice. Traces illustrate excitatory (circle) and inhibitory (triangle) synaptic responses to glutamate uncaging (red line) at the map locations indicated by symbols. Uncaging sites that elicited direct responses at the recorded neuron are indicated in black. **(D)** Changes in synaptic input area and total synaptic charge induced by traumatic noise exposure. Total excitatory charge (right) was decreased in NE-NT mice compared to NE-T mice (Exci Charge, Control= 68.8 ± 25.7 pC; NE-T= 95.8 ± 37.8 pC; NE-NT= 16.4 ± 6.4 pC, n= 36 neurons, n= 19 animals, p= 0.04, Kruskal-Wallis test). In contrast, inhibitory input area (left) and total inhibitory charge (right) were each decreased in NE-T mice compared to control mice (Inhi Area, Control= $2.9 \times 10^5 \pm 0.34 \times 10^5$ μm^2; NE-T= $1.0 \times 10^5 \pm 0.42 \times 10^5$ μm^2; NE-NT= $1.7 \times 10^5 \pm 0.40 \times 10^5$ μm^2, n= 34 neurons, n= 19 animals, p= 0.006, one-way ANOVA) (Inhi Charge, Control= 196.6 ± 66.3 pC; NE-T= 19.7 ± 9.7 pC; NE-NT= 63.1 ± 20.2 pC n= 33 neurons, p= .0009, Kruskal-Wallis test). **(E)** Changes in E:I Index induced by noise-exposure. E:I index measures excitation: inhibition balance and is calculated as excitation minus inhibition, divided by the sum of excitation and inhibition. In NE-T animals, the E:I indices for input area (left) and input charge (right) were shifted from the negative values in control and NE-NT animals, to positive values (Area, Control= -0.50 ± 0.09; NE-T= 0.41 ± 0.14; NE-NT= -0.28 ± 0.10, n= 34 neurons, n= 19 animals, $p < 0.0001$, one-way ANOVA) (Charge, Control= -0.58 ± 0.15; NE-T= 0.57 ± 0.18; NE-NT= -0.57 ± 0.08, n= 33 neurons, n= 19 animals, $p < 0.0001$, one-way ANOVA). Error bars represent SEM. *= $p < 0.05$, **= $p < 0.01$ in post-hoc, pairwise assessments corrected for multiple comparisons. *Mapping data for control animals is same as data shown in Figure 3-6 in Chapter 3.*

All noise-exposed mice showed a reorganization of synaptic input maps of glutamatergic IC neurons, but the nature of this reorganization differed between mice with and without behavioral evidence of tinnitus. In NE-T mice, the size and the strength of excitatory input maps of glutamatergic neurons remained unchanged, as the excitatory input areas and total excitatory postsynaptic charges in NE-T were not significantly different from control animals (Figure 4-4 C, D). However, local synaptic inhibition to glutamatergic neurons was substantially diminished, as evidenced by dramatically smaller inhibitory input maps (NE-T= 34.7% ± 14.4% of control, n= 22 neurons, n= 12 animals) and smaller total inhibitory charges (NE-T= 10.0% ± 4.9% of control, n= 22 neurons, n= 12 animals) (Figure 4-4 C, D). As a consequence, in NE-T mice, the E: I indices for local inputs to glutamatergic neurons were profoundly shifted from the negative values typical for control mice ($E:I_{area}$= -0.50 ± 0.09, $E:I_{charge}$= -0.58 ± 0.15, n= 12 neurons, n= 6 animals), to positive values ($E:I_{area}$= 0.41 ± 0.14, $E:I_{charge}$= 0.57 ± 0.18, n= 10 neurons, n= 6 animals) (Figure 4-4 E). E: I indices were calculated for each neuron as the amount of inhibition (area or charge) received subtracted from the amount of excitation received, together divided by the sum of excitation and inhibition. Negative E: I indices indicate a dominance of inhibition, whereas positive E: I indices indicate a dominance of excitation. Thus, in the IC of control animals, the excitation: inhibition balance arising from local circuits onto glutamatergic neurons is strongly dominated by inhibition, whereas in NE-T mice, local synaptic inputs onto excitatory neurons are strongly dominated by excitation.

Noise-exposed mice without evidence of tinnitus (NE-NT) also showed a reorganization of local inputs to glutamatergic IC neurons, but the pattern of this reorganization was markedly different from that of NE-T mice. First, in NE-NT mice, total excitatory synaptic charge was significantly reduced compared NE-T mice and trended towards being reduced compared to

control mice (p= 0.12, student's t-test) (Figure 4-4 C, D). Secondly, synaptic inhibition onto glutamatergic neurons, which was greatly diminished in NE-T mice, was not significantly reduced in NE-NT mice (Figure 4-4 C, D). Although we observed trends towards both decreased excitatory and inhibitory input map areas in NE-NT mice compared to control mice, neither trend reached statistical significance (Figure 4-4 C, D). As a result, in NE-NT mice there was no significant change of the overall E:I index of local synaptic inputs to glutamatergic neurons, and local inputs remained dominated by inhibition (Figure 4-4 D).

We next characterized noise-induced changes in synaptic input on the level of spontaneous synaptic events, which, in addition to the activity of local IC connections, also captures changes in ascending or descending external inputs (Figure 4-5). Irrespective of the presence or absence of tinnitus, all noise-traumatized mice exhibited increased spontaneous excitatory drive. This increase was reflected by an approximately two-fold increase in the frequency (NE-T= 294% ± 43% of control, NE-NT= 188% ± 20% of control), but not the amplitude of spontaneous excitatory postsynaptic currents (sEPSC) (Figure 4-5 A, C). In contrast, spontaneous inhibitory drive was unaffected by noise exposure, as indicated by stable frequencies and amplitudes of spontaneous inhibitory postsynaptic currents (sIPSC) (Figure 4-5 B, C). To determine the E:I balance of spontaneous synaptic events, we calculated the E:I index for the total synaptic strength received by individual excitatory neurons over a 60 s period (see Methods; 3.2.11). Similar to the E:I index of intrinsic input maps, the E:I index of spontaneous synaptic events shifted to positive values in NE-T mice, but was unchanged in NE-NT mice (Figure 4-5 D).

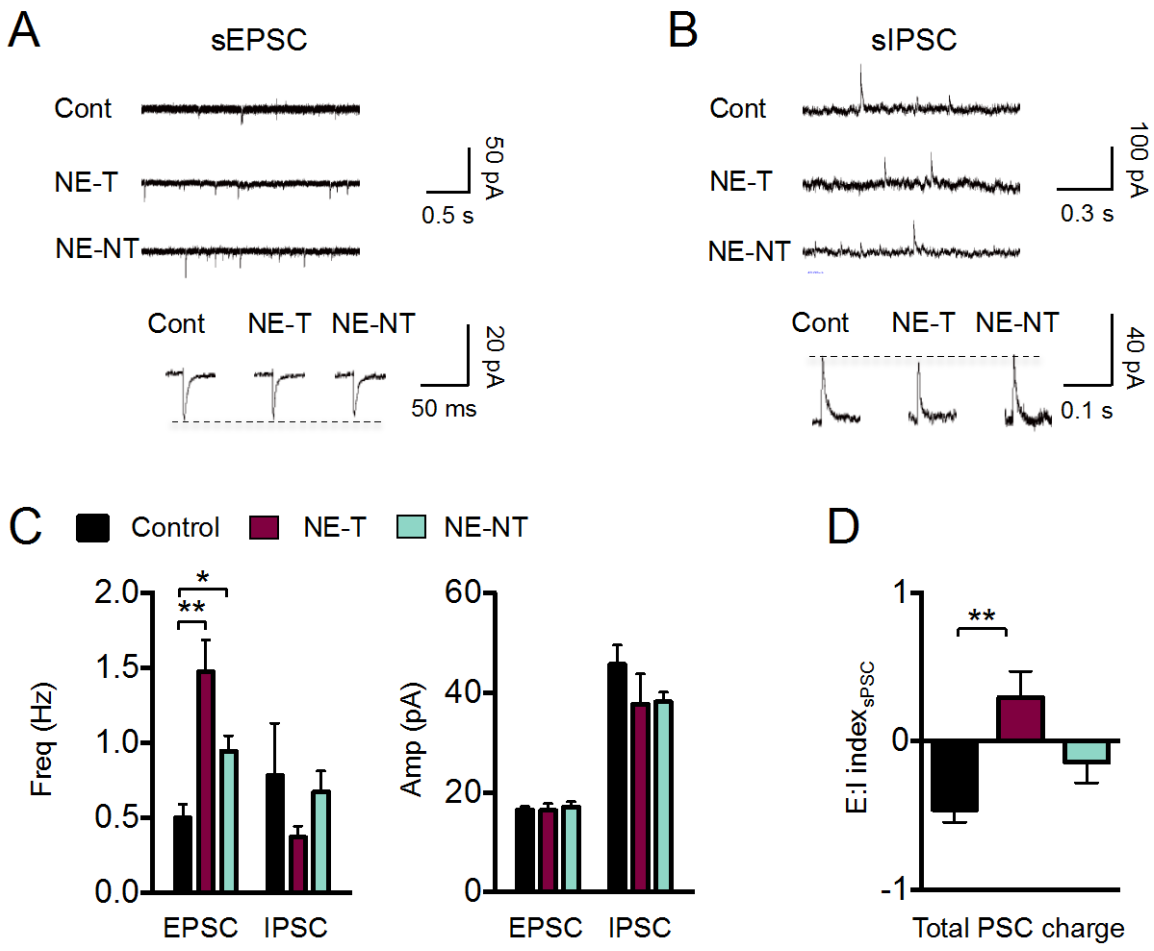

Figure 4-5. Spontaneous synaptic events onto glutamatergic IC neurons in noise-traumatized mice.

(A) Example traces of sEPSCs. Individual event traces are average of 30-100 **e**vents from single cell. **(B)** Same as A, but for sIPSCs. **(C)** Summary graphs for frequency (left) and amplitude (right) of sPSCs. sEPSC frequency was increased in both NE-T and NE-NT mice compared to control mice (Control= 0.50 ± 0.09 Hz; NE-T= 1.47 ± 0.21 Hz; NE-NT= 0.94 ± 0.10 Hz, n=32 neurons, n= 19 animals, p= 0.0002, Kruskal-Wallis test). sIPSC frequency was indistinguishable between groups (p= 0.40, Kruskal-Wallis test). Amplitudes of sEPSC and sIPSC did not differ between control and noise-exposed groups (sEPSC Amp, n= 32 neurons, n= 19 animals, p=0.87, one-way ANOVA; sIPSC Amp, n= 29 neurons, n= 19 animals, p= 0.18, Kruskal-Wallis test). **(D)** The E:I index calculated for the sum of PSC amplitudes over 60s was increased in NE-T mice relative to control mice (Control= -0.46 ± 0.09; NE-T= 0.29 ± 0.18; NE-NT= -0.14 ± 0.14, n= 29 neurons, n= 19 animals, p= 0.002, one-way ANOVA). Error bars represent SEM. *= p< 0.05, **= p< 0.01 in post-hoc, pairwise assessments corrected for multiple comparisons.

In summary, our results demonstrate that traumatic noise exposure leads to a notable reorganization of synaptic inputs received by glutamatergic IC neurons and that the specific nature of this reorganization is distinct in mice that do and do not develop behavioral evidence of tinnitus. In NE-NT mice, the pattern of synaptic reorganization maintains the overall excitation: inhibition balance, whereas in NE-T mice the pattern of reorganization leads to a profound shift in excitation: inhibition balance in the direction of excitation.

4.3.3 Two types of GABAergic IC neurons

Having determined how hearing loss affects the synaptic inputs to glutamatergic IC neurons, we next examined the synaptic inputs of inhibitory neurons, which are GABAergic in the IC and constitute 20-25% of the population (Oliver et al., 1994). GABAergic IC neurons were identified using mice in which dtTomato expression is restricted to neurons expressing Cre under the promoter for the vesicular GABA transporter (vgat+), which is a marker of all GABAergic neurons in the IC (Ito et al., 2009). Based on their local inputs, GABAergic IC neurons fell into two categories. Type 1 neurons (21/30 neurons) received both excitatory and inhibitory local synaptic inputs, with a dominance of local inhibition, whereas type 2 neurons (9/30 neurons) received predominantly excitatory inputs with very few or no inhibitory inputs (inhi input area $\leq$ 0.25 x 10^5 μm^2 and inhi input charge $\leq$ 5pC, see Methods; 3.2.12) (Figure 4-6 A). Type 1 and type 2 neurons did not differ in their intrinsic membrane properties (Table 1), but clearly differed in the magnitude of their direct responses to glutamate uncaging at the soma, which were over 2-fold larger in type 2 neurons than in type 1 neurons (Figure 4-6 A, B). In addition, type 2 neurons received greater amount of spontaneous excitatory drive, as indicated by greater amplitudes and frequencies of sEPSCs (freq, type 2= 481% ± 175% of type 1, n= 21 neurons, n= 13 animals;

amp, type 2= 165% ± 24% of type 1, n= 21 neurons, n= 13 animals) (Figure 4-6 C). These two types of GABAergic IC neurons likely correspond to the two major classes of inhibitory neurons previously described in the IC (Ito et al., 2009; Ito and Oliver, 2012; Ito and Oliver, 2014). Type 2 neurons likely correspond to collicothalamic GABAergic projection neurons, which receive dense, axosomatic and dendritic glutamatergic synapses, whereas type 1 neurons likely correspond to local GABAergic interneurons, which receive fewer glutamatergic inputs, that are also located predominantly on dendrites (Ito and Oliver, 2012; Ito and Oliver, 2014).

The excitatory input maps of type 1 and type 2 GABAergic IC neurons were similar to each other, and also were similar to the excitatory input maps of glutamatergic IC neurons (mean input area: p= 0.31, n= 43 neurons, n= 19 animals; mean postsynaptic charge: p= 0.98, n= 43 neurons, n= 19 animals) (Figure 4-4, Figure 4-7 and Figure 4-9). The inhibitory input maps of type 1 GABAergic neurons, on the other hand, tended to be smaller than the inhibitory input maps of glutamatergic neurons, though the difference did not reach statistical significance for either input area (p= 0.28, n= 33 neurons, n= 16 animals) or input charge (p= 0.22, n= 33 neurons, n= 16 animals) (Figure 4-4 C and Figure 4-7 C). As a consequence, the E:I indices for input map area and input charge were both significantly more positive for type 1 GABAergic neurons than for glutamatergic neurons (Table 2), indicating that E: I equilibrium for type 1 inhibitory IC neurons is more balanced compared to glutamatergic neurons. In summary, our results identified three types of local IC networks: 1) glutamatergic neurons that receive excitation and inhibition with an E:I index that is strongly dominated by inhibition, 2) type 1 GABAergic inhibitory neurons that receive excitation and inhibition with an E:I index that is weakly dominated by inhibition and 3) type 2 GABAergic inhibitory neurons that receive excitation, but minimal local inhibition.

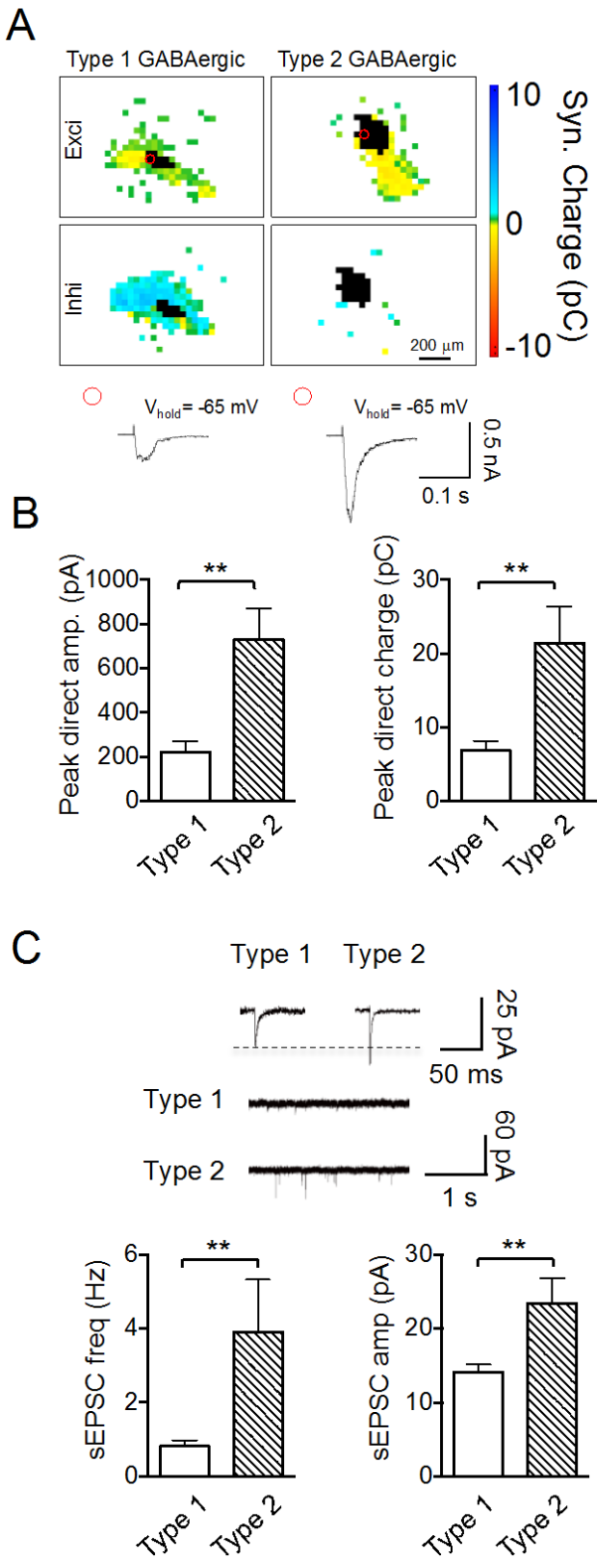

Figure 4-6 Two types of GABAergic IC neurons.

Figure 4-6. Two types of GABAergic IC neurons.

(A) Excitatory and inhibitory input maps from type 1 (left) and type 2 (right) vgat+ GABAergic neurons. Type 1 neurons receive both excitatory and inhibitory inputs (left), but type 2 neurons receive predominantly excitatory inputs (right). Stimulation sites eliciting direct glutamate responses are in black. Traces show membrane currents elicited by glutamate uncaging over the soma. Circle indicates location of stimulation site. **(B)** Direct response amplitude (left) and charge (right) are larger in type 2 than in type 1 neurons (Peak Amplitude, type 1= 223.0 ± 47.6 pA; type 2= 730.0 ± 139.2, pA, n= 30 neurons, p= 0.0007, Mann-Whitney test) (Peak Charge, Type 1= 6.9 ± 1.3 pC; Type 2= 21.4 ± 5.0 pC, n= 30 neurons, p= 0.005, Mann-Whitney test). **(C)** Spontaneous EPSCs of type 1 and type 2 neurons. The mean frequency and the mean amplitude of sEPSCs are greater for type 2 neurons than for type 1 neurons. (Frequency, type 1= 0.81 ± 0.16 Hz; Type 2= 3.9 ± 1.4 Hz, n= 21 neurons, n= 10 animals, p= 0.006, Mann-Whitney test) (Amplitude, type 1= 14.2 ± 1.0 pA; Type 2= 23.5 ± 3.4 pA, n= 24 neurons, p= 0.008, Mann-Whitney test). Error bars represent SEM. Stars indicate statistical significance. *= $p < 0.05$, **= $p< 0.01$.

Table 1. Intrinsic properties of type 1 and type 2 GABAergic IC neurons.

All recordings performed in vgat+ IC neurons from non-noise-exposed animals (input resistance, type 1: n = 10 neurons, n= 5 animals, type 2: n = 6 neurons, n= 4 animals, p = 0.82; depolarization slope, type 1: n = 9 neurons, n= 5 animals, type 2: n = 6 neurons, n= 5 animals, p = 0.79; repolarization slope, type 1: n = 9 neurons, n= 5 animals, type 2: n = 6 neurons, n= 4 animals, p = 0.53; half height width, type 1: n = 9 neurons, n= 5 animals, type 2: n = 6 neurons, n= 4 animals, p = 0.55; spike threshold, type 1: n = 10 neurons, n= 5 animals, type 2: n = 6 neurons, n= 4 animals, p = 0.82). Depolarization slope: maximum depolarizing slope, repolarization slope: minimum repolarizing slope, spike threshold: minimum voltage of first spike generation.

GABAergic Neuron	Input Resistance (MΩ)	Depolarization Slope (V/S)	Repolarization Slope (V/s)	Half height width (ms)	Spike threshold (mV)
Type 1	262.8 ± 42.9	38.7 ± 4.4	-38.0 ± 3.4	1.4 ± 0.1	-33.1 ± 1.8
Type 2	245.7 ± 53.9	40.4 ± 3.5	-41.2 ± 3.3	1.4 ± 0.1	-32.5 ± 1.7

Table 2. Excitation: inhibition balance for excitatory and inhibitory IC neurons.

All recordings were performed in either vgat+ or vglut2+ IC neurons from non-noise-exposed animals (E:I Index input area, vglut2+: n= 12 neurons, n= 6 animals, vgat+: n= 18 neurons, n= 10 animals, p= 0.030, Student's t test; E:I index input charge, vglut2+: n= 12 neurons, n= 6 animals, vgat+: n= 20 neurons, n= 10 animals, p= 0.048, Mann-Whitney test; E:I Index spontaneous events, vglut2+: n= 10 neurons, n= 6 animals, vgat+: n= 14 neurons, n= 10 animals, p=0.25, Student's t test).

	vglut2+	Type 1 vgat+	p value
E:I Index Input Area	-0.50 ± 0.09	-0.23 ± 0.07	0.030
E:I Index Input Charge	-0.58 ± 0.15	-0.28 ± 0.1	0.048
E:I Index Spont. Events	-0.46 ± 0.09	-0.27 ± 0.12	0.25

4.3.4 Reorganization of synaptic inputs onto GABAergic IC neurons

The effects of noise trauma on the input maps of type 1 and type 2 GABAergic neurons differed substantially from each another, as well as from glutamatergic neurons (Figures 4-7, 4-8 and 4-9). In NE-T mice, the excitatory input maps of type 1 GABAergic neurons dramatically decreased by 72% in size and by 83% in total synaptic charge, whereas the inhibitory input maps remained unchanged (Figure 4-7 B). As a result, the mean E:I index of input maps from type 1 neurons shifted to a significantly more negative value (Figure 4-7 D). Along the same lines, the mean E: I index of spontaneous synaptic events for type 1 GABAergic neurons trended towards decreasing, though this difference did not reach statistical significance (Figure 4-8 D). Thus, in NE-T mice, there is increased net inhibition of type 1 GABAergic neurons (disinhibition) and an increased net excitation of glutamatergic IC neurons, both of which may act synergistically to increase IC excitability.

In NE-NT mice, inhibitory input maps for type 1 GABAergic neurons decreased significantly, and excitatory input maps exhibited a trend towards decreasing that did not reach statistical significance ($p= 0.06$) (Figure 4-7 C). However, these changes did not disturb the mean E: I index, which remained stable compared to controls (Figure 4-7 D). Despite the stability of E:I balance on the level of local input maps for NE-NT animals, there was an increase in the spontaneous excitatory drive to these neurons (sEPSC amplitudes, $p= 0.05$, 172% ± 28% of control, $n= 21$ neurons, $n= 13$ animals; sEPSC frequencies 275% ± 100% of control, $p<0.02$, $n= 21$ neurons, $n= 13$ animals) (Figure 4-8 A, C), whereas sIPSCs were unaffected (Figure 4-8 B, C). As a result, the mean E: I index of spontaneous synaptic events for type 1 neurons from NE-NT mice shifted from the negative values present in control and NE-T mice, to a positive value (Figure 4-8 D), indicating increased synaptic excitation of type 1 neurons.

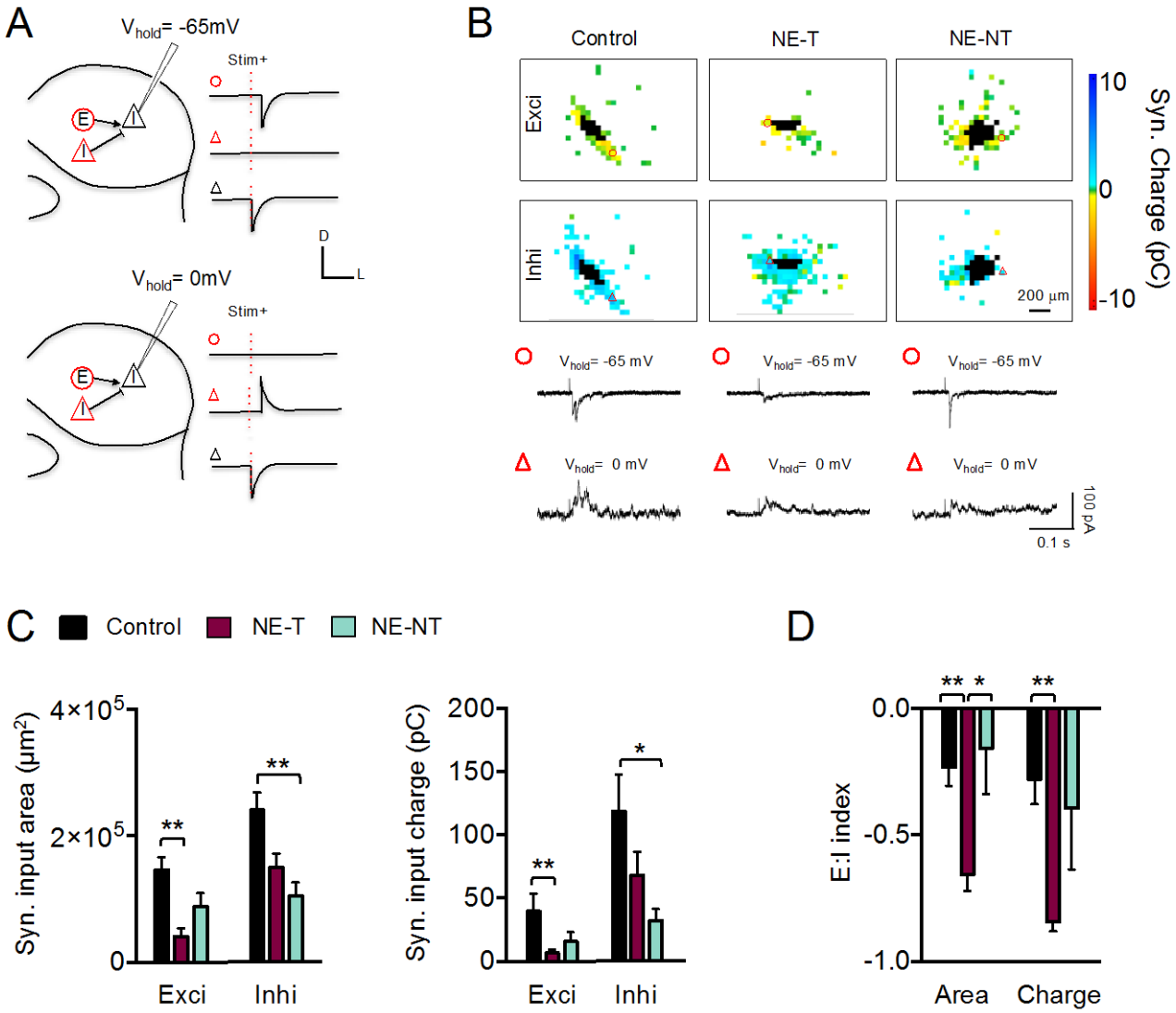

Figure 4-7. Noise-induced reorganization of synaptic input maps onto type 1 GABAergic neurons.

Figure 4-7. Noise-induced reorganization of synaptic input maps onto type 1 GABAergic neurons.

(A) Schematic of synaptic input mapping of vgat+ GABAergic neurons (black triangle). Excitatory (circle) and inhibitory (triangle) inputs are shown in red. **(B)** Examples of excitatory and inhibitory input maps from control, NE-T, and NE-NT mice. Current traces illustrate excitatory (circle) and inhibitory (triangle) synaptic responses to glutamate uncaging (red line) at the locations indicated by symbols. Uncaging sites that elicited direct responses at the recorded neuron are in black. **(C)** Changes in synaptic input area and total synaptic charge following traumatic noise exposure. Excitatory input area and total excitatory charge were decreased in NE-T mice, as compared to control mice (Exci Area, Control= $1.47 \times 10^5 \pm 0.20 \times 10^5$ μm^2; NE-T=$0.41 \times 10^5 \pm 0.14 \times 10^5$ μm^2; NE-NT= $0.88 \times 10^5 \pm 0.22 \times 10^5$ μm^2; n= 40 neurons, n= 21 animals, $p<0.0001$, Kruskal-Wallis test) (Exci Charge, Control= 39.6 ± 14.0 pC; NE-T=6.8 ± 2.4 pC; NE-NT= 15.8 ± 7.3 pC, n= 40 neurons, n= 21 animals, p= 0.005, Kruskal-Wallis test). Inhibitory input area and total inhibitory charge were decreased in NE-NT mice compared to control mice (Inhi Area, Control= $2.41 \times 10^5 \pm 0.27 \times 10^5$ μm^2; NE-T=$1.50 \times 10^5 \pm 0.21 \times 10^5$ μm^2; NE-NT= $1.0 \times 10^5 \pm 0.21 \times 10^5$ μm^2; n= 43 neurons, n= 21 animals, p= 0.004, Kruskal-Wallis test) (Inhi Charge, Control= 118.8 ± 28.8 pC; NE-T=68.0 ± 18.5 pC; NE-NT= 31.9 ± 9.6 pC, n= 43 neurons, n= 21 animals, p= 0.049, Kruskal-Wallis test). **(D)** Changes in E:I index induced by noise-exposure. In NE-T animals, the E:I indices for input area and input charge were shifted to more negative values relative to both control and NE-NT mice (Area, Control= -0.23 ± 0.07; NE-T= -0.66 ± 0.07; NE-NT= -0.16 ± 0.18, n= 40 neurons, n= 21 animals, p= 0.002, Kruskal-Wallis test) (Charge, Control= -0.28 ± 0.10; NE-T=-0.84 ± 0.03; NE-NT= -0.39 ± 0.24, n= 40 neurons, n= 21 animals, p= 0.001, Kruskal-Wallis test). Error bars represent SEM. *= $p< 0.05$, **= $p< 0.01$ in post-hoc, pairwise assessments corrected for multiple comparisons. *Mapping data for control animals is same as data shown in Figure 3-1 in Chapter 3.*

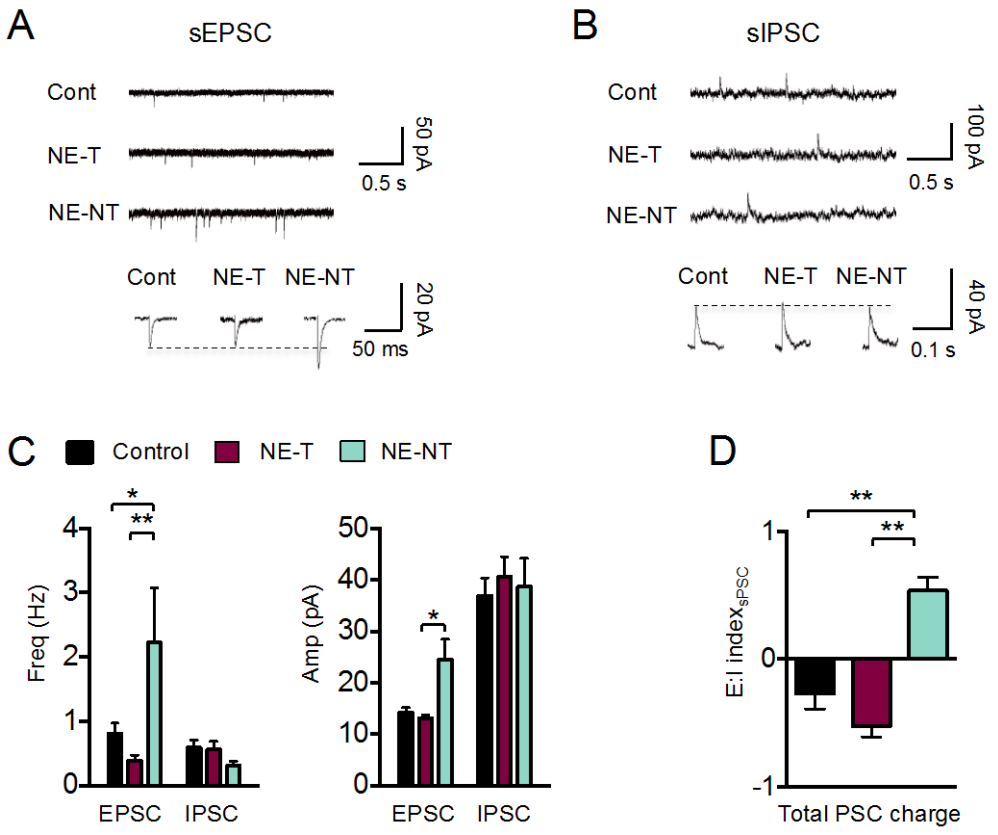

Figure 4-8. Spontaneous synaptic events onto type 1 GABAergic neurons in noise-traumatized mice.

(A) Example traces of sEPSCs. Individual event traces are average of 30-100 events from single cell. **(B)** Same as A, but for sIPSCs. **(C)** Summary graphs for frequency and amplitude of sPSCs. Frequency of sEPSCs was increased in NE-NT mice relative to control mice and both frequency and amplitudes of sEPSCs were increased in NE-NT mice relative to NE-T mice (sEPSC Freq, Control= 0.81 ± 0.16 Hz; NE-T= 0.39 ± 0.08 Hz; NE-NT= 2.26 ± 0.84 Hz, n= 36 neurons, n= 17 animals, p= 0.0022, one-way ANOVA) (sEPSC Amp, Control= 14.2 ± 1.0 pA; NE-T= 13.1 ± 0.68 pA; NE-NT= 24.4 ± 4.0 pA, n= 36 neurons, n= 17 animals, p= 0.0123, Kruskal-Wallis test). In contrast, frequency and amplitudes of sIPSCs were each indistinguishable between groups (sIPSC Freq, n= 36 neurons, n= 17 animals, p= 0.33, one-way ANOVA) (sIPSC Amp, n= 36 neurons, n= 17 animals, p= 0.79, one-way ANOVA) **(D)** The E:I index calculated for the sum of PSC amplitudes over 60s was increased in NE-NT mice relative to both NE-T and control mice (Control= -0.27 ± 0.12; NE-T= -0.53 ± 0.08; NE-NT= 0.54 ± 0.11, n= 36 neurons, n= 17 animals, p< 0.0001, one way ANOVA). Error bars represent SEM. *= p< 0.05, **= p< 0.01 in post-hoc, pairwise assessments corrected for multiple comparisons.

Noise-trauma had no effect on the synaptic inputs of type 2 GABAergic neurons (Figure 4-9). Both in NE-T and NE-NT mice, the excitatory input maps of type 2 GABAergic neurons were indistinguishable from control mice with respect to excitatory input area as well as and total excitatory charge (Figure 4-9 B). Additionally, both the frequency and the amplitudes of sEPSCs were unaffected by noise trauma (Figure 4-9 C). Taken together, these results demonstrate cell-type and input specific reorganizations of synaptic connections onto GABAergic IC neurons, whose nature varies with the presence or absence of behavioral evidence of tinnitus. Similar to what we observed for glutamatergic IC neurons, the noise-induced reorganization of synaptic inputs to GABAergic neurons changed the balance of synaptic excitation and inhibition only in mice with behavioral evidence for tinnitus.

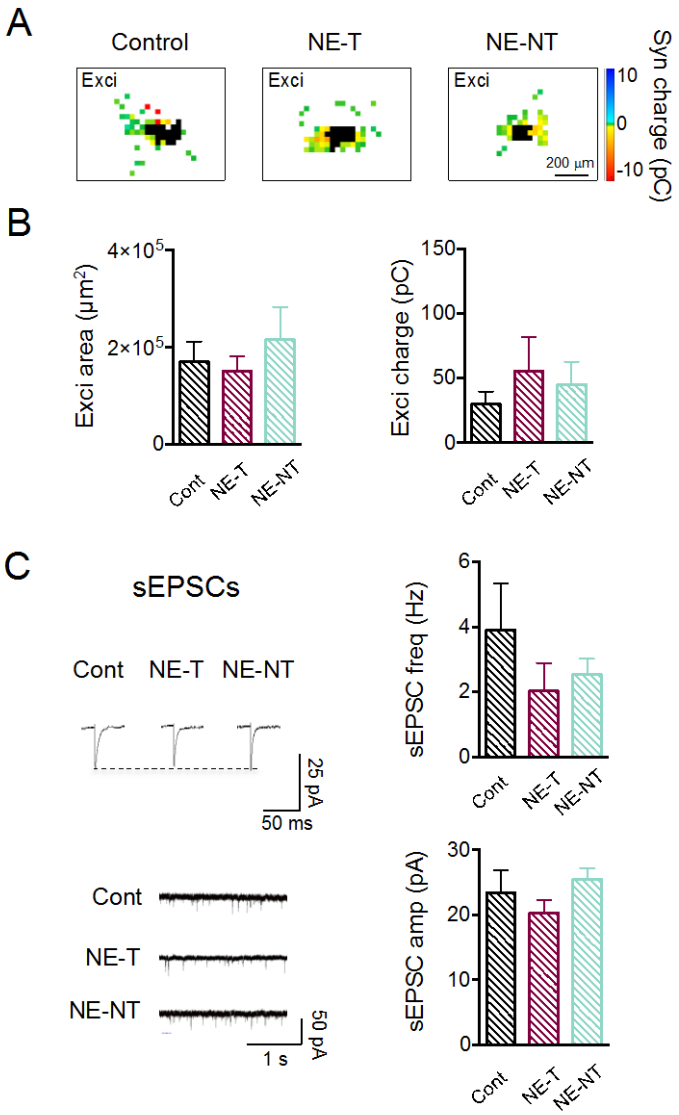

Figure 4-9. Synaptic inputs onto type 2 GABAergic neurons are stable in noise-traumatized mice.

(A) Examples of excitatory input maps from control, NE-T, and NE-NT mice. Uncaging sites that elicited direct responses at the recorded neuron are indicated in black **(B)** Noise-exposure has no effect on excitatory input area (left) (n= 26 neurons, n= 17 animals, p= 0.97, Kruskal-Wallis test) or on total excitatory postsynaptic charge (right) (n= 26 neurons, n= 17 animals, p= 0.62, one-way ANOVA). **(C)** Spontaneous EPSCs are unchanged by noise-trauma. Left, example traces of sEPSCs. Individual event traces (top) are average of 30-100 events. Right, noise trauma does not change the frequency (n= 23 neurons, n= 17 animals, p= 0.38, one-way ANOVA) or the amplitude (n= 23 neurons, n= 17 animals, p= 0.34, one-way ANOVA) of sEPSCs received by type 2 GABAergic neurons. Error bars represent SEM.

4.3.5 Post-traumatic acoustic enrichment prevents circuit reorganization and the behavioral correlates of tinnitus

In the visual and auditory cortices, sensory deprivation can open periods of enhanced synaptic plasticity, which, similar to developmental critical periods, makes neuronal circuits sensitivity to sensory experience (He et al., 2006; Zhou et al., 2011; Zhu et al., 2014). We therefore speculated that noise-induced hearing loss might open a similar sensitive period that enables the synaptic reorganizations in the IC. This scenario would predict that the noise-induced reorganizations of IC circuits could be influenced by changes in the post-trauma acoustic environment. To test this hypothesis, we exposed noise-traumatized mice for 7 days to moderate intensity pulsed white noise (75 dB white noise in pulses of 138 ms duration, delivered pseudo-randomly at intervals from 0 to 450 ms, duty cycle 47%, n= 25 animals). For these initial experiments, we chose pulsed white noise because of its strong effect in preventing map refinement in the developing primary auditory cortex (Zhang et al., 2002) and in interfering with developmental sharpening of sound frequency tuning of IC neurons (Sanes and Constantine- Paton, 1985), while having no effect on the tonotopic refinement in lower brainstem nuclei (Clause et al., 2014).

In support of our hypothesis, post-trauma acoustic enrichment (AE) prevented noise-induced reorganization of both excitatory and inhibitory input maps to glutamatergic as well as GABAergic IC neurons (Figure 4-10). In noise-exposed mice that received AE (NE-AE), excitatory and inhibitory input maps of glutamatergic IC neurons remained undistinguishable compared to maps in control mice (no noise trauma), as evidenced by similar excitatory input areas ($p > 0.05$, n=25 neurons, n= 10 animals) (Figure 4-10 A), inhibitory input areas ($p > 0.05$, n= 22 neurons, n= 10 animals) (Figure 4-10 B), and E:I indices ($p > 0.05$, n= 21 neurons, n= 10 animals) (Figure 4-10 C). In addition, the excitatory and inhibitory input maps of type 1

GABAergic neurons were also indistinguishable between NE-AE and control mice, as evidenced by similar excitatory input areas (n= 26 neurons, n= 14 animals, p> 0.05) (Figure 4-10 D), inhibitory input areas (n= 22 neurons, n= 14 animals, p> 0.05) (Figure 4-10 E), and E:I indices (n= 22 neurons, n= 14 animals p> 0.05) (Figure 4-10 F). Therefore, in NE-AE mice, the overall excitation: inhibition balance in the IC remained at control levels for both glutamatergic and GABAergic neurons. Acoustic enrichment by itself had no effect on IC circuits, because control mice which did not receive prior noise trauma, but received the same AE, showed no changes in intrinsic IC circuitry, as indicated by stable excitatory input maps, inhibitory input areas and E:I indices for glutamatergic neurons (all p values> 0.05, n= 21 neurons, n= 10 animals) (Figure 4-10 G, I) as well as type 1 GABAergic neurons (all p values> 0.05, n=29 neurons, n= 13 animals) (Figure 4-10 H, I). Thus, post-traumatic AE prevented noise-induced circuit reorganization in both excitatory and inhibitory IC neurons without having an effect on IC circuits in age-matched, non-traumatized control mice.

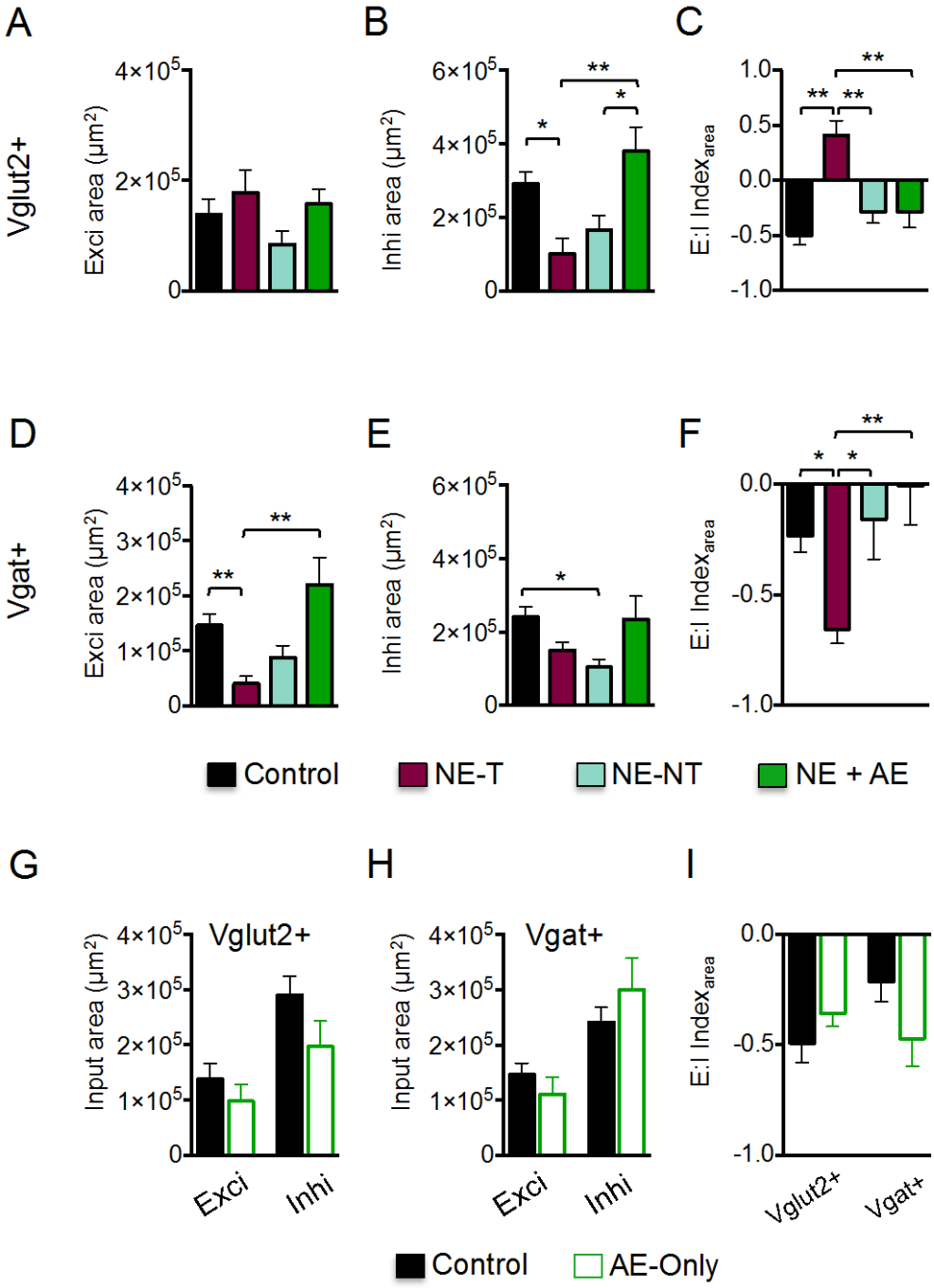

Figure 4-10. Acoustic enrichment with pulsed white noise inhibits post- traumatic circuit reorganization.

Figure 4-10. Acoustic enrichment with pulsed white noise inhibits post- traumatic circuit reorganization.

(A) Noise-exposure-related changes in excitatory input maps of glutamatergic neurons (Vglut2+) in NE-NT and NE-T animals (same data as in Figures 1-2) were absent in animals that received AE (green bars, Exci Area, Control= $1.38 \times 10^5 \pm 0.29 \times 10^5$ μm^2; NE-AE= $1.58 \times 10^5 \pm 0.27 \times 10^5$ μm^2, n= 25 neurons, n= 10 animals, p> 0.05, corrected pairwise comparison after one-way ANOVA). **(B)** Same as A, but for inhibitory input maps (Inhi Area, Control= $2.9 \times 10^5 \pm 0.34 \times 10^5$ μm^2; NE-AE= $3.8 \times 10^5 \pm 0.66 \times 10^5$ $\mu m2$, n= 22 neurons, n= 10 animals, p> 0.05, corrected pairwise comparison after one-way ANOVA). **(C)** E:I indexes in excitatory neurons from NE-AE animals remained at control levels (Control= -0.50 ± 0.09; NE-AE= -0.29 ± 0.14, n= 21 neurons, n= 10 animals, p> 0.05, corrected pairwise comparison after one-way ANOVA). **(D-F)** Same as in A-C, but for type 1 GABAergic neurons (vgat+). **(D)** Excitatory input maps (Exci Area, Control= $1.47 \times 10^5 \pm 0.20 \times 10^5 \mu m^2$; NE-AE= $2.2 \pm 0.50 \times 10^5$ μm^2, n= 28 neurons, n= 13 animals, p> 0.05, corrected pairwise comparison after one-way ANOVA**). (E)** Inhibitory input maps (Inhi Area, Control= $2.41 \times 10^5 \pm 0.27 \times 10^5$ μm^2; NE-AE= $2.34 \times 10^5 \pm 0.63 \times 10^5$ μm^2, n= 29 neurons, n= 13 animals, p> 0.05, corrected pairwise comparison after one-way ANOVA). **(F)** E:I indices in type 1 GABAergic neurons from NE-AE (E:I index, Control= -0.23 ± 0.07; NE-AE= -0.00 ± 0.18, n= 28 neurons, n= 13 animals, p> 0.05, corrected pairwise comparison after one-way ANOVA). **(G)** AE had no effect on input maps for glutamatergic neurons (vglut2+) from non-noise-traumatized control mice (Exci Area, n= 22 neurons, n= 10 animals, p= 0.41, Student's t-test: Inhi Area, n= 19 neurons, n= 10 animals, p= 0.12, Student's t-test). **(H)** Same as G, but for type 1 GABAergic neurons (vgat+) (Exci Area, n= 29 neurons, n= 13 animals, p= 0.33, Student's t-test, Inhi Area, n= 29 neurons, n= 13 animals p= 0.29, Student's t test). **(I)** E:I indices for both glutamatergic neurons and type 1 GABAergic neurons from control mice were not changed by AE (vglut2+ neurons, n= 19 neurons, n= 10 animals, p= 0.30, Student's t-test: vgat+ neurons, n= 29 neurons, n= 13 animals, p= 0.09, Student's t-test). Error bars represent SEM. *= p< 0.05, **= p< 0.01. *Mapping data for AE-alone animals in G-I is same data shown for noise-reared animals in Figures 3-3 and 3-8 in Chapter 3*.

Interestingly, AE also prevented the emergence of behavioral evidence of tinnitus, because noise-traumatized mice with AE had stable gap detection ratios before and after noise exposure (Gap Ratio Change, NE-AE= 0.02 ± 0.02, n= 84 tested sound frequencies) (Figure 4-11 A, B). Acoustic enrichment reduced the percentage of noise-exposed animals that developed tinnitus from 51% (19/37 animals) to 12% (3/25 animals) (Figure 4-11 C). AE also had no effect on pre-pulse inhibition of the ASR compared to control animals (PPI Ratio Change, NE-AE= -0.16 ± 0.04, n= 89 tested sound frequencies, Control= -0.12 ± 0.03, n= 90 tested sound frequencies) (Figure 4-11). This indicates that the effect of AE was specific for gap detection, and that AE did not affect hearing sensitivity or the neuronal circuits that mediate acoustic startle behavior. In addition, the protective effects of AE against noise-induced circuit reorganization and the emergence tinnitus were not due to a maintenance or restoration of hearing (Zhu et al., 2014), because AE did not reverse ABR threshold shifts that occur following traumatizing noise exposure for either low (10-16 kHz, p= 0.472, n= 30 animals) or high (20-32 kHz, p= 0.85, n= 30 animals) sound frequencies (Figure 4-11 D). Finally, the effects of AE on gap detection behavior were only present in noise-traumatized mice, since non-noise-traumatized control mice receiving identical AE showed no changes in gap inhibition of the ASR (p= 0.59, n= 16 animals) (Figure 4-11 E), paired-pulse inhibition of the ASR (p= 0.83, n=16 animals) (Figure 4-11 F) or hearing thresholds (10-16 kHz: p= 0.44, 20- 32 kHz: p= 0.60, n= 6 animals) (Figure 4-11 G).

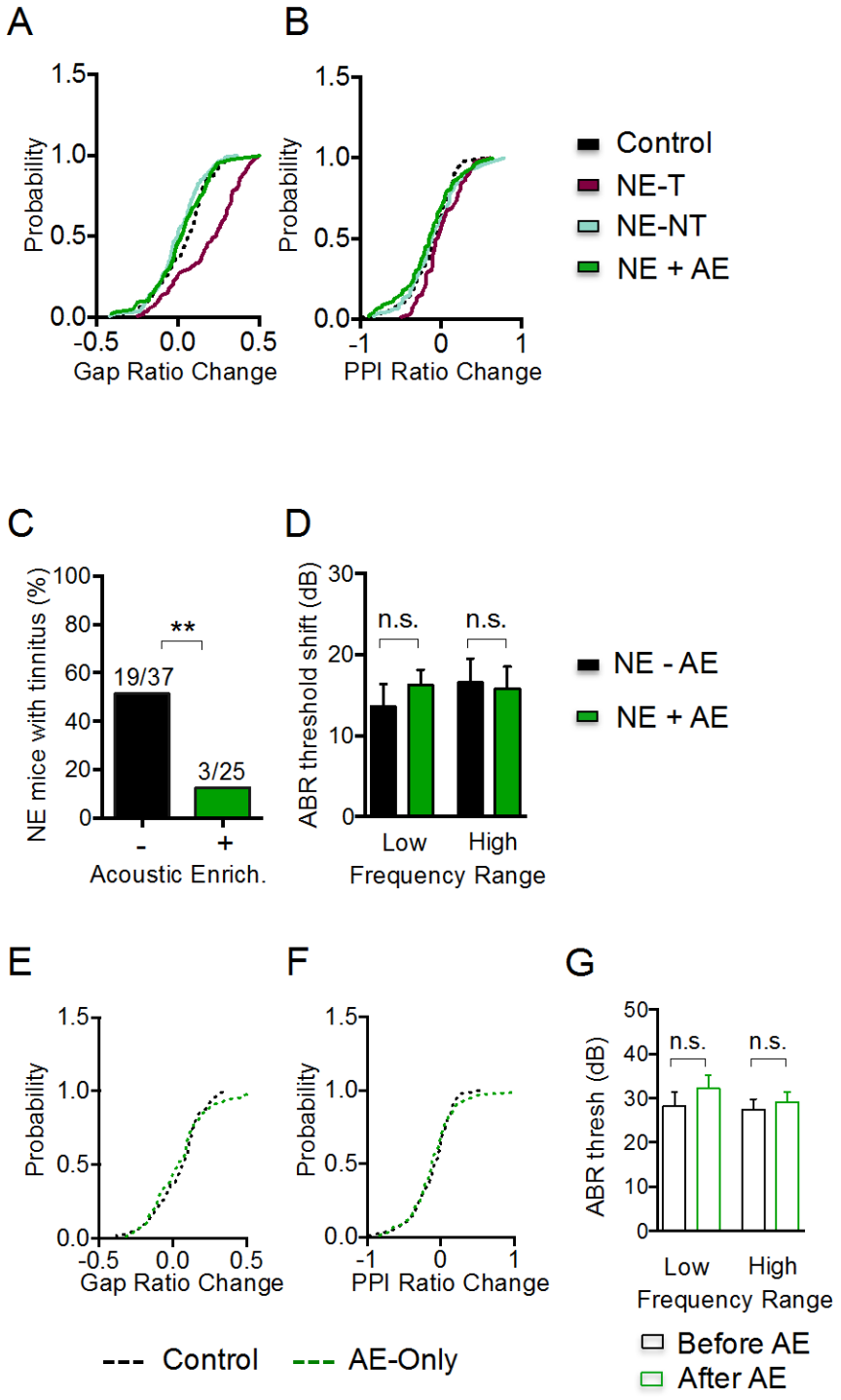

Figure 4-11. Acoustic enrichment prevents the development of behavioral evidence of tinnitus.

Figure 4-11. Acoustic enrichment prevents the development of behavioral evidence of tinnitus.

(A) Acoustic enrichment prevented noise-induced increases in gap detection ratios (left) (Gap Ratio Change, Control= 0.03 ± 0.02; NE-T= 0.18 ± 0.02, NE-NT= 0.00 ± 0.01, NE-AE= 0.02 ± 0.02, n= 376 sound frequencies, $p<0.0001$, Kruskal-Wallis test). **(B)** Prepulse inhibition of the startle response was unchanged following traumatic noise exposure or AE compared to control mice (PPI Ratio Change, Control= -0.12 ± 0.03; NE-T= 0.00 ± 0.03, NE-NT= -0.10 ± 0.04, NE-AE= -0.15 ± 0.04, n= 344 sound frequencies). **(C)** The percentage of noise-exposed animals that developed behavioral evidence of tinnitus (black) was decreased by AE (green) (n= 62 animals, p= 0.003, Fischer Exact Test) **(D)** AE did not affect noise-induced ABR threshold shifts in low (10-16 kHz, NE-AE= 13.6 ± 2.8 dB, NE+AE= 16.2 ± 2.0 dB, n= 30 animals, p= 0.47, Student's t test) or high (20-32 kHz, NE-AE= 16.5 ± 3.0 dB, NE+AE= 15.8 ± 2.7 dB, n= 30 animals, p= 0.85, Student's t test) sound frequencies. **(E)** AE delivered to non noise-traumatized control mice had no effect on gap detection ratios relative to age-matched control mice that did not receive AE (Gap Ratio Change, Control= 0.03 ± 0.01, AE-only= 0.04 ± 0.02, n= 164 sound frequencies, p= 0.59, Kolmogorov-Smirnov test). **(F)** Same as E, but for PPI inhibition of the ASR (PPI Ratio Change, Control= -0.12 ± 0.03, AE-only= -0.11 ± 0.04, n= 164 sound frequencies, p= 0.83, Kolmogorov-Smirnov test). **(G)** Summary graph of ABR thresholds before (black) and 7d after (green) AE for low (n= 6 animals, p= 0.43, Wilcoxin test) and high (n= 6 animals, p= 0.60, Paired t-test) sound frequencies in non-noise-traumatized mice. Error bars are SEM.

4.4 DISCUSSION

In this study, we demonstrate an unexpected level of plasticity of excitatory and inhibitory intrinsic circuits in the central nucleus of the IC of mice following mild hearing loss. By combining behavioral testing and synaptic circuit mapping with LSPS, we were able to link specific patterns of circuit reorganization to the presence or absence of behavioral evidence of tinnitus. While hearing loss led to a substantial reorganization of synaptic connectivity in all noise-exposed mice, the specific pattern of this reorganization differed substantially between NE-T and NE-NT mice. In NE-T mice, glutamatergic IC neurons show stable excitatory input maps but greatly diminished inhibitory input maps, which together lead to a shift in the synaptic excitation: inhibition balance in favor of excitation (Figure 4-4 B-D). Type 1 GABAergic IC neurons show the reverse effect, having smaller excitatory input maps but unchanged inhibitory input maps, leading to a shift the excitation: inhibition balance towards inhibition (Figure 4-7 B-D). In combination, these circuit changes lead to a functional 'dis-inhibition' of the IC in NE-T mice.

In contrast, the synaptic reorganizations that take place in the IC of NE-NT mice preserve the overall excitation: inhibition balance at control levels for both glutamatergic (Figure 4-4 D) and GABAergic (Figure 4-7 D) neurons. Finally, we demonstrate that post-traumatic AE with patterned noise completely prevents noise-induced circuit reorganization of intrinsic IC circuits (Figure 4-10), and dramatically reduces the percentage of noise-traumatized mice that develop behavioral evidence of tinnitus (Figure 4-11). Taken together, these results establish a link between cell-type specific patterns of local circuit reorganization in the IC and the presence of behavioral evidence of tinnitus (Figure 4-12). Our results also encourage further investigation of using post-traumatic acoustic stimulation as a means to prevent the development of tinnitus.

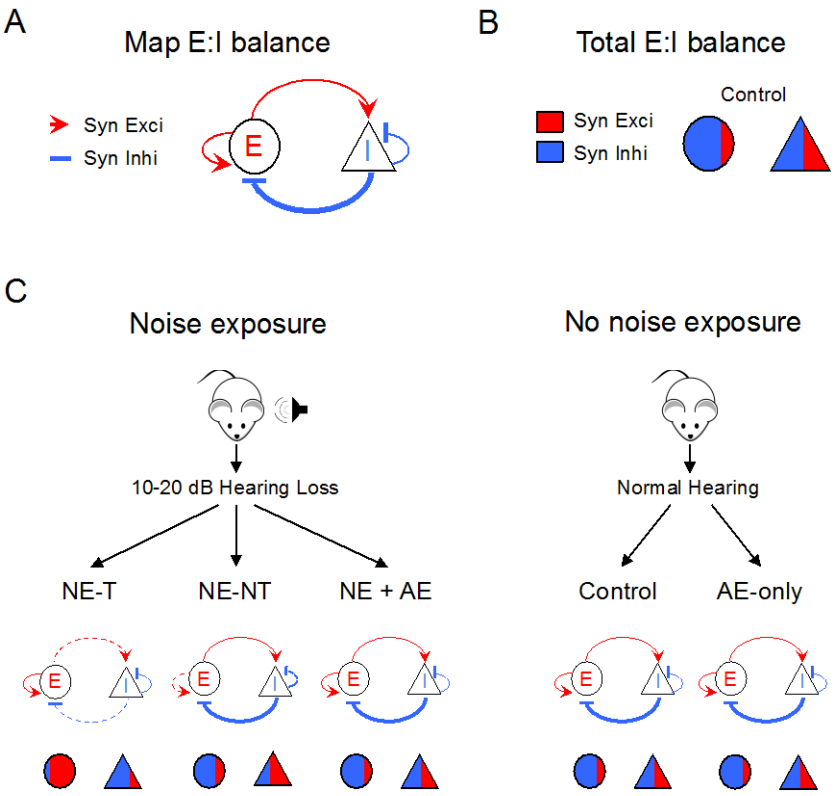

Figure 4-12. Summary of IC network reorganization after noise exposure and/or acoustic enrichment.

(A) Schematized intrinsic IC circuit with excitatory neurons (circle) and type 1 inhibitory neurons (triangle). Red arrows depict the population of excitatory connections and blue lines depict inhibitory connections. Input strength is indicated by the widths of connecting lines. In control mice, the total E:I balance for synaptic input maps is strongly dominated by inhibition for excitatory neurons and is weakly dominated by inhibition for type 1 inhibitory neurons. **(B)** Total E:I balance incorporates spontaneous synaptic drive as well as synaptic input maps. In control mice, the total E:I balance is dominated by inhibition for both excitatory neurons and type 1 inhibitory neurons. **(C)** Changes in connectivity strength in noise-exposed mice with (NE-T) and without tinnitus (NE-NT), and in noise-exposed mice that received acoustic enrichment (NE+ AE). Dashed lines indicate weakened connections. Lower row summarizes E:I balance after noise exposure and/or acoustic enrichment.

4.4.1 Gap detection as a method for tinnitus detection

Since its inception (Turner et al., 2006), gap-inhibition of the ASR has become a widely used behavioral assay for evaluating tinnitus in animal models, and numerous studies utilizing this paradigm have shed significant light on the likely synaptic, cellular and molecular underpinnings of tinnitus (Wang et al., 2009; Engineer et al., 2011; Middleton et al., 2011; Dehmel et al., 2012; Li et al., 2013; Kalappa et al., 2014; Kalappa et al., 2015; Li et al., 2015). This rise in popularity of the gap-inhibition paradigm can be attributed to a number of features. First, compared to other tinnitus behavior paradigms, many of which require extensive conditioning regimens (Bauer and Brozoski, 2001; Lobarinas et al., 2004), the ASR-based method is faster and requires no training period beyond test chamber adaptation. Second, unlike conditioning paradigms, the ASR-based method requires no food or water restriction, and therefore controls against the confounding effects of metabolic disturbances. Finally, since the ASR is a reflex behavior, it is less sensitive to shifts in animal attention compared to the learned behaviors utilized by most other tinnitus paradigms (Jastreboff et al., 1988a/b; Bauer and Brozoski, 2001; Heffner and Harrington, 2002; Lobarinas et al., 2004).

Despite its wide usage, however, the validity of using gap detection as an indicator of tinnitus has recently come under scrutiny. In particular, the concept that gap detection deficits represent evidence of a tinnitus percept “filling in” the silent gap has been questioned (Fournier and Hebert, 2013; Hickox and Liberman, 2014). It has also remained unclear whether and to what degree deficits in gap detection correspond to tinnitus perception in humans. Although deficits in gap detection have been found in humans, they do not appear to be restricted to the sound frequency range of reported tinnitus percepts (Fourner and Hebert, 2013). Additionally, a number of studies have reported normal gap detection in humans with tinnitus (Campolo et al.,

2013; Boyen et al., 2015). Together, these findings underscore the need for animal models that more realistically and reliably depict subjective tinnitus found in humans. However, while gap detection deficits should be interpreted with caution, gap-mediated inhibition of the ASR currently represents the state of the art in animal research on tinnitus.

4.4.2 Cell-type specific organization of synaptic input maps in the CNIC

Synaptic mapping of identified glutamatergic and GABAergic IC neurons enabled us to identify three, cell-type specific input map configurations in the CNIC. First, glutamatergic neurons receive local excitatory and inhibitory inputs, with an exhibition: inhibition balance that is strongly biased towards inhibition (Figure 4-4). This input configuration in four-week old mice is similar to the configuration we observed previously in a population of unidentified, but most likely predominantly glutamatergic IC neurons in three week-old mice (Chapter 2; Sturm et al., 2014), suggesting that the developmental refinement of intrinsic IC circuits is largely completed by the end of the third postnatal week. Second, type 1 GABAergic neurons, which may resemble inhibitory interneurons (Ito et al., 2009), also receive both excitatory and inhibitory intrinsic inputs, but the excitation: inhibition index for type 1 neurons is more balanced and is only slightly biased towards inhibition (Figure 4-7). Finally, type 2 GABAergic neurons, receive predominantly excitatory intrinsic inputs (Figure 4-6). Although this study did not identify the projection patterns of type 1 and type 2 GABAergic neurons, the properties of type 2 neurons resemble those of thalamic-projecting neurons (Ito et al., 2009), and the lack of local inhibitory inputs to type 2 neurons is consistent with their role of providing fast and direct feed-forward inhibition from the colliculus to the thalamic medial geniculate nucleus (Ito and Oliver, 2012). The organization of synaptic maps to glutamatergic and GABAergic neurons suggest that the

fundamental intrinsic synaptic network in the CNIC, in its simplest form, supports intracollicular inhibition.

4.4.3 Reorganization of intrinsic CNIC circuits following noise-trauma

Noise-induced hearing loss, regardless of whether or not it was accompanied by behavioral evidence of tinnitus, led to a substantial reorganization of the intrinsic IC network and to an increase in the spontaneous excitatory drive of glutamatergic IC neurons. However, apart from a general increase in sEPSC frequency, which likely reflects a homeostatic up-regulation of excitatory drive due to decreased sensory-evoked activity (Maffei et al., 2004), the specific patterns of synaptic reorganization otherwise correlated with the presence or absence of tinnitus. Only NE-T mice exhibit a functional dis-inhibition of local IC circuitry. In NE-T mice, glutamatergic IC neurons lose local inhibition, which causes a profound shift in their excitation: inhibition balance towards excitation (Figures 4-4 and 4-5). Reciprocally, type 1 GABAergic IC neurons lose synaptic excitation, which causes a shift in their excitation: inhibition balance towards inhibition (Figures 4-7 and 4-8). Together, these specific circuit reorganizations may give rise to the IC hyperactivity that is characteristic of tinnitus in both rodent models (Bauer et al., 2008; but see Ropp et al., 2014) and human patients (Melcher et al., 2000). The fact that GABAergic neurotransmission is decreased in glutamatergic IC neurons of NE-T mice, but not NE-NT mice, provides a possible explanation for the often-conflicting results of prior studies describing global up- or down-regulation of indicators of GABAergic neurotransmission in the IC after cochlear trauma in animals that were not tested for behavioral signs of tinnitus (Berger and Coomber, 2015). The shifts in excitation: inhibition balance in our study, which only occurred in NE-T animals, could help to discern which aspects of IC hyperactivity, such as

increased spontaneous firing rates (Ma et al., 2006; Bauer et al., 2008; Dong et al., 2009; Mulders and Robertson, 2009; Dong et al., 2010), increased burst firing (Bauer et al., 2008; Wang et al., 2011), and gain (Wang et al., 2002; Niu et al., 2013), are specifically related to tinnitus. Those forms of IC hyperactivity that correlate with tinnitus-associated shifts in excitation: inhibition balance are most likely related to tinnitus pathophysiology, whereas those that occur in all noise-traumatized mice may be due more generally to hearing loss.

Very few studies have examined the central effects of noise-trauma in behaviorally tested animals that lack signs of tinnitus. A recent study in the mouse DCN demonstrated that resilience against tinnitus depends upon the recovery of noise-induced reductions in KCNQ2/3 channel activity (Li et al., 2015), which otherwise contribute to the emergence of hyperactivity and tinnitus (Li et al., 2013; Kalappa et al., 2015). In this study, noise-exposed mice that lacked signs of tinnitus one week after acoustic trauma also exhibited a reduction of hyperpolarization-activated cyclic nucleotide-gated channel (HCN) currents in DCN fusiform cells (Li et al., 2015). Together, these findings indicate that the post-traumatic dynamics of KCNQ2/3 and HCN channels likely determine whether noise exposure leads to DCN hyperactivity in tinnitus. However, whereas noise-induced hyperactivity in the DCN is restricted to noise-exposed mice that show signs of tinnitus (Le et al., 2013; Stefanescu et al., 2015), in the rat IC, increased firing rates have been found in all noise-exposed animals, regardless of their tinnitus classification (Ropp et al., 2014). These findings are at odds with the distinct IC circuit reorganizations we identified in NE-T and NE NT animals. The fact that IC circuits of NE-NT mice differ substantially from those of non-exposed control mice opens an opportunity to investigate the role of intrinsic IC circuits in auditory processing by comparing auditory response properties of IC neurons or auditory perceptions between NE-NT mice and control mice.

Why do only half of noise-exposed mice exhibit the shift in collicular E:I balance that is associated with behavioral evidence of tinnitus? Inter-mouse differences in auditory nerve activity after hearing loss are unlikely to account for this split, because NE-NT and NE-T mice had similar degrees of hearing loss. Additionally, differences in the pre- or post-traumatic acoustic environment are unlikely explanations, since NE-NT and NE-T animals were both raised and housed in the same room and often in the same cages. Genetic predisposition may be a contributing factor, but its influence seems to be weak considering that the fraction of NE-T mice was similar for both sexes (50% for males, n=14; 50% for females, n=20), and across different mouse strains (this study; Li et al, 2013). It is possible that inter-mouse variability in the baseline intrinsic and/or synaptic properties of IC neurons predisposes certain mice to noise-induced circuit reorganizations that disrupt E:I balance and lead to tinnitus, a possibility which may be addressable with in vivo imaging. In addition to determining whether there are pre-exposure differences in the organization of IC circuits in mice that become NE-T or NE-NT mice after noise-exposure, such studies could also provide a fine-grained characterization of the time course of synaptic reorganization after noise-trauma, which would illustrate whether the reorganizations of synaptic inputs onto glutamatergic and GABAergic IC neurons occur independently, or whether some circuit changes trigger changes in others. In cortical circuits, decreased inhibition has emerged as a key step to initiate plasticity (Takesian and Hensch, 2013; Keck et al., 2011; Hübener and Bonhoeffer, 2014). The decrease in inhibitory drive of glutamatergic IC neurons and/or the decreased excitatory drive on GABAergic neuron in noise traumatized mice may thus represent the first steps in the reorganization of IC circuitry and its magnitude may set the direction of subsequent changes.

It remains to be shown whether the functional circuit reorganizations demonstrated in this

study are accompanied or followed by structural reorganizations (i.e. by axonal pruning/growth or remodeling of dendritic branches and spines). Few studies have investigated the effects of hearing-loss on structural IC connectivity (Nordeen et al., 1983; Moore and Kowalchuk, 1988) and none have examined intrinsic connections or neuronal morphology. However, considering the close relationship of functional and structural reorganization (Hensch, 2005; Holtmaat and Svoboda, 2009; Clause et al., 2014), structural remodeling of intrinsic IC connections after cochlear trauma is highly plausible. Compared to the dynamic regulation of synaptic strengths and of neuronal membrane excitability, remodeling of neuronal circuits is considered long lasting and can permanently impair sensory processing (Wiesel and Hubel, 1963; Linkenhoker et al., 2005; Hofer et al., 2009; Sengpiel, 2014). The substantial remodeling of intrinsic IC circuits may thus represent changes that support the often life-long persistence of tinnitus.

4.4.4 IC circuit reorganization and tinnitus

Although increased activity in the IC is already evident shorty after noise trauma (Willot and Lu, 1982), several prior studies indicated that during the first weeks of tinnitus development, IC hyperactivity is mainly due to increased afferent drive from fusiform cells in the DCN (Mulders and Robertson, 2011). DCN ablation shortly after noise exposure abolishes increased IC firing rates and tinnitus behavior (Brozoski et al., 2012; Manzoor et al., 2012), whereas DCN ablation after several months has no effect on tinnitus (Brozoski and Bauer 2005). The shift in the E:I balance in the IC of NE-T but not NE-NT animals, which is already present at least 7 days after noise trauma, suggests that the IC is also involved in the early stages of tinnitus, perhaps via an additional amplification or synchronization of ascending hyperactivity. This additional augmentation may be required to trigger the cortical reorganizations that correlate with tinnitus

(Noreña and Eggermont, 2003; Llano et al., 2012; Engineer et al., 2011). On the other hand, since the IC receives efferent cortical projections, which not only dynamically influence the response properties of IC neurons (Suga et al., 2002), but also play an important role in mediating plasticity in the IC (Bajo et al., 2010), it is possible that either the initiation or the direction of IC circuit reorganization is mediated by these descending pathways.

4.4.5 Prevention of circuit reorganization by acoustic enrichment

Our results demonstrate that immediate, post-traumatic acoustic enrichment with pulsed white noise prevents circuit reorganization in the IC (Figure 4-10). Previous studies have shown that stimulation with pulsed white noise prevents the developmental refinement of both cortical tonotopic maps and frequency tuning in IC neurons (Zhang et al., 2002; Sanes and Constantine-Paton 1983). However, it is unlikely that the effects of pulsed white noise we observed are due to a disturbance of developmental IC refinement, since pulsed white noise had no effect on non-noise-traumatized control mice. This is consistent with previous studies showing that the IC has reached a mature state around the third postnatal week (Shnerson and Willott, 1979; Ehret and Romand, 1992; Yu et al., 2005). A more likely explanation for the blockade of IC circuit refinement by pulsed white noise is that noise-trauma re-opened a ‘sensitive period’ in the IC, which made IC circuits permissive to reorganization by processes that are sensitive to auditory experience. This scenario is reminiscent of the re-opening of critical period plasticity in adult auditory cortex by long-term noise exposure (Zhou et al., 2011) and in visual cortex by dark exposure (He et al., 2006). It also is consistent with previous studies showing that acoustic enrichment can alleviate the reorganization of cortical tonotopic maps induced by traumatizing noise exposure, although some of these effects may have resulted from a recovery of ABR

thresholds (Noreña and Eggermont, 2005). Re-activation of critical period plasticity in cortex involves a down regulation of GABAergic inhibition (Huang et al., 2010; Zhou et al., 2011), which also occurs in the IC after noise trauma (this study; Milbrandt et al., 2000; Dong et al., 2010), suggesting that down-regulation of inhibition may be a crucial step in the initiation of trauma-induced enhanced plasticity in the IC.

4.4.6 Prevention of tinnitus behavior by acoustic enrichment

In addition to preventing noise-induced synaptic circuit reorganization in the IC, post-traumatic acoustic enrichment also substantially reduced the percentage of noise-traumatized mice that developed behavioral evidence of tinnitus (from 51% to 12%) (Figure 4-11), further supporting a role of IC reorganization in the generation of tinnitus. This result also points to the possibility of using immediate acoustic stimulation as a prophylactic measure to prevent the development of tinnitus after acoustic trauma. Compared to most other existing treatment options for tinnitus, most of which have proven ineffective (see Folmer et al., 2014 for review), an acoustic-enrichment based method would be safe, inexpensive, and easy to implement. Acoustic stimulation (e.g. sound therapy) to treat tinnitus has been tried for many years, but has been largely unsuccessful (Vanneste et al., 2013; Folmer et al., 2014), perhaps because sound therapy is usually started months or years after tinnitus has developed (i.e. after the closure of a trauma-induced sensitive period). From both a neurobiological as well as a clinical view, it will be interesting to determine what types of acoustic stimulation are most effective in preventing synaptic reorganization in the IC and the emergence of tinnitus. For example, stimulation with pulsed white noise during the critical period produces a permanent disruption of the tonotopic map in auditory cortex (Zhang et al, 2001), while map disruptions by stimulation with

unstructured noise are reversible (Chang and Merzenich, 2003) and, in the case of noise trauma, may delay but not prevent circuit reorganization. A better understanding of the 'rules' by which auditory experience influences post-traumatic refinement, and a greater level of insight into the cellular and molecular mechanisms that open and close sensitive periods in the mature auditory system will help to better define and understand the sensitive period in the adult IC and may open new avenues to harness this type of plasticity for clinical interventions that prevent tinnitus following noise trauma, traumatic brain injury or treatment with ototoxic drugs.

5.0 GENERAL DISCUSSION

5.1 SUMMARY OF FINDINGS

Through the research described in this dissertation, we sought to shed light on the functional organization and experience-dependent plasticity of intrinsic connectivity in the central nucleus of the mouse inferior colliculus.

In Chapter 2, we examined the development of functional synaptic connections in the CNIC during the first three weeks of postnatal life. We found evidence of robust excitatory and inhibitory synaptic connectivity already at P2, with excitatory and inhibitory input maps exhibiting a large degree of spatial overlap, and aligning to the presumed isofrequency axis of the CNIC (Figures 2-4, 2-5, 2-7). Although these overall organization principles were preserved during the first three postnatal weeks, the sizes and strengths of input maps underwent major developmental changes, with an expansion and strengthening of input maps before hearing onset, followed by a period of dramatic refinement of input maps after hearing onset (Figure 2-5). These changes occurred in parallel for excitatory and inhibitory intrinsic connections, yet compared to inhibitory connections, a greater proportion of excitatory connections were functionally eliminated after hearing onset, resulting in a predominance of intrinsic inhibition at the end of the third postnatal week. Taken together, these findings indicate the existence of functional excitatory and inhibitory intrinsic circuits in the CNIC, which are highly plastic during

postnatal development.

In Chapter 3, we explored the role of hearing experience in directing the maturation of intrinsic CNIC circuitry by rearing mice in pulsed white noise during distinct developmental epochs (P12-P25 or P19-25). In these studies, we increased the cell-specificity of our input mapping approach by targeting recordings to glutamatergic or GABAergic neurons using mice that express the fluorescent protein tdTomato in cells that express the vesicular glutamate transporter 2 and the vesicular GABA transporter genes, respectively. We found that noise rearing from P12-25, but not P19-25, led to substantial, cell-specific reorganizations of synaptic input maps received by glutamatergic and GABAergic neurons compared to age-matched control mice. In GABAergic neurons, noise rearing from P12-25 led an expansion of input map areas, specifically in regions where both excitation and inhibition were found, as well as to a strengthening of excitatory, but not inhibitory synaptic inputs (Figures 3-1, 3-2). In glutamatergic neurons, on the other hand, noise rearing from P12-25 led to a functional elimination of excitatory, but not inhibitory synaptic inputs (Figures 3-6, 3-7). This combination of strengthening excitatory inputs onto GABAergic neurons and eliminating excitatory inputs onto glutamatergic neurons results in a 'hyper-inhibited' state of intrinsic CNIC circuitry at P26-30. Taken together, these findings indicate that the nature of acoustic experience plays a profound role in sculpting intrinsic synaptic connectivity in the CNIC, particularly during an early critical period.

In Chapter 4, we investigated the impact of noise-induced hearing loss on the organization of intrinsic CNIC circuitry in mice that did and did not develop behavioral evidence of tinnitus. Furthermore, we explored the role of the early, post-traumatic acoustic environment in directing hearing-loss-induced plasticity. We found that hearing loss leads to a profound

reorganization of local excitatory and inhibitory synaptic circuits received by both glutamatergic and GABAergic IC neurons. However, only in mice that showed behavioral evidence of tinnitus did these reorganizations lead to significant disruptions in excitation: inhibition balance (Figures 4-1, 4-5). In mice with behavioral signs of tinnitus, glutamatergic neurons exhibited a functional elimination of inhibitory synaptic inputs, whereas GABAergic neurons exhibited an elimination of excitatory synaptic inputs. Together, these synaptic changes resulted in a 'dis-inhibited' state of the CNIC, which likely contributes to patterns of neuronal hyperactivity that have been tied to tinnitus. Most surprisingly, one week of acoustic enrichment with non-traumatic pulsed white noise, delivered immediately after noise trauma, was sufficient to prevent both patterns of synaptic reorganization and to substantially reduce the percentage of noise-traumatized mice that developed behavioral evidence of tinnitus (from 51% to 12%). Taken together, these findings suggest that acoustic trauma opens a 'sensitive window' in the CNIC, during which excitatory and inhibitory synaptic networks are subject to significant experience-dependent modification. The nature of auditory experience during this window appears to determine whether patterns of synaptic reorganization that contribute to the development of tinnitus take place.

5.2 ADVANTAGES AND LIMITATIONS OF MAPPING SYNAPTIC CONNECTIVITY WITH LSPS

Laser-scanning photostimulation with caged glutamate is a robust and reliable tool that has been used to map the strength and spatial distribution of synaptic networks in a number of experimental systems (Callaway and Katz, 1993; Zhao et al., 2009; Shepherd, 2012; Sturm et al.,

2014). However, as with any experimental tool, LSPS has certain advantages and limitations (Shepherd, 2012; Sturm et al, 2015).

A major advantage of LSPS over both optical-fiber-based glutamate uncaging (Kandler et al., 2013) and more traditional electrical stimulation methods is that LSPS can be used to map synaptic connectivity over large areas of neural tissue in relatively short periods of time. Prior to the research described in this dissertation, neither the location nor the extent of intrinsic synaptic connections in the CNIC had been demonstrated. Given this gap in knowledge, it was possible that excitatory and inhibitory intrinsic inputs in the CNIC would arise from either very large or very small tissue areas, and it was therefore necessary to adopt an input-mapping strategy that would be capable of covering large areas of tissue, while at the same time delivering focal presynaptic stimulation. Since LSPS systems use software-controlled mirror galvanometers, it is possible to rapidly scan through a very large number of stimulation sites over short periods of time. Additionally, since ultraviolet light for glutamate uncaging in LSPS is focused through a microscope objective, the uncaging spot can be made very small by using high-magnification objectives, thus affording a relatively high degree of spatial resolution.

One important limitation of using LSPS to map synaptic connectivity is its relatively poor temporal resolution. With LSPS, presynaptic photostimulation often produces complex, multi-peaked synaptic responses at the postsynaptic recorded cell, and it is not possible to determine whether these responses are the product of multiple presynaptic neurons firing action potentials, a single presynaptic neuron firing multiple action potentials, or a combination of both. This limitation can complicate the interpretation of input maps, since the ‘strength’ of synaptic responses recorded in postsynaptic neurons may vary either because of differences in the number

of presynaptic neurons stimulated with LSPS, or because of differences in number of action potentials elicited in a constant number of presynaptic neurons.

A second limitation of using LSPS to map synaptic connectivity is that it does not resolve the type (e.g. excitatory or inhibitory) of presynaptic neurons being photo-stimulated. As long as neurons express functional glutamate receptors, those neurons are likely to be excited in response to glutamate uncaging. In the CNIC, where excitatory and inhibitory neurons are densely packed and uniformly distributed (Ito et al., 2013; Ito et al., 2015), even highly-focused areas of glutamate uncaging are likely to produce action potentials in multiple presynaptic neurons at a time, with the extent of this presynaptic stimulation depending upon the morphological and physiological properties of the presynaptic neurons being stimulated (Kim and Kandler, 2003; Shepherd, 2012). For example, differences in the dendritic geometry and the dendro-somatic distribution of glutamate receptors between CNIC neurons can influence which uncaging positions will generate action potential in different cells types, thereby influencing the spatial resolution of input maps. Although some of this uncertainty can be overcome by generating 'excitability profiles' for putative presynaptic neurons (*see* Chapter 2; Kim and Kandler, 2003; Shepherd, 2012; Sturm et al., 2014), it is impossible with LSPS to determine precisely which presynaptic neurons contribute to a given postsynaptic response at the recorded cell, or to a given synaptic input map.

An alternative approach to LSPS that overcomes these limitations is paired whole-cell recordings. Unlike LSPS, paired recordings allow the experimenter to precisely define both the location and the identity of the presynaptic neurons that provide either excitatory or inhibitory synaptic input to the postsynaptic recorded cell. However, paired recording are, by definition, limited to pairs of synaptically-coupled neurons, and these recordings are therefore not suitable

for estimating the total amounts of excitatory and inhibitory input received by individual neurons. Additionally, depending upon the synaptic connection probability of the brain region being studied (which is often quite low), finding pairs of synaptically coupled neurons can be both challenging and time intensive. Thus, given that a major experimental goal of this dissertation was to map out the spatial extent of functional intrinsic connectivity in the CNIC, LSPS was a more appropriate tool than paired whole-cell recordings.

In contrast to paired whole-cell recordings, optogenetic circuit mapping can be used to map synaptic connections over large areas of tissue (similar to LSPS), while at the same time limiting presynaptic stimulation to specific classes of neurons (Mancuso et al., 2011). In optogenetic circuit mapping, light-sensitive microbial opsins are expressed in specific, genetically defined classes of neurons (typically subsets of excitatory or inhibitory neurons), and photostimulation is used to drive action potential generation in opsin-expressing cells. While the number of presynaptic neurons being stimulated cannot typically be resolved with optogenetic circuit mapping, the type of neurons being stimulated can be more tightly controlled compared to LSPS. However, whereas both the excitatory and inhibitory inputs of individual neurons can be mapped using LSPS, this is more difficult with optogenetic mapping. Unless opsins with distinct light-excitation profiles are expressed in excitatory and inhibitory neuron populations, respectively, in the same experimental animals, it is not possible to resolve both excitatory and inhibitory inputs received by individual neurons. Thus, given that a major experimental goal of this dissertation was to investigate synaptic excitation: inhibition balance in the CNIC, both in development (Chapters 2 and 3) and following hearing loss (Chapter 4), LSPS was a more appropriate tool than optogenetic circuit mapping.

In conclusion, while there are a number of important limitations to consider when using LSPS of caged glutamate, it nevertheless represents a powerful tool for mapping synaptic connectivity. Using LSPS was especially appropriate for mapping intrinsic synaptic connectivity in the CNIC, given the relatively large area of tissue being mapped, and the combination of excitatory and inhibitory synaptic connections received by individual neurons.

5.3 ORGANIZATION OF INTRINSIC CONNECTIVITY IN THE CNIC

Acoustic processing in the mouse CNIC matures rapidly during the first week of hearing experience and reaches an adult-like state by the end of the third postnatal week of life (around P20), as evidenced by adult-like tone-response thresholds, tone-response latencies, frequency tuning and tonotopic organization (Romand and Ehret, 1990; Ehret and Romand, 1992). Evidence from the functional mapping studies discussed in this dissertation indicates that the development of functional intrinsic connectivity in CNIC follows a similar time course, with a period of dramatic refinement occurring during the first week of hearing experience (Chapters 2 and 3). This is in contrast to the extrinsic, ascending synaptic projections received by CNIC neurons, which appear to reach relative maturity before hearing onset (Gabriele et al., 2000a, 2007; Henkel et al., 2007). Accordingly, the rapid maturation of spectrotemporal response properties in the CNIC may relate to the refinement of intrinsic synaptic connectivity.

By P26-30, the intrinsic synaptic networks of CNIC neurons exhibit at least three basic configurations (Figure 5-1). The local input maps of glutamatergic neurons consist of both excitatory and inhibitory synaptic connections, with a strong predominance of intrinsic inhibition

(Figure 3-6, Figure 4-4). The local input maps of type 1 GABAergic neurons also consist of both excitatory and inhibitory local inputs, but with only a slight dominance of synaptic inhibition. Finally, the local input maps of type 2 GABAergic neurons consist of predominantly excitatory inputs, with little or no inhibitory inputs.

Additional studies will be necessary to distinguish between the functions of type 1 and type 2 GABAergic neurons. We predict that type 1 and type 2 GABAergic neurons correspond to the two major classes of GABAergic neurons previously documented in the CNIC: local interneurons and large tectothalamic projection neurons (Ito et al., 2009; Ito and Oliver, 2012). Based upon the findings discussed in this dissertation, we suspect that type 1 neurons correspond to local interneurons, and type 2 neurons correspond to the tectothalamic GABAergic neurons.

Tectothalamic GABAergic neurons are thought to provide fast, feed-forward inhibition to the MGB (Ito et al., 2009; Venkataraman and Bartlett, 2013), a function that would likely be supported by the strong predominance of local excitatory inputs received by type 2 GABAergic neurons. Additionally, tectothalamic GABAergic neurons receive a high density of vglut2-positive axosomatic glutamatergic synapses (Ito et al., 2009), which may explain why type 2 neurons exhibit such strong responses to direct stimulation with glutamate uncaging, as well as why these neurons receive larger and more frequent spontaneous excitatory postsynaptic currents compared to type 1 neurons (Figure 4-6). Comparatively little is known about local GABAergic interneurons in the IC, apart from them being smaller than tectothalamic neurons and lacking vglut2-positive axosomatic glutamatergic synapses (Ito et al., 2009). However, a number of classes of cortical GABAergic interneurons have been found to receive extensive networks of both excitatory and inhibitory inputs, including parvalbumin-positive (PV) basket cells and somatostatin-positive (SST) Martinotti cells (Harris and Shepherd, 2015). This feature is shared

by type 1 GABAergic neurons, suggesting that these neurons may correspond to local inhibitory interneurons. Thus, based upon the combination of their local input map configurations, direct responses to glutamate uncaging and spontaneous excitatory synaptic currents, we predict that type 1 GABAergic CNIC neurons correspond to local interneurons, whereas type 2 GABAergic CNIC neurons correspond to tectothalamic projection neurons.

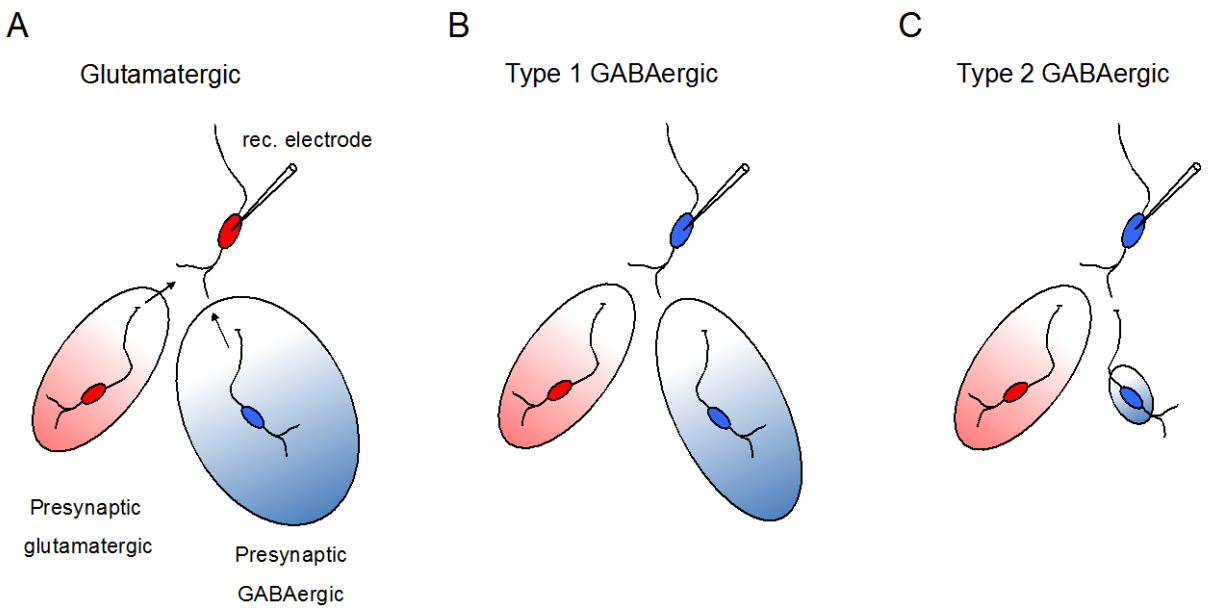

Figure 5-1. Intrinsic input map configurations in the CNIC.

Presynaptic neurons depict populations of synaptic connections. Red and blue circles are glutamatergic and GABAergic neurotransmission, respectively. Size of circles reflects amount of synaptic input received by recorded neuron. **(A)** Glutamatergic CNIC neurons receive local excitatory and inhibitory inputs, with a strong predominance of local inhibition. **(B)** Type 1 GABAergic neurons receive local excitatory and inhibitory inputs, with a slight excess of inhibition. **(C)** Type 2 GABAergic neurons receive substantial local excitatory input, with little or no inhibitory input.

In order to more definitely test the hypothesis that type 1 and type 2 GABAergic neurons correspond to local interneurons, and tectothalamic projection neurons, respectively, studies combing injections of retrograde neural tracers and synaptic input mapping could be performed. For example, injections of green fluorescent RetroBeads (Lumaflour, Inc.) could be performed in the MGB of vgat-ires-cre-dT animals, and CNIC neurons that express both tdTomato (indicating that the cell is GABAergic) and green fluorescent RetroBeads (indicating that the cell projects to the MGB) could be targeted for input mapping. If type 2 GABAergic neurons correspond to tectothalamic GABAergic neurons, then input-mapping studies in Bead+/dT+ neurons should reveal robust local excitatory input maps with minimal local inhibition. Alternatively, if type 1 GABAergic neurons correspond to the tectothalamic projection neurons, then these neurons receive substantial inhibitory input from local sources.

It is also possible that both type 1 and type 2 GABAergic neurons can be either local interneurons or tectothalamic projection neurons. In this case, the differences in local input map organization between type 1 and type 2 neurons may contribute to shaping distinct tuning properties (Egorova et al., 2001; Ehret et al., 2003; Portfors et al., 2011), discharge patterns (Peruzzi et al., 2000; Sivaramakrishnan and Oliver, 2001) and/or evoked response latencies (Hattori and Suga, 1997; Reetz and Ehret, 1999). For example, the significant local inhibition received by type 1 neurons may sharpen tuning curves and raise auditory response thresholds for sound frequencies that flank neurons' characteristic frequencies. The dominance of local excitation received by type 2 neurons, on the other hand, may broaden tuning curves and facilitate rapid sound-evoked response latencies.

In summary, although additional studies are needed to more clearly elucidate the functions of different glutamatergic and GABAergic CNIC neurons, our findings indicate that at

least three basic local circuit configurations are present in the CNIC: 1) glutamatergic neurons which receive local excitatory and inhibitory inputs, with a strong bias towards inhibition, 2) type 1 GABAergic neurons which receive local excitatory and inhibitory inputs, with a slight bias towards inhibition, and 3) type 2 GABAergic neurons which receive a predominance of local excitation, with little or no local inhibition.

5.4 A DEVELOPMENTAL CRITICAL PERIOD FOR INTRINSIC CIRCUIT PLASTICITY IN THE CNIC

Neural circuits are highly sensitive to changes in sensory input during developmental CPs and then become more resistant to reorganization after CP closure (Hensch, 2004). A classic example of the CP principle is seen in the development the visual system, where closure of one eye (monocular deprivation) during the initial weeks of visual experience causes a permanent loss of visual perception through that eye (Hubel and Wiesel, 1964; reviewed by Hensch, 2005). This loss of visual acuity occurs despite there being no damage to the retina or its postsynaptic target, the thalamic lateral geniculate nucleus (LGN), due to an expansion of cortical ocular dominance columns serving the non-deprived eye in primary visual cortex (V1) at the expense of those responding to the deprived eye. This phenomenon, which is referred to as ocular dominance plasticity, only occurs when monocular deprivation is delivered during early visual experience, while the CP is open (Gordon and Stryker, 1996).

In cortical circuits, CP opening occurs soon after the onset of sensory experience and coincides with the maturation of GABAergic neurotransmission (Hensch, 2005). In the CNIC, we demonstrated that excitatory and inhibitory intrinsic input maps undergo a period of dramatic

refinement just after hearing onset, involving a functional elimination of both excitatory and inhibitory inputs (Figure 2-5). However, while inhibitory input map areas are largely stable between P15-22, the functional elimination of excitatory synaptic inputs continues during this period (Figure 2-5 B). Thus, it is plausible that the CP for intrinsic CNIC connectivity is opened shortly after hearing onset, between P12 and P15, coincident with the maturation of local GABAergic inhibition. The continued refinement of synaptic excitation between P15-22, in turn, may reflect ongoing activity-dependent re-modeling of excitatory circuits after CP opening.

While CP opening closely follows the onset of sensory experience in rodents, CP closure often coincides with the developmental time point when neural circuits reach structural and functional maturity. For instance, in primary auditory cortex (A1), the topographic organization of neuronal characteristic frequency (CF) maps (in terms of size, tonotopic gradient and responsiveness) reaches an adult-like state by around P13-14, and the CP for tone-evoked reorganizations of CF organization closes around P13 (de Villers-Sidani et al., 2007; Froemke et al., 2011). In the CNIC, multiple lines of evidence indicate that acoustic response properties reach adult-like levels by the end of the third postnatal week (Willot and Shnerson, 1978; Shnerson and Willott, 1979; Ehret and Romand, 1992; Yu et al., 2005). The CP for experience-driven modifications of acoustic response properties in the CNIC likely closes around this time, since noise rearing beginning at the end of the second postnatal week, but not in adulthood, leads to long-lasting disruptions in the development of frequency tuning in the CNIC (Sanes and Constantine-Paton, 1983; Sanes and Constantine-Paton, 1985; Bures et al., 2014). Our findings that pulsed noise rearing from P12-25, but not P19-25, leads to substantial reorganizations of local synaptic circuits in the CNIC (Chapter 3), indicate that the CP for intrinsic CNIC connectivity also closes by the end of the third postnatal week. Accordingly, noise-rearing-

induced disruptions in frequency tuning in the CNIC may relate to a rewiring of intrinsic circuits.

5.5 INTRINSIC CIRCUIT PLASTICITY AFTER HEARING LOSS

Our findings indicate that noise trauma leads to a substantial reorganization of intrinsic CNIC circuits (Chapter 4), suggesting that cochlear hearing loss opens a 'sensitive window' for local circuit plasticity. This result is conceptually consistent with findings in the visual system, where sensory deprivation via dark exposure restores ocular dominance plasticity in V1 after closure of the developmental CP (He et al., 2006; Stodieck et al., 2014). In the auditory system, prolonged (6 months) noise exposure has been shown to reinstate CP plasticity for CF maps in A1 (Zhou et al., 2011), and this re-activation of plasticity may also relate to deprivation of normal acoustic input. Our results extend upon these studies, highlighting that the capacity for circuit plasticity after CP closure is not unique to cortical circuits, but is also present subcortically, in the auditory midbrain. Similar to cortical circuits, local circuit plasticity in the CNIC can also be unlocked via sensory deprivation.

In cortical circuits, sensory deprivation leads to a robust decrease in GABAergic inhibition (Takesian and Hensch, 2013; Hübener and Bonhoeffer, 2014), which is thought to represent a key step in the re-activation of CP plasticity (Huang et al., 2010; Zhou et al., 2011). In V1, for example, the restoration of ocular dominance plasticity in adulthood by dark exposure has been shown to involve a reduction in PV-expressing GABAergic interneurons, and is prevented by transiently increasing intracortical inhibition with diazepam treatment (Stodieck et al., 2014).

In the CNIC, the reinstatement of plasticity after hearing loss may involve a similar down-regulation of GABAergic inhibition (Chapter 4; Milbrandt et al., 2000; Dong et al., 2010). This down-regulation of inhibition may involve a degradation of perineuronal nets (PNNs), which have been shown to robustly and preferentially enrapture GABAergic neurons in the CNIC (Foster et al., 2014), and which are thought to function as molecular "brakes" on adult plasticity (Baveller et al., 2010). Perineuronal nets are aggregates of extracellular matrix that primarily consist of chondroitin sulfate proteoglycans, and which are thought to maintain excitatory: inhibitory balance in the adult brain (Hartig et al., 1999; Hensch, 2005). In the hippocampus, the degradation of PNNs surrounding GABAergic neurons has been shown to reduce perisomatic inhibition of pyramidal neuron targets (Saghatelyan et al., 2001), suggesting that PNNs are essential for the maintenance of GABAergic neurotransmission. Furthermore, in the visual system, degrading PNNs in V1 by injecting chondroitinase-ABC has been shown to reactivate ocular dominance plasticity in adulthood (Pizzorusso et al., 2002), presumably via a reduction in GABAergic inhibition. Taken together, these findings suggest that PNN degradation is sufficient to both decrease GABAergic inhibition and re-instantiate CP plasticity. In our studies, noise-induced degradation of PNNs surrounding GABAergic CNIC neurons may have contributed to reductions of inhibitory input onto glutamatergic neurons (Figure 4-4), which, in turn, may have re-opened the CP for intrinsic CNIC circuit plasticity and enabled other forms of synaptic reorganization to take place.

It is interesting to note that the effects of pulsed noise rearing delivered from P12-25 on intrinsic CNIC networks were roughly the inverse of the effects of noise-trauma at P21 (Figure 5-2). Pulsed noise delivered during the CP led to a reduction in excitatory input onto glutamatergic neurons, and to an increase in excitatory input onto type 1 GABAergic neurons,

which together produce a ‘hyper-inhibited’ state of the intrinsic CNIC network (Chapter 3). In contrast, noise-trauma led to a reduction of inhibitory input onto glutamatergic neurons and to a reduction of excitatory input onto type 1 GABAergic neurons, which together produced a ‘dis-inhibited’ state of intrinsic CNIC networks in mice with behavioral evidence of tinnitus (Chapter 4). These findings support the view that decreases and increases in GABAergic inhibition can open and close sensitive windows for synaptic circuit plasticity, respectively (Hensch, 2005).

Given that developmental noise rearing effectively results in a hyper-inhibited state of the intrinsic CNIC network, whereas noise trauma produces a dis-inhibited state of the network in mice with behavioral evidence of tinnitus, it is possible that noise-reared mice would exhibit resistance to noise-induced tinnitus. Theoretically, the hyper-inhibited state of the CNIC in noise-reared mice should serve as a buffer against hearing loss-related reductions in inhibition that correlate with tinnitus. To test this hypothesis, gap detection behavior could be compared between noise-reared mice (reared from P12-P25) exposed to acoustic trauma at P26 and age-matched control mice that were reared under normal housing conditions and that received identical acoustic trauma. Since noise rearing is associated with reductions in frequency tuning in the IC (Sanes and Constantine-Paton 1983; Sanes and Constantine-Paton, 1985), it would also be necessary to control for the possibility that noise rearing alone alters gap detection behavior. To account for this, it would be important to include an additional noise-reared control group (reared from P12-25) that that did not receive noise trauma.

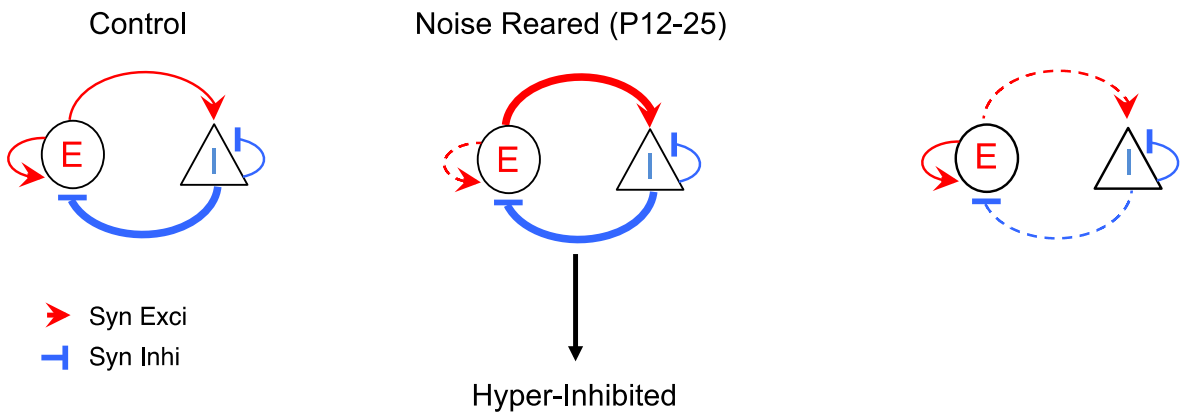

Figure 5-2. Comparison of IC network reorganizations after noise rearing and noise trauma.

Schematized intrinsic IC circuits with glutamatergic neurons (circle) and type 1 GABAergic neurons (triangle). Red arrows depict the population of excitatory connections and blue lines depict inhibitory connections. Input strength is indicated by the widths of connecting lines. Dashed lines indicate weakened connections. In noise-reared mice, glutamatergic neurons lose excitation and GABAergic neurons gain excitation. In noise-traumatized mice with behavioral evidence of tinnitus, glutamatergic neurons lose inhibition and GABAergic neurons lose excitation.

5.6 ACOUSTIC EXPERIENCE AFTER HEARING LOSS

We found that a single week of acoustic enrichment (AE) with non-traumatic patterned white noise, delivered immediately after acoustic trauma, was sufficient to block hearing loss-induced plasticity in intrinsic CNIC networks (Figure 4-10, 4-11). This effect of AE is due to one of two processes: either 1) AE closes the post-traumatic plasticity window before reorganizations take place, or 2) AE reverses reorganizations that have already taken place.

Distinguishing between these two possibilities would require further studies. It would first be necessary to determine the timing of post-traumatic synaptic reorganization in the CNIC, which would involve sequential, day-by-day input mapping studies of intrinsic connectivity after hearing loss (Figure 5-3 A). Once the timing(s) of post-traumatic synaptic reorganization is defined, it would then be possible to divide the post-traumatic plasticity window into two phases: a pre-reorganization phase and post-reorganization phase. If AE closes the post-traumatic plasticity window prior to synaptic reorganizations taking place, as opposed to reversing reorganizations that have taken place, then delivering AE during the post-reorganization phase should not prevent circuit reorganizations from taking place (Figure 5-3 B). Alternatively, if pulsed noise reverses established patterns of circuit reorganization in the CNIC, then AE delivered during the post-reorganization phase should be sufficient to abolish noise-induced synaptic reorganizations (Figure 5-3 B).

It also remains to be determined whether pulsed noise exerts similar effects on the functional organization of intrinsic CNIC circuits during the post-traumatic plasticity window compared to the developmental CP. The first possibility is that pulsed noise closes plasticity windows both during development and following acoustic trauma. If this is the case, then intrinsic input maps in mice exposed to pulsed noise from P12-25 should appear similar to input

maps from mice at P12 (since activity-dependent refinement would be prevented by premature CP closure), and input maps from noise-exposed mice that received AE should appear similar to input maps from non-traumatized mice at P21. However, due to differences in both recording and stimulation conditions between studies, it was not possible to directly compare the input maps from mice aged P26-30 (Chapters 3 and 4) to those from mice aged P2-22 (Chapter 2). Instead, we compared noise-exposed mice that received AE to non-exposed control mice at P26-30. Since intrinsic networks in the CNIC appear to be largely mature by P21, the input maps from non-exposed control mice at P26-30 are likely similar to those at P21. Given that both glutamatergic and GABAergic neurons from noise-exposed mice that received AE exhibited stable excitatory and inhibitory input maps compared to age-matched controls, we suspect that pulsed noise closes plasticity windows after acoustic trauma similar to in development.

There are two alternative explanations. First, rather than closing plasticity windows, pulsed noise might exert similar effects during development and after noise trauma. In this case, input maps from noise-exposed mice that received AE might exhibit a combination of the effects of noise rearing from P12-25 and noise-trauma (since both forms of reorganization would be taking place simultaneously). In this scenario, glutamatergic neurons would exhibit decreased excitatory (from pulsed noise, Figure 3-5) as well as decreased inhibitory input (from noise trauma, Figure 4-4), and GABAergic neurons would exhibit a combination of increased (from pulsed white noise, Figure 3-1) and decreased (from noise trauma, Figure 4-7) excitatory input, perhaps resulting in a maintenance of excitatory inputs compared to control levels. However, our findings were inconsistent with this prediction. While GABAergic neurons from noise-exposed mice that received AE did exhibit stable excitatory input maps compared to controls, glutamatergic neurons did not show reductions in either excitatory or inhibitory input, but rather

appeared similar to age-matched control mice (Figure 4-10).

Second, pulsed noise may exert different effects on intrinsic input maps during development and after noise trauma. In this case, input maps from noise-exposed mice that received AE might exhibit the effects of noise trauma, in addition to pattern(s) of reorganization not found in noise-reared mice. In this scenario, pulsed noise delivered after hearing loss would most likely have led to some change in the organization of intrinsic CNIC networks compared to control mice. However, this was not the case, since both GABAergic and glutamatergic neurons from noise-exposed mice that received AE exhibited excitatory and inhibitory input maps that were comparable to control mice (Figure 4-10). Thus, the most parsimonious explanation of our findings is that pulsed white noise inhibits plasticity in intrinsic CNIC circuits both during development and after hearing loss.

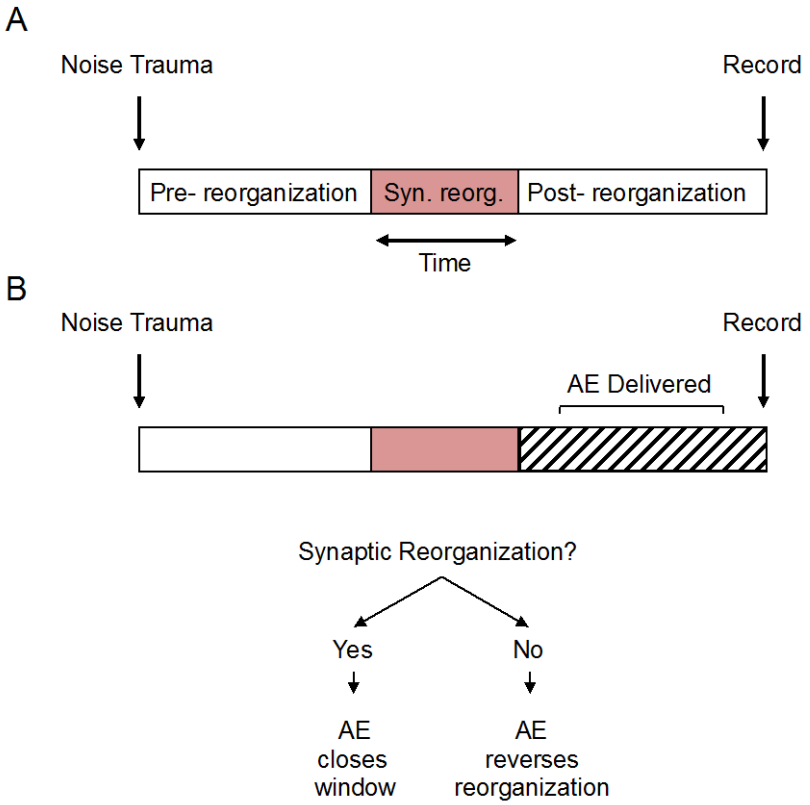

Figure 5-3. Determining how post-traumatic AE prevents synaptic circuit reorganization after hearing loss. **(A)** After noise trauma, the post-trauma plasticity window is divided into pre-reorganization and post-reorganization phases (yet to be experimentally determined). **(B)** Delivering AE during the post-reorganization phase will illustrate whether AE prevents changes from occurring in local CNIC networks after hearing loss, or whether it reverses changes that have occurred. **Legend**: AE; Acoustic enrichment with pulsed white noise.

5.7 CLINICAL RELEVANCE OF DISSERTATION FINDINGS: TINNITUS

We found that immediate, post-traumatic acoustic stimulation dramatically reduces the percentage of noise-traumatized mice that develop behavioral evidence of tinnitus as measured by acoustic gap detection (Turner et al., 2006; Li et al., 2014) (Figure 4-11). This result points to the exciting possibility of using post-traumatic acoustic stimulation as a prophylactic measure to prevent the development of tinnitus after noise trauma in humans. Although acoustic stimulation (e.g. sound therapy) has been used in the treatment of tinnitus for many years, it has been largely unsuccessful (Vanneste et al., 2013; Folmer et al., 2014). This ineffectiveness may relate to the fact that sound therapies are typically delivered long after tinnitus has developed, presumably after the post-traumatic plasticity window has closed.

Why is post-traumatic acoustic stimulation effective in preventing the emergence of behavioral evidence of tinnitus? One possibility is that acoustic enrichment bolsters overall levels of sound stimulation, and in doing so, prevents deprivation-induced reorganizations of auditory circuits from taking place. In this case, the precise spectrotemporal nature of the enriching stimulus might have little impact on its effectiveness in preventing tinnitus, and many different stimuli may prove effective. Alternatively, the nature of the post-traumatic AE stimulus may be crucial. For example, in the developing A1 of rodents, stimulation with pulsed white noise during the developmental critical period produces a permanent disruption of tonotopic maps (Zhang et al, 2002), whereas map distortions caused by stimulation with unstructured noise are reversible (Chang and Merzenich, 2003). Similar principles may govern the post-traumatic plasticity window, in which case the precise patterning of AE may be important in closing the window and preventing tinnitus-related circuit reorganizations from occurring after acoustic trauma. Distinguishing between these possibilities will involve comparing the effectiveness of a

variety of post-traumatic acoustic stimuli in preventing the emergence of behavioral evidence of tinnitus.

In addition to determining the importance of AE stimulus makeup in preventing the emergence of tinnitus behavior, it will also be critical to define the length of the post-traumatic window where AE is effective. A recent study revealed that in a subset of noise-traumatized mice, reductions in the activity of KCNQ2/3 potassium channels in fusiform cells of the DCN, which are critical for the induction of tinnitus (Li et al., 2013), recover between 4 and 7 days after acoustic trauma, and in doing so, boost resilience to tinnitus (Li et al., 2015). Noise-induced reductions of KCNQ2/3 channel activity are necessary for the emergence of tinnitus-related increases in spontaneous firing rates (SFRs) of DCN fusiform cells (Li et al., 2013), and since the CNIC is the major postsynaptic target nucleus of these cells, changes in the firing rates of DCN neurons after noise trauma likely either drive or parallel synaptic reorganizations that take place in local CNIC circuits (Manzoor et al., 2012). It remains to be determined whether post-traumatic AE promotes the recovery of KCNQ2/3 channel activity in DCN fusiform cells and/or prevents the emergence of increased SFRs in these cells, but it is reasonable to predict that AE would be effective in preventing the development of tinnitus as long as it is delivered before tinnitus-related changes in the DCN and CNIC are permanently instantiated. Thus, it is likely that the post-traumatic window where AE is effective in preventing tinnitus closes between 4 and 7d after noise trauma, when reductions in KCNQ2/3 channel activity in the DCN that lead to hyperactivity in the ascending auditory pathway are reversible.

It will also important to determine whether the CNIC retains the capacity for further CP induction after an initial episode of hearing loss has taken place, since the majority of tinnitus patients present for treatment long after the inciting acoustic overexposure has taken place,

Effectively treating these chronic tinnitus sufferers may require the ability to harness CP plasticity long after the noise-induced neural circuit reorganizations that lead to their tinnitus have occurred. It will be therefore be important to determine whether additional episodes of acoustic trauma delivered to mice with established tinnitus are able to re-open CP plasticity, and in particular, whether AE is able to reverse tinnitus in these animals. The ability to re-open plasticity windows in the auditory system, whether by acoustic deprivation or other means, may dramatically improve the efficacy of current and future sound-based therapies in the treatment of tinnitus and other hearing disorders.

5.8 CLINICAL RELEVANCE OF DISSERTATION FINDINGS: HEARING DEVELOPMENT

We found that introducing pulsed white noise during an early critical period of hearing experience has a profound impact on the maturation of neuronal circuitry in the auditory midbrain. Although it has been recognized for some time that developmental hearing loss can disrupt neuronal development (see Butler and Lomber, 2013 for review) and produce long-lasting hearing deficits (see Whitton and Polley, 2011 for review), our results highlight that even a seemingly benign manipulation like introducing mild pulsed white noise can have dramatic effects on the maturation of auditory circuits. Furthermore, while a number of studies have demonstrated changes in auditory cortical processing after developmental hearing loss (Popescu and Polley, 2007; Polley et al., 2013; Buran et al., 2014; Mowery et al., 2014; Caras and Sanes, 2015; see Kral et al., 2005 for Review) or noise rearing (Zhang et al., 2001; Zhang et al., 2002; Chang et al., 2005; Zhou and Merzenich, 2008), our findings provide the first evidence that

developmental noise rearing can produce substantial synaptic circuit reorganization subcortically, at the level of the inferior colliculus.

These findings may have a number of important clinical implications. Although prior human studies have demonstrated that children who experience developmental hearing loss (even reversible) are at an increased risk for abnormalities in brainstem physiology (Gravel et al., 2006), binaural hearing (Gunnarson and Finitzo, 1991; Gravel et al., 2006) and receptive language skills (Mody et al., 1999; Catts et al., 1999; Paradise et al., 2003), comparatively little is known about the importance of patterned acoustic stimulation for the normal development of the human auditory system . Based upon our results, we extrapolate that children growing up in different acoustic environments, who are exposed to different patterns of acoustic stimulation during early hearing development, may exhibit fundamentally different patterns of auditory circuit organization. For example, children who are raised in densely populated, urban environments may exhibit differently organized central auditory pathways from children who are raised in lightly populated, rural environments. Different acoustic rearing environments may result in neuronal circuit arrangements that are adaptive for processing sound attributes prevalent in some settings (likely those encountered in early development) and not others. This line of reasoning leads to the prediction that when adults who grew up in cities move to rural environments (or vice versa), they may experience diminished auditory processing capabilities, particularly for types of sounds that are exclusive to their new settings.

In addition to raising questions about the importance of patterned acoustic stimulation during childhood, our findings may also have important implications for the care of preterm infants in neonatal intensive care units (NICU). Pre-term infants are especially sensitive to environmental noise, due of the early developmental stage of their auditory systems (McMahon

et al., 2012), and the noisy, high frequency sounds found in the NICU differ substantially from the predominately low frequency sounds encountered in the protected environment of the womb (Lahav and Skoe, 2014). Apart from qualitatively differing from the sounds encountered in the womb, noise encountered in the NICU can also mask human speech sounds, potentially limiting the richness of linguistic stimulations. In response to these concerns, some have advocated for a "culture of silence" in NICU settings (Swathi et al., 2014). However, we have concerns with this approach as well. Given our findings that the "nature" of early acoustic experience can be as crucial as the "level" of sound exposure for the development of the central auditory pathways, we suspect that silence may also be detrimental to proper neuronal development. In addition to keeping overall sound levels at non-traumatic intensities, it may be important to design acoustic environments for NICU infants that incorporate the low frequency sounds that they would likely encountered in the womb had they not been born early.

5.9 OVERALL CONCLUSION

Taken as a whole, evidence from the studies in this dissertation shed significant light on the development and plasticity of intrinsic connectivity in the mammalian auditory midbrain. Our findings support a view of local circuit connectivity in the CNIC where excitatory and inhibitory neurons receive extensive, cell-specific patterns of synaptic input. These local circuits undergo substantial developmental refinement, in a manner that is highly sensitive to changes in acoustic experience during an early critical period. These circuits also undergo substantial reorganizations after hearing loss, the nature of which specifically correlate with the presence or absence of behavioral evidence of tinnitus. As in development, hearing-loss-induced circuit reorganizations

are highly sensitive to changes in the acoustic environment, and can be prevented by delivering early, post-traumatic acoustic enrichment. Most surprisingly, post-traumatic acoustic stimulation also dramatically reduces the percentage of noise-traumatized animals that develop tinnitus.

BIBLIOGRAPHY

Adams JC (1979) Ascending projections to the inferior colliculus. *J. Comp. Neurol.* **183**: 519 – 538.

Adams JC (1980) Crossed and descending projections to the inferior colliculus. *Neurosci. Lett.* 19: 1-5.

Aitkin L (1979) The auditory midbrain. *Trends in Neurosciences* **2**: 308-310.

Aitkin LM & Phillips SC (1984b) Is the inferior colliculus an obligatory relay in the cat auditory system? *Neuroscience Letters* **44**: 259-264.

Aitkin LM & Schuck D (1985) Low frequency neurons in the lateral central nucleus of the cat inferior colliculus receive their input predominantly from the medial superior olive. *Hearing Res.* **17**:87–93.

Alvarado JC, Fuentes-Santamaria V, Franklin SR, Brunso-Bechtold JK, Henkel CK (2005) Unilateral cochlear ablation in adult ferrets results in upregulation in calretinin immunostaining in the central nucleus of the inferior colliculus. *Neuroscience* **136(3):** 957-969.

Andersen RA, Roth GL, Aitkin LM & Merzenich MM (1980) The efferent projections of the central nucleus and the pericentral nucleus of the inferior colliculus in the cat. *J. Comp. Neurol*. **194(3):** 649-662.

Baguley D, McFerran D & Hall D (2013) Tinnitus. *The Lancet*. **382**: 1600-1607.

Bajo VM & King AJ (2013) Cortical modulation of auditory processing in the midbrain. *Front. Neural Circ*uits **6:** 10.3389.

Bajo VM & Moore DR (2005) Descending projections from the auditory cortex to the inferior colliculus in the gerbil, Meriones unguiculatus. *J. Comp. Neurol.* ***486*****:** 101–116.

Bajo VM, Nodal FR, Moore DR & King AJ (2010) The descending corticocollicular pathway mediates learning-induced auditory plasticity. *Nat. Neurosci*. **13(2):** 253-260.

Bao S, Chang EF, Davis JD, Gobeske KT & Merzenich MM (2003) Progressive Degradation and Subsequent Refinement of Acoustic Representations in the Adult Auditory Cortex. *J. Neurosci.* **23**(**34**): 10765-10775.

Bauer CA & Brozoski TJ (2001) Assessing tinnitus and prospective tinnitus therapeutics using a psychophysical animal model. *J. Assoc. Res. Otolaryngol*. **2**: 54-64.

Bauer CA, Brozoski TJ, Holder TM & Caspary DM (2000) Effects of chronic salicylate on GABAergic activity in rat inferior colliculus. *Hearing Res*. **147**: 175-182.

Bauer CA, Turner JG, Caspary DM, Myers KS & Brozoski TJ (2008) Tinnitus and inferior colliculus activity in chinchillas related to three distinct patterns of cochlear trauma. *J. Neurosci. Res*. **86**: 2564-2578.

Baveller D, Levi DM, Li RW, Dan Y & Hensch T (2010) Removing Brakes on Adult Brain Plasticity: From Molecular to Behavioral Interventions. *J. Neursoci.* **30(45**): 14964-14971.

Bennet JE & Bair W (2015) Refinement and Pattern Formation in Neural Circuits by the Interaction of Traveling Waves and Spike-Timing Dependent Plasticity. *PLoS Comput. Biol.* **11(8**): e1004422.

Berger JI & Coomber B (2015) Tinnitus-related changes in the inferior colliculus. *Front. Neurol*. **6**: 61.

Bledsoe SC Jr, Nagase S, Miller JM & Altschuler RA (1995) Deafness-induced plasticity in the mature central auditory system. *Neuroreport* **7(1):** 225-229.

Boyen K, Baskent D & van Dijk P (2015) The Gap Detection Test: Can It Be Used to Diagnose Tinnitus? *Ear Hear*. **36(4):** e138-145.

Bregman AS, Abramson J, Doehring P & Darwin CJ (1985) Spectral integration based on common amplitude modulation. *Percept Pscyhophys*. **37**: 483-493.

Brozoski TJ & Bauer CA (2005) The effect of dorsal cochlear nucleus ablation on tinnitus in rats. *Hear. Res.* **206(1-2):** 227-236.

Brozoski TJ, Bauer CA & Caspary DM (2002) Elevated fusiform cell activity in the dorsal cochlear nucleus of chinchillas with psychophysical evidence of tinnitus. *J. Neurosci.* **22**: 2382-2389.

Brozoski TJ, Wisner KW, Sybert LT & Bauer CA (2012) Bilateral dorsal cochlear nucleus lesions prevent acoustic-trauma induced tinnitus in an animal model. *J. Assoc. Res. Otolaryngol*. **13(1):** 55-66.

Brunso-Bechtold JK, Thompson GC & Masterton RB (1981) HRP study of the organization of auditory afferents ascending to central nucleus of inferior colliculus in cat. *J Comp. Neurol.* 197:705–722.

Butler BE & Lomber SG (2013) Functional and structural changes throughout the auditory system following congenital and early onset deafness: implications for hearing restoration. *Front. Syst. Neurosci*. **7**: 92.

Buran BN, Sarro EC, Manno FA, Kang R, Caras ML & Sanes DH (2014) A sensitive period for the impact of hearing loss on auditory perception. *J. Neurosci*. **24(6):** 2276-2284.

Bures Z, Bartosova J, Lindovsky J, Chumak T, Popelar J & Syka J (2014) Acoustic enrichment during early postnatal development changes response properties of inferior colliculus neurons in rats. *Eur. J. Neurosc*i**. 40**: 3674-3683.

Burger RM & Pollak GD (2001) Reversible inactivation of the dorsal nucleus of the lateral lemniscus reveals its role for processing multiple sound sources in the inferior colliculus. *J. Neurosci*. **21**:4830–4843.

Callaway EM & Katz LC (1993) Photostimulation using caged glutamate reveals functional circuitry in living brain slices. *Proc. Natl. Acad. Sci.* **90(16):** 7661-7665.

Case DT, Zhao X & Gillespie DC (2011) Functional refinement in the projection from ventral cochlear nucleus to lateral superior olive precedes hearing onset in rat. *PLoS One* **6(6):** e20756.

Caicedo A & Herbert H (1993) Topography of descending projections from the inferior colliculus to auditory brainstem nuclei in the rate. *J. Comp. Neurol.* **328**: 377-392.

Campagnola L & Manis PB (2014) A map of functional synaptic connectivity in the mouse anteroventral cochlear nucleus. *J. Neurosci*. 21: 4830-4843.

Calford MB & Aitkin LM (1983) Ascending projections to the medial geniculate body of the cat: evidence for multiple parallel auditory pathways through thalamus. *J. Neurosci*. **3(11**): 2365-2380.

Campolo J, Lobarinas E and Salvi R (2013) Does tinnitus “fill in” the silent gaps? *Noise Health*. **15**: 398-405.

Cant NB & Benson CG (2006) Organization of the inferior colliculus of the gerbil (Meriones unguiculatus): differences in distribution of projections from the cochlear nuclei and the superior olivary complex. *J. Comp. Neurol.* **495**: 511–528.

Cant NB, & Benson CG (2008) Organization of the inferior colliculus of the gerbil (Meriones unguiculatus): projections from the cochlear nucleus. *Neuroscience* **154**: 206–217.

Catts HW, Fey ME, ZhangX, TomblinJB (1999) Language basis of reading and reading disabilities: evidence from a longitudinal investigation. *Sci Stud Reading* **3**:331–361.

Caras ML & Sanes DH (2015) Sustained Perceptual Deficits from Transient Sensory Deprivation. *J. Neursoci*. **35(30):** 10831-10842.

Casseday JH, Fremouw T & Covey E (2002) The inferior colliculus: a hub for the central auditory system. In: Integrative functions in the mammalian auditory pathway, pp 238–318. New York: Springer.

Chandrasekaran L, Xiao Y & Sivaramakrishnan S (2013) Functional architecture of the inferior colliculus revealed with voltage-sensitive dyes. *Front. Neural Circ*. **7**: 41.

Chang EF, Bao S, Imaizumi K, Schreiner CE & Merzenich MM (2005) Development of spectral and temporal response selectivity in the auditory cortex. *Proc. Natl. Acad. Sci*. **102(45):** 16460-16465.

Chang EF & Merzenich MM (2003) Environmental Noise Retards Auditory Cortical Development. *Science* **300**: 498-502.

Clause A, Kim G, Sonntag M, Weisz CJ, Vetter DE, Rubsamen R & Kandler K (2014) The precise pattern of prehearing spontaneous activity is necessary for tonotopic map refinement. *Neuron* **82**: 822-835.

Clause A, Nguyen T & Kandler K (2012) An acoustic startle-based method of assessing frequency discrimination in mice. *J. Neurosci. Methods*. **200**: 63-67.

Coomber B, Berger JI, Kowalkowski VL, Schackleton TM, Palmer AR & Wallace MN (2014) Neural changes accompanying tinnitus following unilateral acoustic trauma in guinea pigs. *Eur. J. Neurosci*. **40**: 2427-2421.

Covey E, Kauer JA & Casseday JK (1996) Whole-cell patch-clamp recordings reveals subthreshold sound-evoked postsynaptic currents in the inferior colliculus of awake bats. *J. Neurosci.* **16**: 3009-3018.

de Villers-Sidani E, Chang EF, Bao S & Merzenich MM (2007) Critical period window for spectral tuning defined in primary auditory cortex (A1) in the rat. *J. Neurosci.* **27(1**): 180-189.

de Villers-Sidani E, Simpson KL, Lu Y-F, Lin RCS & Merzenich MM (2008) Manipulating critical period closure across different sectors of primary auditory cortex. *Nat. Neurosci*. **11**(8): 957-965.

Delage H & Tuller L (2007) Language development and mild-to-moderate hearing loss: does language normalize with age? *Journal of Speech, Language, and Hearing Research : JSLHR*, **50:** 1300–1313

Dehmel S, Eisinger D & Shore SE (2012) Gap prepulse inhibition and auditory brainstem-evoked potentials as objective measures for tinnitus in guinea pigs. *Front. Syst. Neurosci.* **6**: 42

Dille MF, Konrad-Martin D, Gallun F, Helt W, Gordon J, Reavis KM, Bratt, GW & Fausti A. (2010). Tinnitus onset rates from chemotherapeutic agents and ototoxic antibiotics; results of a large prospective study. *J. Am. Acac. Audiol*. **21**: 409-417.

Dong S, Mulders WH, Rodger J & Robertson D (2009) Changes in neuronal activity and gene expression in guinea-pig auditory brainstem after unilateral partial hearing loss. *Neuroscience*. **159**: 1164-1174

Dong S, Mulders WH, Rodger J, Woo S & Robertson D (2010) Acoustic trauma evokes hyperactivity and changes in gene expression in the guinea pig auditory brainstem. *Eur. J. Neurosci*. **9**: 1616-1628

Dong S, Rodger J, Mulders WH & Robertson D (2010) Tonotopic changes in GABA receptor expression in guinea pig inferior colliculus after partial unilateral hearing loss. *Brain Res*. **1342**: 24-32.

Egorova M & Ehret G (2008) Tonotopy and inhibition in the midbrain inferior colliculus shape spectral resolution of sounds in neural critical bands. *Eur. J. Neurosc*i. **28**: 675– 692.

Egorova M, Ehret G, Vartanian I & Esser KH (2001) Frequency response areas of neurons in the mouse inferior colliculus: I. Threshold and tuning characteristics. *Exp. Brain Res.* **140**:145–161.

Ehret G & Merzenich MM (1998): Complex sound analysis (frequency resolution, filteraing and spectral integration) by single units in the inferior colliculus of the cat. *Brain Res.* **472(2):** 139-163.

Ehret G & Romand R (1992) Development of tone response thresholds, latencies and tuning in the mouse inferior colliculus. *Brain Res. Dev. Brain. Res.* **67(2):** 317-326.

Ehret G & Romand R (1994) Development of tonoptopy in the inferior colliculus II: 2-DG measurements in the kitten. *J. Neurosci*. 6: 1589-1595.

Ehret G, Egorova M, Hage SR & Muller BA (2003) Spatial map of frequency tuning-curve shapes in the mouse inferior colliculus. *Neuroreport* **14**: 1365-1369.

Engineer ND, Riley JR, Seale JD, Vrana WA, Shetake JA, Sudanagunta SP, Borland MS & Kilgard MP (2011) Reversing pathological neural activity using targeted plasticity. *Nature* **470:** 101-104.

Escabi MA & Schreiner CE (2002) Nonlinear spectrotemporal sound analysis by neurons in the auditory midbrain. *J. Neurosci.* 22: 4114-4131.

Fagiolini M & Hensch TK (2000) Inhibitory threshold for critical-period activation in primary visual cortex. *Nature* **404(6774**): 183-186.

Faingold CL (2002) Role of GABA abnormalities in the inferior colliculus pathophysiology-audiogenic seizures. *Hearing Res.* **168(1-2**): 223-237.

Faingold CL, Anderson CA & Randall ME (1993) Stimulation or blockade of the dorsal nucleus of the lateral lemniscus alters binaural and tonic inhibition in contralateral inferior colliculus neurons. *Hearing Res*. **69**: 98–106.

Fathke RL & Gabriele ML (2009) Patterning of multiple layered projections to the auditory midbrain prior to experience. *Hearing Res*. **249**:36–43.

Folmer RL, Theodoroff SM, Martin WH & Whi Y (2014) Experimental, controversial and futuristic treatments for chronic tinnitus. *J. Am. Acad. Audiol*. **35(1):** 106-125.

Foster NL, Mellott JG & Schofield BR (2014) Perineuronal nets and GABAergic cells in the inferior colliculus of guinea pigs. *Front. Neuroanat*. **7**: 53.

Fournier P & Hebert S (2013) Gap detection deficits in humans with tinnitus as assessed with the acoustic startle paradigm: does tinnitus fill in the gap? *Hear. Res.* **295:** 16-23.

Franklin SR, Bruso-Bechtold JK & Henkel CK (2006) Unilateral cochlear ablation before hearing onset disrupts the maintenance of dorsal nucleus of the lateral lemniscus projection patterns in the rat inferior colliculus. *Neuroscience* **143 (1):** 105-115.

Franklin SR, Bruso-Bechtold JK & Henkel CK (2008) Bilateral cochlear ablation in neonatal rats disrupts development of banded pattern of projections from the dorsal nucleus of the lateral lemniscus to the inferior colliculus. *Neuroscience* **154(1):** 346-354

Froemke RC & Jones BJ (2011) Development of auditory cortical synaptic receptive fields. *Neuroscience and Biobehavioral Reviews* **35**: 2105-2113.

Fubara BM, Casseday JH, Covey E & Schwartz-Bloom RD (1996) Distribution of GABAA, GABAB, and glycine receptors in the central auditory system of the big brown bat, Eptescus fuscus. *J.Comp. Neurol.* **369**: 83-92.

Fuzesseery ZM, Richardson MD & Coburn MS (2006) Neural mechanisms underlying selectivity for the rate and direction of frequency-modulated sweeps in the inferior colliculus of the pallid bat. *J. Neurophysiol*. **96**: 1320-1336.

Gabriele ML, Brunso-Bechtold JK & Henkel CK (2000a) Development of afferent patterns in the inferior colliculus of the rat: projection from the dorsal nucleus of the lateral lemniscus. *J Comp. Neurol.* **416:** 368 –382.

Gabriele ML, Brunso-Bechtold JK & Henkel CK (2000b) Plasticity in the development of afferent patterns in the inferior colliculus of the rat after unilateral cochlear ablation. *J. Neurosci.* **20** :6939–6949.

Gabriele ML, Shahmoradian SH, French CC, Henkel CK & McHaffie JG (2007) Early segregation of layered projections from the lateral superior olivary nucleus to the central nucleus of the inferior colliculus in the neonatal cat. *Brain Research* **1173**: 66–77.

Gao E & Suga N (1998) Experience-dependent corticofugal adjustment of midbrain frequency map in bat auditory system. *Proc. Natl. Acad. Sci*. **95**, 12663-12670.

Gittelman JX, Li N & Pollak GD (2009) Mechanisms underlying directional selectivity for frequency-modulated sweeps in the inferior colliculus revealed by in vivo whole-cell recordings. *J. Neurosci*. **29:** 13030-13041.

Glendenning KK & Masterton RB (1983) Acoustic chiasm: efferent projections of the lateral superior olive. *J. Neurosci*. **3**: 1521-1537.

Gold JR & Bajo VM (2014) Insult-induced adaptive plasticity of the auditory system. *Front. Neurosci*. **8**: 110.

González-Hernández T, Mantolán-Sarmiento B, González-González B & Pérez-González H (1996) Sources of GABAergic input to the inferior colliculus of the rat. *J. Comp. Neurol*. **372(2):** 309-326.

Goodman CS, Shatz CJ. Developmental mechanisms that generate precise patterns of neuronal connectivity. Cell, 1993; 72.

Gordon JA & Stryker MP (1996) Experience-dependent plasticity of binocular responses in the primary visual cortex of the mouse. *J. Neurosci*. **16(10):** 3274-3286.

Gravel JS, Wallace IF & Ruben RJ (1996) Auditory consequences of early mild hearing loss associated with otitis media. *Acta Otolaryngol* **116** :219 –221

Gravel JS, Roberts JE, Roush J, Grose J, Besing J, Burchinal M, Neebe E, Wallace IF & Zeisel S (2006) Early otitis media with effusion, hearing loss, and auditory processes at school age. *Ear Hear*. **27**: 353–368

Grecova J, Bures Z, Popelar J, Suta D & Syka J (2009) Brief exposure of juniveline rats to noise impairs the development of the response properties of inferior colliculus neurons. *Eur. J. Neurosc*i**. 29**: 1921-1930.

Grimsley CA, Sanchez JT & Sivaramakrishnan S (2013) Midbrain local circuits shape sound intensity codes. *Front. Neural Circuits*. **7**: 174.

Groves GM, Boyle RD, Welker RL & Miller SW (1974) On the mechanism of prepulse inhibition. *Physiol. Behav.* **5**: 367-375.

Guinnan JJ Jr, Guinan SS & Norris BE (1972a) Single auditory units in the superior olivary complex. I: Responses to sounds and classifications based on physiological properties. *Int. J. Neurosci* **4**: 101-120.

Guinnan JJ Jr, Norris BE & Guinan SS (1972b) Single auditory units in the superior olivary complex. II: Locations of unit categories and tonotopic organization. *Int. J. Neurosci.* **4**: 147-166.

Gunnarson AD & Finitzo T (1991) Conductive hearing-loss during infancy—effects on later auditory brain-stem electrophysiology. *J Speech Hear Res.* **34**:1207–1215

Haas JS, Nowotny T & Arbarbanel HD (2006) Spike-timing dependent plasticity of inhibitory synapses in entorhinal cortex. *J. Neurophys.* **96**(6): 3305-3313.

Harris KD & Shepherd GMG (2015) The neocortical circuit: themes and variations. *Nat. Neuroscience.* **18***:* 170-181.

Harrison RV, Ibrahim D & Mount RJ (1998) Plasticity of tonotopic maps in auditory midbrain following partial cochlear damage in the developing chinchilla. *Experimental Brain Research* **123**: 449-460.

Härtig W, Derouiche A, Welt K, Brauer K, Grosche J, Mäder M, Reichenbach A & Brückner G (1999) Cortical neurons immunoreactive for the potassium channel Kv3.1b subunit are predominantly surrounded by perineuronal nets presumed as a buffering system for cations. *Brain Res*. **842(1):** 15-29.

Hattori T & Suga N (1997) The inferior colliculus of the mustached bat has the frequency-vs-coordinates. *J. Comp. Physiol. A.* **180**: 271-284.

He HY, Hodos W, Quinlan EM (2006) Visual deprivation reactivates ocular dominance plasticity in adult visual cortex. *J. Neurosci.* **26(11):** 2951-2955.

Hefner HE & Harrington IA (2002) Tinnitus in hamsters following exposure to intense sound. *Hear. Res*. **170**: 83-95.

Helfer TM, Jordan NN, Lee RB, Pietrusiak P, Cave K & Schairer K (2011) Noise-induced hearing injury and comorbidities among postdeployment U.S. Army soldiers: April 2003-June 2009. *Am. J. Audiol*. **20**: 33-41.

Henkel CK, Gabriele ML & McHaffie JG (2005) Quantitative assessment of developing afferent patterns in the cat inferior colliculus revealed with calbindin immunohistochemistry and tract tracing methods. *Neuroscience* **136**:945–955

Henkel CK, Keiger CJ, Franklin SR & Brunso-Bechtold JK (2007) Development of banded afferent compartments in the inferior colliculus before onset of hearing in ferrets. *Neuroscience* **146**:225–235.

Hensch TK (2004) Critical period regulation. *Annu. Rev. Neurosci.* **27**: 549–579.

Hensch TK (2005) Critical period mechanisms in developing visual cortex. *Curr. Top. Dev. Biol.* **69:** 214-237.

Hensch TK (2005) Critical Period Plasticity in Local Cortical Circuits. *Nat. Rev. Neurosci.* **6**: 877-888.

Hensch TK & Stryker MP (2004) Columnar architecture sculpted by GABA circuits in developing cat visual cortex. *Science* **303(5664):** 1678-1681.

Hickox AE & Liberman MC (2014) Is noise-induced cochlear neuropathy key to the generation of hyperacusis or tinnitus? *J. Neurophysiol*. **111**: 553-564.

Hirtz JJ, Braun N, Griesemer D, Hannes C, Janz K, Lohrke S, Muller B & Friauf E (2012) Synaptic refinement of an inhibitory topographic map in the auditory brainstem requires functional CaV1.3 calcium channels. *J. Neurosci.* 42: 14602-14616.

Hofer SB, Mrsic-Flogel TD, Bonhoeffer T, Hübener M (2009) Experience leaves a lasting structural trace in cortical circuits. *Nature* **457(7227):** 313-317.

Holtmaat A & Svoboda K (2009) Experience-dependent structural synaptic plasticity in the mammalian brain. *Nat. Rev. Neurosci*. **10(9):** 647-658.

Huang S, Gu Y, Quinlan EM & Kirkwood A (2010) A refractory period for rejuvenating GABAergic synaptic transmission and ocular dominance plasticity with dark exposure. *J. Neurosci.* **30**: 16636-16642.

Huang S, Gu Y, Quinlan EM & Kirkwood A (2010) A refractory period ofr rejuvenating GABAergic synaptic transmission and ocular dominance plasticity with dark exposure. *J. Neurosci*. **30(49):** 16636-16642.

Hubel DH & Wiesel TN (1964) Effects of Monocular Deprivation in Kittens. *Naunyn Schmiedebergs Arch Exp Pathol Pharmakol*. **248**:492-7.

Hübener M & Bonhoeffer T (2014) Neuronal Plasticity: Beyond the Critical Period. *Cell* **159**: 727-737.

Huberman AD, Feller MB & Chapman B (2008) Mechanisms underlying development ovisual maps and receptive fields. *Ann. Rev. Neurosci*. **31**: 479-509.

Insanally MN, Albanna BF & Bao S (2010) Pulsed Noise Disrupts Complex Sound Representations. *J. Neurophys.* **103**: 2611-2617.

Insanally MN, Kover H, Kim H & Bao S (2009) Feature-dependent sensitive periods in the development of complex sound representation. *J. Neurosci.* **29**(17): 5456-5462.

Ito T, Bishop DC & Oliver DL (2011) Expression of glutamate and inhibitory amino acid vesicular transporters in the rodent auditory brainstem. *J. Comp. Neurol.* **519(2)**: 316-340.

Ito T, Inoue K & Takada M (2015) Distribution of glutamatergic, GABAergic and glycinergic neurons in the auditory pathway of macaque monkeys. *Neuroscience* **310**: 128-151.

Ito T & Oliver DL (2012) The basic circuit of the IC: tectothalamic neurons with different patterns of synaptic organization send different messages to the thalamus. *Front. Neural. Circ*. **6:** 48.

Ito T & Oliver DL (2014) Local and commissural IC neurons make axosomatic inputs on large GABAergic tectothalamic neurons. *J. Comp. Neurol*. **522**: 3539-3554.

Ito T, Bishop DC & Oliver DL (2009) Two classes of GABAergic neurons in the inferior colliculus. *J. Neurosci*. **29:**13860 –13869

Iwai Y, Faglioni M, Obata K & Hensch TK (2003) Rapid critical period induction by tonic inhibition in visual cortex. *J. Neurosci.* **23**(17): 6695-702.

Jastreboff PJ, Brennan JF & Sasaki CT (1988a) An animal model for tinnitus. *Laryngoscope* **98**: 280-286.

Jastreboff PJ, Brennan JF, Coleman JK & Sasaki CT (1988b) Phantom auditory sensation in rats: an animal model for tinnitus. *Behav. Neurosci.* **102(6)**: 811-822.

Jones TA, Leake PA, Snyder RL, Stakhovskaya O, & Bonham B (2007) Spontaneous discharge patterns in the cochlear spiral ganglion cells before the onset of hearing in Cats. *J. Neurophys.* **98**: 1989-1908.

Kalappa BI, Brozoski TJ, Turner JG & Caspary DM (2014) Single unit hyperactivity and bursting in the auditory thalamus of awake rats directly correlates with behavioral evidence of tinnitus. *J. Physiol*. **592**: 5065-5078.

Kalappa BI, Soh H, Duigan KM, Furuya T, Edwards S, Tzingounis AV & Tzounopoulos. (2015) Potent KCNQ2/3-specific channel activator suppresses in vivo epileptic activity and prevents the development of tinnitus. *J. Neurosci.* **35(23):** 8829-8842.

Kaltenbach JA (2007) The dorsal cochlear nucleus as a contributor to tinnitus: mechanisms underlying the induction of hyperactivity. *Prog. Brain Res*. **166**: 89-106.

Kandler K (2004) Activity-dependent organization of inhibitory circuits: lessons from the auditory system. *Curr. Opin. Neurobiol.* **14(1):** 96-104.

Kandler K & Friauf E (1993) Pre- and postnatal development of efferent connections of the cochlear nucleus in the rat. J. *Comp. Neurol*. **328**: 161-184.

Kandler K, Clause A & Noh J (2009) Tonotopic reorganization of developing auditory brainstem circuits. *Nat. Neurosci.* **12(6):** 711-717.

Kandler K, Nguyen T, Noh J & Givens RS (2013) An optical fiber-based uncaging system. *Cold Spring Harb Protoc*. **2:** 118-121.

Katz LC & Shatz CJ (1996) Synaptic activity and the construction of cortical circuits. *Science* **274(5290):** 1133-1138.

Keck T, Scheuss V, Jacobsen RI, Wierenga CJ, Eyesel UT, Bonhoeffer T & Hübener M (2011) Loss of Sensory Input Causes Rapid Structural Changes of Inhibitory Neurons in Adult Mouse Visual Cortex. *Neuron* **71:** 869-882.

Kim G & Kandler K (2003). Elimination and strengthening of glycinergic/GABAergic connections during tonotopic map formation. *Nat. Neurosci.* **6:** 282-90.

Kirkby LA, Sack GS, Firl A & Feller MB (2013) A role for correlated spontaneous activity in the assembly of neural circuits. *Neuron* **80(5):** 1129-1144.

Klug A, Bauer EE, Hanson JT, Hurley L, Meitzen J & Pollak GD (2002) Response selectivity for species-specific calls in the inferior colliculus of Mexican free-tailed bats is generated by inhibition. *J. Neurophysiol*. 88: 1941-1954.

Knipper M, Van Diijk P, Nunes I, Rüttiger L & Zimmermann U (2013) Advances in the neurobiology of hearing disorders: recent developments regarding the basis of tinnitus and hyperacusis. *Prog. Neurobiol*. **111**: 17-33.

Koch M & Schnitzler H-U (1997) The acoustic startle response in rats: circuits mediating evocation, inhibition and potentiation. *Behav. Brain Res*. **89(1-2):** 35-49.

Kral A, Tillein J, Heid S, Hartmann R & Klinke R (2005) Postnatal cortical development in congenital auditory deprivation. *Cerebral Cortex* **15(5):** 555-562.

Krapfer C, Seidl AH, Schweizer H, & Grothe B (2002) Experience-dependent refinement of inhibitory inputs to auditory coincidence-detector neurons. *Nat. Neuroscience* **5**: 247-253.

Kuhlman SJ, Olivas ND, Tring E, Ikrar T, Xu X, & Trachtenberg JT (2013) A disinhibitory microcircuit initates critical period plasticity in visual cortex. *Nature* **501**(7468): 543-546.

Kuwada S, Batra R, Yin TC et al (1997) Intracellular recordings in response to monaural and binaural stimulation of neurons in the inferior colliculus of the cat. *J. Neurosci*. **17:** 7565-7581.

Lahav A & Skoe E (2014) An acoustic gap between the NICU and womb: a potential risk for compromised neuroplasticity in the auditory system in preterm infants. *Front. Neurosci*. **8**: 381.

Leaver AM, Renier L, Chevillet MA, Morgan S, Kim HJ & Rauschecker JP. (2011). Dysregulation of limbic and auditory networks in tinnitus. *Neuron* **69**: 33-43.

Leitner DS, Hammond GR, Springer CP, Ingham KM, Mekilo AM, Bodison PR, Aranda MT & Shawaryn MA (1993) Parameters affecting gap detection in the rat. *Perception & psychophysics* **54**: 395-405

Lesica NA & Grothe B (2008) Efficient temporal processing of naturalistic sounds. *PLoS One* **3**: e1655

Li N & Pollak GD (2013) Circuits that innervate excitatory-inhibitory cells in the inferior colliculus obtained with in vivo whole cell recordings. *J. Neurosci*. **33:** 6367-6379.

Li S, Choi V & Tzounopoulos T (2013) Pathogenic plasticity of Kv7.2/3 channel activity is essential for the induction of tinnitus. *Proc. Natl. Acad. Sci*. **110**: 9980- 9985.

Li S, Kalappa BI & Tzounopoulos (2015) Noise-induced plasticity of KCNQ2/3 and HCN channels underlies vulnerability and resilience to tinnitus. *Elife* **4**: 07242.

Linkenhoker BA, von der Ohe CG & Knudsen EI (2005). Anatomical traces of juvenile learning in the auditory system of adult barn owls. *Nat. Neurosci*. **8(1):** 93-98.

Llano DA, Turner JG & Caspary DM (2012) Diminished cortical inhibition in an aging mouse model of chronic tinnitus. *J. Neurosci*. **32**: 16141-16148.

Lobarinas E, Sun W, Cushing R & Salvi R (2004) A novel behavioral paradigm for assessing tinnitus using shcedul-induced polydipsia avoidance conditioning (SIP-AC). *Hear. Res.* **190**: 109-114.

Loftus WC, Bishop D & Oliver DL (2010) Differential patterns of inputs create functional zones in central nucleus of inferior colliculus. *J. Neurosci.* **30**:13396 –13408.

Loftus WC, Bishop DC, Saint Marie RL & Oliver DL (2004) Organization of binaural excitatory and inhibitory inputs to the inferior colliculus from the superior olive. *J. Comp. Neurol.* **472**: 330 –344.

Luo H, Pace E, Zhang X & Zhang J (2014) Blast-Induced tinnitus and spontaneous firing changes in the rate dorsal cochlear nucleus. *J. Neurosci. Res.* **92:** 1466-1477.

Ma WL, Hidaka H & May BJ (2006) Spontaneous activity in the inferior colliculus of CBA/J mice after manipulations that induce tinnitus. *Hear. Res*. **212:** 9-21.

Ma X & Suga N (2001) Corticofugal modulation of duration-tuned neurons in the midbrain auditory nucleus in bats. Proc. Natl. Acad. Sci. 98(24): 14060-14065.

Ma X & Suga N (2008) Corticofugal modulation of the paradoxical latency shifts of inferior collicular neurons. *J. Neurophysiol*. **100(2):** 1127-1134.

Maffei A Nelson SB & Turrigiano GG (2004) Selective reconfiguration of layer 4visual cortical circuitry by visual deprivation. *Nat. Neurosci.* **7**: 1353- 1359.

Maffi CL & Aitkin LM (1987) Differential neural projections to regions of the inferior colliculus of the cat responsive to high frequency sounds. *Hearing Res*. **26**: 211–219.

Magnusson AK, Kapfer C, Grothe B & Koch U (2005) Maturation of glycinergic inhibition in the gerbil medial superior olive after hearing onset. *J. Physiology* **568**: 497-512.

Maling DH (1993) Coordinate systems and map projections, Ed2. Amsterdam: Elsevier.

Malmierca MS, Blackstad TW, Osen KK, Karagu¨lle T, Molowny RL (1993) The central nucleus of the inferior colliculus in rat: a Golgi and computer reconstruction study of neuronal and laminar structure. *J Comp Neurol*. **333**:1–27.

Malmierca MS, Hernandez O & Rees A (2005) Intercollicular commissural projections modulation neurons responses in the inferior colliculus. *Eur. J. Neurosci.* **21(10):** 2701-10.

Malmierca MS, Izquierdo MA, Cristaudo S, Hernánndez O, Perez-Gonzalez D, Covey E & Oliver DL (2008) A discontinuous tonotopic organization in the inferior colliculus of the rat. *J. Neurosci.* **28**: 4767– 4776.

Malmierca MS, Le Beau FEN & Rees A (1996) The topographical organization of descending projections from the central nucleus of the inferior colliculus in guinea pig. *Hearing Res*. **93**: 167-180.

Malmierca MS, Merchán MA, Henkel CK & Oliver DL (2002) Direct projections from cochlear nuclear complex to auditory thalamus in the rat. *J. Neurosci.* **22**:10891–10897.

Malmierca MS, Saint Marie RL, Merchan MA & Oliver DL (2005). Laminar inputs from dorsal cochlear nucleus and ventral cochlear nucleus to the central nucleus of the inferior colliculus: two patterns of convergence. *Neuroscience*. **136**: 883–894.

Malmierca, MS (2004) The Inferior Colliculus: A Center for Convergence of Ascending and Descending Auditory Information. *Neuroembryology and Aging*. doi:10.1159/000096799

Mancuso JJ, Kim J, Lee S, Tsuda S, Chow NB & Augustine GJ (2011) Optogenetic probing of functional brain circuitry. *Exp. Physiol*. **96(1):** 26-33.

Manzoor NF, Licari F, Klapchar M, Elkin RL, Gao Y, Chen G & Kaltenbach JA (2012) Noise-induced hyperactivity in the inferior colliculus: its relationship with hyperactivity in the dorsal cochlear nucleus. *J. Neurophys.* **108(4):** 976-988.

Manzoor NR, Gao Y, Licari F & Kaltenbach JA (2012) Comparison and contrast of noise-induced hyperactivity in the dorsal cochlear nucleus and inferior colliculus. *Hear. Res*. **294**: 114-123.

McCalpine D, Martin RL, Mossop JE & Moore DR (1997) Response properties of neurons in the inferior colliculus of the monaurally deafened ferret to acoustic stimulation of the intact ear. *J. Neurophys*. **78(2):** 767-779.

McMahon E, Wintermark P & Lahav A (2012) Auditory brain development in premature infants: the importance of early experience. *NY Acad. Sci.* **1252**: 17-24.

Meininger V, Pol D & Derer P (1986) The inferior colliculus of the mouse: a Nissl and Golgi study. *Neuroscience* **17**:1159 –1179.

Melcher JR, Sigalovsky IS, Guinan JJ Jr. & Levine RA (2000) Lateralized tinnitus studied with functional magnetic resonance imaging: abnormal inferior colliculus activation. *J. Neurophysiol.* **83**: 1058-1072.

Mellot JG, Foster NL, Ohi AP & Schofield BR (2014) Excitatory and inhibitory connections in parallel pathways from the inferior colliculus to the auditory thalamus. *Front. Neuroanat.* **8**: 124.

Merzenich MM & Reid MD (1974) Representation of the cochlea within the inferior colliculus of the cat. *Brain Research* **77**: 397-415.

Middleton JW, Kiritani T, Pedersen C, Turner JG, Shepherd GM & Tzounopoulos T (2011) Mice with behavioral evidence of tinnitus exhibit dorsal cochlear nucleus hyperactivity because of decreased GABAergic inhibition. *Proc. Natl. Acad. Sci.* **108**: 7601-7606.

Milbrandt JC, Holder TM, Wilson MC, Salvi RJ & Caspary DM (2000) GAD levels and muscimol binding in rat inferior colliculus following acoustic trauma. *Hear. Res.* **147**: 251-260.

Miller KE, Casseday JH & Covey E (2005) Relation between intrinsic connections and isofrequency contours in the inferior colliculus of the big brown bat, Eptesicus fuscus. *Neuroscience* **136**: 895–905.

Mody M, Schwartz RG, Gravel JS & Ruben RJ (1999) Speech perception and verbal memory in children with and without histories of otitis media. J. Speech Lang. *Hear Res.* **52(5):** 1069-1079.

Moore DR & Kowalchuck NE (1988) Auditory brainstem of the ferret: effects of unilateral cochlear lesions on cochlear nucleus volume and projections to the inferior colliculus. *J. Comp. Neurol.* **272(4)**: 503-515.

Moore DR, Kotak VC & Sanes DH (1998) Commissural and lemniscal synaptic input to the gerbil inferior colliculus. *J. Neurophysiol.* **80**: 2229-2236.

Morest DK & Oliver DL (1984) The neuronal architecture of the inferior colliculus in the cat: defining the anatomy of the auditory midbrain. *J. Comp. Neurol.* **222:** 209 –236

Mossop JE, Wilson MJ, Caspary DM & Moore DR (2000) Down-regulation of inhibition following unilateral deafening. *Hearing Res.* **147(1-2):** 183-187.

Mowery TM, Kitak VC & Sanes DH (2015) Transient Hearing Loss Within a Critical Period Causes Peristent Changes to Cellular Properties in Adult Auditory Cortex. *Cerebral Cortex* **25(8):** 2083-2094.

Mulders WH & Robertson D (2011) Progressive centralization of midbrain hyperactivity after acoustic trauma. *Neuroscience* **192**: 753-760.

Mulders WH, Roberston D (2009) Hyperactivity in the auditory midbrain after acoustic trauma: dependence on cochlear activity. *Neuroscience* **164**: 733- 746.

Myoga MH, Lehnert S, Leibold C, Felmy F & Grothe B (2014) Glycinergic inhibition tunes coincidence detection in the auditory brainstem. *Nat. Commun*. **5**: 3790.

Nagase S, Miller JM, Dupont J, Lim HH, Sato K & Altschuler RA (2000) Changes in cochlaer electrical stimulation induced Fos expression in the rat inferior colliculus following deafness. *Hearing Res*. **147**: 242-250.

Nakahara H, Zhang LI & Merzenich MM (2004) Specialization of primary auditory cortex processing by sound exposure in the "critical period." *Proc. Natl. Acad. Sci*. **101(18**): 7170-7174.

Nakamoto KT, Jones SJ & Palmer AR (2008) Descending projections from auditory cortex modulate sensitivity in the midbrain to cues for spatial position. *J. Neurophysiol.* **99(5):** 2347-2356.

Niu Y, Kamaraguru A, Wang R & Sun W (2013) Hyperexcitability of inferior colliculus neurons caused by acute noise exposure. *J. Neurosci. Res*. **91**: 292-299.

Noh J, Seal RP, Garver JA, Edwards RH & Kandler K (2010) Glutamate co-release at GABA/glycinergic synapses is crucial for the refinement of an inhibitory map. *Nat. Neurosci.* **13**: 232-8.

Nondahl DM, Cruickshanks KJ, Huang GH, Klein BE, Klein R, Nieto FJ & Tweed TS (2011) Tinnitus and its risk factors in the Beaver Dam offspring study. *Int. J. Audiol*. **50**: 313-320.

Nordeen KW, Killackey HP & Kitzes LM (1983) Ascending auditory projections to the inferior colliculus following unilateral cochlear ablation in the neonatal gerbil, Meriones unguicatus. *J. Comp. Neurol*. **214(2):** 144-153.

Noreña AJ & Eggermont JJ (2003) Changes in spontaneous neural activity immediately after an acoustic trauma: implications for neural correlates of tinnitus. *Hear. Res.* **183**: 137-153.

Noreña AJ & Eggermont JJ (2005) Enrichment acoustic environment after noise trauma reduces hearing loss and prevents cortical map reorganization. *J. Neurosci.* **25**: 699-705

Okoyama S, Moriizumi T, Kitao Y, Kawano J, & Kudo M (1995) Postnatal development of the projection from the medial superior olive to the inferior colliculus in the rate. *Hearing Res.* **88**: 65-70.

Oliver DL (1984) Dorsal cochlear nucleus projections to the inferior colliculus in the cat. A light and electron microscopic study. *J. Comp. Neurol*. **224**: 24-46.

Oliver DL (1987) Projections to the inferior colliculus from the anteroventral cochlear nucleus in the cat: possible substrates for binaural interaction. *The J. Comp. Neurol.* **264**: 24–46.

Oliver DL (2000) Ascending efferent projections of the superior olivary complex. *Microscopy Research and Technique* **51**: 355–363.

Oliver DL & Morest DK (1984) The central nucleus of the inferior colliculus in the cat. *J. Comp. Neurol*. **222**: 237-264.

Oliver DL, Beckius GE and Shneiderman A (1995) Axonal projections from the lateral and medial superior olive to the inferior colliculus of the cat: a study using electron microscopic autoradiography. *J. Comp. Neurol.* **360**: 17-32.

Oliver DL, Beckius GE, Bishop DC & Kuwada S (1997) Simultaneous anterograde labeling of axonal layers from lateral superior olive and dorsal cochlear nucleus in the inferior colliculus of cat. *J. Comp. Neurol.* **382**: 215–229.

Oliver DL, Izquierdo MA & Malmierca MS (2011) Persistent Effects of Early Augmented Acoustic Environment on the Auditory Brainstem. *Neuroscience* **184**: 75-87.

Oliver DL, Kuwada S, Yin TC, Haberly LB & Henkel CK (1991) Dendritic and axonal morphology of HRP-injected neurons in the inferior colliculus of the cat. *J. Comp. Neurol*. **303**: 75–100.

Oliver DL, Winer JA, Beckius GE & Saint Marie RL (1994) Morphology of GABAergic neurons in the inferior colliculus of the cat. J. Comp. Neurol. **340**: 27– 42.

Ono M & Oliver DL (2014) The balance of excitatory and inhibitory synaptic cinputs for coding sound location. *J. Neurosci*. **34(10**): 3779-3792.

Ono M, Yanagawa Y & Koyano K (2005) GABAergic neurons in inferior colliculus of the GAD67-GFP knock-in mouse: electrophysiological and morphological properties. *Neurosci Res*. **51**: 475– 492.

Orton LD & Rees A (2014) Intercollicular commissural connections refine the representation of sound frequency and level in the auditory midbrain. *Elife* **18(3):** doi: 10.7554.

Oviedo HV, Bureau I, Svoboda K & Zador AM (2010) The functional asymmetry of auditory cortex is reflected in the organization of local cortical circuits. *Nat. Neurosci.* **13**: 1413-1420.

Paradise JL, Feldman HM, Campbell TF, Dollaghan CA, Colborn DK, Bernard BS, Rockette HE, Janosky JE, Pitcairn DL, Sabo DL, Kurs-Lasky M & Smith CG (2003) Early versus delayed insertion of tympanostomy tubes for persistent otitis media: developmental outcomes at the age of three years in relation to prerandomization illness patterns and hearing levels. *Pediatr Infect Dis J*. **22**: 309–31

Pedemonte M, Torterolo P & Velluti RA (1997) In vivo intracellular characteristics of inferior colliculus neurons in guinea pigs. *Brain Res.* **759**: 24-31.

Peruzzi D, Sivaramakrishnan S, Oliver DL (2000) Identification of cell types in brain slices of the inferior colliculus. *Neuroscience.* **101**: 403– 416.

Phillips MA, Colonnesse MT, Goldberg J, Lewis LD, Brown EN & Constantine-Paton M (2011) A synaptic strategy for consolidation of convergent visuotopic maps. *Neuron* **71**(4): 710-724.

Pilati N, Ison MJ, Barker M, Mulheran M, Large CH, Forsythe ID, Matthias J & Hamann M (2012b) Mechanisms contributing to central excitability changes during hearing loss. *Proc. Nat. Acad. Sci*. **109**: 8292-8297.

Pilati N, Large C, Forsythe ID & Hamann M (2012a) Acoustic over-exposure triggers burst firing in dorsal cochlear nucleus fusiform cells. *Hear. Res*. **283**: 98-106.

Pizzorusso, T. et al. (2002) Reactivation of ocular dominance plasticity in the adult visual cortex. *Science* **298**: 1248–1251.

Pollak GD, Xie R, Gittelman J, Andoni S & Li N (2011) The dominance of inhibition in the inferior colliculus. *Hearing Res*. **274**:27–39.

Polley DB, Thompson JH & Guo W (2013) Brief hearing loss disrupts binaural integration during two early critical periods of auditory cortical development. *Nat. Commun.* **4**: 2547.

Popescu MV & Polley DB (2010) Monaural deprivation disrupts development of binaural selectivy in auditory midbrain and cortex. *Neuron*. **65(5):** 718-31.

Portfors CV, Felix RA 2nd (2005) Spectral integration in the inferior colliculus of the CBA/CaJ Mouse. *Neuroscience* **136**: 1159- 1170.

Portfors DV, Mayko ZM, Jonson K, Cha GF & Roberts PD (2011) Spatial organization of receptive fields in the auditory midbrain of awake mouse. *Neuroscience* 1**93**: 429-439.

Razak KA, Richardson MD & Fuzessery ZM (2008) Experience is required for the maintenance and refinement of FM sweep selectivity in the developing auditory cortex. *Proc. Natl. Acad. Sci* **105**(11): 4465-4470.

Reetz G & Ehret (1999) Inputs from three brainstem sources to identified neurons of the mouse inferior colliculus slice. *Brain Res*. **816**: 527-543.

Roberts LE, Eggermont JJ, Caspary DM, Shore SE, Melcher JR & Kaltenbach JA (2010) *J. Neurosci.* **30(45):** 14972-14979.

Rodriguez FA, Read HL & Escabi MA (2010) Spectral and temporal modulation tradeoff in the inferior colliculus. *J. Neurophysiol*. **103(2**): 887-903.

Romand R & Ehret G (1990) Development of tonotopy in the inferior colliculus: Electrophysiological mapping in house mice. *Dev Brain Res* **54**: 221–234.

Ropp TJ, Tiedemann KL, Young ED & May BJ. (2014) Effects of Unilateral Acoustic Trauma on Tinnitus-Related Spontaneous Activity in the Inferior Colliculus. *J. Assoc. Res. Otolaryngol*. **6**: 1007-1022.

Rubel EW (1984) Ontogeny of auditory system function. *Annu Rev Physiol.* **46**: 213-229.

Ruben RJ (1992) The ontogeny of human hearing. *Acta Otolaryngol* **112**: 192-196.

Saghatelyan AK, Dityatev A, Schmidt S, Schuster T, Bartsch U & Schachner M (2001) Reduced perisomatic inhibition, increased excitatory transmission, and impaired long-term potentiation in mice deficient for the extracellular matrix glycoprotein tenascin-R. *Mol. Cell Neurosci.* **17(1):** 226-240.

Saint Marie RL, Ostapoff EM, Morest DK & Wenthold RJ (1989) Glycine-immunoreactive projection of the cat lateral superior olive: possible role in midbrain ear dominance. *J. Comp. Neurol*. **279**: 382-396.

Saint Marie RL, Shneiderman A & Stanforth DA (1997) Patters of γ–aminobutyric acid and glycine immunoreactivities reflect structural and functional differences of the cat lateral lemniscal nuclei. *J. Comp. Neurol*. **389:** 264-276.

Saitoh I & Suga N (1995). Long delay lines for ranging are created by inhibition in the inferior colliculus of the mustached bat. *J. Neurophysiol.* **74(1):** 1-11.

Saldaña & Merchán MA (2005) Intrinsic and Commissural Connections of the Inferior Colliculus. In: *The Inferior Colliculus*, New York: Springer.

Saldaña E & Merchán MA (1992) Intrinsic and commissural connections of the rat inferior colliculus. *J. Comp. Neurol.* **319**: 417– 437.

Saldaña E, Feliciano M & Mugnaini E (1996) Distribution of descending projections from primary auditory neocortex to inferior colliculus mimics the topography of intracollicular projections. *J. Comp. Neurol*. **371**, 15-40.

Salvi RJ, Powers NL, Saunders SS, Boettcher F & Clock AE (1992) Enhancement of evoked response amplitude and single unit activity after noise exposure. In: Dancer A, Henderson D, Salvi RJ & Hamernik RP (eds). *Noise-Induced Hearing Loss*. Mosby Year Book, St. Louis, pp. 156-171.

Sanes DH & Constantine-Paton M (1983) Altered activity patterns during development reduce neural tuning. *Science* **221**: 1183-1185.

Sanes DH & Constantine-Paton M (1985) The sharpening of Frequency Tuning Curves Requires Patterned Activity during Development in the Mouse, *Mus musculus*[1]. *J. Neurosci.* **5**(5): 1152-1166.

Sanes DH & Siverls V (1991) Development and specificity of inhibitory terminal arborizations in the central nervous system. *J. Neurobiol.* **22(8**): 837-854.

Saunders J, Dolgin K & Lowry L (1980) The maturation of frequency selectivity in C57BL/6J mice studies with auditory evoked response tuning curves. *Brain Res.* **187**: 69-79.

Schaette R & Kempter R (2009) Predicting tinnitus pitch from patient's audiograms with a computational model for the development of neuronal hyperactivity. *J. Neurophysiol.* **101**: 3042-3052.

Schnerson A & Willott JF (1979) Development of inferior colliculus response properties in C57BL/6J mouse pups. *Exp. Brain Res.* **37**: 373-385.

Schofield BR (2001) Origins of projections from the inferior colliculus to the cochlear nucleus in guinea pigs. *J. Comp. Neurol*. **429**: 206-220.

Schreiner CE & Langner G (1988) Periodicity coding in the inferior colliculus of the cat: II. Topographic organization. *J. Neurophysiol.* **60**: 1823-1840.

Schreiner CE & Langner G (1997) Laminar fine structure of frequency organization in auditory midbrain. *Nature* **388**:383–386.

Seidle AH & Grothe B (2005) Development of Sound Localization Mechanisms in the Mongolian Gergil is Shaped by Early Acoustic Experience. *J. Neurophysiol*. **94(2):** 1028-1036.

Seki S & Eggermont JJ (2003) Changes in spontaneous firing rate and neural synchrony in cat primary auditory cortex after localized tone-induced hearing loss. *Hear. Res*. **180**: 28-38.

Sengpiel F (2014) Plasticity of the visual cortex and treatment of amblyopia. *Curr. Biol*. **24(18)**: 936-940.

Sereda M, Edmondson-Jones M & Hall DA (2014) Relationship between tinnitus pitch and edge of hearing loss in individuals with a narrow tinnitus bandwidth. *Int. J. Audiol.* 1-8.

Shargorodsky J, Curhan GC & Farwell WR (2010) Prevalence and characteristics of tinnitus among US adults. *Am. J. Med.* **123**: 711-718.

Shepherd GM (2012) Circuit mapping by UV uncaging of glutamate. *Cold Spring Harb Protoc*. **9:** 998-1004

Shneiderman A & Henkel CK. (1987) Banding of lateral superior olivary nucleus afferents in the inferior colliculus: a possible substrate for sensory integration. *J. Comp. Neurol.* **266:** 519–534. doi:10.1002/cne.902660406.

Shneiderman A, Oliver DL & Henkel CK (1988) Connections of the dorsal nucleus of the lateral lemniscus: an inhibitory parallel pathway in eh ascending auditory system? *J. Comp. Neurol*. **276**: 188-208.

Sivaramakrishnan S & Oliver DL (2001) Distinct K currents result in physiologically distinct cell types in the inferior colliculus of the rat. *J. Neurosci*. **21**: 2861–2877.

Sivaramakrishnan S & Oliver DL (2006) Neuronal responses to lemniscal stimulation in laminar brain slices of the inferior colliculus. *J. Assoc Res. Otolaryngol*. **7**: 1-14.

Spitzer NC (2006) Electrical activity in early neuronal development. *Nature.* **444(7120):** 707-712.

Stebbings KA, Lesicko AMH & Llano DA (2014) The Auditory Corticocollicular System: Molecular and Circuit-Level Considerations. *Hearing Res*. **314**: 51-59.

Stefanescu RA, Koehler SD & Shore SE (2015) Stimulus-timing dependent modifications in the rate-level functions in animals with and without tinnitus. *J. Neurophysiol.* **113**: 956-970.

Stiebler I, & Ehret G (1985) Inferior colliculus of the house mouse. I. A quantitative study of tonotopic organization, frequency representation, and ton-threshold distribution. *J. Comp. Neurol*. **238 (1):** 65-76.

Stodieck SK, Greifzu F, Goetze B, Schmidt KF & Lowel S (2014) Brief dark exposure restored ocular dominance plasticity in aging mice and after cortical stroke. *Exp. Gerontol*. **60:** 1-11.

Sturm J, Nguyen T & Kandler K (2014) Development of Intrinsic Connectivity in the Mouse Inferior Colliculus. *J. Neurosci*. **34(45)**: 15032-15046.

Sturm JJ, Nguyen T & Kandler K (2015) Mapping Synaptic Circuits with Photostimulation of Caged Glutamate. Auditory Vestibular Research Methods, New York: Springer. *Accepted.*

Suga N, Xiao Z, Ma X & Ji W (2002) Plasticity and corticofugal modulation for hearing in adult animals. *Neuron* **36(1):** 9-18.

Sun YJ, Wu GK, Liu BH, Li P, Zhou M, Xiao Z, Tao HW & Zhang L (2010). Fine-tuning of pre-balanced excitation and inhibition during auditory cortical development. *Nature* **465(7300):** 927-931.

Suneja SK, Potashner SJ & Benson CG (2000b) AMPA receptor binding in adult guinea pig brain stem auditory nuclei after unilateral cochlear ablation. *Experimental Neurology* **165**: 355-369.

Swathi S, Ramesh A, Nagapoornima M, Fernandes LM, Jisina C, Suman Rao PN & Swarnarekha A (2014) Sustaining a “culture of silence” in the neonatal intensive care unit during nonemergency situations: a grounded theory on ensuring adherence to behavioral modification to reduce noise levels. *Int. J. Qual Stud. Heath Well-being.* **9**: 10.3402.

Takesian AE & Hensch TK (2013) Balancing plasticity/stability across brain development. *Prog. Brain. Res*. **207**: 3-34.

Tan ML, Theeuwes HP, Feenstra L & Borst JG (2007) Membrane properties and firing patterns of inferior colliculus neurons: an in vivo patch-clamp study in rodents. *J. Neurophysiol.* **98**: 443– 453.

Tibussek D, Meister H, Walger M, Foerst A & von WH (2002). Hearing loss in early infancy affects maturation of the auditory pathway. *Developmental Medicine and Child Neurology*, ***44*:** 123–129.

Thompson GC, Cortez AM & Lam DM-K (1985) Localization of GABA immunoreactivity in the auditory brainstem of guinea pigs. *Brain Res*. **339**: 119-122.

Tritsch NX & Bergles DE (2010). Developmental regulation of spontaneous activity in the Mammalian cochlear. *J. Neurosci.* **30(4):** 1539-1550.

Tritsch NX, Yi E, Gale JE, Glowatzki E & Bergles DE (2007) The origin of spontaneous activity in the developing auditory system. *Nature* **450**(7166): 50-55.

Turner JG, Brozoski TJ, Bauer CA, Parrish JK, Meyers K, Hughes LF & Caspary DM (2006) Gap detection deficits in rats with tinnitus: a potential novel screening tool. *Behav. Neurosci.* **112:** 188-195.

Tzounopolous T, Rubio ME, Keen JE & Trussel LO (2007). Coactivation of Pre- and Postsynaptic Signaling Mechanisms Determines Cell-Specific Spike-Timing-Dependent Plasticity. *Neuron* **54(2**): 291-301.

Tzounopoulos T, Kim Y, Oertel D & Trussell LO (2004). Cell-specific, spike timing-dependent plasticities in the dorsal cochlear nucleus. *Nat. Neurosci*. **7**:719–72.

Vale C & Sanes DH (2002) The effect of bilateral deafness on excitatory and inhibitory synaptic strength in the inferior colliculus. *Eur. J. Neurosci.* **16(12):** 2394-2404.

Vale C, Juiz JM, Moore DR & Sanes DH (2004) Unilateral cochlear ablation produces a greater loss of inhibition in the contralateral inferior colliculus. *Eur. J. Neurosci*. **20(8):** 2133-2400.

Vanneste S, van Dongen M, Dre Vree B, Hiseni S, van der Velden E, Strydis C, Joos K, Norena A, Serdijn W& De Ridder D (2013) Does enriched acoustic environment in humans

abolish chronic tinnitus clinical and electrophysiologically? A double blind placebo controlled study. *Hearing Res*. **296**: 141-148.

Vater M & Feng AS (1990) Functional organization of ascending and descending connections of the cochlear nucleus of horseshoe bats. *J. Comp. Neurol.* **292**: 373-395.

Venkataraman Y & Bartlett EL (2013) Postnatal development of synaptic properties of the GABAergic projection from the inferior colliculus to the auditory thalamus. *J. Neurophysiol*. **109(12):** 2866-2882.

Vetter DE, Saldaña E & Mugnaini E (1992) Input from the inferior colliculus to medial olivocochlear neurons in the rat: a double label study with PHA-L and cholera toxin. *Hearing Res*. **70**: 173-186.

Vogler DP, Robertson D & Mulders WH (2011) Hyperactivity in the ventral cochlear nucleus after cochlear trauma. *J. Neurosci*. **31**: 6639-6645.

Von der Behrens (2014) Animal models of subjective tinnitus. *Neural. Plast.* 741452.

Wallace MM, Kavianpour SM & Gabriele ML (2013) Ephrin_B2 reverse signaling is required for topography but not pattern formation of lateral superior olivary inputs to the inferior colliculus. *J. Comp. Neurol***. 7**: 1585-1597.

Wallace MN, Shackelton TM & Palmer AR (2012) Morphological characteristics of laminar cells in the central nucleus of the inferior colliculus. *Front. Neur. Circ*. **6**: 55.

Wang H, Brozoski JT & Caspary DM (2011) Inhibitory neurotransmission in animal models of tinnitus: maladaptive plasticity. *Hear. Res.* **279**: 111-117.

Wang H, Brozoski TJ, Turner JG, Ling L, Parrish JL, Hughes LF & Caspary DM (2009) Plasticity of glycinergic synapses in dorsal cochlear nucleus of rats with behavioral evidence of tinnitus. *Neuroscience*. **164**: 747-759.

Wang J, Ding D, Salvi RJ (2002) Functional reorganization in chinchilla inferior colliculus associated with chronic and acute cochlear damage. *Hear. Res*. **168**: 238-249.

Wenstrup JJ & Grose CD (1995) Inputs to combination-sensitive neurons in the medial geniculate body of the mustached bat: the missing fundamental. *J. Neurosci*. **15**: 4693-4177

Wenstrup JJ & Portfors CV (2011) Neural processing of target distance by echolocating bats: functional roles of the auditory midbrain. *Neurosci. Biobehav. Rev.* **35(10)**: 2073-2083.

Wenstrup JJ, Ross LS & Pollak GD (1986) Binaural response organization within a frequency-band representation of the inferior colliculus: implications for sound localization. *J. Neurosci*. **6**: 962–973.

Werthat F, Alexandrova O, Grothe B, & Koch U (2008). Experience-Dependent Refinement of the Inhibitory Axons Projecting to the Medial Superior Olive. *Developmental Biology* **68(13):** 1454-1462.

Whitton JP & Polley DB (2011) Evalutating the perceptual and pathophysiological consequences of auditory deprivation in early neonatal life: a comparison of basic and clinical studies. *J Assoc. Res. Otolaryngol.* **12(5):** 535-547.

Wiesel TN & Hubel DH (1963) Single-cell responses in striate cortex of kittens deprived of vision in one eye. *J. Neurophysiol*. **26**: 1003-10017.

Willott JF & Lu SM (1982) Noise-induced hearing loss can alter neural coding and increase excitability in the central nervous system. *Science* **216(4552)**: 1331-1334.

Willott JF & Shnerson A (1978) Rapid development of tuning characteristics of inferior colliculus neurons in mouse pups. *Brain Res.* **148**: 230 –233.

Wilmington D, Gray L & Jahrsdoerfer R (1994) Binaural processing after corrected congenital unilateral conductive hearing loss. *Hear. Res.* **74**: 99 –114.

Winer JA & Morest DK (1983) Axons of the dorsal medial geniculate body of the cat: a study with the rapid Golgi method. *J. Comp. Neurol*. **224(3):** 344-370.

Winer JA & Morest DK (1983) The medial division of the medial geniculate body of the cat: implications for thalamic organization. J. *Neurosci.* **3(12):** 2629- 2651.

Winer JA & Schreiner CE (2005) The Inferior Colliculus. pp 24. New York: Springer

Winer JA, Larue DT & Pollak (1995) GABA and glycine in the central auditory system of the mustache bat: structural substrates for inhibitory neuronal organization. *J. Comp. Neurol.* **355**: 317-353.

Winer JA, Larue DT, Diehl JJ & Hefti BJ (1998) Auditory cortical projections to the cat inferior colliculus. *J. Comp. Neurol.* **400**:147–174.

Winer JA, Saint Marie RL, Larue DT et al (1996) GABAergic feedforward projections from the inferiror colliculus to the medial geniculate body. *Proc. Natl. Acad. Sci.* **93**: 8004-8010.

Wong RO (1993) The role of spatio-temporal firing patterns in neuronal development of sensory systems. *Curr. Opin. Neurobiol*. **3(4):** 595-601.

Xiao Z & Suga N (2005) Asymmetry in corticofugal modulation of frequency-tuning in mustached bat auditory system. *Proc. Natl. Acad. Sci*. **102(52):** 19162-19167.

Xie R, Gittelman JX & Pollak GD (2007) Rethinking tuning: in vivo whole-cell recordings of the inferior colliculus in awake bats. *J. Neurosci.* **27**: 9469-9481.

Xiong XR, Liang F, Li H, Mesik L, Zhang KK, Polley DB, Tao HW, Xiao Z & Zhang L (2013) Interaural level difference-dependent gain control and synaptic scaling underlying binaural computation. *Neuron*. **79(4):** 738-753.

Xiong XR, Liang F, Zingg B, Ji XY, Ibrahim LA, Tao HW & Zhang L (2015). Auditory cortex controls sound-drive innate defense behavioral through corticofugal projections to inferior colliculus. *Nat. Communications* **6:** 7224.

Xu J, Yu L, Cai R, Zhang J & Sun X (2009) Early Continuous White Noise Exposure Alters Auditory Spatial Sensitivity and Expression of GAD65 and GABAA Receptor Subunits in Rat Auditory Cortex. *Cerebral Cortex* **20**: 804-812.

Xu J, Yu L, Zhang J, Cai R, Sun X (2010) Early Continuous White Noise Exposure Alters L-α-Amino-3-Hydroxy-5-methyl-4-Isoxazole Propionic Acid Receptor Subunit Glutamates Receptor 2 and γ-Aminobutyric Acid Type A Receptor Subunit β3 Protein Expression in Rat Auditory Cortex. *Journal of Neuroscience Research* **88**: 614-619.

Yan J, Zhang Y & Ehret G (2005). Corticofugal shaping of frequency tuning curves in the central nucleus of the inferior colliculus of mice. *J. Neurophysiol*. **93(1):** 71-83.

Yang S, Weiner BD, Zhang LS, Cho S-J & Bao S (2011). Homeostatic plasticity drives tinnitus perception in an animal model. *Proc. Natl. Acad. Sci*. **108**: 14974- 14979.

Yankaskas K (2013) Prelude: noise-induced tinnitus and hearing loss in the military. *Hear. Res*. **294**: 3-8.

Yu X, Wadghiri YZ, Sanes DH & Turnbull DH (2005) In vivo auditory brain mapping in mice with Mn-enhanced MRI. *Nat Neurosci*. **8(3**): 961-96.

Yurgil KA, Clifford RE, Risbrough VB, Geyer MA, Huang M, Barkauskas DA, Vasterling JJ, Baker DG & MRS team. (2015). Prospective Associations Between Traumatic Brain Injury and Postdeployment Tinnitus in Active-Duty Marines. *J. Head. Trauma Rehabil*. PMID: 25699623

Zhang Li & Poo MM (2001) Electrical activity and development of neural circuits. *Nat. Neurosci*. **4**: 1207-1214.

Zhang LI, Bao S & Merzenich MM (2001) Persistent and specific influences of early acoustic environments on primary auditory cortex. *Nat. Neurosci.* **4**: 1123-1130.

Zhang LI, Bao S & Merzenich MM (2002) Disruption of primary auditory cortex by synchronous auditory inputs during a critical period. *Proc. Natl. Acad. Sci.* **99**(4): 2309-2314.

Zhao C, Kao JP & Kanold PO (2009) Functional excitatory microcircuits in neonatal cortex connect thalamus and layer 4. *J. Neurosci*. **29(49):** 15479-15488.

Zhou X & Merzenich MM (2008) Enduring effects of early structures noise exposure on temporal modulation in the primary auditory cortex. *Proc. Natl. Acad. Sci.* **105**(11): 4423-4428.

Zhou X, Panizzutti R, de Villers-Sidani E, Madeira M & Merzenich MM (2011) Natural Restoration of Critical Period Plasticity in the Juvenile and Adult Primary Auditory Cortex. *J. Neurosci*. **31(15):** 5625-5634.

Zhu X, Wang F, Hu H, Sun X, Kilgard MP, Merzenich MM & Zhou X (2014) Environmental acoustic enrichment promotes recovery from developmentally degraded auditory cortical processing. *J Neurosci.* **34**: 5406- 5015.